

**Mechanisms of Ryanodine Receptor 2 Regulation
in Cardiac Pathophysiology**

by

Francisco Alvarado Guillén

A dissertation submitted in partial fulfillment
of the requirements for the degree of
Doctor of Philosophy
(Molecular and Integrative Physiology)
in The University of Michigan
2017

Doctoral Committee:

Professor Héctor H. Valdivia, Chair
Associate Professor Sharlene M. Day
Professor José Jalife
Associate Professor Daniel E. Michele

Francisco Alvarado Guillén

falvara@umich.edu

ORCID iD: [0000-0003-0552-9029](https://orcid.org/0000-0003-0552-9029)

© Francisco Alvarado Guillén 2017

DEDICATION

“La educación es la única herencia que dura para toda la vida”

A mis padres, Javier y Goretty, por todo su esfuerzo, dedicación y sacrificios a través de los años para darme la mejor educación posible.

ACKNOWLEDGEMENTS

The work described in this dissertation is the result of a collaborative effort developed in the Valdivia Laboratory, and with colleagues and friends from the University of Michigan and other institutions all over the world. Without the contributions of these great scientists, none of this would have been possible. Each chapter includes a short section highlighting the scientific contributions of the people that participated in these projects. I specially thank Carmen, Dawn, Julieta, Keita, and Michelle proof-reading the many drafts that came before this document was completed. To my Dissertation Committee, Dan Michele, Pepe Jalife and Sharlene Day, I am grateful for their critical feedback, tough questions, and thoughtful advice.

Héctor, my mentor, needs special recognition not only for his scientific acumen, which was fundamental for this research and crucial for my graduate training, but for his great personality and paternalistic mentoring approach, which have made my experience in his lab remarkable. Since I joined Héctor's group in 2011, he has provided me with nothing but endless and sincere support every step of the way in the best working environment a student can hope for. But beyond what I have learned from Héctor about science, ryanodine receptors and calcium, I want to thank him for what he has taught me about life, humility, and tequila. Thank you Héctor! I also want to sincerely thank Carmen for always making feel part of the Valdivia family.

I owe endless gratitude to all my Valdivia lab mates throughout these years: Carmen, Randall, Jonathan, Julieta, Xi, Yanting, Michelle, Roberto, Emmanuel, Erika, Liang, Jing, Yan, Dawn, Edgar, Mario, Keita, Dani Robledo, Sharon, and many others ... To all the members of the Center for Arrhythmia Research I am thankful for their support and friendship, especially Guadalupe and Dani Ponce. The Department of Molecular and Integrative Physiology deserves special credit because the scientific, professional, and personal development opportunities offered to graduate students are difficult to find elsewhere. I appreciate the opportunity of going through graduate school in this great institution. Together with NIH who granted thousands of research dollars to Héctor, I want to acknowledge other funding sources that have paid the bills for my experiments and traveling endeavors, especially the American Heart Association, Rackham Graduate School and the MIP Graduate Education Fund. Also, the University of Costa Rica for continued support in Costa Rica.

I leave my family last — mom, dad, Liana, Demetrio, Isaac, Daniel, Luis Daniel, Felipe, Sofi and all others close to me — not because I've forgotten them, but because to them I owe the largest gratitude, and it is difficult to find words to express it. It is not easy to move thousands of miles away from home and settle in another country to follow a personal goal. The tremendous support from my family has been vital to continue following my dreams regardless of the tough circumstances. They have never stopped cheering for me and that gives me strength. To my dad, who passed away while I was away from home, I want to thank for always trying to understand what I do, asking me tough questions about life and science, providing me valuable advice, and giving me far more credit than I will ever deserve. ¡Gracias totales!

TABLE OF CONTENTS

DEDICATION	ii
ACKNOWLEDGEMENTS	iii
LIST OF TABLES	ix
LIST OF FIGURES	x
ABSTRACT	xiii
CHAPTER 1	
Background and Significance	
1.1. Introduction	1
1.2. Overview of Calcium Homeostasis in the Heart	2
1.3. Adrenergic Regulation of Calcium Homeostasis	4
1.4. Ryanodine Receptor Structure and Function	6
1.4.1. Structural Hierarchy	7
1.4.2. Macromolecular Complex Formation	8
1.4.3. Regulation by Phosphorylation	10
1.5. Ryanodine Receptor Dysfunction in Heart Disease	13
1.5.1. Catecholaminergic Polymorphic Ventricular Tachycardia	13
1.5.2. Heart Failure	16
1.5.3. Inherited Structural Cardiomyopathy	19

1.6. Scope of this Dissertation	23
1.7. Acknowledgements	26

CHAPTER 2

Ablation of RyR2-S2808 Phosphorylation Does Not Alter the Adrenergic Response or the Progression to Heart Failure in Mice

2.1. Introduction	32
2.2. Results	34
2.2.1. Direct Sequencing of Ryr2	34
2.2.2. Analysis of Cardiac Function and Structure After Myocardial Infarction	35
2.2.3. Expression and Phosphorylation of E-C Coupling Proteins	36
2.2.4. Cardiac Response to Adrenergic Stimulation	37
2.2.5. Cellular Ca ²⁺ Handling Kinetics	38
2.3. Discussion	38
2.4. Methods	45
2.5. Acknowledgements	50

CHAPTER 3

RyR2 Haploinsufficiency is Compensated by Fine-tuning Channel Activity Through Phosphorylation

3.1. Introduction	60
3.2. Results	63
3.2.1. Genetic Characterization of RyR2-KO Rabbits.	63
3.2.2. Assessment of RyR2 Expression and Phosphorylation	63

3.2.3. Cardiac Structure and Function	65
3.2.4. Expression of E-C Coupling Proteins	66
3.2.5. Assessment of RyR2 Activity	66
3.2.6. Association of RyR2 with Protein Phosphatases	67
3.2.7. Adrenergic Response of Isolated Hearts	68
3.2.9. Arrhythmia Susceptibility	71
3.3. Discussion	73
3.4. Methods	79
3.5. Acknowledgments	86

CHAPTER 4

A Novel RyR2 Mutation Associated with Hypertrophic Cardiomyopathy Induces Hypertrophy and Arrhythmia in Mice

4.1. Introduction	101
4.2. Results	103
4.2.1. Identification of RyR2-P1124L in a Human Patient	103
4.2.2. Localization of P1124L in the Three-dimensional Structure of RyR2	105
4.2.3. Molecular Phenotype of P1124L Channels	106
4.2.4. Spontaneous Ca ²⁺ Oscillations in HEK Cells Expressing RyR2	106
4.2.5. Single Channel Recordings	108
4.2.6. Cardiac Structure of Mice Harboring P1124L	109
4.2.7. Signaling Pathways Associated with Cardiac Hypertrophy	110
4.2.8. Arrhythmia Susceptibility of P1124L Mice.	111

4.2.9. Cellular Ca ²⁺ Handling in Ventricular Myocytes	113
4.3. Discussion	113
4.4. Methods	119
4.5. Acknowledgments	126
CHAPTER 5	
Conclusions and Perspectives	
5.1. Summary of Key Findings	149
5.2. Genetically-Engineered Rabbit Models to Study Cardiac Physiology	152
5.3. Mouse vs. Rabbit Cardiac Electrophysiology and Ca ²⁺ Handling	157
5.4. RyR2 Regulation by Phosphorylation	161
5.5. Clinical Significance of RyR2 Variants and Polymorphisms	165
5.6. RyR2-Associated Structural Cardiomyopathy	168
5.7. Future Directions	171
5.7.1. S2808A Mouse Models and the Never-Ending Controversy	171
5.7.2. The Three Phosphorylation Sites and Their Role in RyR2 Regulation	171
5.7.3. RyR2 distribution and Ca ²⁺ handling in RyR2-KO Rabbits	172
5.7.4. Chronic Response of RyR2-KO Rabbits to Stress	174
5.7.5. Hypertrophic Signaling Pathways Activated by P1124L	174
BIBLIOGRAPHY	180

LIST OF TABLES

Table 1.1. Characterized Phosphorylation Sites in RyR2	31
Table 2.1. Echocardiographic Parameters to Assess HF Progression in S2808A Mice	57
Table 2.2. Echocardiographic Parameters to Assess the Adrenergic Response in S2808A Mice	58
Table 2.3. Cardiac Function Parameters in Langendorff-perfused S2808A Hearts	59
Table 2.4. Ca ²⁺ Handling Parameters to Assess Adrenergic Response in isolated S2808A myocytes	59
Table 3.1. Echocardiographic Parameters to Assess Cardiac Structure and Function in RyR2-KO Rabbits	98
Table 3.2. Electrocardiographic Parameters in RyR2-KO Rabbits Undergoing Arrhythmia Challenge	99
Table 3.3. Cardiac Function Parameters in Langendorff-perfused RyR2-KO Hearts	100
Table 4.1. X-ray crystallography data collected and refinement statistics	145
Table 4.2. Echocardiographic Parameters in 8-month-old P1124L Mice	146
Table 4.3. Echocardiographic Parameters in 12-month-old P1124L Mice	147
Table 4.4. Ca ²⁺ Handling Parameters in Isolated P1124L Myocytes	148
Table 5.1. RyR2 Mutations Reported in both Clinical Cases and WES Studies	179

LIST OF FIGURES

Figure 1.1. Cardiac Excitation-Contraction Coupling	27
Figure 1.2. Ryanodine Receptor Structure and Domain Assignment	28
Figure 1.3. In vitro Phosphorylation of RyR2 by PKA and CaMKII	28
Figure 1.4. Cellular Mechanisms of CPVT	29
Figure 1.5. RyR2 Mutations Associated with CPVT	30
Figure 2.1. Experimental Model to Assess HF Progression in S2808A Mice	51
Figure 2.2. Direct Sequencing of the Region Ryr2 Containing S2808	52
Figure 2.3. Cardiac Function Post-MI in S2808A Mice	53
Figure 2.4. Tissue Remodeling post-MI in S2808A Mice	53
Figure 2.5. E-C Coupling Protein Expression and Phosphorylation in S2808A Hearts	54
Figure 2.6. Cardiac Response to Adrenergic Stimulation in S2808A Mice and Isolated Hearts	55
Figure 2.7. Ca ²⁺ Transients and SR Ca ²⁺ Load in S2808A Cardiomyocytes	56
Figure 3.1. Generation of the RyR2-KO Rabbit Model	87
Figure 3.2. RyR2 Sequence Alignment of the WT and KO Allele Products	88
Figure 3.3. RyR2 Expression and Phosphorylation in LV Samples	89
Figure 3.4. Cardiac Structure and Function In Vivo	90
Figure 3.5. Expression of E-C Coupling Proteins in LV Samples	91

Figure 3.6. Assessment of RyR2 Activity Using [³ H]Ryanodine Binding Assays	92
Figure 3.7. RyR2 Association with Protein Phosphatases in LV Samples	93
Figure 3.8. Cardiac Response to Adrenergic Stimulation in KO Rabbits	94
Figure 3.9. Representative Ca ²⁺ transient and SR load trace	95
Figure 3.10. Cellular Ca ²⁺ Handling in Rabbit Myocytes	95
Figure 3.11. Representative ECG Traces from Rabbits Undergoing Arrhythmia Challenge	96
Figure 3.12. Scheme of Functional Compensation in RyR2-KO Rabbits	97
Figure 4.1. Electrocardiogram Recordings from the Patient Harboring the P1124L Mutation	128
Figure 4.2. Location of P1124L in the Context of the RyR2 Mutation “Hotspots”	129
Figure 4.3. Amino Acid Sequence Alignment of RyR Isoforms from Various Species	129
Figure 4.4. Structure of the SPRY2 Domain at 1.44 Å resolution	130
Figure 4.5. Location of P1124L Within the SPRY2 Domain of RyR2	131
Figure 4.6. RyR2-P1124L Activity Measured with [³ H]Ryanodine Binding Assays	132
Figure 4.7. Abnormal Termination of Spontaneous Ca ²⁺ Release in HEK293 Cells Expressing RyR2	133
Figure 4.8. RyR2 Expression in Stable HEK Cells	134
Figure 4.9. Generation of the P1124L Mouse Model	135
Figure 4.10. Single RyR2 Recordings from Cardiac Microsomes	136
Figure 4.11. Cardiac Hypertrophy in 12-month-old P1124L Mice	137
Figure 4.12. RyR2 Expression and Phosphorylation in 12-month-old Mice	138
Figure 4.13. Expression of E-C Coupling Proteins in 12-month-old Mice	139

Figure 4.14. Ventricular Myocyte Size	140
Figure 4.15. Expression of Hypertrophic Genes in 12-month-old Mice	140
Figure 4.16. Hypertrophic Signaling Pathways	141
Figure 4.17. Susceptibility to Ventricular Arrhythmia in P1124L Mice Challenged with Epinephrine/Caffeine	142
Figure 4.18. Ca ²⁺ Transients and SR Load	143
Figure 4.19. Susceptibility to Spontaneous Ca ²⁺ Release in Ventricular Myocytes	144
Figure 5.1. Overview of Cardiac Physiology in Mouse, Rabbit, and Human	175
Figure 5.2. Comparison of Cardiac Function between Mouse and Rabbit	176
Figure 5.3. Comparison of Ca ²⁺ Transients and Action Potentials in Ventricular Myocytes from Mouse and Rabbit	177
Figure 5.4. RyR2 Regulation by Phosphorylation	178

ABSTRACT

The Ryanodine Receptor type 2 (RyR2) the major calcium-release channel in the heart, where it is fundamental for excitation-contraction coupling, the process transducing electrical signals into mechanical contraction. The role of RyR2 dysfunction as a trigger of cardiac arrhythmia due to inherited mutations is firmly established, but the fundamental mechanisms of RyR2 regulation in normal cardiac physiology, and dysregulation in other forms of inherited and acquired heart disease remain partially understood. In this dissertation, we took advantage of three novel genetically-engineered animal models with mutations in RyR2 to better understand of the role of this ion channel in the healthy and diseased heart.

First, we derived a congenic mouse line with ablation of the S2808 phosphorylation to revisit the hypothesis that this site is critical for RyR2 regulation, and sort out one of the differences between two mouse models generated by different laboratories that have fueled a long-standing controversy: the genetic background. Consistent with previous studies performed in Sv129/C57Bl6 mice, our data demonstrate that S2808A mice in the C57Bl/6 background behave like WT when subjected to acute and chronic stress. These data support the idea that S2808 phosphorylation is unlikely fundamental for RyR2 regulation during the normal adrenergic response or heart failure progression. Furthermore, they suggest that the genetic background may not be the cause for the opposing results obtained with S2808A mice from different laboratories.

Second, we used a novel RyR2 knock-out rabbit model to elucidate the effects of decreased RyR2 expression on cardiac function and the possible underlying compensatory mechanisms. We show that homozygous knock-out of RyR2 is lethal, while heterozygous knock-out decreases RyR2 expression by 60% without producing an abnormal phenotype. Our data indicate that RyR2 deficiency is likely compensated by upregulation of channel function by decreasing the phosphorylation of S2031. Hence, RyR2 function is likely backed by a protein reserve, and channel deficiency is readily compensated. Nonetheless, during acute adrenergic stimulation the contraction velocity and calcium release are slower in cardiomyocytes from mutant animals, suggesting that a 40% RyR2 level may be insufficient to maintain calcium release flux during acute stress. These results give additional significance to phosphorylation of S2031, a site often ignored in the regulatory scheme of RyR2.

Third, we performed a multi-level characterization of the novel mutation P1124L, identified in a patient with hypertrophic cardiomyopathy. Since this is one of a handful of RyR2 mutations associated with structural remodeling of the heart, its study may uncover novel pathogenic mechanisms of RyR2 dysregulation. We show that P1124L induces conformational changes in the SPRY2 domain of RyR2, affecting the sensitivity of the channel to cytosolic and luminal calcium. In a mouse model, P1124L produces cardiac hypertrophy and increases the susceptibility to arrhythmia. While we have yet to fully elucidate the underlying pathogenic mechanisms, these studies suggest that specific RyR2 mutations may cause cardiac hypertrophy while at the same inducing arrhythmias that are typical of previously-described mutations.

These three stories share a common aim: to obtain a better understanding of RyR2 regulation in cardiac pathophysiology. From the regulatory role of phosphorylation to the clinical relevance of mutations in the RYR2 gene and the underlying pathogenic mechanisms, each model addressed in this dissertation provides novel insights into the role of RyR2 as an essential player in excitation-contraction coupling, and the possible culprit of severe cardiac disease.

CHAPTER 1

Background and Significance

1.1. Introduction

Calcium (Ca^{2+}) is the most ubiquitous and versatile signaling molecule in living organisms. In the heart, Ca^{2+} plays a remarkable dual role, serving as both signaling molecule for gene transcription and triggering signal for contraction. Hence, the cardiac regulation of intracellular $[\text{Ca}^{2+}]$ ($[\text{Ca}^{2+}]_i$) is a particularly complex process that follows an exquisitely orchestrated sequence of events, ultimately allowing cardiac myocytes to differentiate the global, rapid and cyclic $[\text{Ca}^{2+}]_i$ oscillations required for contraction — excitation-contraction (e-c) coupling — from the localized, subcellular and typically long-term changes in $[\text{Ca}^{2+}]_i$ that regulate gene transcription. Indeed, there is a ~20,000-fold transmembrane $[\text{Ca}^{2+}]$ gradient that is essential for endowing Ca^{2+} with such versatility.

During the last two decades, hundreds of mutations in Ca^{2+} handling proteins have been linked to inherited cardiac disorders, offering genetic evidence that dysregulation of Ca^{2+} homeostasis has profound pathological relevance. The inherited phenotype most associated with cardiac Ca^{2+} dysregulation is an electrical disturbance (arrhythmia); catecholaminergic polymorphic ventricular tachycardia (CPVT) is the quintessential manifestation of arrhythmogenic Ca^{2+} disorders of the heart. Nevertheless, as genetic testing becomes more widespread in the clinic and gene panels are extended, new

evidence suggests that cardiac Ca^{2+} dysregulation accounts for more than arrhythmia and may lead to structural cardiomyopathy and more complex phenotypes as well.

The cardiac Ryanodine Receptor (RyR2), the subject of this dissertation, is one of the most relevant Ca^{2+} handling proteins because it conducts most of the Ca^{2+} required for heart contraction. Numerous studies have associated RyR2 dysfunction with heart failure progression, arrhythmia and, more recently, with structural remodeling of the cardiac muscle. This chapter reviews the relevant literature in the field and provides a framework for the latter chapters, which address specific questions about RyR2 regulation and function in health and disease.

1.2. Overview of Calcium Homeostasis in the Heart

While studying the effect of inorganic salts on several tissues in the late 19th century, physiologist Sidney Ringer realized that Ca^{2+} is an essential ion for cardiac contraction. Working with isolated heart preparations, he noticed that removing Ca^{2+} from his buffers stopped hearts from beating, while adding it back restored and maintained their contractility.¹ At the time, Ringer almost certainly was unaware that extracellular Ca^{2+} only accounts for a small fraction of the Ca^{2+} needed for the heart to contract. Every action potential (AP) in a cardiac myocyte is accompanied by a transient elevation of the free $[\text{Ca}^{2+}]_i$ from approximately 100 nM during diastole to nearly 1 μM during systole in order to activate the myofilaments and produce contraction.² This series of events, through which membrane depolarization is converted to mechanical contraction, is termed excitation-contraction (e-c) coupling (Figure 1.1). In adult cardiomyocytes, the amount of extracellular Ca^{2+} entering the cell during an action potential is insufficient to elicit a full contraction. Instead, most of the Ca^{2+} required for contraction (approximately 70% in

humans and 90% in mice) flows out of the sarcoplasmic reticulum (SR),³ an intracellular Ca^{2+} store, through the amplifying mechanism of Ca^{2+} -induced Ca^{2+} release (CICR).⁴

The e-c coupling in cardiac muscle mechanism begins during the AP, when a relatively small inward Ca^{2+} current (I_{CaL}) from L-type Ca^{2+} channels (LTCCs) activates RyR2 channels, which in turn release more Ca^{2+} from the SR. Hence, RyR2 acts as both an intracellular Ca^{2+} sensor and a Ca^{2+} channel, amplifying a small Ca^{2+} signal and potentially turning CICR into a self-sustaining, regenerative process. However, CICR reliably stops in intact, healthy cardiomyocytes, and relaxation ensues once Ca^{2+} is removed from the cytosol. Several mechanisms have been proposed to terminate CICR: stochastic attrition, which implies that all LTCC and RyR2 channels within a specific region shut down simultaneously;² RyR2 adaptation, which suggests that channels are unable to reopen until they recover due to a decrease in their responsiveness to sustained increases of $[\text{Ca}^{2+}]$;⁵⁻⁷ and local depletion of the SR, in which release termination occurs when the regions of the SR store reach a critical minimum threshold that closes local RyR2s.⁸ None of these mechanisms have been demonstrated to work independently; therefore, it is reasonable to assume that, under normal circumstances, a combination of the three are likely to work in concert to terminate CICR.⁹

Following release termination, two main molecular players contribute to cytosolic Ca^{2+} removal: the sarco/endoplasmic reticulum Ca^{2+} -ATPase (SERCA2a) refills the SR, while the $\text{Na}^+/\text{Ca}^{2+}$ exchanger (NCX) extrudes Ca^{2+} from the cell. To maintain Ca^{2+} equilibrium during repetitive contractions, Ca^{2+} that enters the cell through LTCC must be extruded by the NCX, while the Ca^{2+} released by RyR2 must return to the SR. A smaller proportion of Ca^{2+} removal (less than 2% in rabbit myocytes) is performed by slow

mechanisms such as the sarcolemmal Ca^{2+} ATPase (PMCA) and the mitochondrial Ca^{2+} uniporter.³ NCX is an electrogenic transporter, which transports three Na^+ ions in one direction while carrying a single Ca^{2+} ion in the opposite direction; hence, the extrusion of Ca^{2+} via NCX creates an inward depolarizing current that becomes more evident in the late phases of the AP.

CICR takes place at specialized regions of the cell where the external membrane is near the SR, mostly within the T-tubule (TT) network of the myocyte. In these tightly spaced microdomains, clusters of ~20 LTCCs provide the activating Ca^{2+} signal for ~100 RyR2s, forming a Ca^{2+} release unit (CRU).³ Any Ca^{2+} release event originating from a single CRU is referred to as a Ca^{2+} spark, while the global cytosolic Ca^{2+} transient results from the temporal and spatial summation of Ca^{2+} sparks coordinated during e-c coupling by the AP and I_{CaL} .¹⁰ Isolated Ca^{2+} sparks during diastole are normal and most likely originate from activation of a single CRU through stochastic openings of RyR2 channel or LTCC.¹¹ However, diastolic propagation of Ca^{2+} sparks through the cell as Ca^{2+} waves and synchronization of spontaneous sparks into diastolic Ca^{2+} transients are often observed in pathologic conditions.

1.3. Adrenergic Regulation of Calcium Homeostasis

The sympathetic branch of the autonomous nervous system increases the dynamic output of the heart in response to increased metabolic demand of the organism. Indeed, this system provides an essential component of the cardiac fight-or-flight response through activation of β_1 -adrenergic receptors (β_1 -AR) by catecholamines: for example, heart rate increases due to direct effect on the sinus node (positive chronotropic effect), while the contractility and rate of relaxation increase due to a direct effect on

ventricular myocytes (positive inotropic and lusitropic effect, respectively), among others. Although the role of Ca^{2+} signaling in sinus node automaticity is still emerging,¹² its importance for modulating inotropy (cardiac muscle contractility) and lusitropy (rate of cardiac muscle relaxation) has long been established.² Canonical β_1 -AR signaling in the heart involves activation of adenylyl cyclase (AC), which converts adenosine triphosphate (ATP) into cyclic adenosine monophosphate (cAMP). cAMP stimulates protein kinase A (PKA) activation, which in turn phosphorylates at least three key players of e-c coupling: LTCC, enhancing peak I_{CaL} and promoting increased SR Ca^{2+} content; phospholamban (PLB) at S16, relieving its partial inhibition on SERCA2a and thus accelerating SR refilling; and cardiac troponin I (cTnI), decreasing the Ca^{2+} affinity of the myofilaments and accelerating cross-bridge detachment. These effects result in larger and faster Ca^{2+} transients, hence increasing contractile force and allowing faster relaxation. PKA also phosphorylates RyR2 in at least two sites (S2031 and S2808, human nomenclature), but the physiological role of these modifications is still unclear.^{13,14}

Non-canonical β_1 -AR signaling, on the other hand, requires the exchange protein directly activated by cAMP 2 (Epac2) to activate the Ca^{2+} /calmodulin-dependent kinase II (CaMKII) through an unknown mechanism.^{15,16} CaMKII, which is also independently activated during adrenergic stimulation by the increased Ca^{2+} cycling, phosphorylates many of the same protein targets of PKA, including LTCC, PLB (at T17) and RyR2 (at S2808 and S2814); yet, chronic activation of CaMKII is considered more deleterious.¹⁷ A key difference is that CaMKII increases SR Ca^{2+} leak — as observed in heart failure — perhaps by phosphorylating RyR2-S2814, while the role of PKA in SR Ca^{2+} leak is a matter of intense debate.¹⁸⁻²⁰ Whatever the downstream signaling pathways and

regardless of the specific controversies, it is sufficiently clear that adrenergic signaling in the heart boosts Ca^{2+} cycling by directly affecting e-c coupling machinery at all levels: sarcolemma, SR, and myofilaments.

1.4. Ryanodine Receptor Structure and Function

The Ca^{2+} -release channel/Ryanodine Receptor (RyR) is the largest ion channel known in nature. It derives its name from the alkaloid ryanodine, found in the plant *Ryania speciosa*,²¹ a high-affinity ligand that binds to the open state of the channel and locks it in a sub-conductance state.²² Ryanodine was fundamental for the initial purification and characterization of the channel, hence the name.^{23,24} Four identical subunits, each containing nearly 5000 amino acids and a combined molecular mass >2 million Da, form a functional channel (Figure 1.2). There are three mammalian isoforms, each encoded by a different gene contained in a different chromosome, that share ~65% sequence identity: RyR1 is predominantly expressed in skeletal muscle, RyR2 is the cardiac isoform, and RyR3, the least known of the three isoforms, is expressed in several tissues including the brain.²⁵ RyRs are expressed in several other tissues, including vascular smooth muscle and regions of the brain; however, the best-studied function of RyR is in e-c coupling in skeletal (RyR1) and cardiac (RyR2) muscle. It should be noted that RyR2 is commonly referred to as the “cardiac isoform,” which is true (it is the only isoform expressed in the heart) but misleading, since RyR2 is also the major isoform expressed in the brain.²⁶ The 35% sequence difference between RyR1 and RyR2 accounts for dramatic differences in e-c coupling mechanism,²⁵ sensitivity to Ca^{2+} ,²⁷ and regulation by native partners²⁸ and exogenous agents.²⁷

RyR2 is well-conserved among species. The human RyR2 (hRyR2), for example, shares 97% sequence identity with the mouse RyR2 (mRyR2; the primary model organism used in the field), 99% with the rabbit RyR2 (rRyR2; a larger mammalian model commonly used in heart failure studies), and >99% with the porcine RyR2 (pRyR2; the species used for the most recent structural studies described below). In this introductory chapter and in the concluding remarks in CHAPTER 5 hRyR2 nomenclature will be used unless specifically stated otherwise. In the chapters discussing experimental models, the nomenclature of the species under study will be used: mRyR in CHAPTER 2 and CHAPTER 4; rRyR2 in CHAPTER 3. Please note that in the following sections “RyR” will be used as a collective reference to the three isoforms whenever such generalization is necessary.

1.4.1. Structural Hierarchy

Elucidating the molecular architecture of RyR has been difficult, in part because its colossal size makes the channel nearly impossible to crystallize. The most informative approach for studying the molecular structure of the channel is cryo-electron microscopy (cryo-EM), which initially yielded maps of RyR1 with overall resolution of up to 9.6 Å.²⁹ Later, discrete domains were crystallized, solved at resolutions below 2 Å,³⁰⁻³² and docked into previous cryo-EM maps, providing a general idea of protein architecture, as well as domain arrangement and interaction. The size hurdle was partially overcome using a combination of enhanced computer power, clever purification steps and improved detector, when three laboratories published the highest-resolution cryo-EM structures of RyR1 available to date at a maximum average resolution of 3.8 Å.³³⁻³⁵ More recently, Peng et al. elucidated the structure of the closed and open RyR2 at 4.1 Å and 4.2 Å,

respectively.³⁶ des Georges et al. went even further, obtaining ~4 Å maps of RyR1 in various states, including structures with Ca²⁺, ATP, caffeine, and ryanodine bound to the channel.³⁷

Remarkably, both RyR1 and RyR2 share a similar structural hierarchy (Figure 1.2), which includes: 1) a central tower forming the core of the protein and including, from top to bottom, N-terminal domain (NTD), and central (CD) and pore-forming (PFD) domains on the C-terminus end; 2) a corona, which tops the central tower and is formed by two helical domains (HD1 and HD2) and the handle domain; and 3) a peripheral region, composed of five smaller domains (SPRY1-3, P1-2). Even with these high-resolution maps, docking known crystal structures of individual domains in cryo-EM structures remains problematic, particularly in the periphery of the channel where the resolution of the cryo-EM maps is poor. However, the central tower has the highest level of detail. Opening of the channel involves an intricate reorganization of specific motifs within the central tower, in which the NTD and CD act as scaffolds that integrate and transmit signals to the PFD. The PFD is made by 6 transmembrane segments per subunit, and the S6 helix forms the Ca²⁺-conducting pore. Furthermore, the C-terminal end of the protein, located after the cytosolic extension S6, docks in a pocket of the CD, forming an “activation module” where Ca²⁺, ATP, and caffeine bind to RyR.³⁷ Finally, each subunit has an S1-S2 luminal loop^{33,34,37} that might serve as an interaction site for other SR proteins such as triadin, junctin, and calsequestrin.

1.4.2. Macromolecular Complex Formation

The bulk of RyR2 is localized in the cytoplasm, and spans most of the gap between the SR and the TT membrane. This large cytosolic shell contains anchoring points for a

variety of proteins that serve as accessory regulators of the channel. Many of these proteins bind to RyR2 permanently, while others do so in a Ca^{2+} -dependent manner.³⁸ Hence, some authors have called RyR2 channels “allosteric giants”,³⁹ not only because of their colossal size, but because of their role as scaffolds of a macromolecular complex. Some components of this complex include calmodulin (CaM), two FK506-binding proteins (FKBP12 and FKBP12.6) and the soluble resistance-related Ca^{2+} binding protein (sorcin). These three RyR2 partners are briefly discussed below, but RyR2 also binds to PKA, protein phosphatases 1 (PP1) and 2A (PP2A), phosphodiesterase 4D3 and CaMKII.⁴⁰ Certainly, this suggests that regulation of RyR2 by phosphorylation is important, but this claim requires further examination.

CaM is a 149-amino acid, 16.7 kDa Ca^{2+} -binding protein ubiquitously expressed from three different genes (*CALM1*, *CALM2* and *CALM3*) encoding for the same protein product, is the best-known partner of RyR2. The importance of CaM in regulating numerous cellular functions is highlighted by this apparent genetic redundancy. Each terminus of the protein forms a globular domain that contains two Ca^{2+} -binding sites, and these regions are joined by a flexible linker that allows conformational changes upon binding of Ca^{2+} .⁴¹ CaM, in its Ca^{2+} -bound or Ca^{2+} -free forms, directly interacts with RyR2. At high [Ca^{2+}] Ca^{2+} -CaM decreases the open probability of RyR2.⁴² Interestingly, mice expressing RyR2 channels unable to bind CaM develop severe cardiac hypertrophy and die perinatally.⁴³

FKBP12 and FKBP12.6 are two immunophilins named after their molecular weight that bind to RyR with high affinity. The recent cryo-EM studies took advantage of this interaction to purify the channels.^{33,34,36,37} Interestingly, the FKBP12-RyR1 interaction is

maintained throughout the purification steps and both appear in the cryo-EM micrographs.³³ RyR2, on the other hand, dissociates from FKBP12 during the purification (Figure 1.2).³⁶ In the heart, the expression of FKBP12 is higher than that of FKBP12.6, but the latter has much higher affinity for RyR2.⁴⁴ Hence, RyR2 channels bind both isoforms, but Guo et al. determined that only 10–20% of RyR2 channels contain FKBP12.6, while all FKBP12.6 is bound to RyR2. FKBP12.6 is thought to stabilize the closed state of RyR2, thus some refer to it as Ca²⁺-channel-stabilizing protein 2 (calstabin 2). Nevertheless, the physiological role of this interaction is widely disputed.

Finally, sorcin is a 21.6 kDa Ca²⁺-binding protein expressed in several tissues. In the heart, sorcin is thought to modulate Ca²⁺ by directly interacting with several e-c coupling targets,^{45,46} including RyR2,⁴⁷ SERCA2a,⁴⁸ and NCX.^{49,50} The specific role of sorcin in regulating cardiac function and in the development of heart disease is currently under investigation in our laboratory.

1.4.3. Regulation by Phosphorylation

hRyR2 contains 353 serine and 222 threonine residues, many of which are susceptible to phosphorylation based on computational analysis of consensus sequences.⁵¹ Experimentally, however, only three phosphorylation sites have been identified (S2031, S2808, and S2814), which are phosphorylated by two kinases (PKA and CaMKII).

S2808 was the first site to come under scrutiny after Witcher et al.⁵² identified it as a CaMKII-dependent phosphorylation site in 1991. More than 10 years later, the Marks laboratory published a series of elegant studies in which S2808 was relabeled as a PKA-dependent phosphorylation site^{53,54} essential for the adrenergic response of the heart^{55,56}

and critically involved in heart failure (HF) progression.^{53,54} This site has a high level of basal phosphorylation^{20,57} and is phosphorylated *in vitro* by both CaMKII and PKA (Figure 1.3, Table 1.1). According to Marks' hypothesis, S2808 phosphorylation increases further in ischemic HF, causing the channel to be unstable or "leaky". However, several studies from many laboratories have challenged these conclusions (reviewed in refs. 14,19,58). This phospho-site will be discussed in more detail in CHAPTER 2.

S2814 was identified by Wehrens et al. in 2004 as a CaMKII-dependent phosphorylation site.⁵⁹ Respress et al.⁶⁰ later implicated this site in the pathogenesis of non-ischemic HF where the phosphorylation level is significantly increased. Thus, genetic ablation of this site by substituting serine with the non-phosphorylatable residue alanine (S2814A) resulted in relative protection against the deleterious effects of transverse aortic constriction — but not myocardial infarction — in mice. In this context, phosphorylation of S2814 by CaMKII results in hyperactive or "leaky" RyR2 channels. Like S2808, this site is highly phosphorylated in the absence of adrenergic stimulation.^{57,58} However, S2814 is only phosphorylated *in vitro* by CaMKII (Figure 1.3, Table 1.1).

Finally, in 2005 Xiao et al. introduced S2031 as an exclusive PKA site,⁶¹ despite being part of a CaMKII consensus sequence.⁵¹ Remarkably, it can be phosphorylated *in vitro* by activation of endogenous CaMKII (Figure 1.3); however, this is not the case in HEK293 cells transfected with RyR2 and CaMKII.⁶¹ S2031 has not been studied to the same extent as the previous two phosphorylation sites. Unlike S2814, basal phosphorylation of S2031 is low but detectable.⁵⁷ It also is readily phosphorylated by PKA *in vitro*^{57,61,62} and *ex vivo*.¹³ Mice with genetic ablation of the S2031 site (S2030A, as per mouse nomenclature; developed in our laboratory) show cardiac hypertrophy, suggesting

that, despite the low basal phosphorylation, S2031 has an important regulatory role at least in rodents. This site will be discussed in more detail in CHAPTER 3.

Despite the solid experimental evidence suggesting that RyR2 is phosphorylated downstream of β_1 -AR activation,¹³ it is unclear whether RyR2 phosphorylation is *required* for the adrenergic response.⁵⁸ So far, the description of the three known phosphorylation sites suggests that phosphorylation of RyR2 results in increased channel activity. By removing SR load and I_{CaL} regulation by β_1 -AR activation, Ginsburg and Bers⁶³ elegantly demonstrated that RyR2 phosphorylation may be involved in speeding up Ca^{2+} release, while SR load and I_{CaL} mediate the actual increase in the amount Ca^{2+} release. Furthermore, Valdivia et al. showed that single channels phosphorylated by PKA respond with higher open probabilities (P_O) upon rapid exposure to increased $[Ca^{2+}]$.⁷ However, they rapidly undergo adaptation and stabilize at a *lower* P_O than non-phosphorylated channels.⁶⁴ Remarkably, three expected functional outcomes of phosphorylation have been reported for channel activity: increase,^{52,54} decrease,^{65,66} and no effect.⁶⁷ Many of these studies have looked at the overall phosphorylation state of the channel rather than focusing on a single phosphorylation site. From the size of the channel, and the multitude of phosphorylation sites, it is apparent that interpretation of these data is difficult, as phosphorylation sites may work in concert rather than independently to modulate RyR2 function.

Using ^{32}P incorporation assays, Takasago et al.⁶⁸ showed that RyR2 can be phosphorylated *in vitro* by CaMKII, PKA, and protein kinases C and G (PKC and PKG, respectively). Furthermore, CaMKII-dependent incorporation of ^{32}P was ~ 4 times greater than that of PKA, suggesting the presence of at least 4 CaMKII phosphorylation sites for

each PKA site. These data indicate that at least 6 more CaMKII sites remain to be discovered. Finally, it is important to mention that other post-translational modifications of RyR2 have been reported to influence channel function, even synergistically with phosphorylation.⁵⁵

1.5. Ryanodine Receptor Dysfunction in Heart Disease

Congenital mutations and acquired post-translational modifications of several Ca²⁺ handling proteins may lead to cardiac arrhythmia and heart failure. Here our discussion will be focused on catecholaminergic polymorphic ventricular tachycardia, heart failure, and inherited structural cardiomyopathies

1.5.1. Catecholaminergic Polymorphic Ventricular Tachycardia

CPVT is a severe inherited syndrome characterized by ventricular tachyarrhythmias triggered by physical or emotional stress in the absence of structural disease or changes in the resting electrocardiogram.⁶⁹⁻⁷¹ Patients often develop bidirectional tachycardia, potentially leading to ventricular fibrillation and sudden cardiac death; however, idiopathic ventricular fibrillation has also been observed.⁷² Mutations in four genes are currently implicated in the pathogenesis of CPVT, resulting in four CPVT types: ryanodine receptor 2 (*RYR2*, CPVT1),⁷³ calsequestrin 2 (*CASQ2*, CPVT2),⁷⁴ triadin (*TRDN*, CPVT3),^{75,76} and calmodulin (*CALM*, CPVT4).⁷⁷

CPVT is a disorder that may be entirely attributed to altered intracellular Ca²⁺ cycling. The most accepted mechanism for the onset of arrhythmia involves spontaneous release of Ca²⁺ from the SR during diastole in myocytes harboring RyR2 channels destabilized by mutations in the channel protein itself or in the ancillary proteins of RyR2.³⁸ As discussed above, NCX is the fastest and largest pathway for Ca²⁺ extrusion

from the cell, and is also an electrogenic transporter. Thus, if the spontaneous Ca^{2+} release is synchronized and of sufficient critical mass, the resulting inward NCX current can drive the membrane potential to threshold and trigger an extemporaneous action potential known as a delayed after depolarization (DAD; Figure 1.4 **B,D**). Further repetition of this cycle and spontaneous synchronization of DADs occurring in a large group of myocytes may lead to ventricular arrhythmias,¹¹ which become polymorphic as sites of ectopic electrical activity appear in different regions of the heart.⁷⁸ Recent evidence suggests that arrhythmogenic focal activity may be more prominent in Purkinje cells where the subcellular structure, limited inter-cellular connections, and low electrotonicity favor the generation and propagation of DADs.^{79,80}

More than 200 different mutations in *RYR2* have been identified in patients with CPVT1 (this number is steadily increasing); however, only a handful have been fully characterized. Historically, three regions of RyR2 are considered canonical clusters of CPVT1 mutations. These regions — CPVT-I (residues 77–466), CPVT-II (residues 2246–2534), and CPVT-III (residues 3778–4967) — are arbitrarily defined based on mutation frequency, location of putative regulatory regions, and overlap with mutation sites in RyR1 associated with skeletal muscle diseases;⁸¹ furthermore, CPVT1 clusters are often depicted in a linear representation of an RyR2 subunit (see figure 2 in ref. 81), oversimplifying the complex three-dimensional structure of the protein. With the recent high resolution cryo-EM maps, it is possible to limit these sections to four specific structural domains (Figure 1.5 **C**); of the mutation sites, 17% are localized in the NTD (residues 1–642, CPVT-I), ~21% occur within HD1 (residues 2110–2678, CPVT-II), and ~55% are located in the CD (residues 3612–4206, ~27%), the PFD (residues 4485–4967,

~25%), corresponding to CPVT-III and CPVT-IV, respectively. Intriguingly, only ~7% of the mutations fall in the peripheral domains (residues 643–2109 and 2679–3611), located outside the canonical CPVT regions, while the clear majority falls within the central tower of the channel (Figure 1.5 **B**). If genetic mutations are equally likely to arise anywhere in *RYR2*, those occurring in the peripheral domains are either more deleterious (or perhaps lethal) or they are innocuous compared to those within the canonical sites, and thus do not appear in the clinical spectrum. However, over 1000 variants scattered all over *RYR2* (background genetic testing noise) are present in whole-exome sequencing studies (WES) of the general population,^{82,83} and some disease-causing mutations may appear in these studies with low frequency.

The specific molecular mechanism(s) by which RyR2 mutations produce arrhythmia is still unclear. To date, three specific hypotheses have been proposed to explain arrhythmogenesis due to RyR2 mutations that cause CPVT: defective inter-domain interaction,⁸⁴ enhanced dissociation of FKBP12.6,^{85,86} increased sensitivity to activation by luminal⁶⁹ and cytosolic Ca^{2+} ,⁸⁷ or a combination thereof. The molecular heterogeneity associated with RyR2 mutations has become more evident in studies of novel mutations; two examples in the literature provide solid experimental evidence. V2475F produces at least three molecular defects that contribute to pathogenicity: increased sensitivity to *cytosolic* Ca^{2+} , increased sensitivity to *luminal* Ca^{2+} , and altered PKA phosphorylation.⁸⁷ The relative contribution of each molecular defect to arrhythmogenesis was not assessed independently. A4860G is, perhaps, a more evident example of mechanistic heterogeneity because it is not activated by neither luminal⁸⁸ nor cytosolic⁸⁹ Ca^{2+} ; thus, it is a loss-of-function mutation. In this case, the lack of luminal and

cytosolic activation of A4860G channels promotes SR overload. Eventually, SR overload, I_{CaL} , and other sympathetically-induced activating factors converge to produce a burst of Ca^{2+} that prolongs the AP due to enhanced activation of NCX (Figure 1.4 **C,E**). The latter may lead to reactivation of other depolarizing currents, EADs, focal ectopic activity, and ultimately ventricular fibrillation.

As more RyR2 mutations undergo molecular scrutiny, the variety of arrhythmia mechanisms will undoubtedly increase. Due to the staggering number of possible functional alterations, it remains to be seen whether it will be possible to predict the dominant molecular defects leading to arrhythmia based upon the location of the mutation in the overall structure of RyR2. This remains challenging, but doing so would enable therapies to be tailored for CPVT1 according to the RyR2 domain affected. Confounding this goal is the fact that the overall clinical phenotype of CPVT1 is shared by most RyR2 mutations, regardless of the underlying molecular phenotype.

1.5.2. Heart Failure

HF is the advanced and typically progressive manifestation of other underlying conditions that deteriorate cardiac function, such as myocardial infarction or cardiomyopathy, making the heart unable to meet the metabolic demands of the organism.⁹⁰ As such, the clinical definition and diagnosis of HF are complex, and the structural, functional, and electrophysiological remodeling occurring in failing hearts is intricate and likely dependent on the underlying etiology. Hence, not all studies agree on whether specific changes in protein expression or function are relevant for HF.^{91,92} Nevertheless, Ca^{2+} mishandling is a common finding in failing hearts, and involves dysfunction of the e-c coupling apparatus.^{93,94} Cardiac myocytes from failing hearts have

prolonged action potentials, decreased SR Ca^{2+} content and decreased Ca^{2+} release.⁹⁵ Furthermore, the contribution of NCX to cytosolic Ca^{2+} removal is increased compared to that of non-failing cardiac myocytes,⁹⁵ while the activity and expression of SERCA2a are decreased.⁹⁶ Hence, the higher NCX and lower SERCA2a synergize to decrease the SR content, lower Ca^{2+} release and, ultimately, produce contractile dysfunction and weak failing hearts.

Patients with HF are also more susceptible to develop cardiac arrhythmia. Pogwizd et al. showed, using a rabbit model of non-ischemic HF, that arrhythmogenesis is enhanced by increased activity of NCX, reduced I_{K1} — the current determining the resting membrane potential — and residual responsiveness to β -AR stimulation.⁹⁷ Also, failing myocytes show increased SR Ca^{2+} leak mediated by RyR2, as shown by Shannon et al.⁹⁸ Therefore, the cellular mechanisms for cardiac arrhythmias in HF are similar to those of CPVT: β_1 -AR activation promotes increased SR Ca^{2+} content — as in normal conditions — which leads to enhanced spontaneous Ca^{2+} release (SCR) during diastole in failing hearts due to “leaky” RyR2 channels. When this extemporaneous Ca^{2+} is extruded by NCX, the cell membrane depolarizes possibly triggering DADs. Moreover, since I_{K1} is lower, any given amount of Ca^{2+} extruded by NCX will have a larger depolarizing effect on the membrane potential than in healthy hearts.

One area of controversy in the field of HF is regarding the role of RyR2 on the pathophysiology of the syndrome. Several studies have noticed variability in the expression and function of RyR2 in human and animal HF.^{3,92,99,100} Zhang et al., for example, did not detect a change in RyR2 expression in mice four weeks after myocardial infarction,¹⁰¹ while we observed an evident tendency toward decreased expression using

the same approach (Figure 2.5).¹⁰² Hence, the study of the effect of RyR2 expression on cardiac function has generated sparse interest in the field. But regardless of protein expression level, the most contentious issue is the phosphorylation of the channel. In a seminal study, Marx et al. showed that in human failing hearts, PKA-mediated “hyperphosphorylation” of RyR2 is increased, prompting the dissociation of FKBP12.6 from the macromolecular complex.⁵⁴ In single channels, phosphorylation of RyR2 by PKA produced sub-conductance states — partial conductance because of incomplete closing of the channel — that make the channels “leaky”⁵⁴ and might account for the increased escape of Ca^{2+} from the SR as measured by Shannon et al.⁹⁸ Later, the same laboratory showed that this is mediated exclusively by PKA phosphorylation of S2808.⁵³ Thus, S2808A mice were partially protected against HF in a model of ischemic HF — i.e. after myocardial infarction. As discussed in previous sections, this is controversial for many reasons including the already high basal phosphorylation level of S2808. The lack of confirmatory studies from independent investigators of key aspects of this hypothesis is, perhaps, the strongest argument against it.^{19,51,103} However, the low abundance of FKBP12.6 — only enough to occupy a small fraction of the total RyR2 content of a myocyte — and the RyR2-FKBP12.6 binding affinity and kinetics^{19,104} are also important aspects to consider.

The more recent study suggesting that S2814 phosphorylation by CaMKII is the underlying cause of SR Ca^{2+} leak in HF seems to hold better against scrutiny.⁶⁰ With the exception of FKBP12.6 dissociation from RyR2 and the appearance of sub-conductance states, the general idea is the same as described above: RyR2 gets “hyperphosphorylated” by a different kinase at a different phosphorylation site and the channels

become “leaky.” The caveat is that in the authors’ scheme, S2814 is only relevant in non-ischemic HF, while S2808 is relevant only in ischemic HF. This idea, however, is difficult to reconcile with both phosphorylation sites located within the same domain of RyR2. Nonetheless, the experimental evidence in support of the pathogenic role of S2814 phosphorylation in HF and other forms of heart disease continues to grow. Ultimately, the existence of Ca²⁺ mishandling in HF is well-documented, and elucidating the role of RyR2 will require further investigation.

1.5.3. Inherited Structural Cardiomyopathy

Structural cardiomyopathies are a complex and heterogeneous group of heart diseases that involve mechanical dysfunction of the heart, often from genetic etiology, and display ventricular hypertrophy or dilation.^{105,106} Among them, hypertrophic cardiomyopathy (HCM) is the most common congenital cardiac disease, affecting one in every 500 individuals.^{107,108} HCM is considered to be a sarcomeric disease because the vast majority of patients with a positive genetic diagnosis carry a mutation in the genes encoding myosin-binding protein C (*MYBPC3*), β -myosin heavy chain (*MYH7*), or another component of the myofilaments.¹⁰⁹ Nonetheless, approximately half of the patients undergoing genetic testing are negative for mutations in the HCM panel, which screens ~15 associated genes.¹⁰⁹ These are considered idiopathic cases; however, mutations in several other genes have been recently identified in HCM patients, including those encoding Ca²⁺ handling proteins such as PLB, CASQ2, junctophilin 2, sorcin, and RyR2.¹¹⁰ It is noteworthy that at least two of these proteins are also involved in CPVT.

The first direct evidence suggesting that RyR2 mutations can lead to structural cardiomyopathy came from a series of studies by the Meissner laboratory, which

characterized a mouse model expressing a mutant RyR2 with impaired regulation by CaM (RyR2-W3587A/L3591D/F3603A, ADA).^{43,111,112} Interestingly, mice homozygous for the mutation developed severe hypertrophy and died within two weeks of birth, a phenomenon likely associated with increased Erk1/2-p90RSK-GSK-3 β rather than CaM-CaN-NFAT and CaM-CaMKII-HDAC signaling.¹¹¹ The observation that a mutation in RyR2 is sufficient to induce severe hypertrophy, albeit not being a clinically relevant mutation, suggested that RyR2 could cause cardiomyopathy in humans. To date, three types of cardiomyopathy have been associated with RyR2 mutations in the clinical setting, all with low confidence levels: HCM (T1107M),¹¹³ left ventricular non-compaction (LVNC, in-frame deletion of exon 3)¹¹⁴⁻¹¹⁶ and arrhythmogenic right ventricular cardiomyopathy (ARVC, several mutations).^{117,118}

In an effort to determine the pathogenic mechanisms associated with these mutations, Tang et al.¹¹⁹ measured the activation and termination threshold for spontaneous Ca²⁺ release (SCR) in a heterologous system with RyR2 expression. All CPVT, LVNC, and ARVC mutations studied increased both activation and termination thresholds for SCR. Importantly, A1107M, the mouse analog of T1107M, behaved differently from all the other mutations, showing normal activation but decreased termination threshold, and was thus classified as a loss-of-function. Lau and Van Petegem³⁰ mapped A1107 to SPRY2, a small but structurally complex domain. SPRY2 is one of the peripheral domains of RyR2 not considered a hotspot for CPVT mutations (Figure 1.5, discussed above); however, it might be relevant for inter-subunit interactions because it spans the gap between the handle domain and HD2 of two adjacent protomers.³³ Crystallographic data of the isolated SPRY2 further suggest that position

1107 can easily accommodate an alanine or a threonine, while the bulkier side chain of methionine produces a shift in the amino acid backbone, affecting interactions with neighboring amino acids.³⁰ Remarkably, T1107M has also been identified in patients with CPVT.⁸¹ Altogether, these data strengthen the overall pathogenic role of T1107M, but weakens its role in structural cardiomyopathy.

The in-frame deletion of exon 3, associated with LVNC, showed similar SCR properties to other CPVT and ARVC mutations studied by Tang et al.¹¹⁹ Nevertheless, the same group created a mouse with a comparable genetic deletion to characterize the *in vivo* phenotype.¹²⁰ The homozygous mutation was embryonic lethal, but heterozygous mice survived with no evident changes in cardiac structure and normal susceptibility to stress-induced arrhythmia. Remarkably, these mice had decreased cardiac expression of RyR2, similar to a previously characterized RyR2 heterozygous knock-out mice.¹²¹ Because there are no reports quantifying RyR2 expression in patients harboring an *RYR2* allele with exon 3 deletion, it is difficult to assess whether the clinical phenotype is associated with decreased RyR2 expression or with the presence of the mutant protein product. Nevertheless, exon 3 deletion also appears in cohorts of CPVT patients.⁸¹

Finally, ARVC is an autosomal dominant congenital cardiomyopathy characterized by progressive fibro-fatty replacement of the myocardium that can lead to ventricular arrhythmias and heart failure. ARVC is more often caused by mutations in genes encoding components of the cardiac desmosome, including plakophilin-2 (*PKP2*), plakoglobin (*JUP*), and others; however, as many as 40–50% of patients do not harbor mutations in the five main desmosomal ARVC genes.¹²² Rampazzo et al.¹²³ first mapped a mutation in a family with an autosomal dominant form of ARVC to chromosome 1q42-

q43. Tiso et al.¹¹⁷ later identified *RYR2* as the gene harboring the disease-causing mutation. Interestingly, the clinical presentation of ARVC2 in these patients resembled CPVT in that arrhythmias could be elicited by exercise, had high penetrance, and affected males and females equally¹¹⁷ — characteristics that are not typical of ARVC. Although a clear association between RyR2 mutations and ARVC remains unproven, a recent study that analyzed 64 “typical” ARVC patients without desmosomal mutations found 6 rare missense *RYR2* variants yielding 9% incidence among probands (6/64) — clearly higher than the control population.¹²⁴ Thus, although the causal association between RyR2 variants and ARVC was not direct, the study reopened the possibility that RyR2 mutations may lead to structural alterations characteristic of ARVC. Alternatively, it is possible that specific RyR2 variants may aggravate the phenotype associated resulting from mutations in other proteins present in these patients.¹²⁵

Important steps have been taken to establish a definitive link between RyR2 mutations and structural cardiomyopathy; yet, all efforts are overshadowed by reports associating specific variants with both arrhythmogenic disorders and structural cardiomyopathy.^{81,118} Thus, the mechanism(s) by which a given mutation in *RYR2* triggers pathological remodeling instead of a purely arrhythmogenic syndrome (CPVT) remains unknown. However, it is evident that RyR2 mutation can produce a wide spectrum of cardiac alterations — yet the underlying mechanisms that determine the phenotype will remain unknown until novel mutations identified only in patients with structural cardiomyopathy are fully characterized. The most straightforward link between Ca²⁺ dysregulation and structural cardiomyopathy involves activation of the CaM-CaN-NFAT and CaM-CaMKII-HDAC signaling pathways because both are Ca²⁺-dependent

and have been shown to be relevant to hypertrophy and heart failure.¹²⁶ Nevertheless, the lack of a connection between these pathways and the hypertrophic phenotype of the ADA mouse discussed above foreshadows a more complex mechanism.

1.6. Scope of this Dissertation

Ca²⁺ signaling is pivotal for the control of contractility, action potentials, gene transcription, mitochondrial activity, and several other important functions of cardiac cells. As the regulatory valve of SR Ca²⁺ release in the heart, RyR2 has an undeniable role in each of these processes. Today, the role of RyR2 dysregulation as a trigger of cardiac arrhythmias has been firmly established. CPVT, caused by mutations in RyR2 and/or its accessory proteins, is the most salient example of intracellular Ca²⁺ signaling gone awry and causes lethal ventricular arrhythmias. HF, on the other hand, offers a provocative example of how similar arrhythmogenic mechanisms are also associated with acquired, rather than inherited, Ca²⁺ mishandling and RyR2 dysfunction. As our understanding of the intimate and bidirectional connection between RyR2 dysfunction and membrane potential increases, this frontier is extending ever more firmly beyond CPVT and into the territories of atrial fibrillation, long QT syndrome, and other arrhythmogenic syndromes that will require ample discussion in the future. Although Ca²⁺-dependent arrhythmias are known to exacerbate the malignancy of structural diseases such as HCM and heart failure, no study has yet established a *direct* causal relationship between RyR2 dysregulation and pathological structural remodeling. The idea that they *directly* cause such diseases remains tantalizing at best. Moreover, no animal model generated to date harboring such mutations recapitulates the cardinal signs of any structural cardiomyopathy syndrome.

This project was initially intended to study the mechanisms by which RyR2 mutations, specifically the novel HCM-associated mutation P1124L, might produce structural cardiomyopathy rather than CPVT. Along the way, the scope of the project was expanded to include two aspects of RyR2 regulation that contribute not only to pathogenesis, but to normal cardiac function: phosphorylation and expression. While seemingly independent, these three subprojects respond to the same general aim: to obtain better understanding about RyR2 regulation in the healthy and diseased heart. Our overall working hypothesis is that RyR2 expression and phosphorylation are fundamental to control cardiac function, and may be involved in dysregulation of Ca²⁺ handling in heart disease. Each of the subprojects discussed in the following chapters takes advantage of an animal model harboring specific RyR2 mutations used to test this hypothesis:

CHAPTER 2 discusses a series of experiments developed using a mouse derived from the S2808A model published by our laboratory in 2007.¹³ This project was designed to sort out one of the fundamental differences between two mouse models generated by different laboratories that have fueled a long-standing controversy regarding the role of S2808 phosphorylation on RyR2 regulation. The aim of these experiments was to test the hypothesis that the genetic background of S2808A mice contributes to impairing their cardiac adrenergic response and abating their progression to heart failure after myocardial infarction. This chapter uses mRyR2 nomenclature (Table 1.1).

CHAPTER 3 discusses the characterization of a novel RyR2 knock-out rabbit model, which we used as a tool to test the hypothesis that decreased RyR2 expression is sufficient to cause cardiac dysfunction in rabbits as compared to the relative lack of effect of decreased RyR2 expression previously observed in mice. Homozygous deletion

of RyR2 is embryonic-lethal, but heterozygotes show haploinsufficiency. Decreased RyR2 expression is commonly observed in failing hearts⁹² and in patients with HCM.^{99,100} We also discussed earlier that decreased expression of RyR2 was reported in mice with deletion of exon 3 associated with LNVC and CPVT. Hence, this rabbit model allowed us to understand the contribution of RyR2 expression to the pathology of heart disease in a mammalian model closer to the human. This chapter uses rRyR2 nomenclature (Table 1.1).

CHAPTER 4 discusses the molecular, cellular and whole-animal characterization of P1124L, an RyR2 mutation identified by Michael Ackerman's laboratory in a patient with HCM. This mutation is a good candidate to elucidate the mechanisms of RyR2 dysfunction that might lead to structural cardiomyopathy because it has only been associated with human HCM. We determined that this mutation induces cardiac hypertrophy and arrhythmia in mice. In this chapter, we use mRyR2 nomenclature, unless otherwise stated.

Finally, CHAPTER 5 integrates the key findings described in the previous chapters into the larger scheme of RyR2 regulation. While this dissertation does not put an end to specific controversies or affirms beyond doubt the role of RyR2 in generating structural cardiomyopathy, it certainly improves our understanding of RyR2 regulation in the context of cardiac function and leads to important advances in the field of cardiac e-c coupling. This final chapter also discusses future research avenues directly derived from the data discussed henceforth.

1.7. Acknowledgements

Sections of this chapter are in the process of being published: Alvarado FJ, Valdivia HH. Chapter 53: Inheritable Phenotypes Associated with Altered Intracellular Calcium Handling. *In* Zipes DP, Jalife J & Williamson WG. Cardiac Electrophysiology: From Bench to Bedside. 7th Edition. Elsevier, 2017.

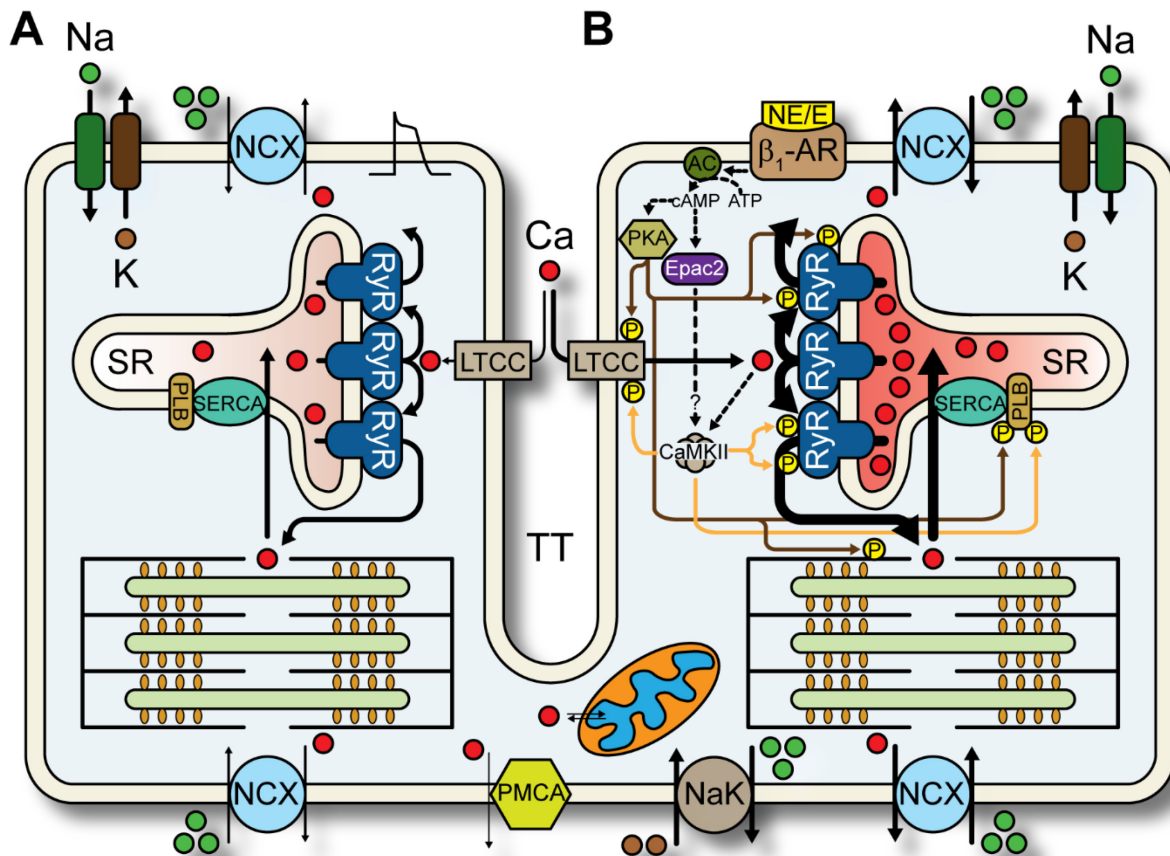


Figure 1.1. Cardiac Excitation-Contraction Coupling.

Schematic representation of excitation-contraction coupling in a ventricular myocyte. Panel **A** represents the cell under basal conditions and panel **B** under adrenergic stimulation. Each panel is to be interpreted independently, but the plasma-membrane Ca²⁺ ATPase (PMCA), Na⁺/K⁺ ATPase (NaK), and mitochondrion shown at the bottom are common both panels.

A. Cardiac excitation-contraction coupling in basal conditions. Ca²⁺ current through L-type Ca²⁺ channels (LTCC) activates ryanodine receptors 2 (RyR2), which in turn release Ca²⁺ from the sarcoplasmic reticulum (SR) leading to contraction of the myofilaments. Ca²⁺ is then extruded from the cell through the Na⁺/Ca²⁺ exchanger (NCX) and resequenced into the SR by the sarco/endoplasmic reticulum Ca²⁺ ATPase (SERCA). Other players such as PMCA and mitochondria also participate in Ca²⁺ extrusion from the cytosol to a lesser extent. **B.** Stimulation of β₁-adrenergic receptors (β₁-AR) by catecholamines (NE/E) promotes activation adenylyl cyclase (AC), which converts ATP into cAMP. The latter activates PKA, which phosphorylates (P) several protein targets including LTCC, RyR2, phospholamban (PLB), and troponin I. This leads to increased Ca²⁺ cycling and positive inotropy and lusitropy. Non-canonical β₁-AR signaling that leads to activation of CaMKII is indicated. CaMKII is also activated by enhanced Ca²⁺ cycling during adrenergic stimulation.

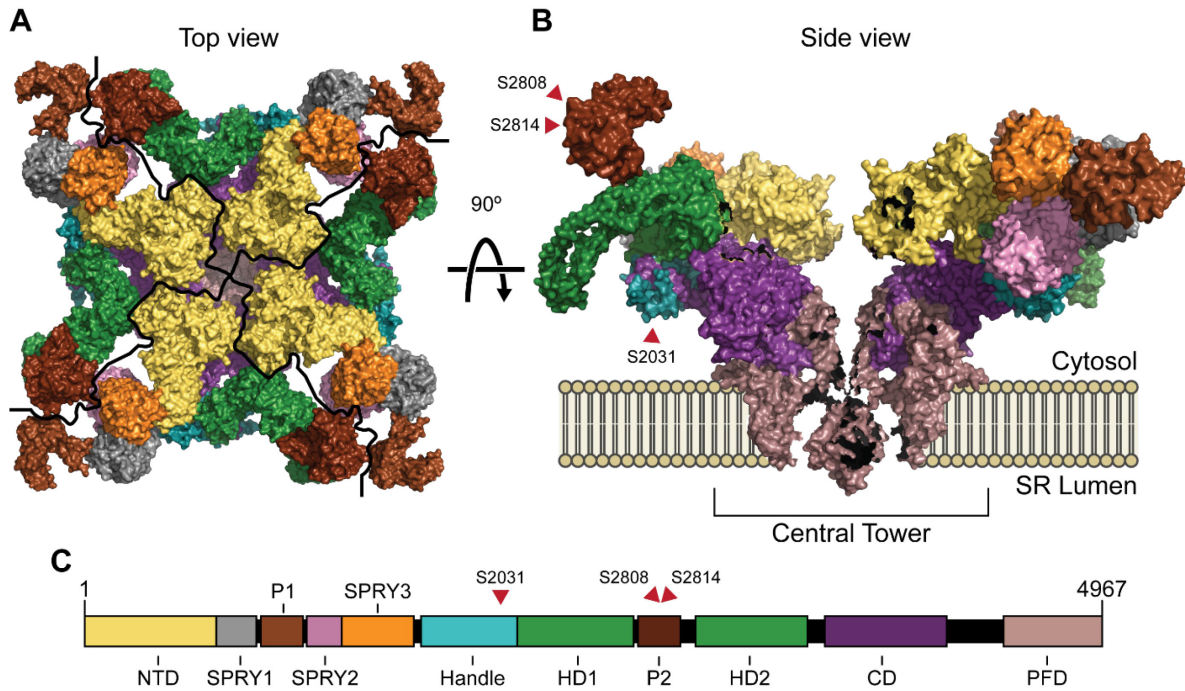


Figure 1.2. Ryanodine Receptor Structure and Domain Assignment.

The atomic coordinates and domains of the porcine RyR2 as reported by Peng et al.³⁶ (PDB ID 5GO9) were used to identify equivalent domains in the human RyR2. Domains are color-coded in all panels. **A**. Single RyR2 channel observed from the dyadic cleft. Black lines delimit the four subunits. **B**. Side view of an RyR2 channel showing two opposite subunits. The central tower of the channel, composed, from top to bottom, by the N-terminal domain (NTD), the central domain (CD), and pore-forming domain (PFD), is highlighted. **C**. Schematic of a single RyR2 subunit drawn to scale. Black boxes indicate inter-domain regions. Panels **A-B** were prepared using PyMOL Molecular Graphics software. Arrowheads indicate the approximate location of the three known phosphorylation sites.

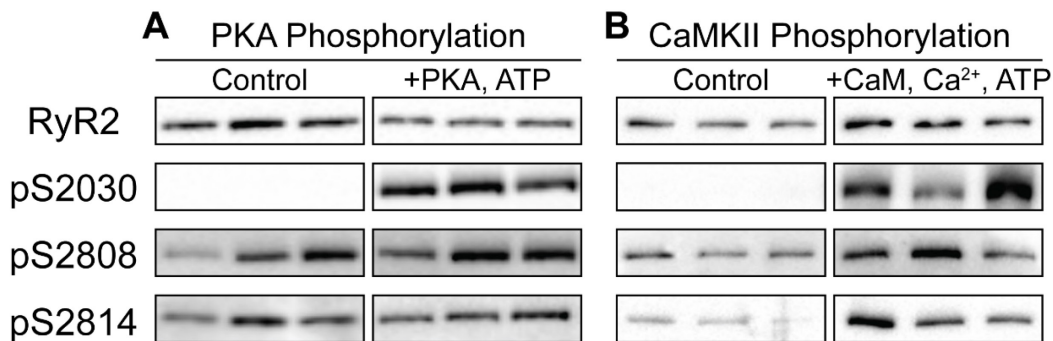


Figure 1.3. *In vitro* Phosphorylation of RyR2 by PKA and CaMKII.

RyR2 from mouse heart homogenates was back-phosphorylated *in vitro* with the addition of either the catalytic subunit of PKA and ATP (**A**), or the addition of CaM, Ca²⁺, and ATP to activate the endogenous CaMKII (**B**). Control reactions were performed in the absence of PKA (**A**) and CaM (**B**). Phosphorylation levels were assessed using phospho-specific antibodies. Western blots were performed as described in the following chapters.

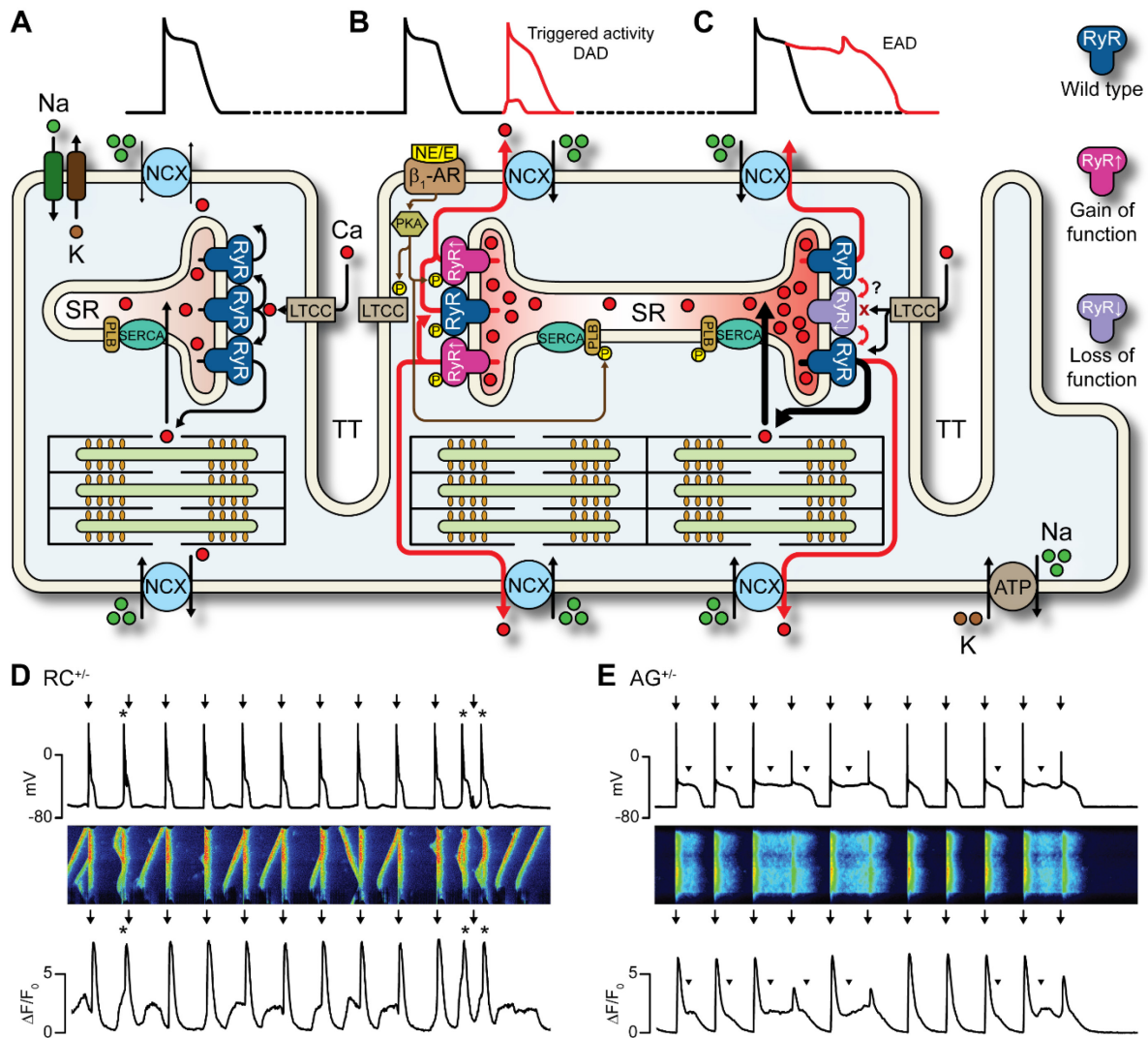


Figure 1.4. Cellular Mechanisms of CPVT.

A. Cardiac excitation-contraction coupling and action potential wave-form in a normal myocyte. **B.** Spontaneous Ca^{2+} release in myocytes harboring gain-of-function RyR2 mutations and stimulated with catecholamines. Extemporaneous Ca^{2+} release during diastole due to increased cytosolic and/or luminal sensitivity to Ca^{2+} can produce delayed after-depolarization (DAD) and lead to trigger activity. **C.** RyR2 channels harboring a loss-of-function mutation do not respond to luminal or cytosolic Ca^{2+} . When the SR reaches a critical Ca^{2+} load during an AP, both wild type and hypoactive channels produce a burst of Ca^{2+} that prolongs the AP by activating the NCX, leading to an early after-depolarization (EAD). **D-E.** Representative action potential (top panel) and Ca^{2+} transient (middle and lower panels) traces recorded in cardiac myocytes from heterozygous RyR2-R4496C ($\text{RC}^{+/-}$, gain-of-function) and RyR2-A4860G ($\text{AG}^{+/-}$, loss-of-function) mice stimulated at 1Hz in the presence of 300 nM isoproterenol. In panel D, notice the several Ca^{2+} waves unable to trigger full APs in the **D**. Arrows indicate triggered stimuli. Asterisks indicate DADs and arrowheads indicate AP prolongation and EADs. (For **D-E**, data kindly provided by Xi Chen and Yan-Ting Zhao from the University of Michigan Center for Arrhythmia Research).

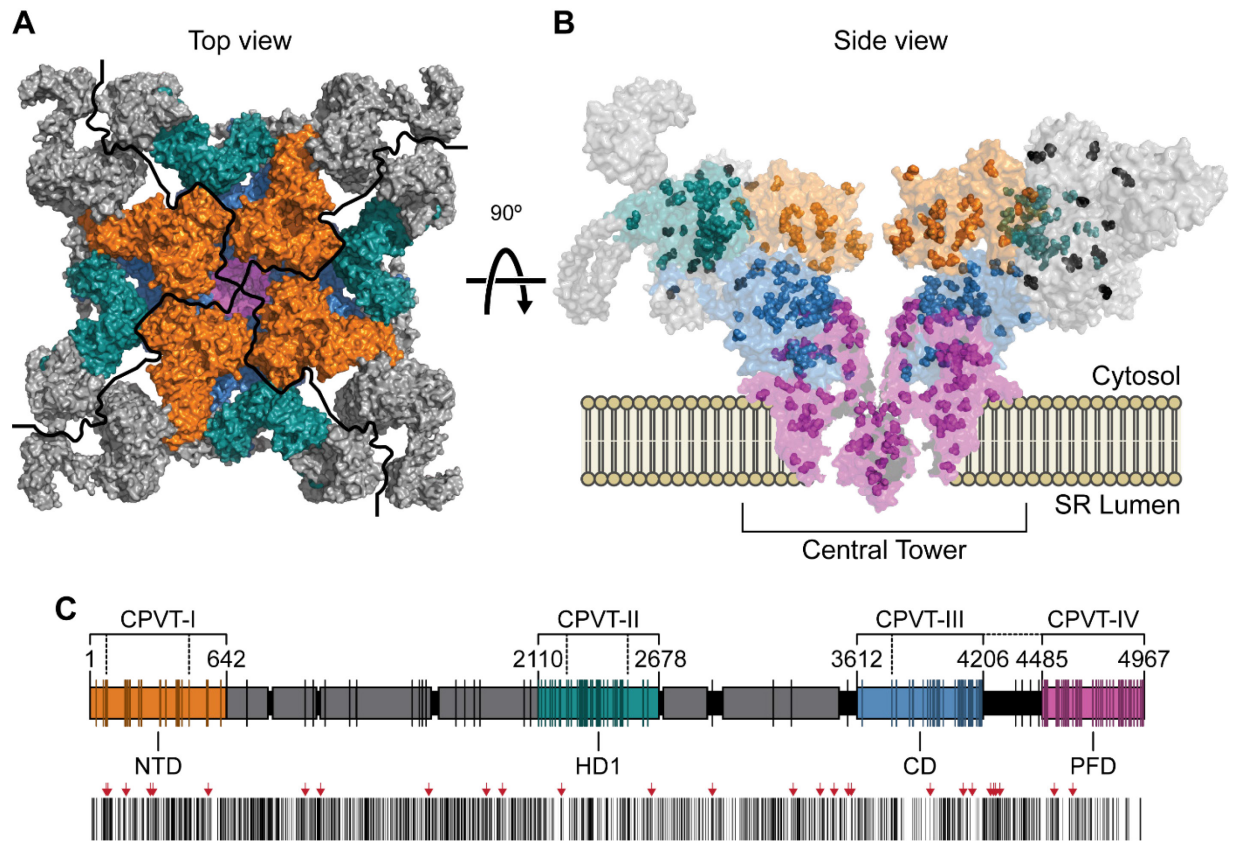


Figure 1.5. RyR2 Mutations Associated with CPVT.

The four domains containing most of the CPVT mutations are color-coded in all panels: N-terminal domain (NTD), orange; helical domain 1 (HD1), green; central domain (CD), blue; and pore-forming domain (PFD), magenta. All other domains are colored gray. **A.** Single RyR2 channel observed from the dyadic cleft. Black lines delimit the four subunits. **B.** Side view of an RyR2 channel showing two opposite subunits. The side chain of ~200 residues susceptible to CPVT mutations are identified with spheres and colored according to the domain. **C. Top.** Schematic of a single RyR2 subunit drawn to scale with superimposed lines representing the location of 200 residues susceptible to CPVT mutations. The current delimitation of the three CPVT mutation clusters, as defined by Medeiros et al.,⁸¹ is indicated with dashed lines. Solid lines indicate a proposed delimitation based on specific domains (mutation data compiled from the Human Gene Mutation Database¹²⁷ and from the literature). **Bottom.** Location of 1422 RyR2 residues with reported missense variants, drawn at the same scale as top panel. Arrows indicate the position of 29 variants that introduce stop codons and truncate the protein (data from the Genome Aggregation Database⁸³).

Table 1.1. Characterized Phosphorylation Sites in RyR2.

Current nomenclature, basal phosphorylation, kinase, and initial reference of the three known phosphorylation sites of RyR2. Reference sequences of RyR2 are: human Q92736, rabbit P30957, mouse E9A401 (Uniprot¹²⁸).

Human	Site		Basal Phosphorylation**	Kinase	Reference
	Rabbit	Mouse			
S2031	S2031	S2030	?–Low	PKA	Xiao et al. ⁶¹
S2808	S2809	S2807*	~50%	PKA, CaMKII	Witcher et al. ⁵²
S2814	S2815	S2813*	~50%	CaMKII	Wehrens et al. ⁵⁹

* These sites are referred to in the literature as S2808 and S2814, respectively. Residue numbers changed in February 2015 after the removal of A2266 from the reference sequence. To maintain coherence with the literature, these sites will continue to be referred to as S2808 and S2814 throughout the text.

** Basal phosphorylation levels assessed in rat cardiomyocytes by Huke & Bers.⁵⁷

CHAPTER 2

Ablation of RyR2-S2808 Phosphorylation Does Not Alter the Adrenergic Response or the Progression to Heart Failure in Mice

2.1. Introduction

Heart failure (HF) is a complex, multi-factorial syndrome characterized by incapacity of the heart to meet metabolic demands; HF is clinically manifested by dyspnea, fatigue, limited exercise capacity and fluid retention.⁹⁰ Although the underlying mechanisms of HF are varied and complex, dysregulation of intracellular calcium (Ca^{2+}) handling is a defining feature that is thought to be involved in the most prominent pathophysiological observations: structural remodeling of the heart, impaired cardiac contractility, and increased propensity to arrhythmia.^{95,97,129}

Cardiac contraction requires Ca^{2+} cycling for excitation-contraction (e-c) coupling, the process transducing electrical signals into mechanical force. A normal contraction occurs when ryanodine receptors (RyR2) release Ca^{2+} from the sarcoplasmic reticulum (SR) upon activation by a small inward Ca^{2+} current (I_{CaL}) mediated by L-type Ca^{2+} channels. Relaxation then ensues from the removal of Ca^{2+} from the cytosol by the SR Ca pump (SERCA2a) and the $\text{Na}^+/\text{Ca}^{2+}$ exchanger (NCX). In HF, the abundance, phosphorylation levels, and activity of several e-c coupling proteins and their regulatory partners are altered.^{92,130} In 2000, Marks et al communicated that in HF, RyR2 is hyperphosphorylated at its S2808 phospho-site, which triggers dissociation of the

regulatory protein FKBP12.6 and renders the channel hyperactive by inducing long-lasting sub-conductance states.⁵⁴ In subsequent papers, the group provided compelling evidence that S2808 is the only PKA phosphorylation site in RyR2⁵⁴ and that ablation of this site in mice (S2808A) blunts the normal cardiac adrenergic response⁵⁵ and improves the outcome of ischemic HF.⁵³ Thus, Marks et al. assigned the Ca²⁺ mishandling characteristic of HF to S2808 hyperphosphorylation and subsequent dissociation of FKBP12.6. However, many laboratories have failed to reproduce key elements of this hypothesis.^{19,58} Our laboratory independently generated a S2808A mouse model and observed a normal progression to HF following transverse aortic constriction.¹³ Later, Houser's group, using the same mice, reported normal adrenergic response¹³¹ and unaltered progression to HF following myocardial infarction (MI).¹⁰¹

Although the discrepancies between these two mouse models are striking, the underlying causes have not been explored yet. One of the most patent differences between both S2808A models is the genetic background: the studies by the Marks laboratory were conducted using mice on the C57Bl/6 background, while the Valdivia and Houser laboratories used a mixed Sv129/C57Bl6 background.^{13,53} This variable is relevant, since important phenotypic differences have emerged from identical genetic alterations in various mouse strains. Background genes from the parental strains may interact with the mutated gene in a manner that could severely compromise the interpretation of phenotype. In this study, we explored the effect of the genetic background as the source of these divergent results. We backcrossed the Valdivia lab's mouse model into a congenic C57Bl/6 strain and followed an experimental approach similar to previous reports using these models.^{13,101,131} We found that S2808A mice in the

C57Bl/6 genetic background (1) have a normal response to adrenergic stimulation at the whole animal and cellular levels, and (2) show identical progression towards HF compared to wild type controls up to four weeks after MI. Therefore, it is unlikely that the genetic background of the mice is the source of the diametrically opposite results obtained by the Marks and Valdivia/Houser groups. These data support the notion that phosphorylation of S2808 is unlikely to be essential for the cardiac adrenergic response and is perhaps irrelevant in HF progression.

2.2. Results

2.2.1. Direct Sequencing of Ryr2

For this work, we derived a congenic mouse line in the C57Bl/6 genetic background from the S2808A mice generated in our laboratory (Figure 2.1) and first described by Benkusky et al.¹³ This model has been thoroughly characterized by our laboratory¹³ and several collaborators.^{101,131-133} All these reports have used Western blots to confirm the absence of S2808 phosphorylation in homozygous mice. However, changes in neighboring amino acids that alter the antibody epitope can produce a confounding result. Therefore, we sequenced the genomic region containing the underlying mutation to validate the model from a genetic perspective.

This mouse was created using homologous recombination with a targeting vector containing exons 54-56 and a floxed neomycin (NEO) resistance cassette within an intronic region. We amplified and sequenced the region of exon 56 containing the codon of interest together with a fragment of the downstream intron. Three mutations were identified in exon 56 of S2808A mice (Figure 2.2): two of them were silent mutations in codons 2804 and 2805; the third was the missense mutation that changed codon 2808

from encoding a serine to an alanine substitution. Thus, we confirmed that the genetic mutation is at the expected location within *Ryr2* and that the surrounding exon encodes for the same amino acid sequence as the WT gene. The intron downstream of exon 56 contains a short deletion within a non-complexity region (dominated by C and A) and an insertion from the targeting vector containing the remaining loxP site from the Cre-mediated deletion of the NEO resistance cassette.

2.2.2. Analysis of Cardiac Function and Structure After Myocardial Infarction

We utilized a similar approach to that used by Wehrens et al.⁵³ and Zhang et al.¹⁰¹ to assess cardiac function after MI in S2808A mice. Animals were followed using echocardiography up to 4 weeks after the induction of myocardial infarction by ligation of the left anterior descending (LAD) coronary artery (Figure 2.1 **C**). During this period, survival was not statistically different ($p = 0.298$) between WT and S2808A mice (9 out of 12 and 10 out of 11, respectively; Figure 2.1 **D**). Figure 2.3 and Table 2.1 summarize the echocardiographic parameters measured in WT and S2808A mice before, and one and four weeks after MI. Consistent with previous reports,^{13,101,131} we did not observe structural or functional differences between WT and S2808A mice at basal level. Following MI, both groups showed equivalent deteriorating cardiac function that involved a significant decrease in ejection fraction (Figure 2.3 **A**) and fractional shortening (Figure 2.3 **B**), and an increase in LV diameter (Figure 2.3 **C**). The interventricular septum wall thickness (Figure 2.3 **D**) and stroke volume (Figure 2.3 **E**) remained unchanged in both groups. Once established, all deteriorating parameters remained unchanged up until 4 weeks post-MI, with no significant difference between WT and S2808A. This indicates that both groups have a similar progression to HF. Heart rate, on the other hand, was

statistically higher in S2808A mice 4 weeks post-MI (WT 485 ± 22 vs. S2808A 582 ± 19 bpm, $p = 0.009$; Figure 2.3 **F**). Interestingly, heart rate in S2808A mice appeared to be part of a continuum of processes that was uncovered by MI, because it *tended* to be higher at baseline (WT 476 ± 21 vs. S2808A 539 ± 13 bpm, $p = 0.175$) and reached statistical significance 1 week post-MI (WT 484 ± 21 vs. S2808A 563 ± 15 bpm, $p = 0.047$). Finally, cardiac output was not statistically different between WT and S2808A mice 4 weeks post-MI (WT 18.2 ± 1.9 vs. S2808A 23.0 ± 2.1 mL/min, $p = 0.337$), likely reflecting variability in stroke volume (Figure 2.3 **E**).

The structural observations described above were accompanied by a significant and comparable increase of heart weight for both groups (Figure 2.4 **A**). Also, both WT and S2808A mice had a similar, non-significant tendency toward increased lung weight after MI (Figure 2.4 **B**). Finally, liver weight was not significantly different at any time point (Figure 2.4 **C**). The overarching conclusion from this work is that preventing S2808 phosphorylation does not impact the most salient cardiac parameters under basal conditions, nor does it affect their deterioration towards heart failure after MI.

2.2.3. Expression and Phosphorylation of E-C Coupling Proteins

The e-c coupling apparatus relies on a well-organized network of proteins that becomes disrupted during HF. Thus, we measured the abundance and phosphorylation of the major e-c coupling proteins using Western blots. The representative blots and summary plots are shown in Figure 2.5. We observed a similar, non-significant tendency for decreased RyR2 expression in both groups after MI (Figure 2.5 **B**). As expected, we did not observe phosphorylation of S2808 in mutant hearts. WT hearts, on the other hand, had significant basal S2808 phosphorylation and showed a tendency for increased

phosphorylation after MI (Figure 2.5 **C**). Among the other e-c coupling proteins studied, we only detected a significant increase in NCX expression after MI in both groups (Figure 2.5 **F**), consistent with other models of HF. However, there were no differences between WT and S2808A in the abundance and phosphorylation of the proteins analyzed, suggesting both mice undergo similar remodeling of the e-c coupling apparatus after MI, and that S2808A does not prevent such changes.

2.2.4. Cardiac Response to Adrenergic Stimulation

To assess the response of S2808A mice to acute adrenergic stimulation, we used echocardiography and analyzed the cardiac function before and after i.p. injection of 2 mg/kg Isoproterenol (Iso). Consistent with the data shown in Figure 2.3, there were no differences in the basal cardiac function between WT and S2808A mice. Following Iso injection, we observed a robust chronotropic and inotropic response in both groups (Table 2.2), with a significant increase in HR (Figure 2.6 **A**), ejection fraction (EF; Figure 2.6 **B**), and fractional shortening (Figure 2.6 **C**). Interestingly, the stroke volume remained unchanged after Iso (Table 2.2). This was most likely due to insufficient ventricle refilling time, since we also observed a significant decrease of LV diameter and volume in diastole (Table 2.2). We did not observe differences between WT and S2808A mice injected with Iso. To complement these *in vivo* results, we used Langendorff perfusion of isolated hearts to assess the adrenergic response in the absence of neurohormonal and hemodynamic regulation (Table 2.3). Perfusion with 300 nM Iso produced a significant increase in HR (Figure 2.6 **D**), LV-developed pressure (LVDP; Figure 2.6 **E**), and dP/dt (Figure 2.6 **F**). Yet again, none of the parameters were different between WT and S2808A

mice. Taken together, these data suggest that this phosphorylation site is not essential for the normal adrenergic response.

2.2.5. Cellular Ca²⁺ Handling Kinetics

Lastly, we measured the adrenergic response of isolated cardiac myocytes. We loaded the cells with fluo-4 and paced them at 1 Hz. When the Ca²⁺ transient amplitude was stable, 300 nM Iso was perfused for 1 minute, followed by a caffeine pulse to measure the SR Ca²⁺ load (Figure 2.7 **A**). As expected, Iso produced a significant increase in Ca²⁺ transient amplitude (Figure 2.7 **B**). This response, however, was identical in WT and S2808A cardiomyocytes. Additionally, we observed no differences in SR Ca²⁺ load (Figure 2.7 **C**) or in fractional release (percentage of SR Ca load released during pacing, Figure 2.7 **D**) between groups. These data are consistent with the isoproterenol stimulation observed in whole animals and isolated hearts, and further reinforce the notion that the S2808 phospho-site is not critical for adrenergic signaling.

2.3. Discussion

The notion that S2808 phosphorylation (1) is a marker of HF in humans and animal models,⁵⁴ (2) is a critical mediator of the normal adrenergic response of the heart,^{53,55} and (3) that it greatly influences the progression and may actually exacerbate major signs of ischemic HF⁵³ has been extensively documented by Marks et al. Since then, extensive research has focused on obtaining a better understanding of the underlying mechanisms. While the Marks group has produced elegant and comprehensive studies supporting their hypothesis^{53,55,56,134} and extended their central tenets to explain pathogenesis in some forms of Ca²⁺-dependent arrhythmias,²² muscular dystrophy,¹³⁵ seizures,³¹ stress-induced cognitive dysfunction,³² and diabetes,³³ several laboratories have failed to

reproduce fundamental tenets of their model (reviewed in refs. 14,18,19) making this a highly controversial topic. One of the most remarkable aspects of this controversy is that RyR2-S2808A mice developed by the Marks laboratory show a blunted response to adrenergic stimulation⁵³ and better outcomes after MI,⁵⁵ while a different mouse model with the same mutation, generated independently by our laboratory, has a normal adrenergic response¹³¹ and normal progression to HF following TAC¹³ and MI.¹⁰¹ Beyond certain variations in the experimental approach followed by both groups, which have been addressed in previous studies, there are evident differences between both mouse models:^{13,53} (1) the targeting strategy utilized: Marks used a self-excising ACN vector (containing a NEO resistance cassette, Cre recombinase, and a testes-specific promoter, all flanked by loxP sites), while our laboratory employed the classic “floxed” NEO cassette approach, which requires breeding targeted mice with mice expressing Cre-recombinase to excise the cassette; (2) the embryonic stem cells targeted: Marks used MM13 cells from 129S/SvEv mice, we utilized R1 cells derived from (129X1/SvJx129S1/SvImJ)F1 mice; and (3) the genetic background of the final mouse model: Marks backcrossed to the C57Bl/6 background for 10 generations, while we used a Sv129/C57Bl6 mixed background.

Although the impact of the targeting strategies or embryonic stem cells on the final phenotypic outcome is difficult to assess, several instances support the idea that identical mutations expressed in mice of different strains may lead to diverse phenotypes.^{136,137} Rubinstein et al.,¹³⁸ for example, observed that C57Bl/6 mice with heterozygous Nav1.1 deletion closely recapitulate the severe epileptic phenotype of human patients with Dravet Syndrome, while the same mutation expressed in Sv129 mice produces a milder

phenotype. Moreover, mice with mixed genetic background have an intermediate phenotype. In a more dramatic example, mice with a mutant superoxide dismutase transgene on the mixed B6SJL background show abnormalities resembling human amyotrophic lateral sclerosis lesions that are not evident on the C57Bl/6 background.¹³⁹ Thus, the mouse strain can greatly alter the phenotype of a mutant mouse, likely because the targeted gene interacts substantially with background genes. Unfortunately, this sort of in-depth study has not been performed in the context of cardiac proteins.

Some authors have suggested the variable beta-adrenergic response of the mouse strains used as a potential reason for divergent experimental results.¹⁴⁰ Thus, in this study we aimed to determine whether the genetic background confers S2808A mice with a blunted adrenergic response and protection against HF. The experimental approach was straightforward: backcross the S2808A mice with mixed background (Sv129/C57Bl6) into a C57Bl/6 strain (the same strain used by the Marks Laboratory) and replicate several of the key experiments that have fueled this controversy. This approach allowed us to dissect a single variable (genetic background) that is potentially responsible for the conflicting results discussed above.

Our initial mouse model has been characterized thoroughly and shared with several collaborators. Nevertheless, we performed gene sequencing of *Ryr2* in the congenic mouse strain to validate the genetic integrity of the model. We identified a single missense mutation in exon 56, which introduces a serine to alanine substitution in codon 2807 (S2807A). This codon corresponds to the human S2808. Classically, this site has been referred to as S2808 in the mouse nomenclature, but this changed when a revision was introduced to the mouse *Ryr2* reference sequence in February 2015. Here we have

continued using the same numbering to maintain consistency with previous literature and to avoid confusion. Also, both Benkusky et al.¹³ and Wehrens et al.⁵³ reported targeting exon 55 of *Ryr2* to generate their respective models. However, based on the most recent reference sequences available (accession numbers NM_023868.2 and NT_039578.8), this region corresponds to exon 56. Our sequenced amplicons align with this exon (Figure 2.2) and show the missense mutation is at the expected codon, as discussed above.

Following this genetic validation, we selected relevant experiments from previous reports to assess the response of our mice to acute and chronic stress (Iso injections and MI, respectively). If the genetic background were the cause of the conflicting results obtained with the two S2808A models, we expected (1) improved cardiac function after MI and (2) a blunted acute response to Iso, compared to WT. Each set of experiments produced the expected results in terms of the response to MI (LV dilation and deteriorating EF) and to adrenergic stimulation (positive chronotropism and inotropism), but S2808A mice behaved indistinguishably from WT controls. The only difference we detected was that S2808A mice showed a significant increase in HR compared to WT at one and four weeks post-MI. This observation was not reported by previous studies using our mouse,¹⁰¹ or by the Marks laboratory.⁷⁻⁵³ We can only speculate about the potential mechanisms underlying this phenomenon: for example, chronic adrenergic stimulation of WT may reduce SR Ca²⁺ load in pacemaker cells and decrease HR due to decreased entrainment of Ca²⁺ signals and membrane potential;¹⁴¹ however, the absence of significant differences in cardiac output between genotypes after MI suggest that this increase in HR does not improve cardiac function and, therefore, is not protective against MI. Furthermore, a higher HR during the onset of HF could nudge these mice closer to

arrhythmias, potentially *increasing* — rather than decreasing — their vulnerability to MI. Still, the increase in HR after MI in S2808A mice is not logically derived from current models of RyR2 regulation by S2808 phosphorylation and remains to be understood; however, it appears from the multitude of other variables that are similar between the two groups (Table 2.1) that it does not affect the progression to HF.

We also used Western blots to measure the expression of key e-c coupling before and after MI in both WT and S2808A hearts. There were no differences between WT and S2808A before or after MI in any of the proteins analyzed. Expression of RyR2 showed a tendency to be decreased 4 weeks after MI, but the difference did not reach statistical significance. The density of Ca_v1.2, SERCA2a, and PLB was unchanged after MI, whereas that of NCX increased by ~2.5-fold in both groups of mice. Hyperphosphorylation of S2808, a central process in the hypothetical model of Marks,^{53,54} had a modest trend to be increased in WT — but, again, the difference was not statistically significant. Lastly, phosphorylation of PLB-T17, a marker of CaMKII activation, trended to decrease but was not modified by MI. These observations agree with some — but not all — studies that report protein density after MI. There is considerable variability even in closely related models of HF. Hasenfuss¹³⁰ and Houser et al.⁹² noted this variability in several reports from human HF. Nevertheless, our observations here agree with those of Zhang,¹⁰¹ who used our S2808A mice (in the Sv129/C57Bl6 background), suggesting that the transfer of the mutation to a different genetic background did not modify expression of other key proteins. More importantly, a side-by-side comparison of WT and S2808A mice shows that preventing phosphorylation of this site does not alter expression of key proteins of e-

c coupling before or after MI, as expected if the phospho-mutation had the profound changes in e-c coupling postulated by Marks.

Concerning the physiologic response to acute stress, we also failed to detect differences between the two groups in mice in either isolated hearts or in isolated myocytes exposed to Iso. The lack of significant increase in stroke volume (SV) after adrenergic stimulation in both WT and S2808A mice was expected, considering that left ventricular volume at diastole (LVVd) and at systole (LVVs) were modified by Isoproterenol, since $SV = LVVd - LVVs$. However, fractional shortening (FS) and ejection fraction (EF), which directly reflect the inotropic response of the heart, were substantially increased by Isoproterenol in both groups (Table 2.2), thus indicating that the adrenergic response was fully installed in both groups of mice. Furthermore, the nearly-identical increase in LVDP in isolated hearts perfused with Iso (Table 2.3) supports the idea that both WT and S2808A mice show comparable response to acute stress. Again, these data are in agreement with all reports using our mouse model.^{101,131} Marks et al. previously proposed a dose-dependent effect of Iso, with only low doses (2 $\mu\text{g}/\text{kg}$) and concentrations (100 nM) producing blunted responses in S2808A mice. However, the idea of a dose-dependent effect on S2808 is not supported by previous reports that used a broad range of adrenergic agonist — as low as 10 nM Iso in isolated hearts¹³¹ and myocytes¹⁰¹ — and failed to observe differences in S2808A mice. In our whole-animal experiments we used 2 mg/kg Iso; for isolated-heart and cellular experiments we used 300 nM Iso (a dose only 3-fold higher than that used by Shan et al.⁵⁵) — yet there was no statistical difference between groups. All these data, taken together, argue against S2808 phosphorylation mediating the cardiac fight-or-flight response.

In summary, our data are in general agreement with all previous reports using our S2808A mice with mixed Sv129/C57Bl6 background. Therefore, the most logical conclusion is that the genetic background is not the cause of the conflicting results. This leaves the possibility open for other potential reasons, such as animal housing conditions and circadian rhythms, among others proposed by Dobrev & Wehrens.¹⁴⁰ However, the studies using the mouse model generated in our laboratory include data obtained by four independent laboratories (ourselves,¹³ Houser,^{101,131} Niggli,¹³³ and Gyorke¹³²) located in five different academic institutions, which undermines the likelihood that animal housing, circadian rhythms, and animal handling are critical variables. Also, they have involved experiments at all integrating levels of physiology (*in vivo*, *ex vivo*, cellular, and molecular) and have encompassed a wide range of experimental approaches. The real causes of the discrepancy thus remain unsolved, but the complexity and variability of data that have become evident through this journey have prompted us to revise our current model of RyR2 regulation by phosphorylation. A deterministic model in which one site (S2808) controls the fight-or-flight response to stress and prevents ischemic cardiomyopathy, while another site (S2814) defines CaMKII-regulation of Ca²⁺ release and prevents non-ischemic cardiomyopathy, appears now unsustainable and overly simplistic. Instead, it may be instructive to consider a more comprehensive model of RyR2 regulation that (1) includes all phospho-sites known to date (S2808, S2814 and S2030),^{18,61} (2) takes into account the interplay between these sites at baseline and under stress^{57,87} while acknowledging the great likelihood that other critical phospho-sites remain undiscovered,⁵¹ and (3) considers the effect of other post-translational modifications.¹⁸ The proximity and location of S2808 and S2814 within the same flexible loop of the

putative “phosphorylation hot spot” of RyR2,³¹ for example, strongly suggest that it is unlikely that these sites work independently.

Finally, we consider that validation of experimental models by independent laboratories is paramount to resolving controversies. With this in mind, we make our S2808A mice, in either the mixed 129Sv/C57Bl6 or C57Bl/6 strains, available for distribution to all interested parties.

2.4. Methods

2.4.1. General Considerations

All animal experiments were approved by the University of Michigan Institutional Animal Care and Use Committee. All experiments performed at institutional cores were single blind. Unless otherwise stated, all reagents were acquired from Sigma-Aldrich.

2.4.2. Mouse Model

The methods used to create the S2808A mouse model have been previously published.¹³ A congenic S2808A strain in the C57Bl/6 background was developed as follows (Figure 2.1): homozygous S2808A mice in a mixed Sv129/C57Bl6 background and with the floxed Neomycin resistance cassette were crossed with E2a-Cre transgenic mice (Jax Stock No. 003724). Heterozygous S2808A offspring with complete excision of the NEO resistance cassette were crossed with C57Bl/6J mice (Jax Stock No. 000664). S2808A offspring negative for the Cre recombinase were selected and backcrossed for 6 additional generations with C57Bl/6J to create a mouse model with over 99% C57Bl/6 genetic background.¹⁴² Backcrossing was conducted using a male C57Bl/6J and a female S2808A to lock the C57Bl/6 Y-chromosome in the male progeny. The new congenic

RyR2-S2808A colony was then maintained by breeding homozygotes. Age- and gender-matched C57Bl/6J mice were used as WT controls.

2.4.3. DNA Extraction, Sequencing and Genotyping

DNA was extracted from tail biopsies using the GenElute Mammalian Genomic DNA MiniPrep kit (Sigma-Aldrich). Mouse genotyping was carried out with the following primers: 5'-GGTAGTCTGTTTCAGAAC-3' and 5'-CTATATTCCCAAAGTTGGGT-3', amplifying a region including part of Exon 56 and of the downstream intron. PCR products obtained during genotyping were purified using the QIAquick PCR Purification kit (Qiagen) and submitted to the Sequencing Core of the University of Michigan for direct Sanger sequencing, using the primers above. Sequences were compared, using Nucleotide BLAST¹⁴³ to the region of the murine chromosome 13 containing the *Ryr2* (accession number NT_039578.8), as well as the corresponding mRNA (accession number NM_023868.2). In the current version of these sequences, the numbering of the amino acids in the translated mouse RyR2 protein (E9Q401) changed following the removal of the residue A2266; therefore, S2808 is now S2807. Here, we continued using the previous nomenclature, referring to this site as S2808 to avoid confusion.

2.4.4. Myocardial Infarctions

Myocardial Infarction (MI) surgeries using previously described methodologies¹⁴⁴ were performed by the Microsurgery Service of the Frankel Cardiovascular Center Animal Phenotyping Core at the University of Michigan. Briefly, 14–16-week-old mice were anesthetized using 1–5% isoflurane. A skin incision was made on the left side of the thorax, the pectoral muscle was retracted, and the third intercostal space was opened to expose the heart. Using 7-0 silk suture, the LAD artery was permanently ligated

approximately 2–3 mm from its origin. The thorax was closed immediately after ligation, followed by repositioning of the pectoral muscle and closing of the skin incision with surgical clips. Mice undergoing MI were evaluated with an echocardiogram one week prior to the surgery, and one and four weeks post-MI (Figure 2.1 **B**), and euthanized shortly thereafter (18–20 weeks of age). Hearts of control WT and S2808A mice were harvested at 18–20 weeks of age.

2.4.5. Echocardiography

Transthoracic echocardiography (Echo) was performed by the Echocardiography Service of the Frankel Cardiovascular Center Animal Phenotyping Core at the University of Michigan using a Vevo 2100 system with a 22–55 MHz transducer (MS550D; Visual Sonics), as described previously.^{89,145} Mice were anesthetized with 1–5% isoflurane and maintained on a heated platform. Two-dimensionally guided M-mode images of the left ventricle were acquired at the tip of the papillary muscles. Left ventricle diameter, septum wall and posterior wall thickness were recorded to determine the fractional shortening, LV volume, ejection fraction, and heart rate. To measure the adrenergic response, echocardiograms were performed in a different group of mice at basal conditions and 1 min after a 2 mg/kg Iso IP injection, as previously described.^{131,146} All parameters were measured over at least three consecutive cycles.

2.4.6. Tissue Homogenization

Whole heart homogenates were prepared as previously described.¹³ Briefly, frozen hearts were pulverized in liquid nitrogen, suspended in homogenization buffer (0.9% NaCl, Tris-HCl 10 mM pH 6.8, 20 mM NaF, 2 μ M leupeptin, 100 μ M phenylmethylsulphonyl fluoride, 500 μ M benzamidine, 100 nM aprotinin), homogenized

using a Teflon pestle, and centrifuged at 1000 x g for 10 minutes at 4 °C. Supernatants were aliquoted and stored at -80 °C until used. Protein concentrations were determined using the Bradford method (Bio-Rad).

2.4.7. Western Blotting

50 µg of tissue homogenate were suspended in Laemmli buffer and separated by SDS-PAGE in 4-20% TGX or AnyKD precast gels (Bio-Rad). Proteins were then transferred to PVDF membranes using the iblot2 transfer system (ThermoFisher) or overnight wet transfer. Membranes were probed with the following primary antibodies: anti-RyR (1:2000; MA3-925, Thermo), pS2808-RyR (1:5000; A010-30, Badrilla), SERCA (1:1000; ab2861, Abcam), NCX (1:200; ab6495, Abcam), PLB (1:5000; A010-14, Badrilla), pS16-PLB (1:5000; A010-12, Badrilla), pT17-PLB (1:5000; A010-13, Badrilla), Cav1.2 (1:200; ACC-003, Alomone), anti-GAPDH (1:10000; MAB374, Millipore). Secondary antibodies, used as appropriate, were goat anti-mouse-HRP (1:1000; 31437, Thermo) or goat anti-rabbit-HRP (1:2000; 31463, Thermo). Membranes were developed using SuperSignal Femto ECL reagent (Thermo) and imaged with a ChemiDoc MP apparatus (Bio-Rad). Band intensity was quantified with the ImageLab software (Bio-Rad).

2.4.8. Langendorff Perfusions

Perfusion of isolated hearts was performed as previously reported.^{87,131} Mouse hearts were harvested and mounted on a Langendorff apparatus as indicated in section 2.4.9, and perfused with Krebs-Henseleit Buffer (KHB) containing (mM) 118.5 NaCl, 4.7 KCl, 1.2 KH₂PO₄, 1.2 MgSO₄, 11 glucose, 25 NaHCO₃, 1.8 CaCl₂, aerated with 95% O₂, 5% CO₂. The perfusion pressure was adjusted to 70–100 mmHg. A pressure-transducer balloon was inserted into the left ventricle and the end-diastolic pressure was adjusted to

6–15 mmHg. Following a baseline recording of 5 min, hearts were stimulated with 300 nM Iso to record the adrenergic response for an additional 5 min. All parameters were acquired using a PowerLab 8/35 system (ADInstruments) and data were analyzed using LabChart 8 (ADInstruments).

2.4.9. Isolation of Ventricular Myocytes

Ventricular myocytes were isolated as previously described.⁸⁹ Briefly, mice were heparinized (0.5 U/g IP, Sagent Pharmaceuticals) and anesthetized with urethane (1mg/kg IP). The heart was quickly excised, mounted on a Langendorff apparatus, and perfused with Perfusion Buffer (PB) containing (mM) 113 NaCl, 4.7 KCl, 1.2 MgSO₄-7H₂O, 10 HEPES, 0.6 Na₂HPO₄, 12 NaHCO₃, 0.6 KH₂PO₄, 10 KHCO₃, 30 Taurine, 500mM 2,3-Butanedione monoxime, 5.5 glucose, pH 7.46 at 37 °C and 3 mL/min. The heart was then perfused with PB supplemented with 773.48 U/ml Collagenase Type II (Worthington), 0.14 mg/ml Trypsin (Gibco) and 12.5 μM CaCl₂. Once fully digested (5–7 min), the ventricles were minced in PB buffer containing with 10% FBS and 12.5 μM CaCl₂. Tissue pieces were gently pipetted to dissociate cells. Ca²⁺ was reintroduced to 1.8 mM step-by-step and cells were kept in Tyrode's solution containing (mM) 135 NaCl, 4 KCl, 1.8 CaCl₂, 1 MgCl₂, 10 HEPES, 1.2 NaH₂PO₄, and 10 glucose, pH 7.40, until used.

2.4.10. Confocal Ca²⁺ Imaging.

Ca²⁺ transients triggered by field stimulation were recorded from cardiac myocytes as previously described.⁸⁹ Cells were incubated in 10 μM fluo-4 AM (ThermoFisher) with 0.4% Pluronic F-127 (ThermoFisher) at 37 °C for 5 min. Cells were then washed and kept in fresh Tyrode's solution. Longitudinal line-scan images were recorded using a LSM510 Meta confocal microscope (Carl Zeiss) with a 40×/1.2 N.A water immersion objective at

3.072 ms/line. Fluorescence was excited at 488 nm and recorded at >505 nm. Myocytes were first perfused with Tyrode's solution and paced at 1 Hz using a Grass Stimulator. When a stable response was established, cells were perfused with Tyrode's solution containing 300 nM Iso for 1 min. Finally, 20 mM caffeine was applied to measure the SR Ca²⁺ load. The last five Ca²⁺ transients under basal conditions and with Iso were averaged for each cell. The fractional release was calculated as a percentage of the SR Ca²⁺ load released during field stimulation.

2.4.11. Statistical Analysis

All data are presented as mean±SEM. Statistical significance was determined at $p \leq 0.05$ using survival logrank (survival rates), paired t-test (Echos pre- vs. post-MI, Echos pre- vs. post-Iso, Ca²⁺ transients basal vs. Iso, Langendorff perfusions vs. t = 0 of same genotype), one-tailed t-test (Ca²⁺ transients, Langendorff perfusions between genotypes at each time-point), or one-way ANOVA (all other comparisons). Analyses were carried out in SigmaPlot 12.5 (Systat Software).

2.5. Acknowledgements

This chapter previously published: Alvarado FJ, Chen X, Valdivia HH. Ablation of the cardiac ryanodine receptor phospho-site Ser2808 does not alter the adrenergic response or the progression to heart failure in mice. Elimination of the genetic background as critical variable. *J Mol Cell Cardiol* 2017; 103:40-47.

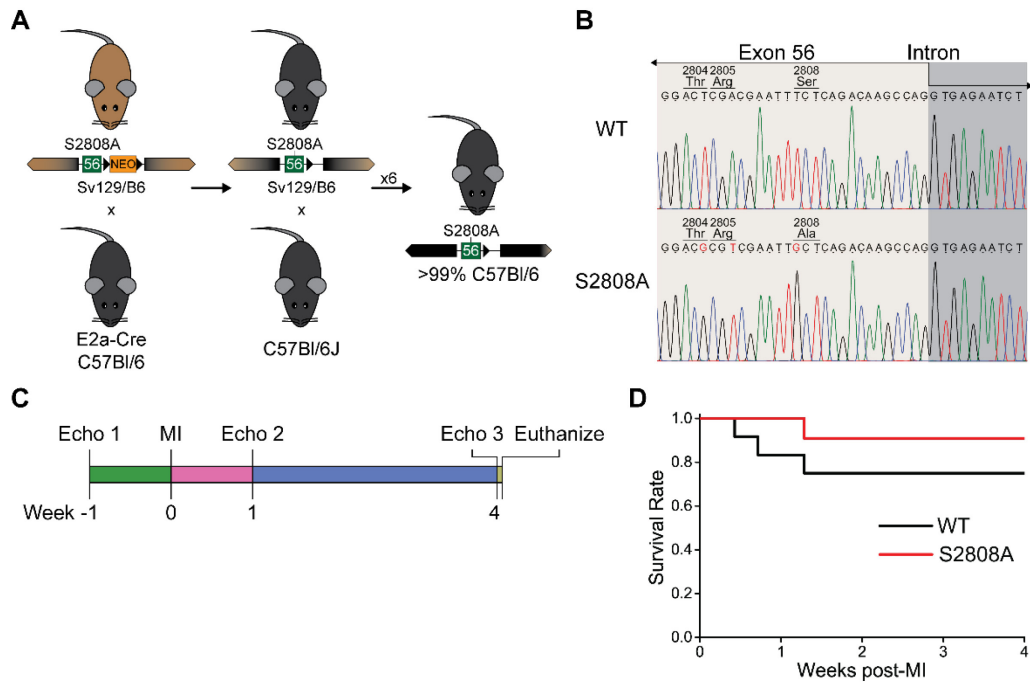


Figure 2.1. Experimental Model to Assess HF Progression in S2808A Mice.

A. Backcrossing scheme used to produce a congenic mouse strain derived from the RyR2-S2808A mouse developed in our laboratory. **B.** Direct sequencing of a portion of exon 55 confirms the presence of the missense mutation in codon 2808 leading to the serine to alanine substitution. Two silent mutations are located in codons 2804 and 2805. **C.** General scheme used to assess cardiac function in mice undergoing myocardial infarction. In this model, each mouse acts as its own control at basal conditions. **D.** Kaplan-Meier plot of survival after MI induction. Survival was slightly higher in S2808A than in WT controls, but this difference is not significant (n = 11-12 per genotype, p = 0.298).

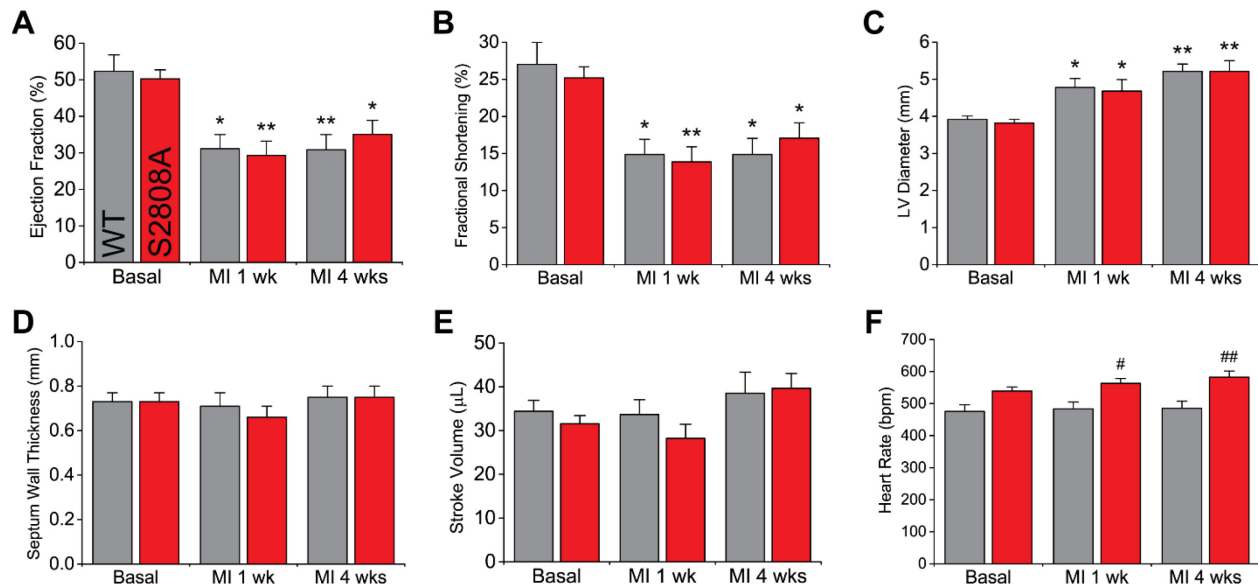


Figure 2.3. Cardiac Function Post-MI in S2808A Mice.

MI due to permanent LAD ligation produced a significant decrease in ejection fraction (A) and fractional shortening (B), and an increase in LV diameter in diastole (C). Septum wall thickness in diastole (D) and stroke volume (E) remained unaltered. Most parameters, measured at one and four weeks after MI, were comparable between S2808A and WT mice, except for heart rate (F) (n = 9 per genotype; * p < 0.05, ** p < 0.01 vs. same genotype basal; # p < 0.05, ## p < 0.01 vs. WT at same time-point).

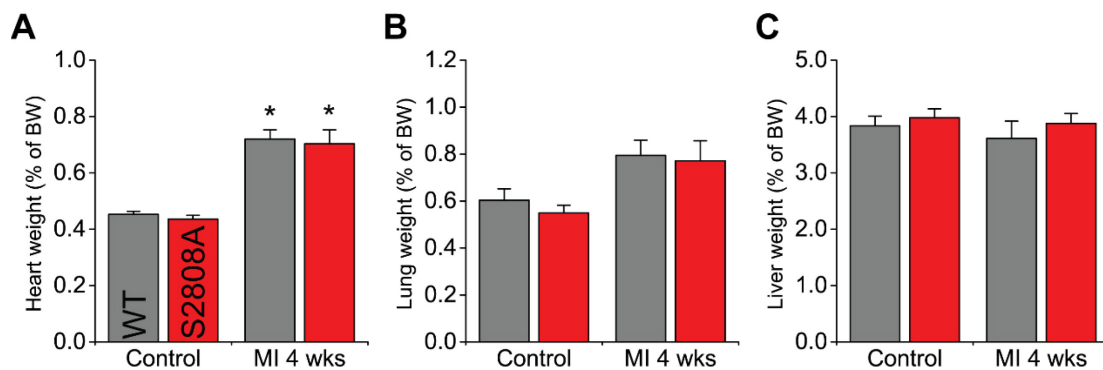


Figure 2.4. Tissue Remodeling post-MI in S2808A Mice.

Heart weight (A), lung weight (B) and liver weight (C) as a percentage of body weight in control mice and 4 weeks after LAD ligation. Only the heart weight was increased in both groups after MI (n = 7-9 per genotype per group; * p < 0.05 vs same genotype control).

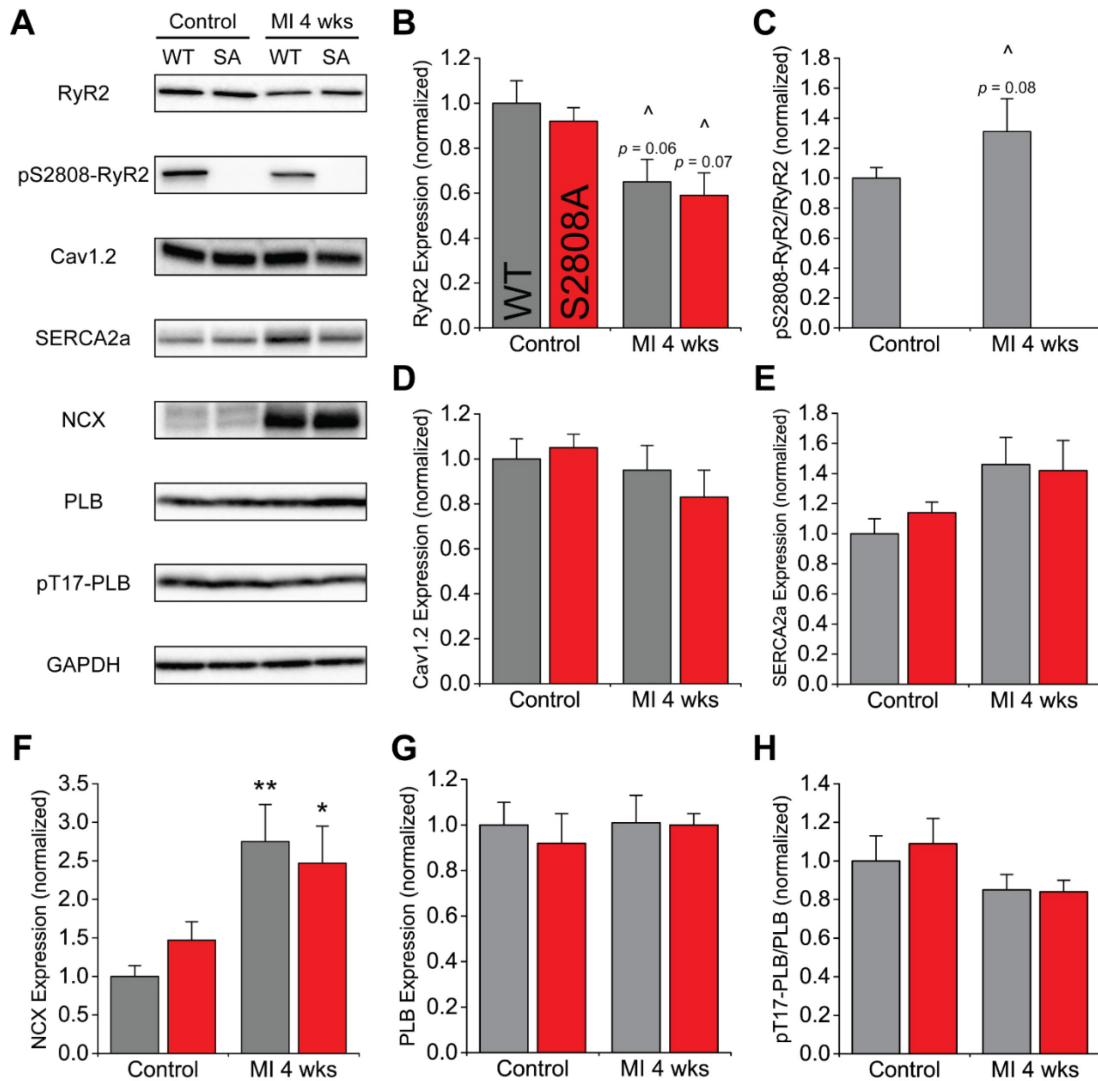


Figure 2.5. E-C Coupling Protein Expression and Phosphorylation in S2808A Hearts.

A. Representative blots. **B.** Expression of RyR2 has a tendency to be decreased 4 weeks after MI. **C.** Phosphorylation level of RyR2-S2808 determined as a ratio between phosphorylated and total protein. Phosphorylation was absent in S2808A mice, and has a tendency to be increased in wild-type animals. **D-G.** Expression level of excitation-contraction coupling proteins Cav1.2, SERCA2a, NCX and PLB. Expression of NCX was nearly 2.5-fold increased after MI. **H.** Phosphorylation level of PLB determined as described above ($n = 6-8$ per genotype per group; * $p < 0.05$, ** $p < 0.01$ vs. same genotype control; \wedge tendency with $p < 0.1$ vs. same group control).

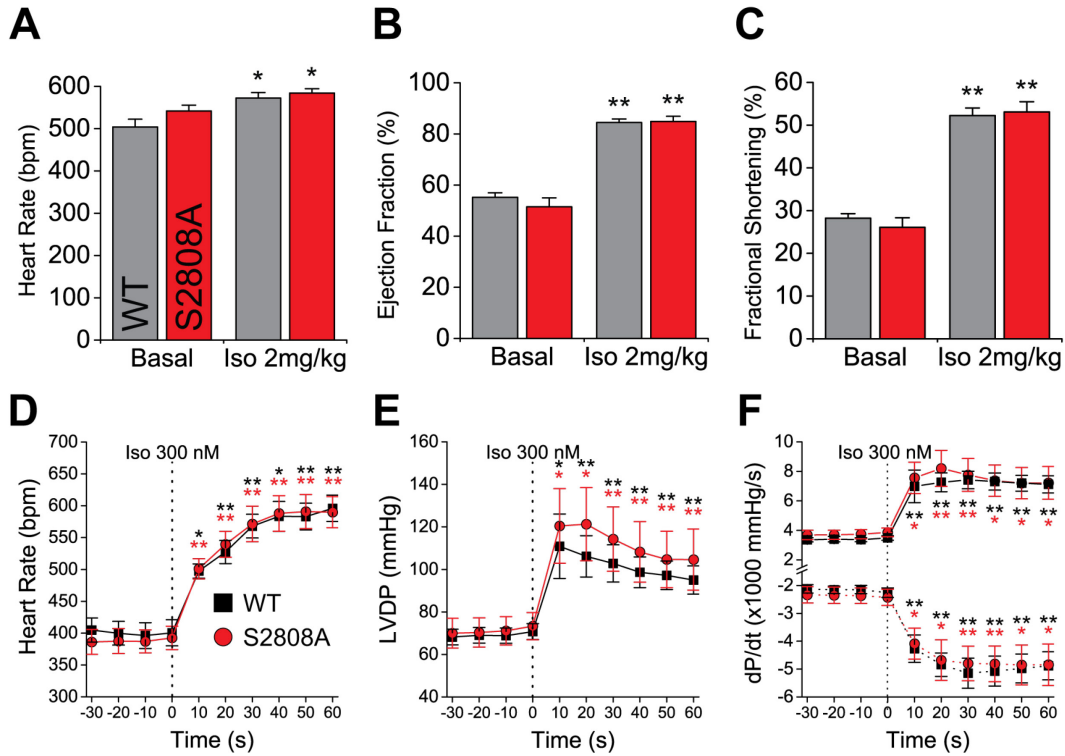


Figure 2.6. Cardiac Response to Adrenergic Stimulation in S2808A Mice and Isolated Hearts.

A-C. IP injection of isoproterenol (2 mg/kg) in anesthetized mice produces a significant increase in cardiac function, including heart rate (**A**), ejection fraction (**B**) and fractional shortening (**C**) (n = 6 per genotype; * p < 0.05, ** p < 0.01 vs. same genotype basal). **D-E.** Langendorff-perfused hearts stimulated with 300 nM Iso show a significant increase in heart rate (**D**), LV-developed pressure (LVDP, **E**) and dP/dt (**F**) (n = 5 per genotype; * p < 0.05, ** p < 0.01 vs. same genotype, as indicated by the color, at t = 0).

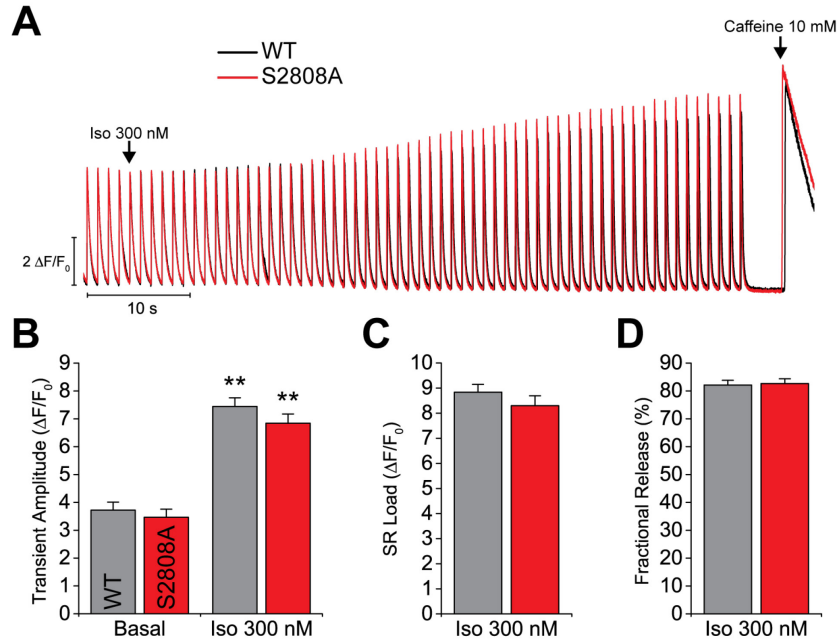


Figure 2.7. Ca^{2+} Transients and SR Ca^{2+} Load in S2808A Cardiomyocytes.

A. Representative traces of field stimulation-triggered Ca^{2+} transients. After obtaining a stable basal response, Iso 300 nM was perfused for 1 min, followed by a pulse of 20 mM caffeine to measure the SR Ca^{2+} load. **B.** Quantification of Ca^{2+} transient amplitude at basal conditions and with Iso stimulation. Both groups showed a significant response to Iso. **C-D.** Quantification of the SR Ca^{2+} load and fractional release (Ca^{2+} transient amplitude/SR Ca^{2+} load) under Iso stimulation. (N = 2 WT, 3 S2808A; n = 16 cells per genotype; ** p < 0.01 vs. same genotype basal).

Table 2.1. Echocardiographic Parameters to Assess HF Progression in S2808A Mice.

Structural and functional parameters measured in WT and S2808A mice at basal level and after induction of a myocardial infarction.

	Basal		1 week Post-MI		4 weeks Post-MI	
	WT	S2808A	WT	S2808A	WT	S2808A
n	9	9	9	9	9	9
BW (g)	22.3±0.7	24.6±1.2	22.2±1.0	24.4±1.4	23±1.2	25.3±1.5
HR (bpm)	476±21	539±13	484±21	563±15 [#]	485±23	582±19 ^{##}
IVSd (mm)	0.73±0.04	0.73±0.04	0.71±0.06	0.66±0.05	0.75±0.05	0.75±0.05
IVSs (mm)	1.05±0.06	1.06±0.06	0.94±0.07	0.93±0.09	1.02±0.07	1.05±0.05
IVSth (%)	44.3±4.3	44.3±4.2	34.8±6.0	40.2±5.8	36.5±4.1	41.6±6.3
PWd (mm)	0.76±0.04	0.75±0.04	0.67±0.04	0.62±0.06	0.73±0.04	0.75±0.07
PWs (mm)	1.06±0.04	1.08±0.05	0.86±0.07	0.77±0.08 [*]	0.96±0.05	0.96±0.07
PWth (%)	42.3±5.8	46.4±4.7	28.2±6.8	24.0±5.1 [*]	31.9±3.5	29.8±6.3
LVDd (mm)	3.92±0.09	3.82±0.10	4.78±0.24 [*]	4.68±0.31 [*]	5.21±0.2 ^{**}	5.21±0.29 ^{**}
LVDs (mm)	2.87±0.16	2.86±0.11	4.10±0.27 [*]	4.07±0.33 ^{**}	4.45±0.26 ^{**}	4.36±0.34 ^{**}
FS (%)	27.0±2.9	25.2±1.5	14.9±2.0 [*]	13.9±2.0 ^{**}	14.9±2.2 [*]	17.1±2.1 [*]
LVVd (uL)	67.1±3.6	63.4±3.8	104.8±14.1	106.9±16.6 [*]	132.2±11.3 ^{**}	131.8±18.0 ^{**}
LVVs (uL)	32.7±4.2	31.8±2.8	71.1±13.7 [*]	78.7±14.8 [*]	93.7±12.8 ^{**}	92.2±16.8 ^{**}
EF (%)	52.3±4.5	50.2±2.4	31.1±3.8 [*]	29.3±3.9 ^{**}	30.8±4.1 ^{**}	35.0±3.8 [*]
SV (uL)	34.4±2.5	31.5±1.9	33.7±3.4	28.2±3.2	38.5±4.8	39.6±3.4
CO (mL/min)	16.5±1.5	16.9±0.9	15.8±1.1	15.8±1.7	18.2±1.9	23.0±2.1
LVmass (% of BW)	0.47±0.04	0.40±0.03	0.59±0.04 [*]	0.47±0.03	0.72±0.04 [*]	0.65±0.06 ^{**}

BW: body weight; HR: heart rate; IVSd: interventricular septum thickness in diastole; IVSs: interventricular septum thickness in systole; IVSth: percent change in IVS between systole and diastole; PWd: posterior wall thickness in diastole; PWs: posterior wall thickness in systole; PWth: percent change in PW between systole and diastole; LVDd: left ventricle diameter in diastole; LVDs: left ventricle diameter in systole; FS: fractional shortening; LVVd: left ventricle volume in diastole; LVVs: left ventricle volume in systole; EF: ejection fraction; SV: stroke volume; CO: cardiac output; LVmass: left ventricle mass.

*: $p < 0.05$, **: $p < 0.01$ vs. same genotype basal, paired t-test.

#: $p < 0.05$, ##: $p < 0.01$ vs. WT at same time-point, one-way ANOVA.

Table 2.2. Echocardiographic Parameters to Assess the Adrenergic Response in S2808A Mice.

Structural and functional parameters measured in WT and S2808A mice at basal level and after IP injection of 2 mg/kg of Iso.

	Basal		Iso 2 mg/kg	
	WT	S2808A	WT	S2808A
n	6	6	6	6
BW (g)	24.0±1.8	25.8±1.6	-	-
HR (bpm)	504±18	542±14	572±13 *	584±10 *
IVSd (mm)	0.81±0.04	0.78±0.03	0.99±0.05 **	0.94±0.03 **
IVSs (mm)	1.20±0.04	1.16±0.05	1.60±0.05 **	1.51±0.04 **
IVSth (%)	47.3±2.5	49.7±1.6	61.9±5.0 *	60.5±3.1 *
PWd (mm)	0.83±0.02	0.85±0.05	0.95±0.03 **	0.92±0.03
PWs (mm)	1.12±0.03	1.14±0.07	1.47±0.07 **	1.49±0.04 *
PWth (%)	36.0±2.8	35.0±4.0	54.3±7.4 *	63.0±6.9 **
LVDd (mm)	3.77±0.10	3.86±0.09	3.00±0.10 **	3.09±0.15 **
LVDs (mm)	2.71±0.11	2.86±0.11	1.43±0.05 **	1.46±0.13 **
FS (%)	28.2±1.1	26.1±2.2	52.2±1.8 **	53.1±2.4 **
LVVd (uL)	61.3±3.8	64.9±3.5	35.3±2.8 **	38.4±4.9 **
LVVs (uL)	27.7±2.7	31.6±3.0	5.4±0.4 **	6.1±1.5 **
EF (%)	55.2±1.8	51.5±3.5	84.5±1.4 **	84.9±2.0 **
SV (uL)	33.5±1.2	33.3±2.7	29.9±2.7	32.4±3.6
CO (mL/min)	16.9±0.9	18.0±1.5	17.3±1.9	19.0±2.3

BW: body weight; HR: heart rate; IVSd: interventricular septum thickness in diastole; IVSs: interventricular septum thickness in systole; IVSth: percent change in IVS between systole and diastole; PWd: posterior wall thickness in diastole; PWs: posterior wall thickness in systole; PWth: percent change in PW between systole and diastole; LVDd: left ventricle diameter in diastole; LVDs: left ventricle diameter in systole; FS: fractional shortening; LVVd: left ventricle volume in diastole; LVVs: left ventricle volume in systole; EF: ejection fraction; SV: stroke volume; CO: cardiac output.

*: $p < 0.05$, **: $p < 0.01$ vs. same genotype basal, paired t-test

Table 2.3. Cardiac Function Parameters in Langendorff-perfused S2808A Hearts.

Functional parameters measured in isolated WT and S2808A hearts perfused in a Langendorff apparatus and stimulated with Iso 300 nM

	Basal (t = 0)		Iso 300 nM (t = 20 s)	
	WT	S2808A	WT	S2808A
n	6	6	6	6
HR (bpm)	400±21	393±18	527±18**	539±20**
ΔHR (%)	-	-	33.2±7.3	38.7±7.3
LVDP (mmHg)	70.7±3.7	73.3±6.4	106.1±9.7**	121.3±17.2*
ΔLVDP (%)	-	-	49.9±10.8	63.0±13.3
+dP/dt (mmHg/s)	3485±154	3862±298	7261±640**	8196±1220**
Δ+dP/dt (%)	-	-	106.5±10.5	108.9±23.2
-dp/dt (mmHg/s)	-2258±172	-2425±290	-4841±421**	-4679±730*
Δ-dP/dt (%)	-	-	113.6±7.6	100.1±27.2

HR: heart rate; LVDP: left ventricle developed pressure (LV pressure max–end-diastolic pressure).
 *: $p < 0.05$, **: $p < 0.01$ vs. same genotype basal, paired t-test

Table 2.4. Ca²⁺ Handling Parameters to Assess Adrenergic Response in isolated S2808A myocytes.

Ca²⁺ transient amplitude and SR Ca²⁺ load measured in basal conditions and with 300 nM Iso stimulation.

	WT	S2808A
Cells (n)	16	16
Mice (N)	2	3
[Ca ²⁺] _i transient amplitude basal (ΔF/F ₀)	3.72±0.29	3.47±0.29
[Ca ²⁺] _i transient amplitude 300 nM Iso (ΔF/F ₀)	7.45±0.31**	6.84±0.33**
SR Ca ²⁺ Load (ΔF/F ₀)	8.84±0.31	8.30±0.40
Fractional release (%)	84.33±2.01	82.65±1.70

** $p < 0.01$ vs. same genotype basal, paired t-test.

CHAPTER 3

RyR2 Haploinsufficiency is Compensated by Fine-tuning Channel Activity Through Phosphorylation

3.1. Introduction

Ryanodine Receptors (RyRs) are the largest ion channels known to date. RyR2, the cardiac isoform, releases Ca^{2+} from the sarcoplasmic reticulum (SR) after being activated by a small inward Ca^{2+} current (I_{CaL}) mediated by L-type Ca^{2+} channels (LTCC). This is the underlying mechanism of excitation-contraction (e-c) coupling, the process that transduces action potentials into mechanical contraction in the heart. Ca^{2+} released from the SR via RyR2 binds to the myofilaments producing contraction. Relaxation is achieved when Ca^{2+} is re-sequestered into the SR through the SR Ca^{2+} pump (SERCA2a) or extruded out of the cell through the electrogenic $\text{Na}^+/\text{Ca}^{2+}$ exchanger (NCX).³

Altered expression and function of many of these proteins have been observed in different forms of human heart disease.^{99,129} Increased expression of NCX and decreased expression of SERCA2a, for example, promote depletion of the Ca^{2+} stored in the SR during heart failure (HF).⁹⁵ This, in turn, is associated with contractile dysfunction. Moreover, bursts of sympathetic activity due to physical and emotional stress can lead to SR overload and spontaneous Ca^{2+} release.^{97,147} Ca^{2+} is then extruded from the cell by NCX, depolarizing the cell and potentially leading to spontaneous APs during diastole (delayed afterdepolarizations or DADs). In this context, RyR2 has been under scrutiny

because studies do not agree on whether its regulation by phosphorylation is important for the onset and progression of HF.⁵⁸ Nevertheless, there is consensus that RyR2 phosphorylation at S2814 by CaMKII increases SR Ca²⁺ leak and this can be pathogenic. Interestingly, several reports in the literature also indicate that expression of RyR2 is decreased in some forms of human heart disease,^{92,99,100,129,130} and in animal models of HF.^{121,148,149}

What is the contribution of decreased RyR2 expression to the pathology of heart disease? To date, there is no clear answer to this question due to the simple fact that no studies have addressed it thoroughly. Nevertheless, there is solid experimental support for the idea that RyR2 dysfunction due to specific mutations is deleterious to cardiac function. Gain-of-function RyR2 mutations are the culprits in catecholaminergic polymorphic ventricular tachycardia (CPVT), a severe inherited arrhythmia in which Ca²⁺ handling dysfunction is the underlying mechanism. On the other side of the spectrum, a loss-of-function RyR2 mutation recently characterized by our laboratory also produces Ca²⁺ mishandling and arrhythmia in mice.⁸⁹ Therefore, RyR2 regulation in a cardiac myocyte requires a fine balance in which too much or too little RyR2 activity is deleterious. Interestingly, two studies reporting a constitutive decrease of RyR2 expression in mice — presumably leading to loss of RyR2 function — did not report harmful phenotypes.^{120,121} Conditional knockout of RyR2 (cRyR2-KO) in adult mice, on the other hand, produces malignant ventricular arrhythmias and eventually death,¹⁵⁰ while heterozygous cRyR2-KO decreases glucose metabolism without grossly affecting cardiac function.¹⁵¹ These data suggest that RyR2 deficiency can be compensated in the heart without evident adverse effects, while complete suppression of RyR2 is catastrophic. All these studies

have been performed using a mouse model. However, cardiac e-c coupling is considerably different between mouse and human, with the SR contributing 90% and 70% of the total Ca^{2+} required for contraction, respectively.³

In this study, we used a constitutive RyR2-KO rabbit model to determine the cardiac effects of decreased RyR2 channel expression. Using a rabbit model gives the important advantage of a species with cardiac physiology closer to human. We observed that homozygous RyR2 deletion in rabbits is embryonic lethal, as is the case in mice. Heterozygotes, on the other hand, show RyR2 haploinsufficiency without an overt phenotype. Further study of these animals allowed for the dissection of the mechanisms that compensate for the lower RyR2 expression. We found that when RyR2 expression is significantly decreased, channel activity is likely upregulated by reducing the basal phosphorylation of the S2031 site, which is mediated by increased association of RyR2 with PP2A. Therefore, upregulation of channel function may offset the effect of lower expression of the protein. These results suggest that a decrease in RyR2 expression observed in different forms of heart disease is not likely pathogenic in and of itself. Most importantly, these data provide novel insights into the regulatory mechanisms of RyR2 via phosphorylation of S2031. This poorly-studied site is often ignored in models of RyR2 regulation; however, these data should prompt the development of more comprehensive models of RyR2 regulation involving all phosphorylation sites known to date and the potential important roles on phosphatase-mediated regulation of RyR2.

3.2. Results

3.2.1. Genetic Characterization of RyR2-KO Rabbits.

For this work, we took advantage of an RyR2-KO rabbit model generated by Center for Advances Models and Translational sciences and Therapeutics (CAMTraST) at the University of Michigan.¹⁵² The model was developed using Crispr/Cas9 endonuclease genome editing and contains a 16 bp deletion in exon 49. This KO allele encodes a normal RyR2 sequence until residue 2462, after which there are 34 scrambled amino acids followed by a termination codon (Figure 3.1 **A**, Figure 3.2). Several more termination codons appear downstream of this position (not shown). Since the PFD of the channel is located at the C-terminal end of the protein (residues 4486–4469), the mutant allele does not encode functional channels. Figure 3.1 **B** shows the offspring distribution obtained from mating heterozygous RyR2-KO rabbits. We have not detected homozygotes ($\chi^2 = 39.96$, $p = 2.4 \times 10^{-6}$, $n = 118$ kits), suggesting that complete lack of RyR2 is embryonic lethal. These data are consistent with previous studies using mice.¹⁵³ Hence, for all the experiments discussed in the following sections, we took advantage of the heterozygous RyR2-KO rabbits (Het), which we obtained in the expected Mendelian ratio.

3.2.2. Assessment of RyR2 Expression and Phosphorylation

The KO allele encodes a product of 2496 amino acids. This protein, which is unable to assemble functional channels, could associate with and destabilize channels properly assembled from the WT allele. We used Western blots (WB) to determine whether the KO allele was being translated into protein. The commercial antibody used for the RyR WB recognizes an epitope corresponding to residues 2722–2769 of RyR2,^{154,155} present

in the full-length but not the truncated RyR2. This antibody also reacts with the other RyR isoforms, RyR1 and RyR3. Hence, we took advantage of the S2031 phosphorylation site, present in both WT and KO proteins (Figure 3.3 **A**), to determine the fate of the product of the KO allele. Since the phosphorylation level of S2031 (pS2031) is low at basal conditions, we used an antibody that recognizes only the dephosphorylated (dpS2031) site. As shown in Figure 3.3 **A**, only a single band was detected with this antibody at the size of the full-length RyR2 (~500 kDa). This indicates that the product of the KO allele is probably absent in Het hearts likely because of premature degradation or because the mutant allele is silent.

We observed a nearly 60% decrease in RyR expression in Het hearts, using RT-PCR to measure *RYR2* gene transcript level (WT 100.0±7.9% vs. Het 43.0±7.1%, $p = 0.0014$; Figure 3.3 **B**) and WBs to detect total protein (WT 100.0±11.6% vs. Het 38.6±6.8%, $p = 0.0011$; Figure 3.3 **C**). These data show that Het rabbits have RyR2 haploinsufficiency. The close agreement between gene (*RYR2*) and protein (RyR) expression suggests that the KO allele is *silenced* and that other RyR isoforms do not compensate for RyR2 deficiency in Het KO hearts. Remarkably, the RyR2 level is well below the expected 50%, suggesting that a single functional allele is insufficient to provide half of the expected protein expression. Since phosphorylation is the best known post-translational modification of RyR2, we also measured the phosphorylation level of the three characterized sites in RyR2 as a ratio of the level of phosphorylation to the total RyR2 expression. While pS2809 (Figure 3.3 **F**) and pS2815 (Figure 3.3 **G**) were not altered, we observed a 52% increase in the dpS2031 level (WT 100.0±8.3% vs. Het 152.0±19.0%, $p = 0.035$; Figure 3.3 **D**). Basal phosphorylation of this site is low (see

section 1.4.3), making it difficult to detect using a *phospho-specific* antibody; however, prolonged incubation with the antibody allowed us to quantify a ~60% decrease in basal phosphorylation (WT 100.0±22.4% vs. Het 39.8±13.9%, $p = 0.045$; Figure 3.3 **E**). Although the signal to noise ratio of this blot is low, it agrees with the *dephosphorylation* level of the residue. These data indicate that the phosphorylation of RyR2 is downregulated in Het KO hearts. This could be a possible compensatory mechanism for RyR2 deficiency.

3.2.3. Cardiac Structure and Function

Next, we tested whether Het rabbits develop a structural or functional cardiac phenotype because of the lower RyR2 expression. Macroscopically, there were no evident differences in the size and morphology of Het hearts (Figure 3.4 **A**, upper panel). Also, histological staining of left atrium and left ventricle (LV) sections of Het hearts did not show significant alterations in the microarchitecture of the cardiac tissue nor evidence of fibrosis, and display normal myocyte size and arrangement (Figure 3.4 **A**, middle and lower panels). M-Mode echocardiography in anesthetized rabbits showed no significant differences in functional parameters such as fractional shortening (FS; Figure 3.4 **B**) and ejection fraction (EF; Figure 3.4 **C**), or in structural parameters including posterior wall (Figure 3.4 **D**) and septal wall thicknesses (Figure 3.4 **E**). The heart rate (HR; Figure 3.4 **F**) and LV mass (Figure 3.4 **G**) were also not altered. A more detailed analysis of additional echocardiographic parameters is shown in Table 3.1. Interestingly, we only observed a decreased septal wall thickness in Het rabbits. This change, which could indicate mild systolic dysfunction, also leads to a non-significant tendency toward lower percent change in septal thickness between systole and diastole. However, since we also

observed normal EF, SV, and cardiac output (CO), we conclude that the overall cardiac function in Het rabbits is normal. Overall, these data suggest that both basal structure and function of the heart are preserved, even in rabbits with RyR2 deficiency. These data suggest that there is a considerable amount of non-essential RyR2 expressed in normal hearts and that cellular and sub-cellular compensatory mechanisms might be triggered to prevent the development of a whole-organ functional phenotype.

3.2.4. Expression of E-C Coupling Proteins

One possible compensatory mechanism could involve changes in the expression of proteins that participate in e-c coupling. These proteins contribute to Ca²⁺ handling during the cardiac cycle and functionally couple with RyR2 to produce the whole-cell Ca²⁺ transient required for contraction. We observed no differences in the expression of Ca_v1.2 (pore-forming subunit of LTCC; Figure 3.5 **B**), NCX (Figure 3.5 **C**), or SERCA2a (Figure 3.5 **D**) in Het KO rabbit hearts compared to WT. The expression of phospholamban (PLB), an inhibitor of SERCA2a, was also unchanged (Figure 3.5 **E**). Finally, no changes were observed in the phosphorylation level of PLB (Figure 3.5 **F-G**). These data suggest that Het hearts do not show significant changes in the expression or function of major Ca²⁺-handling proteins other than RyR2. Furthermore, the unchanged phosphorylation level of PLB suggests that the basal adrenergic tone of Het rabbits is not significantly different than that of WTs.

3.2.5. Assessment of RyR2 Activity

As mentioned before, the assumption that lower RyR2 expression necessarily means lower RyR2 function could prompt a hypothesis suggesting that RyR2 deficiency is deleterious as in the case of loss-of-function mutations. To investigate this possibility,

we used [³H]ryanodine binding experiments to assess RyR2 activity in LV homogenates. The raw [³H]ryanodine binding was ~34% decreased in Het samples (WT 28.91±2.99 fmol/mg of total protein vs. Het 19.14±2.02 fmol/mg of total protein, $p = 0.0211$; Figure 3.6 **A**), as expected from the lower RyR2 expression. Remarkably, there is an evident discrepancy between the RyR2 expression level (~40% of WT) and the [³H]ryanodine binding (~66% of WT) in heterozygous hearts. We found that maximum [³H]ryanodine binding normalized to RyR2 density has a ~2-fold increase in Het samples (WT 29.58±2.28 fmol/mg of total protein vs. Het 56.45±8.34 fmol/mg of total protein, $p = 0.018$; Figure 3.6 **B**). This suggests that, although RyR2 is less abundant, the activity of the remaining channels is increased in Het hearts. Interestingly, the corrected [³H]ryanodine binding had a significant linear relationship with dephospho-S2031 level (Figure 3.6 **C**), suggesting that phosphorylation of this site correlates with channel activity. Finally, we observed no change in RyR2 sensitivity to Ca²⁺, as shown by the superimposable curves normalized to 10 μM [Ca²⁺] (EC₅₀: WT 1.05±0.03 μM vs. Het 1.05±0.09 μM, $p = 0.95$; Figure 3.6 **D**). Hence, RyR2 channels from Het rabbits have higher maximum response to activating [Ca²⁺] without a change in affinity.

3.2.6. Association of RyR2 with Protein Phosphatases

Two phosphatases are known to associate with RyR2: PP1 and PP2A.⁴⁰ Recently, the binding of both enzymes to RyR2 channels from a transgenic rabbit model of long QT syndrome 2 (LQTS2) was found to be increased, thereby affecting the phosphorylation level of the channel.^{156,157} To gain a better understanding of the mechanisms underlying the lower phosphorylation level of S2031, we used WBs and co-immunoprecipitations to measure the total expression of PP1 and PP2A in LV homogenates, together with the

level of RyR2-bound phosphatases. The total expression of both PP1 and PP2A was not different between WT and Het rabbits (Figure 3.7 **B-C**); however, immunoprecipitated RyR2 channels had higher PP2A content than WT (WT $100.0 \pm 9.5\%$ vs. Het $134.2 \pm 9.9\%$ of WT, $p = 0.03$; Figure 3.7 **D**). In contrast to previous reports,¹⁵⁷ we detected no PP1 associated with RyR2 (Figure 3.7 **A**). Therefore, it is likely that PP2A is responsible for maintaining S2031 at a lower phosphorylation level in Het hearts and causing the channels to be more active.

3.2.7. Adrenergic Response of Isolated Hearts

To determine whether RyR2 haploinsufficiency affects the adrenergic response of the rabbit hearts, we used echocardiograms during IV infusion of $0.5 \mu\text{g}/\text{kg}/\text{min}$ Iso. To ensure a stable response, measurements were taken after 15 min of continuous IV infusion. In basal conditions, we did not observe significant differences between Het and WT rabbits in any of the parameters measured. As expected, we detected a significant increase in HR (Figure 3.8 **A**), EF (Figure 3.8 **B**), and FS (Figure 3.8 **C**) after Iso — all indicators of a strong inotropic and chronotropic response (Table 3.3). However, there was no difference between the response of WT and Het rabbits, suggesting that the latter have preserved adrenergic function *in vivo*. Furthermore, the basal difference we observed in septal wall thickness during diastole in Het rabbits (see section 3.2.3) was not evident during Iso. Moreover, the percent change in septal thickness between systole and diastole was significantly increased in Het rabbits after Iso compared to basal conditions. None of the rabbits presented ventricular arrhythmias during the echocardiographic measurements.

To complement these results and to remove neurohormonal and hemodynamic regulation of the heart — autonomous nervous system and preload, respectively — we used Langendorff perfusions of isolated hearts. After stabilization of the baseline recording at a constant maximum LV-developed pressure (LVDP), the hearts were perfused with 100 nM Iso. Both groups showed a rapid and significant increase in HR (Figure 3.8 **D**) and LVDP (Figure 3.8 **E**) with Iso stimulation. HR remained elevated throughout the experiment, while LVDP peaked within 10 seconds of the onset of the Iso response and stabilized at a lower value that was still significantly higher than baseline LVDP. Overall, the response to Iso was comparable between groups (Table 3.3), suggesting that RyR2 deficiency does not grossly impair the adrenergic response of the heart. Nevertheless, there is an overall non-significant tendency for decreased LVDP (the difference was only significant at two time-points). Furthermore, the velocity of contraction and relaxation (dP/dt ; Figure 3.8 **F**, Table 3.3) was significantly lower in Het hearts at the onset of the Iso response, with the lower contraction velocity manifesting at several time-points. These data indicate that, although LVDP is preserved, pressure development is slower in Het hearts perhaps due to a slower Ca^{2+} release or to a change in the Ca^{2+} affinity of the myofilaments. Also, the comparable baseline and Iso-stimulated LVDPs between Het and WT isolated hearts suggest that two possible compensatory mechanisms for RyR2 haploinsufficiency present in whole animals but not isolated hearts — (1) an increased basal adrenergic tone that normalizes contractility and (2) increased end-diastolic filling that normalizes contractile force in Het hearts via a Starling effect — are not likely responsible for normalizing cardiac function in Het rabbits. Lastly, the lack of significant differences in basal and Iso-stimulated heart rates in both whole rabbits and

isolated hearts suggests that RyR2 haploinsufficiency may not affect the Ca²⁺-mediated component of the coupled clock regulating automaticity in the sinus node or the clock's response to Iso stimulation.

3.2.8. Cellular Ca²⁺ Handling

Next, we assessed Ca²⁺ handling in isolated LV myocytes using confocal line scans of fluo-4AM-loaded cells paced at 0.5 Hz. After a train of 20 stimulations, a pulse of 20 mM caffeine was applied to measure SR load (Figure 3.9). First, the Ca²⁺ transient amplitude was comparable between WT and Het myocytes in basal conditions and with 50 nM Iso (Figure 3.10 **A**). This result is in agreement with the results described above from whole animals and isolated hearts undergoing Iso treatment. Remarkably, the time to reach the peak of the Ca²⁺ transient was prolonged in Het cells stimulated with Iso (Figure 3.10 **B**), suggesting that the increased dP/dt we measured in isolated Het hearts is a result of slower Ca²⁺ release rather than a change in the Ca²⁺ sensitivity of the myofilaments. This also suggests that, while the Ca²⁺ transient amplitude release is apparently preserved, haploinsufficiency seems to affect the recruitment of RyR2 channels during Iso stimulation. Based on the comparable expression of SERCA2a, NCX, and PLB, as well as the similar phosphorylation level of PLB between WT and Het (section 3.2.4 and Figure 3.5), we did not expect differences in cytosolic Ca²⁺ removal. Indeed, the 50% decay time of the Ca²⁺ transient was not different between genotypes (Figure 3.10 **C**). We also determined that the SR load was not significantly different WT and Het cells; yet, Iso did not induce an increase in SR load in either group (Figure 3.10 **D**). This observation is at odds with previous literature using rabbit myocytes^{20,157} and with the expected effects of adrenergic stimulation in the heart (section 1.3). One possible

explanation is that our studies were carried out at room temperature, while other groups have measured the Iso response at 37 °C.¹⁵⁷ It is important to consider, however, that the increase in transient amplitude (Figure 3.10 **A**), decrease in time-to-peak (Figure 3.10 **B**), and transient decay acceleration (Figure 3.10 **C**) confirm the adrenergic response to Iso. Then, the increase in I_{CaL} produced by Iso — which we have yet to quantify — may be driving the surge in Ca^{2+} release without overloading the SR. Indeed, we observed that the fractional release of Ca^{2+} is significantly increased in both WT and Het myocytes during Iso stimulation (Figure 3.10 **E**). Interestingly, this value was slightly but significantly lower in Het cells.

3.2.9. Arrhythmia Susceptibility

Up to this point, we have established that heterozygous KO of RyR2 in rabbits does not produce a deleterious phenotype under basal conditions, and that higher RyR2 activity likely compensates for the observed decrease in expression. Next, we studied the response of RyR2-KO rabbits to adrenergic stress. We began by testing the susceptibility of anesthetized rabbits to ventricular arrhythmia. Initially, we tried a less aggressive protocol than that used in mice (see section 4.4.5), using only 2 mg/kg epinephrine IP; however, WT rabbits died after episodes of ventricular tachycardia followed by severe bradycardia and apnea (not shown). Decreasing the dose of epinephrine or changing the administration route to intravenous (IV) produced variable results, ranging from short adrenergic responses to high mortality in WT animals (not shown). The powerful vasoconstriction effect of epinephrine was always evident, as rabbits became cyanotic shortly after injection. Because dobutamine is used in human patients during echocardiogram stress tests,¹⁵⁸ we decided to take advantage of the drug's strong

inotropic and weak vasoactive effects. We tested different IV infusion rates and settled upon 80 $\mu\text{g}/\text{kg}/\text{min}$: a dose two-fold higher than the maximum used in humans.¹⁵⁸ This dose was well-tolerated in WT rabbits and provided enough resolution between heartbeats to measure ECG parameters accurately (Figure 3.11). A higher dose of 100 $\mu\text{g}/\text{kg}/\text{min}$ produced fusion of the T wave with the following P wave (not shown).

Caffeine has been reported to potentiate arrhythmias in rabbits exposed to hazardous chemicals;¹⁵⁹ therefore, we added it to the arrhythmia protocol. Considering the pharmacokinetics of caffeine (half-life 3.8 h, clearance of 0.2 L/kg/min and distribution volume of 0.82 L/kg¹⁶⁰), we surmised that it would take approximately 27 h for caffeine to reach a steady plasma concentration during IV infusion, assuming caffeine follows single-compartment pharmacokinetics. To overcome this issue, we used the following protocol: a loading dose of 9 mg/kg caffeine IV, followed by infusion of 28 $\mu\text{g}/\text{kg}/\text{min}$ caffeine and 80 $\mu\text{g}/\text{kg}/\text{min}$ dobutamine. The half-life of dobutamine is as short as 2 min; thus, it would take approximately 15 min to reach a steady plasma concentration. We observed a maximum increase in HR within 30 min of initiating treatment. After this, the IV infusion was maintained for 30 additional minutes to test arrhythmia susceptibility. During this time, the ECG showed little change and neither WT nor Het rabbits developed ventricular arrhythmia. Furthermore, all ECG parameters measured at baseline and at the peak HR response were comparable between WT and Het rabbits (Table 3.2). From these experiments, we can conclude that RyR2 haploinsufficiency is not expected to predispose rabbits to cardiac arrhythmias even under acute adrenergic stress.

3.3. Discussion

In this study, we report a thorough characterization of the *first rabbit model* with genetic targeting of the *RYR2* gene, specifically a constitutive gene knock out created by Yan et al.¹⁵² using CRISPR/Cas9 technology. The rabbit is a classical model to study cardiac pathophysiology, but targeted genome editing in this species is a recent breakthrough. Until recently, genetic manipulation of rabbits was limited to transgenic overexpression of exogenous genes, such as human HERG channels with a dominant-negative mutation associated with long QT syndrome (LQTS).^{156,157} The newly-developed technique to manipulate endogenous genes in rabbits, on the other hand, offers the same versatility as in the mouse but in a species with cardiac Ca^{2+} handling and electrophysiology more similar to that of the human. To create the rabbit model used in this study, Yan et al. introduced a 16 bp deletion in exon 49 of *RYR2*, changing the reading frame of the gene and truncating RyR2 synthesis before the pore-forming domain. Hence, the mutant allele works as a knock-out allele.

RyR2-KO animals have been the subject of a handful of studies since 1998, when Takeshima et al.¹⁵³ described that constitutive RyR2-KO in mice is also embryonic lethal. In that report, the authors detected contractions of the developing heart at embryonic day E9.5 — suggesting that RyR2 is not essential for the embryonic heart to contract — but RyR2-KO embryos showed vacuolization of the SR and died after embryonic day E10.5. These ultrastructural abnormalities resembled those observed in the skeletal muscle of RyR1-KO and RyR1/RyR3 double-KO mice.^{161,162} However, these animals died perinatally due to respiratory failure, rather than *in utero*. Later, Zou et al. reported lower RyR2 expression in Het KO mice and a lack of an abnormal basal phenotype.¹²¹ Broun

et al., on the other hand, showed that conditional knockout (cKO) of RyR2 in adult mice results in a progressive decline of cardiac function and eventually death,¹⁵⁰ while heterozygous cKO mice only showed reduced heart rate and oxidative metabolism.¹⁶³ Hence, complete lack of RyR2 is lethal, while haploinsufficiency is well-tolerated. Indeed, we determined that homozygous RyR2-KO is also embryonic lethal in rabbits and heterozygous animals have significantly lower expression of RyR2 in the left ventricle (~40% of WT). Then we used a multi-level approach to determine whether RyR2 haploinsufficiency alters cardiac function in rabbits, and the possible underlying mechanisms.

We determined that in basal conditions (1) Het rabbits have normal cardiac structure and function; (2) Het hearts develop the same contractile force as WT hearts; and (3) Ca²⁺ homeostasis is not altered in Het cardiomyocytes. To explain the lack of an abnormal phenotype, we looked at the possible compensatory mechanisms involved. Remarkably, while Het KO hearts showed ~60% lower RyR2 expression — suggesting that a single functional allele is unable to provide half of the protein expression — the remaining RyR2 channels had ~2-fold higher activity than in WT hearts. Therefore, RyR2 deficiency is possibly compensated, at least partially, by an upregulation of channel function. Our data indicate that this is most likely mediated by decreased phosphorylation of S2031 due to enhanced association of PP2A with RyR2. It is important to note that, even though PP1 is also reported to co-immunoprecipitate with RyR2, we did not detect it in our experiments possibly due to a weaker association disrupted during the procedure. Therefore, we cannot discard the possibility that RyR2-bound PP1 is also changed in Het rabbits.

Interestingly, the mechanism above represents the exact opposite of that described in the LQTS rabbits, where lower association of phosphatases with RyR2 increased RyR2 phosphorylation, resulting in abnormal Ca^{2+} release and enhanced arrhythmogenesis.¹⁵⁷ This mechanism agrees with the prevalent idea in the field: more RyR2 phosphorylation promotes increased channel activity, a notion coming from nearly two decades of reports arguing that increased phosphorylation of the two main sites in RyR2 — S2809 and S2815 — produces “leaky” channels that contribute to different forms of heart disease including heart failure,^{53,60} hypertrophic cardiomyopathy,⁹⁹ and even diabetic cardiomyopathy.¹⁶⁴ Nevertheless, there is evidence in the literature suggesting that *dephosphorylation* of RyR2, as we observed in Het hearts, also increases channel activity. Lokuta et al. showed that dephosphorylation of cardiac SR vesicles using acid phosphatase increases the maximum [³H]ryanodine binding and open probability of single RyR2 channels.⁶⁵ Also, Terentyev et al. showed that perfusion of permeabilized rat cardiomyocytes with PP1 increases Ca^{2+} spark frequency and depletes SR Ca^{2+} , a reliable indicator of RyR2 activity.⁶⁶ Moreover, ablation of both S2809 and S2815 phosphorylation sites in a mouse model (S2808A/S2814A, as per the mouse nomenclature), increases Ca^{2+} leak and promotes arrhythmia,¹⁶⁵ probably due to higher RyR2 activity. Together, these reports suggest that both phosphorylation and dephosphorylation of RyR2 may increase channel activity.

At the single channel level, the increase in RyR2 activity we detected using [³H]ryanodine binding experiments must translate into increased open probability. While we did not test this hypothesis, the study by Lokuta et al. reported that dephosphorylated RyR2 has higher open probability due to increased mean open time and opening

frequency.⁶⁵ Hence, the population of RyR2 channels in Het hearts would be able to maintain a normal Ca^{2+} release upon activation by I_{CaL} by decreasing the inactivation time within the timeframe of SR Ca^{2+} flux (up to ~150 ms after activation¹⁶⁶), thus decreasing the refractory period. Indeed, we observed normal Ca^{2+} transient amplitude in Het cardiomyocytes. Previous studies showed that acute pharmacological modulation of RyR2 activity only produces transient changes in Ca^{2+} release with the SR load having a prominent compensatory role.¹⁶⁷⁻¹⁶⁹ Hence, if RyR2 channel activity is acutely reduced — e.g. using tetracaine — systolic Ca^{2+} release will decrease transiently and will recover after the SR load stabilizes at a higher level. Following the same logic, a higher SR Ca^{2+} load could compensate for a lower RyR2 expression, hindering the appearance of a deleterious whole-organ phenotype. Since we measured a comparable basal SR load in WT and Het myocytes, we conclude that modulation of the SR load does not contribute to maintain Ca^{2+} homeostasis in haploinsufficient hearts.

Our results indicate that decreased S2031 phosphorylation may contribute to compensate for RyR2 deficiency in Het rabbits by increasing channel activity, while the phosphorylation level of S2809 and S2815 remains unchanged. S2031 is a phosphorylation site often ignored in the overall scheme of RyR2 regulation.⁵¹ The low basal phosphorylation of this site and initial reports suggesting it is not phosphorylated by PKA — making it irrelevant for the adrenergic response⁵³ — relegated this site to a lower tier than S2809 and S2815. However, S2031 *is* readily phosphorylated by PKA *in vitro* and upon adrenergic stimulation with a high dynamic range (~16-fold increase).^{13,61,62} Correspondingly, S2809, regarded by many researchers as the *only* PKA site in RyR2 and essential for the adrenergic response, has only a 2-fold dynamic range upon Iso

stimulation.¹³ We cannot overlook the fact that S2031 phosphorylation level is low. Then, how does decreasing it further increase channel activity? To fully answer this question, we need more information from animal models with amino acid substitutions ablating (S2031A) or mimicking phosphorylation (S2031D). Interestingly, preliminary data generated in our laboratory show that S2030A mice (as per the mouse nomenclature) develop severe hypertrophy, confirming that phosphorylation of this site, albeit low, is necessary to maintain normal heart homeostasis. The underlying mechanisms for the phenotype of the S2030A mouse model have yet to be elucidated.

We have established so far that the heterozygous ablation of RyR2 does not induce a deleterious basal phenotype. Now, we must consider the response of RyR2 haploinsufficient rabbits to acute adrenergic stimulation. Overall, the adrenergic response was preserved in Het rabbits. Iso induced a comparable increase in ejection fraction and fractional shortening in anesthetized animals, pressure development in isolated hearts, and Ca^{2+} transient amplitude in isolated ventricular myocytes. Stimulation of β -adrenergic receptors (β -ARs) with Iso prompts activation of protein kinase A (PKA), which phosphorylates several targets, including LTCC, PLB (a regulator of SERCA2a) and, most importantly for this discussion, RyR2. This creates an apparent paradox, because PKA phosphorylates S2031 upon activation of β -AR but we postulate that decreased phosphorylation compensates for the lower RyR2 expression. One possible explanation is that the increase in I_{CaL} produced by Iso because of LTCC phosphorylation offsets the overall effect of RyR2 phosphorylation under Iso. Indeed, Ginsburg and Bers determined that the main drivers for the augmented Ca^{2+} release during Iso stimulation are I_{CaL} and SR load,⁶³ while RyR2 phosphorylation only accelerated Ca^{2+} release kinetics.

Interestingly, isolated Het hearts showed slower pressure development immediately after Iso (Figure 3.8) and isolated myocytes showed delayed Ca^{2+} transient time-to-peak compared to WT (Figure 3.10). Altogether, these data suggest that a ~40% RyR2 expression is enough to sustain normal Ca^{2+} , but affects the rate of release during Iso stimulation. Finally, Fu et al. recently reported that RyR2 phosphorylation prompts reorganization of the channels within the dyadic cleft.¹⁷⁰ Unfortunately, we have not performed ultrastructural studies to determine the extent to which RyR2 deficiency affects the number of Ca release units (CRUs) or the content of RyR2 within the CRU. Still, we hypothesize that the microdomain reorganization proposed by Fu et al. is preserved because RyR2 channels from Het rabbits can be phosphorylated in the three phosphorylation sites. Nevertheless, the issue would be with the number of channels recruited.

To conclude, we must consider the pathophysiological relevance of decreased RyR2 expression. Our data suggest that lower RyR2 expression is not a trigger for overt cardiac dysfunction, even in the presence of acute adrenergic stimulation; hence, it is unlikely to contribute to the pathology of HF and HCM. The Genome Aggregation Database (gnomAD)⁸³ — which contains data from over 123,000 human exomes — reports 27 *RYR2* variants (allele frequency of $\sim 1 \times 10^{-4}$) that introduce termination codons before the pore-forming domain of RyR2. Since these variants are equivalent to our rabbit model, it is reasonable to hypothesize that these individuals have lower RyR2 expression as well. Our data provides strong experimental support to classify these truncation variants as benign. Exon 3 deletion in *RYR2*, on the other hand, a mutation potentially associated with stress-induced arrhythmia (CPVT)⁸¹ and structural cardiomyopathy,¹¹⁵

produces haploinsufficiency in a mouse model. Lui et al. argued that the lack of abnormal phenotype was because the mutant allele was silenced, and mouse hearts only expressed the WT allele.¹²⁰ If exon 3 deletion is indeed pathogenic in humans, our data indicate that this is unlikely a result of haploinsufficiency.

In summary, our data show that RyR2 haploinsufficiency — which likely involves fewer RyR2 channels per CRU, fewer CRUs overall or a combination thereof — is compensated at basal conditions, at least partially, by decreasing the phosphorylation level of S2031 and upregulating channel activity (Figure 3.12). This prevents the appearance of deleterious phenotypes. Furthermore, the adrenergic response is preserved in these animals, but the Ca²⁺ release kinetics is significantly slower with low RyR2 expression. Het rabbits showed RyR2 expression levels ranging from 15–69% of the average expression in WT animals, in which the range was 63–150%. Since we also established that complete lack of RyR2 is lethal, then how much RyR2 expression is enough and how much is too little? These are tantalizing questions that will require further study.

3.4. Methods

3.4.1. General Considerations

All animal experiments were approved by the University of Michigan Institutional Animal Care and Use Committee. All experiments performed at institutional cores were single blind. Unless otherwise stated, all reagents were acquired from Sigma-Aldrich.

3.4.2. Generation of the RyR2-KO Rabbit Model

RyR2 knockout rabbits (RyR2-KO) were generated by the Center for Advanced Models and Translational Sciences as previously published.¹⁵² Two KO founders carrying different genetic mutations in *RYR2* were initially used: Founder 6 with a 16 bp deletion (KO allele) and a 12 bp insertion, each in a different allele, and Founder 7 with an 11 bp deletion. These founders were mated and several preliminary experiments were conducted with the offspring. Figure 3.1B summarizes the offspring yield of this mating, in which rabbits carrying both KO alleles were never identified (defined as homozygous KO rabbits or Homo). It is important to note that following Mendel's Law of Segregation, the 12 bp insertion from Founder 6 was inherited by all rabbits labeled as "WT" in Figure 3.1 B, as well as those heterozygotes that inherited the KO allele from Founder 7. This 12 bp insertion results from an in-frame insertion of 4 amino acids into RyR2. Therefore, we carefully selected only those rabbits carrying the KO allele from Founder 6 and a WT allele (data not shown). These rabbits were further mated with New Zealand White rabbits to continue the colony and provide the experimental animals. All data shown in this chapter, except for Figure 3.1 B were gathered using Het rabbits carrying the KO allele from Founder 6.

3.4.3. Tissue Homogenization

Rabbits were heparinized (1000 U/kg, Sagent Pharmaceuticals), sedated with 30 mg/kg ketamine (VETOne) and 5 mg/kg xylazine (Akorn Animal Health), and fully anesthetized with 10 mg/kg propofol (Abbott). The heart was quickly excised, cleaned, section into major regions and flash frozen in liquid nitrogen. Left ventricle homogenates were prepared as described in section 2.4.6 using 1 mL of homogenization buffer per 200 mg of tissue.

3.4.4. Co-immunoprecipitations and Western Blotting

Western blots were carried out as described in section 2.4.7. The following primary antibodies were also used: anti-pS2814 (1:1000, custom¹³), pS2030 (1:1000, custom¹³), dpS2030 (1:1000, custom¹³), PP1 (1:1000; ab150782, Abcam), PP2A (1:250; 610555, BD Biosciences).

RyR2 was immunoprecipitated from LV homogenates as previously described.⁸⁶ Briefly, 5 mg of protein from LV homogenates were diluted in modified RIPA buffer containing 0.9% NaCl, 10 mM Tris pH 6.8, 0.1% Triton X-100, 20 mM NaF, 2 μ M leupeptin, 100 μ M phenylmethylsulphonyl fluoride, 500 μ M benzamidine, 100 nM aprotinin. Samples were incubated for 2 hours at 4 °C with protein-G Dynabeads (ThermoFisher) crosslinked with 5 μ g of anti-RyR2 antibody (MA3-925, ThermoFisher). Crosslinking was done using BS3 (ThermoFisher) following the manufacturer's instructions. Beads were then washed three times with RIPA buffer and incubated with Laemmli buffer at 55 °C for 10 min to elute the protein. Supernatants were used for Western blots as described above.

3.4.5. Gene Expression Analysis

Total RNA was extracted from WT and KO LV samples. Briefly, tissue was homogenized in TRIzol reagent (ThermoFisher) following the manufacturer's instructions. After addition of an appropriate amount of chloroform, mixing, incubation, and centrifugation, the RNA-containing aqueous phase was collected and treated with *DNase* I (Qiagen) for one hour. RNA was subsequently purified using the RNeasy mini kit (Qiagen), following the manufacturer's protocol. First strand cDNA synthesis was performed using the iScript Reverse Transcription Kit (Bio-Rad). To facilitate full length

first strand cDNA synthesis, samples were incubated for 90 minutes at 50 °C prior to heat inactivation of the reverse transcriptase at 70 °C for 15 minutes.

Expression levels of *RYR2* (Oc03398553_m1) and *GAPDH* (Oc03823402_g1) were subsequently assessed using TaqMan gene expression assays (ThermoFisher). 10 ng of cDNA were used as template reaction, together with TaqMan gene expression Master Mix (ThermoFisher). Thermal cycling and fluorescence measurements were performed in a StepOnePlus Real-Time PCR System (ThermoFisher). Data were analyzed using OnePlus software (ThermoFisher). *RYR2* expression levels were calculated using the Δ CT-method, normalized to *GAPDH* expression and calculated as percentage of WT.

3.4.6. [³H]Ryanodine Binding Assays

Binding assays were carried out following a modified version of a protocol previously described.^{87,164} Binding mixtures were prepared containing 100 µg of protein LV homogenate, 0.2 M KCl, 20 mM Na-HEPES pH 7.4, 6.5 nM [³H]ryanodine (NET950, PerkinElmer), and enough CaCl₂ to set free [Ca²⁺] between 100 nM to 100 µM. 1 mM EGTA was used to buffer Ca²⁺. The Ca²⁺/EGTA ratio for these solutions was determined using MaxChelator (WEBMAXCLITE v1.15, <http://maxchelator.stanford.edu/>). The binding reactions were incubated for 2 h at 37°C, then filtered through Whatman GF/B filters and washed three times with 5 mL of distilled water in a Brandel M24-R Harvester. Non-specific binding was determined in the presence of 20 µM unlabeled ryanodine (2153770, MP Biomedicals). [³H]ryanodine binding was measured by liquid scintillation using Bio-Safe II counting cocktail (RPI Research). Corrections for RyR2 expression were determined by dividing the total [³H]ryanodine binding by the normalized band intensity

from Western blots, relative to WT. Hill's equation was used to determine the maximum [³H]ryanodine binding and the EC₅₀ in Origin 9 (Origin Lab).

3.4.7. Histological Staining

LV and left atrium samples were fixed in 10% neutral buffered formalin and processed by the Pathology Core of the Unit for Laboratory Animal Medicine at the University of Michigan. An expert pathologist analyzed the samples looking for alterations of the micro-architecture of the tissue, including hypertrophy, myocyte disarray, and fibrotic infiltrations.

3.4.8. Langendorff Perfusions

Perfusion of isolated hearts was performed as described in section 2.4.8 and in the literature.¹⁷¹ Rabbits were heparinized and anesthetized as indicated in section 3.4.3. The chest was opened and the heart exposed. The aorta was cannulated *in situ* and the heart was excised and mounted on a Langendorff apparatus. A latex balloon (Harvard Apparatus) as introduced in the LV to measure developed pressure. Hearts were perfused with modified Tyrode's solution containing (mM) 130 NaCl, 4 KCl, 1 MgCl₂, 1.2 NaH₂PO₄, 24 NaHCO₃, 5.6 glucose, 1.8 CaCl₂, pH 7.4, aerated with 95% O₂, 5% CO₂. The perfusion pressure was adjusted to 50–70 mmHg (30–45 mL/min). Hearts were stimulated with 100 nM Iso to record the adrenergic response. LV pressure traces were analyzed using the Blood Pressure module of LabChart 8 (ADInstruments) to calculate LVDP, HR, and dP/dt. Five consecutive cardiac cycles were averaged at the indicated time-points.

3.4.9. Echocardiography

Transthoracic echocardiography (Echo) was performed by the Echocardiography Service of the Frankel Cardiovascular Center Animal Phenotyping Core at the University of Michigan as described in section 2.4.5, using a MS200 transducer. Rabbits were lightly sedated with ketamine/xylazine (10 mg/kg and 1 mg/kg, respectively) and anesthetized with 2% isoflurane. The adrenergic response was also determined after 15 minutes of continuous IV infusion of 0.5 μ g/kg/min Iso. All parameters are the average of three consecutive cardiac cycles.

3.4.10. Electrocardiography

Rabbits were anesthetized as indicated in section 3.4.9. Surface electrodes were placed on the limbs to record the ECG in Lead-I and Lead-II configurations using a PowerLab 8/35 system (ADInstruments). After 10 minutes of stabilization and baseline recording, a loading dose of caffeine 9 mg/kg was injected IV followed by IV infusion of dobutamine and caffeine (80 μ g/kg/min and 28 μ g/kg/min, respectively). After reaching a steady HR, the infusion was maintained for 30 min and the ECG was monitored for arrhythmia events. Lead-II ECG traces were analyzed using ECG Analysis module of LabChart 8 (ADInstruments) and averaged over 2 min of basal recording or at the peak HR response

3.4.11. Isolation of Cardiac Myocytes

Cardiac myocytes were isolated as previously described.^{97,98,171} Briefly, rabbits were anesthetized as indicated in section 3.4.9, hearts were mounted on a Langendorff apparatus as described in section 3.4.7 and perfused for 5–10 min (30–40 mL/min, 37 °C) with normal Tyrode's (NT) solution containing (mM) 138 NaCl, 4.4 KCl, 1 MgCl₂, 24 HEPES, 11 glucose, 1.8 CaCl₂, pH 7.4, aerated with 100% O₂. Once blood was

completely removed, perfusion was switched to nominally-free Ca^{2+} Tyrode's solution for 5–10 min until the heart stopped contracting. At this point, the perfusion was changed to nominally-free Ca^{2+} Tyrode's solution supplemented with 200 U/mL collagenase type 2 (Worthington), 1 mg/mL BSA and 36 μM Ca^{2+} , for 20–30 min until the heart became flaccid. The LV was then removed and minced in collagenase solution. Myocytes were dispersed by gentle pipetting. The supernatant was collected and the remaining tissue was further digested in fresh collagenase solution. This process was repeated, every 2–3 min, six times. After gently dispersion, the cell-containing supernatants were centrifuged (100 x g , 1 min) and the myocytes were resuspended in Tyrode's solution containing 1 mg/mL BSA and 36 μM Ca^{2+} . The solution was replaced every 10–15 min to raise $[\text{Ca}^{2+}]$ to 1.8 mM in five steps: 80 μM , 250 μM , 500 μM , 1 mM and, finally, 1.8 mM. 1 mg/mL BSA was added to the first two solutions. Cells were maintained in NT solution until used.

3.4.12. Cellular Ca^{2+} Imaging

Ca^{2+} transients and SR load were recorded as described in 2.4.10 and in the literature.⁸⁹ Cells were plated on laminin-coated glass-bottom dishes with NT solution and in the presence of 50 nM Iso. Longitudinal line-scans were recorded during field stimulation at 0.5 Hz. After 20 pulses 20 mM caffeine was perfused to measure the SR Ca^{2+} load (Figure 3.9).

3.4.13. Statistical Analysis

All data are presented as mean \pm SEM. Statistical significance was determined at $p \leq 0.05$ was indicated. Analyses were carried out in SigmaPlot 12.5 (Systat Software).

3.5. Acknowledgments

This chapter was prepared to be submitted as a manuscript and includes data generated with the following collaborators: Jifeng Zhang, Dongshan Yang, Jie Xu, and Y. Eugene Chen, CAMTraST University of Michigan (creation of the RyR2-KO rabbit model); Roberto Ramos-Mondragón, Xi Chen, and Yan-Ting Zhao, University of Michigan (Ca²⁺ imaging and patch-clamp); Jonathan J. Hernández, University of Wisconsin-Madison (gene expression analysis); Julieta Palomeque, Universidad Nacional de la Plata, Argentina (electrocardiograms and standardization of myocyte isolation).

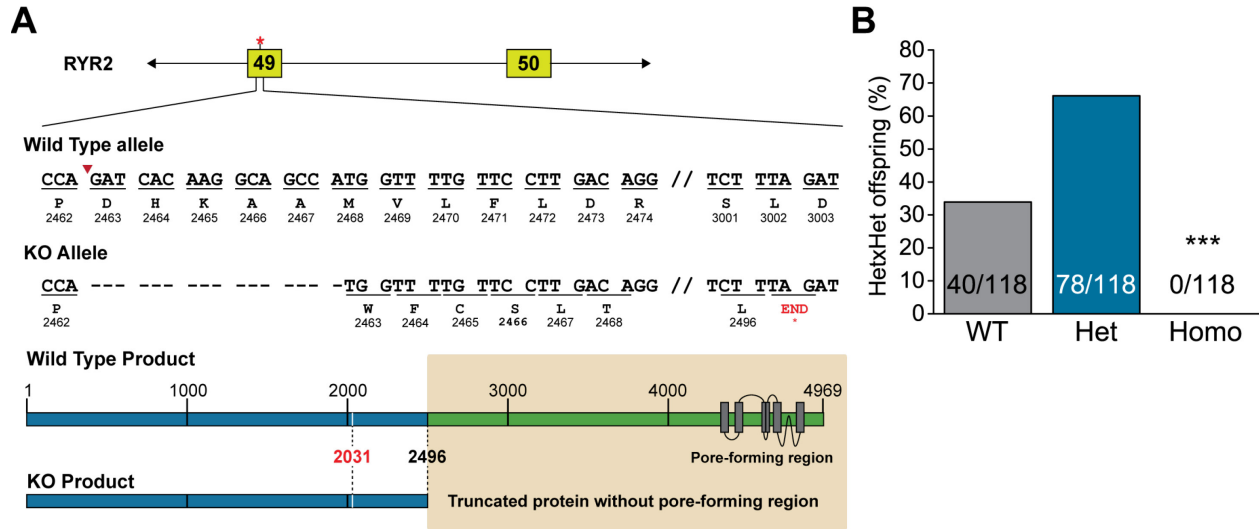


Figure 3.1. Generation of the RyR2-KO Rabbit Model.

A. Strategy to develop the RyR2-KO rabbit. Exon 49 of RYR2 was targeted using the Crispr/Cas9 technology, which generated a 16 bp deletion. Sequence analysis shows a stop codon downstream, which terminates translation after residue 2496. The PFD is not part of the truncated protein, hence the knock-out. The only phosphorylation site present in the truncated protein is S2031. The arrowhead indicates a DpnII restriction site present only in the WT allele **B.** Propagation of KO rabbits upon mating heterozygotes. Homozygotes have not been detected among a total offspring of 118 kits (***: $\chi^2 = 39.96$, $p = 2.4 \times 10^{-6}$).

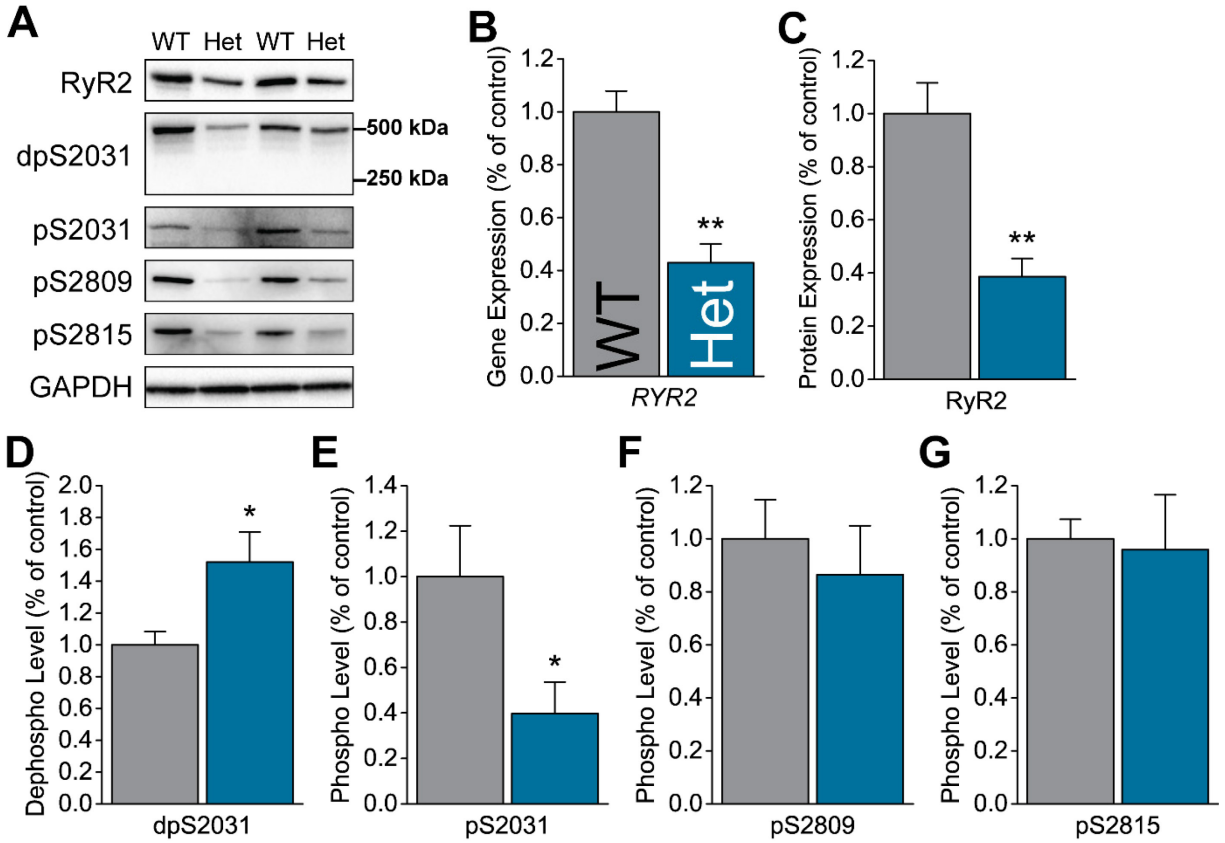


Figure 3.3. RyR2 Expression and Phosphorylation in LV Samples.

A. Representative blots. **B-C.** Expression of RyR2 is decreased in the left ventricle of KO rabbits, as measured by RT-PCR (**B**) and WB (**C**). **D-F.** Phosphorylation levels of the three major RyR2 phospho-sites (dp: dephospho; p: phospho): S2031 (**D,E**), S2809 (**F**), and S2814 (**G**). Basal phosphorylation of S2031 is decreased in heterozygous rabbits. Phosphorylation levels calculated as the ratio between phospho-band and total RyR2 band intensity, expressed as percentage of control (n = 7 per genotype; * $p < 0.05$, ** $p < 0.01$ vs. WT, two-tailed t-test).

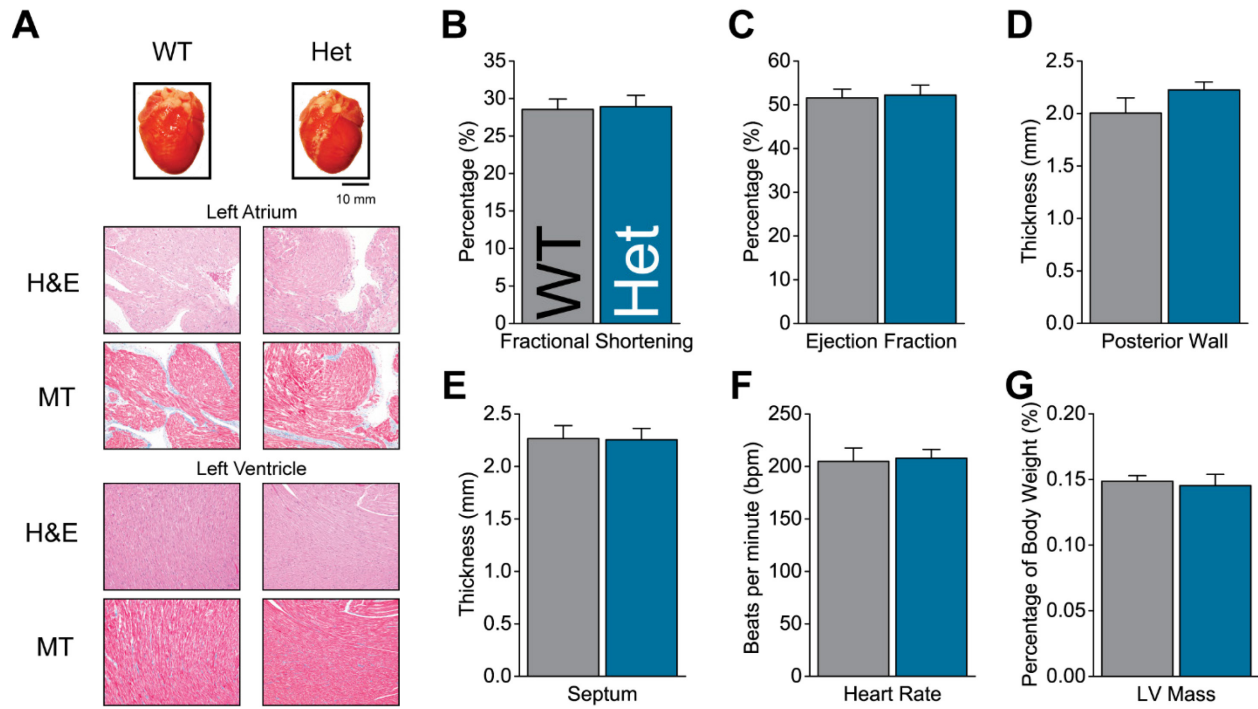


Figure 3.4. Cardiac Structure and Function *In Vivo*.

A. Representative images of whole hearts fixed in formalin (first row), high-magnification micrographs of H&E-stained tissue section (third row), and high-magnification micrographs of Masson's Trichrome-stained tissue sections (fourth row). **B-G.** M-Mode echocardiography measurements of heart rate (**B**), LV Mass (**C**), fractional shortening (**D**), ejection fraction (**E**), and posterior wall (**F**) and septum (**G**) thickness in diastole (n = 5 per genotype, t-test).

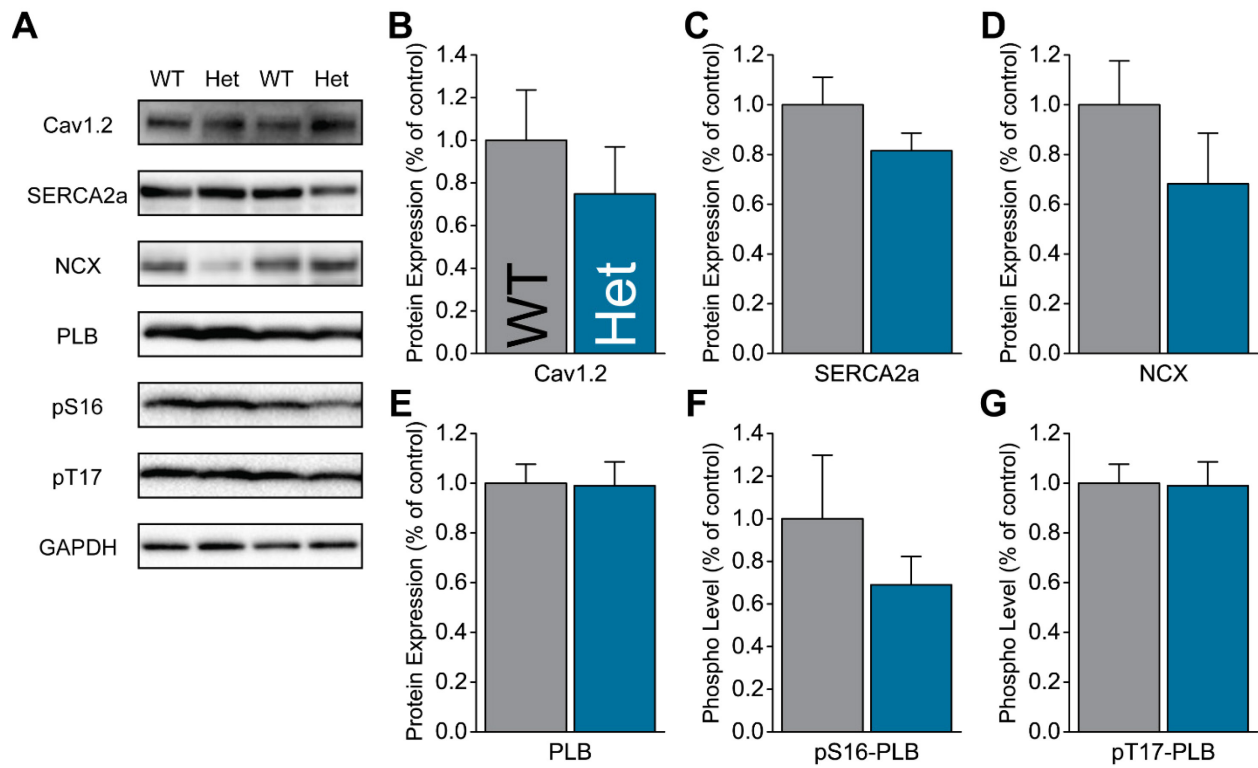


Figure 3.5. Expression of E-C Coupling Proteins in LV Samples.

A. Representative blots. **B-D.** Expression level of excitation-contraction coupling proteins Cav1.2, SERCA2a, NCX, and PLB (n = 5-7 per genotype, two-tailed t-test comparison). **F-G.** Phosphorylation level of PLB at the PKA and CaMKII phosphorylation sites (S16 and T17, respectively).

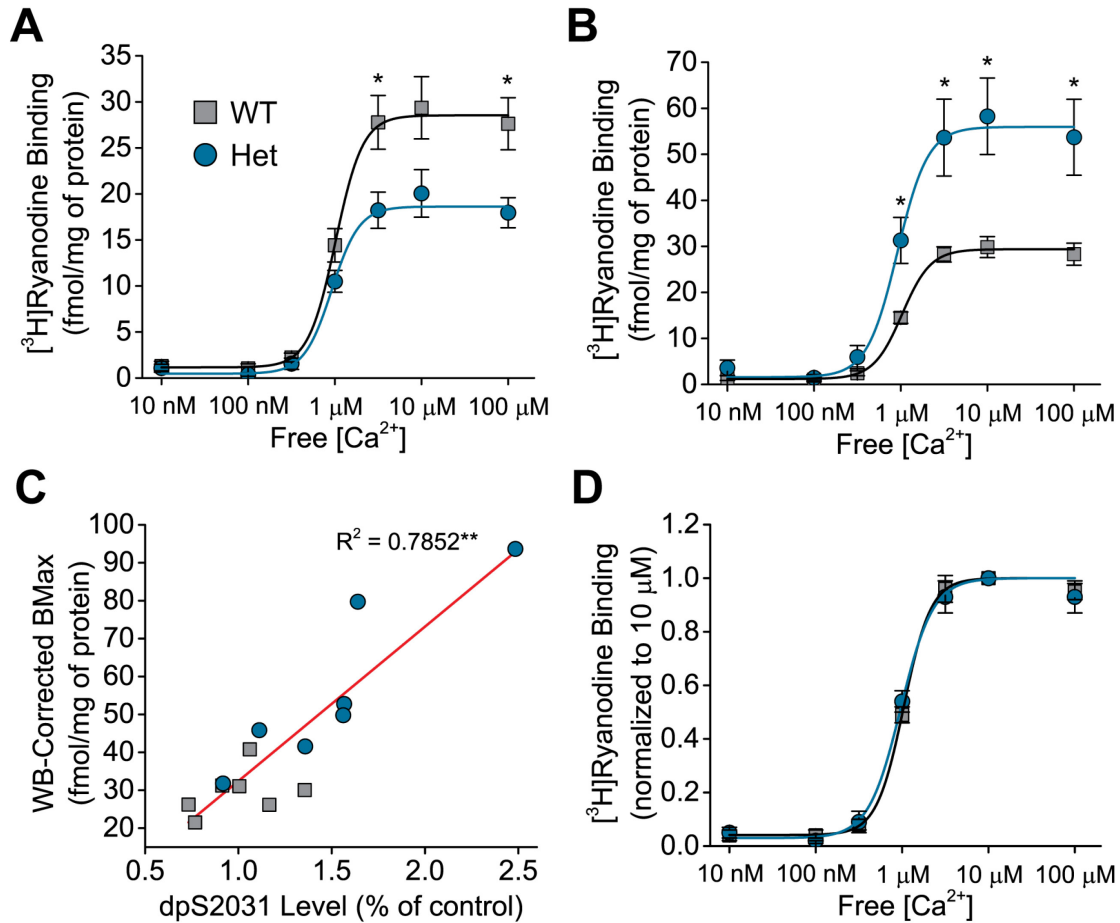


Figure 3.6. Assessment of RyR2 Activity Using [³H]Ryanodine Binding Assays.

A. [³H]ryanodine binding curves quantified in LV homogenate samples. **B.** [³H]ryanodine binding curves corrected for RyR2 expression (Western blot data from Figure 3.3 C). Each sample was normalized to its RyR2 level, determined as the ratio between normalized band intensity and the WT average. **C.** Linear fitting of S2031 dephosphorylation level vs. maximum [³H]ryanodine binding corrected for RyR2 expression determined from B. **D.** [³H]ryanodine binding curves normalized to 10 μM [Ca²⁺] showing a comparable Ca²⁺ sensitivity (n = 7 per genotype; * p < 0.05, ** p < 0.01 vs. WT, t-test).

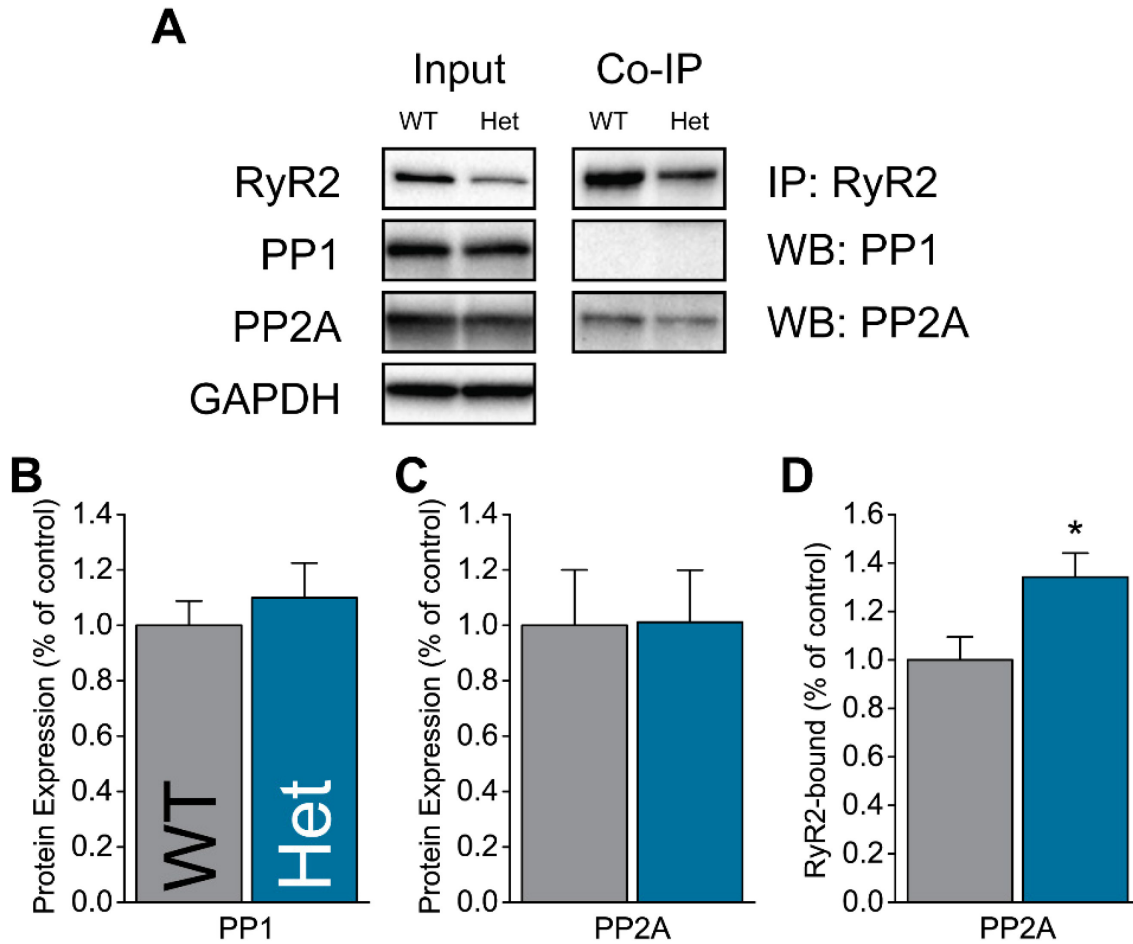


Figure 3.7. RyR2 Association with Protein Phosphatases in LV Samples.

A. Representative blots of PP1 and PP2A expression and association with RyR2 determined through co-immunoprecipitation (co-IP). **B-C.** Quantification of expression of PP1 and PP2A in LV homogenates. **D.** Quantification of RyR2-bound PP2A showing a significant increase in heterozygous LV ($n = 7$ per genotype; $p < 0.05$ vs. WT, t-test).

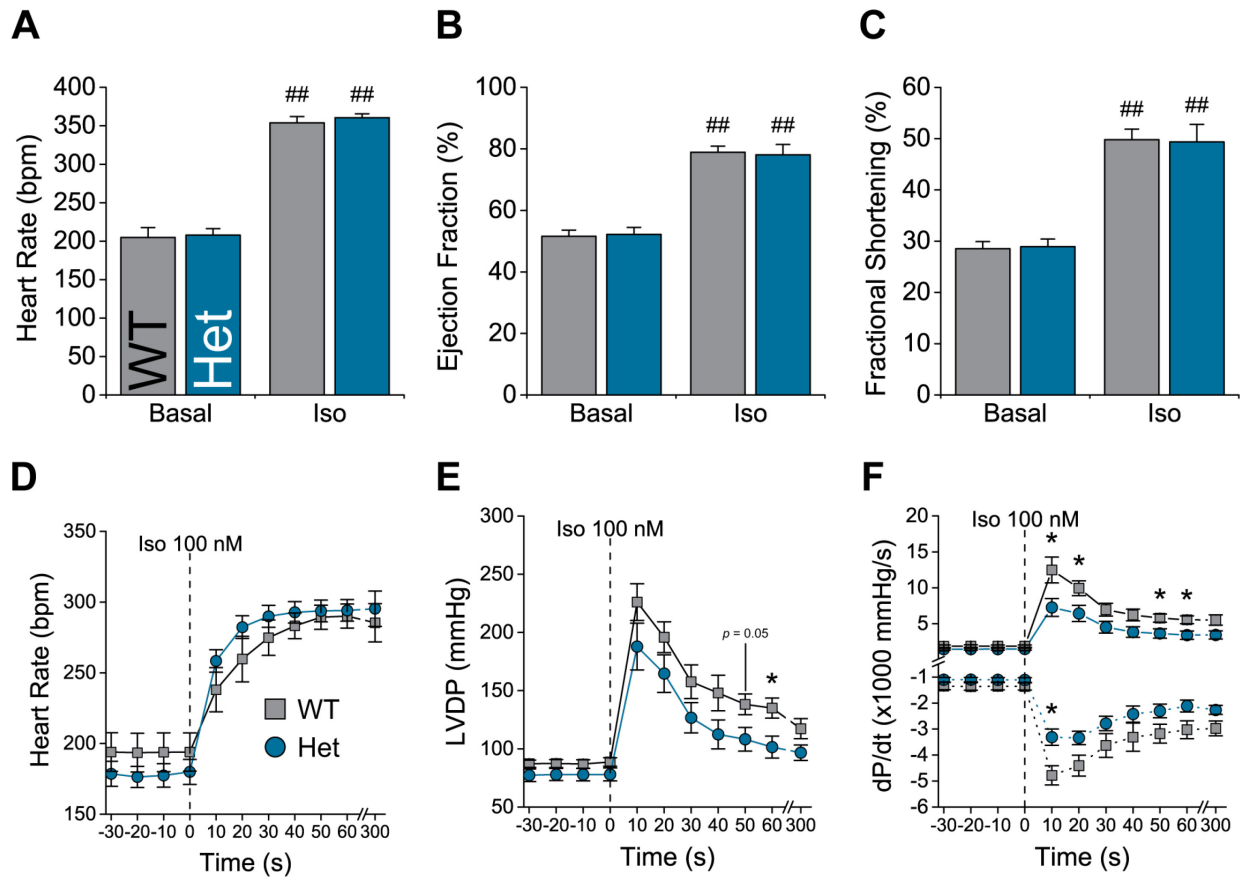


Figure 3.8. Cardiac Response to Adrenergic Stimulation in KO Rabbits.

A-C. IV infusion of isoproterenol (0.5 $\mu\text{g}/\text{kg}/\text{min}$) in anesthetized rabbits produced a significant increase in cardiac function, including heart rate (**A**), ejection fraction (**B**), and fractional shortening (**C**) ($n = 6$ per genotype; ##: $p < 0.01$ vs. same genotype basal, paired t-test). **D-E.** Langendorff-perfused hearts stimulated with 100 nM Iso show a significant increase in heart rate (**D**), LV-developed pressure (LVDP, **E**), and dP/dt (**F**) at all time-points ($n = 5$ WT, 7 Het; * $p < 0.05$, vs WT at same time-point, t-test).

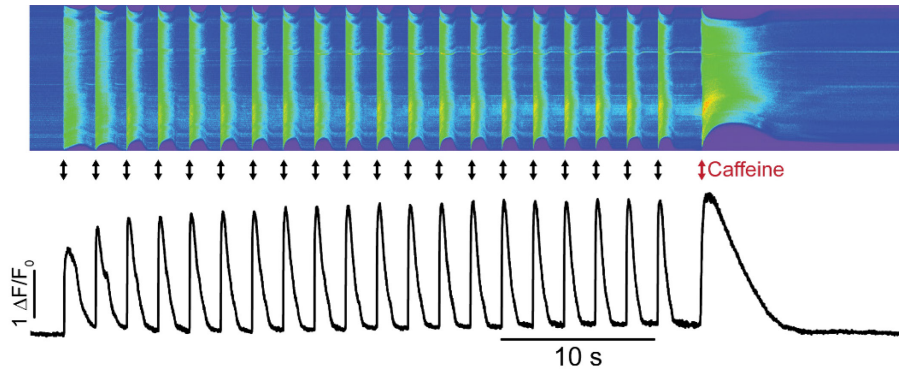


Figure 3.9. Representative Ca^{2+} transient and SR load trace.

Representative line-scan image (*top panel*) and intensity profile (*bottom panel*) of a WT rabbit myocyte paced 20 times at 0.5 Hz with field stimulation (black double arrows) under 50 nM Isoproterenol stimulation. A pulse of caffeine to measure the SR Ca^{2+} load (red double arrow).

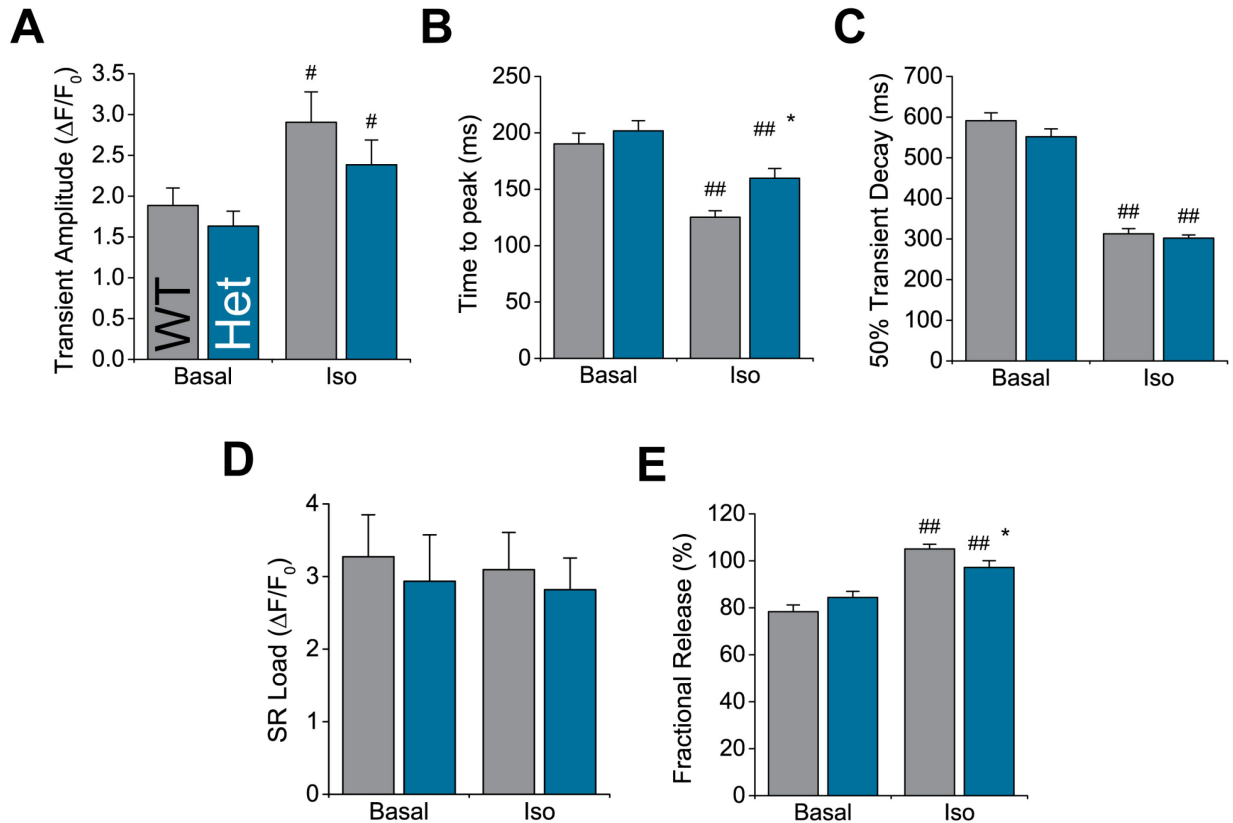


Figure 3.10. Cellular Ca^{2+} Handling in Rabbit Myocytes.

A-C. Quantification of Ca^{2+} transient amplitude (B), time-to-peak (C) and 50% transient decay time (D) during 0.5 Hz field stimulation (Basal WT: N = 4, n = 47-49; Het: N = 5, n = 45-47. Iso WT: N = 3, n = 34-36; Het: N = 3, n = 35-36). **E-G.** Quantification of SR load (E) and fractional release of Ca^{2+} (F) (Basal WT: N = 3, n = 35; Het: N = 3, n = 32. Iso WT: N = 3, n = 33-34; Het: N = 3, n = 34). * $p < 0.05$ vs. WT, same conditions. # $p < 0.05$, ## $p < 0.01$ vs. same genotype basal.

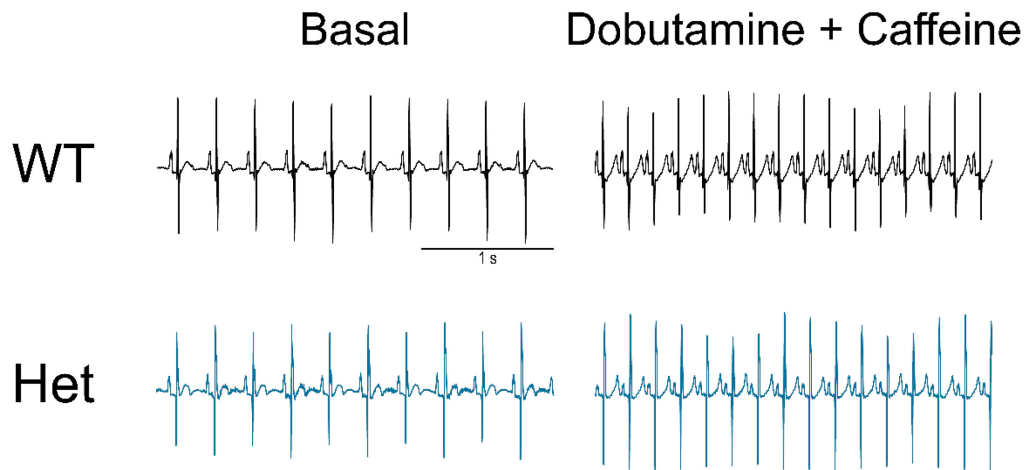


Figure 3.11. Representative ECG Traces from Rabbits Undergoing Arrhythmia Challenge.

Following a 15 min of basal recording, rabbits were challenged with a dobutamine/caffeine cocktail for 30 minutes after reaching the maximum HR. The response of both groups was comparable and no arrhythmia was detected.

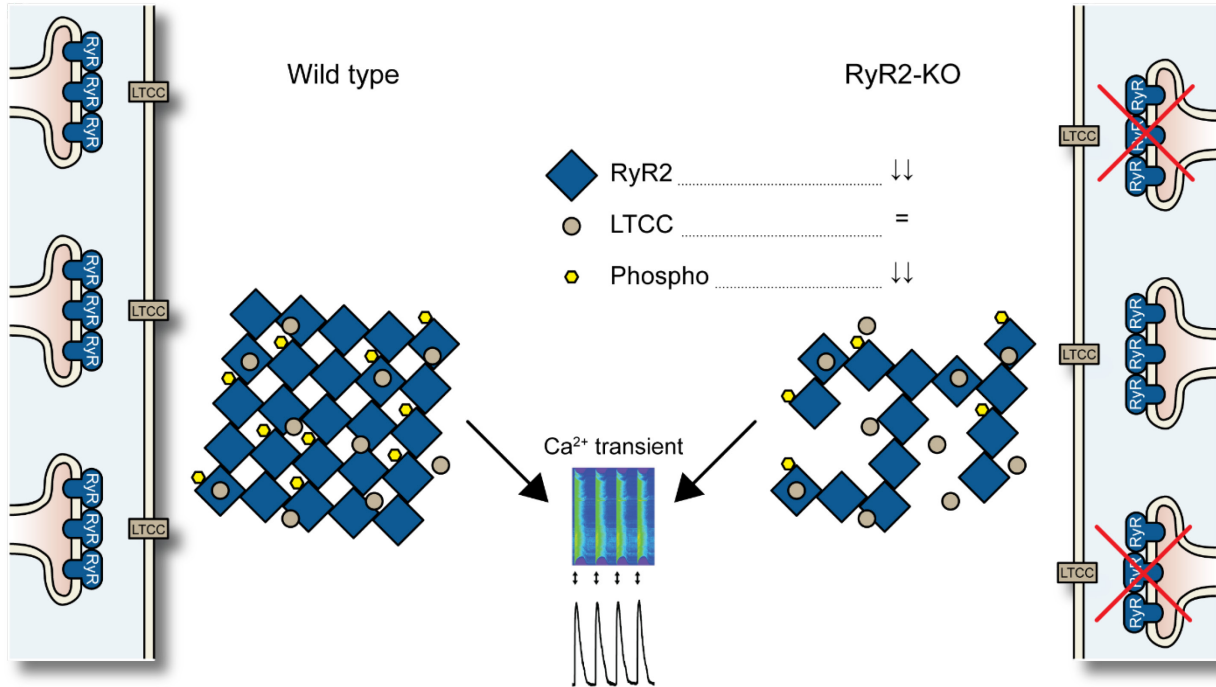


Figure 3.12. Scheme of Functional Compensation in RyR2-KO Rabbits.

Heterozygous knock-out of RyR2 (panels on the right) decrease channel expression, thereby decreasing the number of RyR2s per Ca²⁺ release unit (CRU) or the number of overall number of CRU. Hence, in basal conditions a decrease in the phosphorylation level of S2031 increases channel activity normalizing Ca²⁺ release.

Table 3.1. Echocardiographic Parameters to Assess Cardiac Structure and Function in RyR2-KO Rabbits.

Structural and functional parameters measured in WT and Het rabbits at basal level and after IV infusion of 0.5 µg/kg/min of Iso.

	Basal		Iso 0.5 µg/kg/min	
	WT	Het	WT	Het
n	6	6	6	6
BW (g)	2.5±0.1	2.6±0.1	-	-
LV Mass (% of BW)	0.149±0.004	0.145±0.009	-	-
HR (bpm)	205±13	208±9	354±8 ^{##}	361±5 ^{##}
IVSd (mm)	2.27±0.12	2.25±0.11	3.44±0.14 ^{##}	3.34±0.13 ^{##}
IVSs (mm)	3.38±0.14	2.88±0.15*	5.44±0.21 ^{##}	5.11±0.08 ^{##}
IVSth (%)	50.3±6.7	29.3±9.5	59.0±5.5	54.0±5.0 [#]
PWd (mm)	2.00±0.15	2.22±0.08	3.48±0.12 ^{##}	3.63±0.12 ^{##}
PWs (mm)	3.34±0.2	3.43±0.28	5.23±0.27 ^{##}	5.66±0.25 ^{##}
PWth (%)	68.6±9.8	54.7±12.8	51.6±10.0	56.1±5.6
LVDd (mm)	14.44±0.62	13.94±0.36	9.14±0.59 ^{##}	8.84±0.37 ^{##}
LVDs (mm)	10.31±0.45	9.92±0.40	4.57±0.27 ^{##}	4.43±0.22 ^{##}
FS (%)	28.5±1.4	28.9±1.5	49.8±2 ^{##}	49.3±3.4 ^{##}
LVVd (uL)	1265.5±113.9	1165.8±63.5	475.8±70.6 ^{##}	434.7±39.5 ^{##}
LVV _s (uL)	610.9±57.6	561.2±48.9	98.1±12.7 ^{##}	90.9±10.7 ^{##}
EF (%)	51.6±2.0	52.2±2.3	78.9±2 ^{##}	78.1±3.4 ^{##}
SV (uL)	654.6±69.0	604.6±31.4	377.7±62.4 [#]	343.8±42.9 ^{##}
CO (mL/min)	130.7±9.4	125.3±6.5	132.9±20.7	124.5±16.5

BW: body weight; HR: heart rate; IVSd: interventricular septum thickness in diastole; IVSs: interventricular septum thickness in systole; IVSth: percent change in IVS between systole and diastole; PWd: posterior wall thickness in diastole; PWs: posterior wall thickness in systole; PWth: percent change in PW between systole and diastole; LVDd: left ventricle diameter in diastole; LVDs: left ventricle diameter in systole; FS: fractional shortening; LVVd: left ventricle volume in diastole; LVVs: left ventricle volume in systole; EF: ejection fraction; SV: stroke volume; CO: cardiac output.

*: $p < 0.05$, vs. WT, t-test

#: $p < 0.05$, ##: $p < 0.01$ vs. same genotype basal, paired t-test

Table 3.2. Electrocardiographic Parameters in RyR2-KO Rabbits Undergoing Arrhythmia Challenge.

Average ECG parameters from Lead-II determined as the average of 2 min of recording in basal conditions and at the peak HR response.

	Basal		Dobutamine + Caffeine	
	WT	Het	WT	Het
n	4	8	3	3
HR (bpm)	207±15	211±9	329±5 ^{##}	320±14 ^{##}
delta HR	-	-	109.0±6.7	114.8±14.1
RR (ms)	294.0±22.1	288.5±12.9	182.6±3.0 ^{##}	188.2±8.7 ^{##}
QRS (ms)	27.8±2.6	29.3±1.9	24.0±0.5	26.8±1.7
PR (ms)	57.5±3.7	58.3±2.0	51.7±1.8	52.4±1.2 [#]
QT (ms)	138.4±3.9	138.4±5.2	122.1±2.8	121±8.1
QTc (ms)	155.9±2.4	156.5±5.6	150±3.0	147.7±8.6

[#]: $p < 0.05$, ^{##}: $p < 0.01$ vs. same genotype basal, t-test.

Table 3.3. Cardiac Function Parameters in Langendorff-perfused RyR2-KO Hearts.

Average parameters of cardiac function measured in isolated rabbit hearts perfused in a Langendorff apparatus.

	Basal (t = 0)		Iso 100 nM (t = 10 s)		Iso 100 nM (t = 300 s)	
	WT	Het	WT	Het	WT	Het
n	5	7	5	7	5	7
HR (bpm)	194±14	180±9	238±16 ^{##}	258±8 ^{##}	285±14 ^{##}	295±13 ^{##}
ΔHR (%)	-	-	23.8±7.8	43.5±7.8	48.6±7.0	68.1±7.5
LVDP (mmHg)	88.7±3.6	78.0±5.5	226.0±15.7 ^{##}	187.9±20.1 ^{##}	117.3±8.7 [#]	96.6±6.6 [#]
ΔLVDP (%)	-	-	157.7±24.5	141.5±22.3	32.8±10	17.1±7.0
+dP/dt (mmHg/s)	1889±165	1494±137	12475±1803 ^{##}	7268±1240 ^{*##}	5520±717 ^{##}	3445±568 ^{*.#}
Δ+dP/dt (%)	-	-	572.0±90.6	408.8±81.1	194.9±31.6	135.2±31.5
-dp/dt (mmHg/s)	-1362±139	-1115±92	-4782±368 ^{##}	-3312±313 ^{*.##}	-2976±286 ^{##}	-2266±174 ^{##}
Δ-dP/dt (%)	-	-	269.7±52.1	188.9±22.9	120.5±14.4	89.4±13.8

HR: heart rate; LVDP: LV-developed pressure (LV pressure max–end-diastolic pressure).

*: $p < 0.05$, vs. WT, t-test.

#: $p < 0.05$, ##: $p < 0.01$ vs. same genotype basal, paired t-test.

CHAPTER 4

A Novel RyR2 Mutation Associated with Hypertrophic Cardiomyopathy Induces Hypertrophy and Arrhythmia in Mice

4.1. Introduction

Hypertrophic cardiomyopathy (HCM) is the most common congenital cardiac disease, affecting 1 out of every 500 individuals (0.2% of the general population).¹⁰⁸ HCM is characterized at the tissue level by myocyte hypertrophy and disarray, and interstitial fibrosis; while the clinical features involve thickening of the left ventricle (LV) wall, diastolic dysfunction, heart failure, and increased risk of life-threatening arrhythmias that may lead to sudden cardiac death.¹⁷²⁻¹⁷⁴ More than 1400 mutations¹⁰⁹ affecting over 24 genes¹⁷⁵ have a strong correlation with HCM, with the most commonly affected genes encoding for sarcomeric proteins. HCM patients have the highest prevalence of mutations in *MYH7* and *MYPBC3*, accounting for approximately 50% of the cases with a positive genetic diagnosis. However, approximately half of the patients who meet the diagnostic criteria of HCM and undergo genetic testing do not carry mutations in the genes included in commercial screening tests.¹⁰⁹ As genetic testing has become more common, and the gene panel has expanded, new HCM-associated mutations have been identified in a plethora of genes within the myofilaments and beyond. While rare, there are reports pointing to mutations in Ca²⁺-handling proteins as responsible for HCM, including genes

such as *SRI*, *CASQ2* and *RYR2*.¹¹⁰ None of these mutations has been thoroughly characterized.

RYR2 encodes ryanodine receptor type 2 (RyR2), the major Ca^{2+} -release channel in the heart. During an action potential in cardiac myocytes, a small inward Ca^{2+} current through L-type channels activates RyR2 on the membrane of the sarcoplasmic reticulum, triggering more Ca^{2+} release. RyR2 provides most of the Ca^{2+} required for this process — ~70% in humans² — called excitation-contraction (e-c) coupling. Tight regulation of Ca^{2+} release in the heart, and thus of RyR2 function, is essential because the same calcium used for e-c coupling can induce Ca^{2+} -dependent arrhythmias,⁶⁹ or modulate signaling pathways involved in structural remodeling.¹²⁶

Over the last 20 years, nearly 200 RyR2 mutations have been identified in patients with Catecholaminergic Polymorphic Ventricular Tachycardia (CPVT), a disorder involving severe ventricular arrhythmias triggered by stress, but without structural alterations of the myocardium. The mechanisms underlying this disorder have been the subject of extensive research, uncovering a variety of molecular and cellular alterations producing Ca^{2+} mishandling and, ultimately, arrhythmia. More recently, the first HCM-related RyR2 mutation — T1107M — was reported by a Japanese group.¹¹³ This mutation generated considerable interest in the field, as it was the first RyR2 variant associated with a structural — HCM — rather than an entirely functional disorder — CPVT. Interestingly, A1107M, the mouse analog, behaved considerably different in a heterologous expression system when compared to other CPVT mutations, suggesting a different pathogenic mechanism.¹¹⁹ Furthermore, it produces disruption of the SPRY2 domain of RyR2.³⁰ However, T1107M has also appeared in cohorts of whole-exome

sequencing (WES)¹⁷⁶ and cohorts of CPVT patients,⁸¹ weakening its pathogenic potential. Altogether, these data indicated that RyR2 mutations can produce a wide range of cardiac alterations, but the link between RyR2 mutations and structural cardiomyopathy remains elusive.

In this study, we performed a thorough characterization of the novel mutation P1124L, recently identified in a patient with HCM. Remarkably, P1124L is in the same domain as T1107M. Nonetheless, four criteria support the pathogenicity of P1124L in the context of HCM: (1) the patient is negative for other potential mutations associated with HCM as screened in the clinical test; (2) the patient has a family history of HCM; (3) we provide compelling evidence showing that this mutation produces disruption of RyR2 structure and function; and (4) mice harboring P1124L develop hypertrophy and cardiac arrhythmia. Still, we have yet to identify the specific signaling pathways responsible for the hypertrophic phenotype. Hence, while P1124L represents a new paradigm for the emerging field of RyR2-mediated cardiac remodeling and Ca²⁺-dependent HCM, a detailed elucidation of all the pathogenic mechanisms associated with the mutation will require further investigation.

4.2. Results

4.2.1. Identification of RyR2-P1124L in a Human Patient

The patient harboring the heterozygous RyR2-P1124L mutation was diagnosed at 17 years of age with HCM after a syncopal episode and demonstrated concentric LV hypertrophy most prominent in the lateral and inferolateral walls. Despite beta blocker therapy, he remained symptomatic, experiencing chest tightness and paroxysmal nocturnal dyspnea requiring him to sleep upright. Due to refractory symptoms, he had a

dual-chamber pacemaker (right atrium + right ventricle) placed 4 months later. He has a positive family history of two maternal cousins having HCM, without reported cases of sudden cardiac death. His mother was phenotypically negative for HCM, while his father and three siblings have not been screened. The patient tested negative for the equivalent of the clinical HCM genetic test (sarcomeric genes including *MYBPC*, *MYH7*, *TNNT2*, *TNNI3*, *TNNC1*, *TPM1*, *ACTC*, *MYL2*, and *MYL3*). The only relevant variant identified was the heterozygous RyR2-P1124L. Since DNA samples from immediate relatives were not available, it is not possible to determine co-segregation of the mutation and HCM phenotype within the patient's family.

At a subsequent visit to Mayo Clinic at age 18, he had a 24 mm mid-ventricular septal thickness (basal septum 16 mm) and LVOT obstruction (88 mmHg with Valsalva, 46 mmHg baseline, and systolic anterior movement of the mitral valve) with mitral valve regurgitation. Because of these symptoms, he underwent an extended surgical myectomy. Figure 4.1 shows the complete electrocardiograms recorded before and after the surgery. Pre-surgery, Figure 4.1 **A** shows significant widening of the QRS complex and an elevated heart rate (95 bpm) maintained by firing of the pacemaker (pacing artifact most evident in leads II and V5). After the surgery (Figure 4.1 **B**), sinus rhythm was re-established, and the widening of the QRS complex was significantly decreased.

For the final publication of this chapter in a scientific journal, the Ackerman group, which identified the mutation, must provide additional information including the echocardiograms from previous visits to Mayo, to offer a stronger clinical foundation for the work described henceforth.

4.2.2. Localization of P1124L in the Three-dimensional Structure of RyR2

RyR2 mutations are clustered in four regions of the protein (Figure 4.2): CPVT-I is contained within the N-terminal domain (NTD), CPVT-II is formed by the second helical domain (HD2), CPVT-III and CPVT-IV involve the carboxy-end and comprise the central and pore-forming domains, respectively (CD and PFD). P1124L is a highly conserved residue (Figure 4.3) located outside of these regions in close proximity to T1107M, the only other HCM-associated mutation in RyR2.¹¹³ P1124 is part of SPRY2, one of the three SPRY domains in RyR2.^{33,177} The crystal structure of SPRY2 from RyR2 was recently solved to a resolution of 1.34 Å.³¹ P1124 belongs to a flexible linker connecting β -strands β 2 and β 3 that was not included in the initial SPRY2 model due to poor electron density. We did further refinement of the crystal structure of the wild type SPRY2 and crystalized the domain with the P1124L mutation (Figure 4.4). These new data suggest that the loop containing P1124 is located at the SPRY2-SPRY3 interface (Figure 4.5). Introducing the P to L substitution produces a substantial conformational change that affects neighboring residues, most notably C1122 and D1125, which are now directly facing SPRY3 (Figure 4.5 **D**). While high-resolution structures of SPRY3 are not available yet, modeling of the SPRY2-SPRY3 interface shows that the new position of D1125 facilitates the formation of a salt bridge with R1599 of SPRY3. Therefore, this new inter-domain interaction might promote protein stability. Also, a new salt bridge forms between R1119 and D1132, located in opposite ends of the β 2- β 3 flexible linker. This could also provide rigidity to the linker and contributing to lock the SPRY domains.

4.2.3. Molecular Phenotype of P1124L Channels

To determine the molecular phenotype of RyR2 channels harboring the P1124L mutation, we introduced the mutation into the mouse RyR2 cDNA and expressed the WT or mutant protein in HEK293 cells. 48 hours after transfection, we lysed the cells and performed functional studies. First, we found that P1124L mutant RyR2 expression is significantly reduced in transfected HEK 293 cells compared to the expression of WT RyR2 (49.4±3.4% of WT expression, $n = 6$, $p < 0.01$; Figure 4.6 **A,B**). This is an uncommon observation, as mutation-harboring RyR2 channels are often expressed to the same level as WT channels in this heterologous system.¹¹⁹ Next, we performed [³H]ryanodine binding assays to assess RyR2 channel activity. Ryanodine, the alkaloid which provided the name to RyR2, only binds to the open state of the channel. Hence, ryanodine binding is suitable to evaluate RyR2 activity in a population of channels at varying [Ca^{2+}] exposed to the cytosolic side of the channel. After correcting for RyR2 expression levels by Western blot, we determined that P1124L behaves as a loss-of-function mutation, with lower maximum [³H]ryanodine binding than WT (BMax = 0.44±0.02 vs. 0.60±0.03 pmol/mg of protein, $n = 7$, $p < 0.01$; Figure 4.6 **C,D**) and requiring higher [Ca^{2+}] for activation ($\text{EC}_{50} = 362.9\pm 74.5$ vs. 190.6±9.8 nM, $n = 7$, $p = 0.04$; Figure 4.6 **E,F**).

4.2.4. Spontaneous Ca^{2+} Oscillations in HEK Cells Expressing RyR2

Using an assay involving heterologous expression of RyR2 in HEK293 cells and monitoring of intra-endoplasmic reticulum (ER) [Ca^{2+}]. Tang et al.¹¹⁹ previously determined that some RyR2 mutations induce abnormal termination of spontaneous Ca^{2+} release (SCR), in particular A1107M. We used the same approach to gain a better

understanding of the possible mechanisms underlying the pathogenicity of P1124L. HEK293 cells stably expressing RyR2 were transfected with the FRET-based endoplasmic reticulum (ER) Ca^{2+} sensor D1ER. Then, cells were perfused with 2 mM Ca^{2+} to fill the ER and induce luminal $[\text{Ca}^{2+}]$ oscillations due to RyR2 activation. In this experiment, luminal Ca^{2+} oscillations are observed as a decrease in the FRET ratio. Figure 4.7 **A** shows representative FRET traces measured in cells expressing WT and P1124L channels. From these recordings, we determined the FRET level at which Ca^{2+} oscillations are triggered (F_{Act}) and terminated (F_{Termi}). Then, we perfused the cells with tetracaine to inhibit RyR2 and determine the FRET level at maximum store capacity (F_{Max}), followed by caffeine to empty the ER and determine the residual FRET signal (F_{Min}). In both groups, Ca^{2+} oscillations activated at ~80% the maximum ER store capacity (Figure 4.7 **B**). However, P1124L showed a significant reduction in the termination threshold for $[\text{Ca}^{2+}]$ oscillations (Figure 4.7 **C**), resulting in a larger fractional release (Figure 4.7 **D**). Interestingly, the ER store capacity was also decreased in the cells expressing P1124L channels (Figure 4.7 **E**). Similar to HEK293 cells with transient transfection of P1124L, cells with stable expression of these channels also showed lower RyR2 expression (Figure 4.8), which could account for the change in store capacity. This observation was not reported by Tang et al.¹¹⁹, who did not observe changes in RyR2 expression among the variants they tested.

Ultimately, these data suggest that P1124L channels have impaired luminal regulation and, upon activation, release more Ca^{2+} than WT channels. In the context of a myocyte, the implication may be that upon reaching a threshold SR load, P1124L channels would spontaneously release more Ca^{2+} . This would lead to higher local,

subcellular $[Ca^{2+}]$ potentially leading to activation of entire clusters of RyR2 that propagate as Ca^{2+} waves.

4.2.5. Single Channel Recordings

Recombinant RyR2 from a heterologous system is expressed in the absence of other important regulatory co-factors. Therefore, we prepared SR-enriched microsomal fractions from pooled WT or homozygous P1124L mouse hearts to assess RyR2 activity from *native* channels reconstituted in artificial planar lipid bilayers. Knock-in P1124L mice were generated following the strategy summarized in Figure 4.9 **A**. Using homologous recombination, we introduced three mutations in exon 28 of *Ryr2* (Figure 4.9 **B**): a silent A to G substitution in codon 1123, creating a PvuII restriction site; and two substitutions in codon 1124, accounting for the P to L change. P1124L mice have Mendelian propagation (Figure 4.9 **C**), and show heart rate (Figure 4.9 **D**) and RyR2 expression (Figure 4.9 **E**) comparable with WT controls.

Figure 4.10 **A** shows representative current traces and histograms normalized to the average current of the open state obtained from single RyR2 channels from SR microsomes. We observed that P1124L channels have lower open probability than WT channels ($P_o = 0.113 \pm 0.046$, $n = 3$ channels vs. 0.515 ± 0.143 , $n = 5$ channels, $p < 0.01$; Figure 4.10 **B**) at nominally-free $[Ca^{2+}]$ ($\sim 3-5 \mu M$). These data agree with the $[^3H]$ ryanodine binding assays and support the idea that P1124L shows a cytosolic loss-of-function at physiologically-relevant cytosolic $[Ca^{2+}]$. The average conductance of WT and P1124L was not different, as determined based on the single channel currents recorded at 0 mV in a Cs^+ gradient (trans/cis 300/50 mM). We have yet to titrate the

sensitivity of P1124L channels to luminal $[Ca^{2+}]$, to confirm our findings on the termination threshold of SCR presented in the previous section.

4.2.6. Cardiac Structure of Mice Harboring P1124L

We determined that P1124L mice develop mild hypertrophy at 12-months of age (Figure 4.11, Table 1.1). This phenotype is evident in both homozygous (Homo) and heterozygous (Het) mice, and involves thickening of the posterior wall (Figure 4.11 **B**) and septum (Figure 4.11 **C**), without deterioration of the ejection fraction (Figure 4.11 **D**). In Het and HOMO mice we also observed a significant increase in heart weight as percentage of body weight (Figure 4.11 **E**). However, we did not observe microscopic alterations of the cardiac muscle or fibrotic infiltrations (fibrosis quantification; WT: $4.54 \pm 0.57\%$, Het: $5.21 \pm 0.74\%$, HOMO: $4.19 \pm 0.57\%$; $p > 0.05$). At this age, we did not detect differences in the expression and phosphorylation of RyR2 (Figure 4.12) or other e-c coupling proteins (Figure 4.13). However, there was significant variability within samples of the same genotype, and tendencies, such as an increase in NCX expression, were not significant (Figure 4.13 **B**). Nevertheless, GAPDH expression showed little variability suggesting that the variability in in the e-c coupling proteins is not due to inadequate normalization (Figure 4.13 **I**).

To complement these results, we isolated and measured ventricular myocytes from P1124L mice. Figure 4.14 **A** shows representative transmitted-light images of these cells. We observed that HOMO myocytes were significantly longer than WT and Het myocytes, and wider than WT cells (Figure 4.14 **B**). This results in HOMO myocytes having a significantly larger surface area than WT (Figure 4.14 **C**). Het myocytes, on the other hand, were only significantly wider than WT (Figure 4.14 **B**), showing no difference in

length and surface area. Finally, we measured the cardiac expression of three hypertrophy marker genes using RT-PCR: atrial natriuretic peptide (*Nppa*), brain natriuretic peptide (*Nppb*), and β -myosin heavy chain (*Myh7*). Consistent with the mild hypertrophy we observed in Homo mice, we only measured a significant increase in *Nppa* expression in Homo mice (Figure 4.15).

Taken together, these data suggest that P1124L produces mild cardiac hypertrophy in mice. This phenotype is detectable in both Homo and Het mice, as determined at the whole-heart and cellular level. Overall, the number of significant differences in indexes of hypertrophy were greater in Homo mice. To our knowledge, P1124L mice are the first animal model harboring a clinically-relevant RyR2 mutation that induces structural remodeling of the cardiac muscle.

4.2.7. Signaling Pathways Associated with Cardiac Hypertrophy

To determine the mechanisms by which P1124L might induces hypertrophy, we used Western blots to measure the expression and phosphorylation of relevant signaling molecules in 12-month-old hearts. First, we looked at the two Ca^{2+} -dependent signaling pathways: CaM-CaMKII-HDAC and CaM-CaN-NFAT. In both cases, Ca^{2+} binds to calmodulin (CaM), which in turn activates either the Ca^{2+} /CaM-dependent kinase II (CaMKII) or the serine/threonine phosphatase calcineurin (CaN). Downstream, each pathway follows a different signaling cascade that ultimately activates hypertrophic genes.¹⁷⁸ We did not detect a difference in the expression of CaMKII between genotypes (Figure 4.16 **B**), although there was a tendency for an increase in Homo mice. Upon activation CaMKII auto-phosphorylates at residue T287 which confers it with Ca^{2+} /CaM-independent activity.¹⁷ Hence, even if expression is not altered, increased auto-

phosphorylation indicates pathologic activity, as occurs in human HCM.^{99,100} After several trials adjusting the blotting conditions and using different lots of antibody, we did not detect phosphorylation of T287 in any of the three genotypes (data not shown). This is unlikely due to an issue with the antibody, since we have successfully used it with samples from younger mice, atrial tissue, and other species. We also measured the expression of CnA, the catalytic subunit of CaN (Figure 4.16 **B**). Again, there was no significant difference between WT, Het, and Homo mice.

Yamaguchi et al. also failed to detect differences in Ca²⁺-dependent signaling while studying a mouse model expressing RyR2 channels unable to bind CaM.^{43,111} Hence, they looked at other pathways also related to cardiac hypertrophy:¹¹¹ Erk1/2 — extracellularly responsive kinases part of the MAPK family — and Akt — also known as protein kinase B, part of the PI3K/Akt/GSK-3 cascade.¹⁷⁸ We tested the same signaling molecules by Western blotting, but did not observe significant differences in expression or phosphorylation (Figure 4.16 **C,D**). Altogether, these data suggest (1) that the mild cardiac hypertrophy of P1124L mice is likely not mediated by Ca²⁺-dependent signaling pathways, and (2) Erk1/2 and Akt do not appear to be responsible for the cardiac hypertrophy. Hence, we have yet to determine the specific link between the RyR2 dysfunction produced by P1124L and the cardiac hypertrophy developed in 12-month-old mice.

4.2.8. Arrhythmia Susceptibility of P1124L Mice.

RyR2 mutations are commonly associated with cardiac arrhythmia in the absence of gross remodeling of the heart. Therefore, we tested whether P1124L is sufficient to induce arrhythmia in mice. We used an arrhythmia challenge protocol (IP injection of

epinephrine 2 mg/mg and caffeine 120 mg/kg⁸⁷) during surface ECG recording, to determine the susceptibility of P1124L mice to develop ventricular arrhythmia. We performed this test in 8-month-old mice because at this age they do not show signs of cardiac hypertrophy. Figure 4.17 **A** shows representative 2-seconds long lead-II ECG recordings. Most of the arrhythmias we quantified were ventricular bigeminy (alternated premature and sinus beats, Figure 4.17 **Aiii**) and ventricular tachycardia (3 or more consecutive premature beats, Figure 4.17 **Aiv**). The effect of the arrhythmogenic cocktails was minimal in WT mice, which only showed premature ventricular beats (PVB, Figure 4.17 **Aii**) and non-sustained arrhythmias lasting less than 5 seconds (Figure 4.17 **C**). P1124L mice exhibited a non-significant tendency to develop more PVBs than WT (Figure 4.17 **B**), which coalesced into significantly more episodes of arrhythmia in Homo mice during 30 min post-challenge (Figure 4.17 **C-D**), including bidirectional ventricular tachycardia (BDVT, Figure 4.17 **E**), the pathognomonic sign of RyR2-induced arrhythmia. Again, Het mice had an intermediate phenotype between WT and Homo. While the difference in the number of episodes of sustained arrhythmia and incidence of BDVT was not statistically different between WT and Het mice, WT animals did not show these types of events, consistent with the literature. This suggests that the phenotype of Het mice is significant.

In summary, P1124L predisposes 8-month-old mice to develop cardiac arrhythmia before the onset of the structural remodeling at 12 months of age. This suggests that the arrhythmia is a result of RyR2 dysfunction rather than a result of the cardiac structural remodeling.

4.2.9. Cellular Ca²⁺ Handling in Ventricular Myocytes

To understand the cellular mechanisms for the cardiac arrhythmia, we measured the kinetics of Ca²⁺ handling in isolated myocytes. We first paced at the cells at 1 Hz to quantify the properties of the cellular Ca²⁺ transient at basal conditions and then during 300 nM Isoproterenol (Iso) perfusion. Figure 4.18 summarizes these data, which show no differences in Ca²⁺ release, Ca²⁺ removal, or SR content between WT and P1124L mice. Next, we studied the propensity for spontaneous Ca²⁺ release using a different protocol: cells were paced at 3 Hz for 30 s, followed by a resting period of 30 s. During this time, we monitored the cells for episodes of spontaneous Ca²⁺ release (SCR), manifested as Ca²⁺ waves (Figure 4.19). The incidence of SCR was higher in Homo myocytes at basal conditions, compared to WT and Het. This difference dissipated with Iso; however, the frequency of SCR was significantly higher in Homo myocytes treated with Iso than WT. Het myocytes displayed an intermediate phenotype, with a non-significant tendency for higher SCR frequency under Iso compared to WT. Incidentally, SCR frequency was not statistically different between Het and Homo under Iso. These data suggest that the cellular mechanism for the ventricular arrhythmias in P1124L mice is SCR during diastole.

4.3. Discussion

Since HCM was first described by Teare in 1957,¹⁷⁹ and the identification of the first associated mutation affecting β -myosin heavy chain in 1990 (MYH7-R403Q),¹⁸⁰ the number of genes and genetic variants related to the disease continues to grow steadily. Most of these mutations affect components of the contractile machinery of the heart, commonly MYH7 of the thick filaments and myosin-binding protein C of the intermediate filaments.¹⁰⁹ Considering the role of Ca²⁺ as a master regulator not only of contractility,

but also hypertrophic signaling, it is quite surprising that genetic mutations in Ca^{2+} -handling proteins are rare among HCM patients. In 2006, Fujino et al. reported, for the first time, an RyR2 mutation occurring in a family with HCM — T1107M.¹¹³ While *in vitro* studies suggested this is a loss-of-function mutation¹¹⁹ that alters the SPRY2 domain of RyR2,³⁰ T1107M is not a good tool to study the mechanisms by which RyR2 dysfunction and any associated Ca^{2+} mishandling produces cardiac hypertrophy for two main reasons. On the one hand, Medeiros-Domingo et al. identified this mutation in patients with CPVT, the inherited arrhythmia already strongly associated with RyR2 dysfunction,⁸¹ weakening its association with HCM. Yet, at least two studies question the pathogenicity T1107M altogether,^{176,181} since it appears with high frequency in whole-exome sequencing (WES) cohorts. Hence, Landstrom et al. demoted T1107M from disease-causative to variant of unknown significance (VUS).¹⁷⁶

In this report, we thoroughly characterized the novel mutation P1124L in RyR2. P1124L was detected in a patient with severe HCM, who underwent surgical myectomy to relieve an LVOT obstruction producing symptoms of HF. Among all the RyR2 mutations reported to date (over 200), this is the first with a strong correlation with structural cardiomyopathy rather than cardiac arrhythmia. P1124L also appears in the gnomAD, a WES database, albeit with significantly lower frequency than T1107M — i.e. ~2 in 100,000 vs. ~4 in 10,000 for T1107M.⁸³ Hence, to our knowledge this is the first comprehensive, multi-level study — from molecule to whole animal — of an RyR2 mutation strongly associated with structural remodeling of the heart.

First, we show that P1124L, a highly conserved residue among RyR isoforms and species (Figure 4.3), is located within SPRY2, one of the peripheral domains of RyR2,

where it produces structural disturbances affecting the arrangement of a flexible linker and the interface between the SPRY2 and SPRY3 domains. P1124L is one of a handful of mutations that fall outside of the canonical mutation “hotspots” of RyR2 (Figure 4.2). These regions, which contain ~95% of the disease-causing RyR2 mutations, involve the N-terminal domain (CPVT-I), the helical domain 1 (CPVT-II), the central domain (CPVT-III) and the pore-forming domain (CPVT-IV). Recent high-resolution studies of RyR1 and RyR2 described in detail the movement of the central domains during RyR activation and gating;^{36,37} unfortunately, the resolution of the peripheral domains does not allow such a detailed analysis. Nevertheless, our model of the SPRY2/SPRY3 interface suggests that P1124L creates an inter-domain ionic bridge that could provide stability to this region of the channel. Ultimately, the consequence of these structural alterations is a cytosolic loss-of-function of the channel, as we determined using two complementary assays — [³H]ryanodine binding with recombinant protein and single channel recordings with mouse SR microsomes — and a luminal gain-of-function, which we measured in the SCR assay in HEK293 cells. While these experiments were carried out using homozygous P1124L channels, in the heterozygous condition — as in the patient — any phenotype will be the result of a heterogeneous population of channels containing anywhere between zero and four mutant subunits. We have previously discussed this issue for two CPVT related mutations.^{87,89}

Second, we show that mice expressing P1124L channels develop cardiac hypertrophy at 12 months of age. This phenotype, albeit mild, involves an increase in LV wall thickness, myocyte size and ANP expression in homozygous mice. Het hearts, on the other hand, have a tendency for hypertrophy and have a significant increase in

myocyte width. There are two possible reasons for the discrepancy in the phenotypic penetrance in mice compared to the human patient. For one, there are significant differences between mouse and human cardiac physiology³ that can hamper the expected phenotype. An example of this in the HCM field is for mutations that truncate the myosin-binding protein C (MyBP-C), which only produce hypertrophy in homozygous mice.¹⁸² The same occurs in MyBP-C knockout mice.^{145,183} It is possible that the patient carries specific epigenetic markers or modifiers that enhance the pathogenicity of P1124L. This could also explain the report of P1124L in WES cohorts, in which carriers devoid of these markers might have a mild, sub-clinical phenotype.¹⁸⁴ Further study of carriers of the mutation can strengthen this idea. Nevertheless, the presence of hypertrophy in mice supports the pathogenicity of P1124L, which is a not a dominant negative mutation — i.e. the phenotype increases with the P1124L content.

To our knowledge, this report is the first instance in which a clinically-relevant RyR2 mutation produces cardiac hypertrophy in mice. Previously, the Meissner laboratory reported a mouse model with three amino acid substitutions in RyR2 (W3587A/L3591D/F3603A, ADA), impairing the association with calmodulin (CaM), a regulatory partner.⁴³ Cardiomyocytes from homozygous ADA mice showed aberrant Ca²⁺ handling, and mice developed severe cardiac hypertrophy and died within 13–15 days of birth. Interestingly, none of the two Ca²⁺-dependent signaling pathways (CaM-CaN-NFAT and CaM-CaMKII-HDAC) was required for these mice to develop the hypertrophy.¹¹¹ Instead, the authors observed increased phosphorylation of GSK-3 β , most likely mediated by early activation of Erk1/2 kinase signaling but not Akt.¹¹¹ These pathways are also known involved in cardiac hypertrophy.¹⁷⁸ We found that the expression and

phosphorylation levels of CaMKII, Akt and Erk1/2 are unchanged in mice harboring P1124L, suggesting these pathways do not mediate the hypertrophic phenotype we observed. It is also possible that, since we only detected mild hypertrophy, these mediators are not significantly altered yet. Hence, further studies will be required to determine the specific signaling pathways necessary to trigger cardiac hypertrophy due to RyR2 dysfunction. Yet, our results provide concrete evidence that a clinically-relevant RyR2 mutation can trigger cardiac hypertrophy in mice, in the absence of other experimental manipulations.

Third, we observed cardiac arrhythmia — particularly BDVT — in 8-month-old P1124L mice undergoing a challenge with epinephrine and caffeine. In HCM, arrhythmia often develops because of the extensive structural and electrophysiological remodeling.^{99,100} Interestingly, P1124L mice show both structural (hypertrophy) and functional (arrhythmia) phenotypes independently, with the latter occurring at younger ages. Hence, these animals develop arrhythmia solely due to RyR2 dysfunction induced by the mutation. Unlike hypertrophy though, it is not surprising that an RyR2 mutation produces cardiac arrhythmia, since more than 200 mutations have been found in patients with CPVT. Commonly, these RyR2 gain-of-function mutations sensitize channels to luminal $[Ca^{2+}]$, triggering spontaneous Ca^{2+} release during *diastole*, delayed afterdepolarizations and, ultimately, arrhythmia.⁶⁹ The only other described loss-of-function mutation, on the other hand, produces bursts of Ca^{2+} during *systole*, leading to early afterdepolarizations and arrhythmia.⁸⁹ In myocytes expressing P1124L we observed stable Ca^{2+} handling during stimulation and SCR during resting periods, which is more consistent with the cellular mechanism underlying arrhythmia due to gain-of-function

mutations.^{69,185} Hence, from the molecular phenotypes we uncovered for P1124L channels — i.e. cytosolic loss-of-function and luminal gain-of-function — the latter seems to drive the arrhythmia: spontaneous activation of P1124L channels in conditions of high SR load will produce a larger Ca^{2+} signal that can diffuse to neighboring clusters, and propagate as Ca^{2+} waves. These events would activate NCX during diastole and produce triggered activity due to delayed afterdepolarizations. As shown in Figure 4.17, Homo mice have higher incidence of arrhythmia than Hets. It is important to underline that even though the difference in BDVT incidence between Het and WT mice is not statistically significant, none of the latter developed episodes of sustained arrhythmia. Therefore, the phenotype of Het mice cannot be overlooked. In these animals, permutation analysis predicts that most RyR2 channels should contain at least one P1124L subunit, and ~6% of the channels should contain four P1124L subunits.^{87,89} In the cellular mechanism described above, these are the channels that would likely promote larger SCR and Ca^{2+} waves.

Overall, P1124L represents a new paradigm for the emerging field of RyR2-mediated cardiac remodeling and Ca^{2+} -dependent HCM, as the first RyR2 mutation able to induce cardiac hypertrophy in a mouse model. Although we did not determine the signaling pathways underlying the hypertrophic phenotype, this is not discouraging. Similar to the reports by the Meissner laboratory using the ADA mouse, the lack of involvement of Ca^{2+} -dependent pathways foresees a more complex panorama that will require further investigation. Hence, at this point it is difficult to assess which of the molecular mechanisms we identified for P1124L — cytosolic loss-of-function and luminal gain-of-function — drives the hypertrophic remodeling. The mechanisms underlying the

arrhythmia, on the other hand, seem to be consistent with previously-studied CPVT mutations, and are expected to originate because of the luminal gain-of-function.

4.4. Methods

4.4.1. Identification of P1124L in a Human Patient

P1124L was identified in a patient with HCM referred to Mayo Clinic for evaluation. Michael Ackerman's groups at Mayo did the clinical evaluation and genetic testing that identified P1124L. In the final version of this chapter before publication as a scientific paper, we will include a section detailing the relevant work by Dr. Ackerman's laboratory that lead to the identification of P1124L.

4.4.2. Generation of the RyR2-P1124L Targeted Mice

The RyR2-P1124L-KI targeting vector was constructed using a combination of traditional cloning techniques and "recombineering", a highly efficient phage-based *Escherichia coli* homologous recombination system.^{186,187} The RyR2- P1124L-KI targeting vector was linearized by digestion with *NotI* and electroporated into murine SV/129 AB2.2 embryonic stem cells.¹⁸⁸ ES cells that integrated the targeting vector either by homologous or random integration were selected by growth on G418. The presence of gancyclovir (GANC) selected against clones that contained the HSV-TK cassette, thus enriching for clones that integrated the Neo cassette by homologous recombination. 472 Neo^r, GANC^r colonies were selected, replicated and expanded. DNA was isolated from 192 replica ES clones, digested with *BamHI* restriction endonuclease, electrophoresed on agarose gels, transferred to charged nylon membranes and hybridized to radiolabeled 3' probe. 36 correctly targeted clones were identified by the appearance of a 17.2 kb band

in addition to the 21.7 kb native band. DNA from 19 clones that appeared to be correctly targeted on the 3' side were digested with *Nco1* electrophoresed on agarose gels, transferred to charged nylon membranes and hybridized to radiolabeled 5' probe. Nineteen positive clones were identified. Six clones (2B2, 2C3, 2E5, 2B9, 2C9 and 2G9 1F2) were thawed from the master plate and fully expanded. The remaining 13 clones were partially expanded and cryopreserved. The expanded clones were genotyped using both the 5' and 3' probes. Correctly targeted clones were identified by the presence of a 21.7 kb native band and a 17.2 kb altered band when digested with *BamH1*, transferred to a charged nylon membrane and hybridized to the 3' probe, and the presence of a 15.2 kb native band and an 8.7 kb altered band when digested with *Nco1* and hybridized with the 5' probe. DNA sequence analysis was used to identify the correctly targeted clones and to confirm the presence of the floxed Neo cassette and the P to L substitution at position 1124. The chromosomes of 2 Ryr2-P1124L clones were counted and both clones were found to be euploid. Clones RyR2-P1124L 2E5 and RyR2-P1124L 2B2 were microinjected into C57Bl/6 blastocyst to produce chimeric founders. Highly chimeric males were crossed with C57Bl/6J females (000664, Jackson Laboratory). Agouti pups carrying the P1124L chromosome were identified by PCR. The floxed Neo cassette was excised by mating heterozygous RyR2-P1124L mice with Ella-Cre transgenic mice (003724, Jackson Laboratory). Pups with complete excision of the Neo cassette were identified by PCR and then backcrossed with C57Bl/6J mice. RyR2-P1124L pups negative for the Cre recombinase gene were further backcrossed for 7 additional generations to obtain a 99%+ congenic strain.¹⁴² Direct sequencing of the region of *Ryr2* containing the mutation (exon 28) was performed as described in section 2.4.3, using the

following primers: 5'-CGCATCTTCAGGGCAGAG-3' and 5'-GAGTGAAGCGGGAATGTC-3'. The sequences obtained were compared with the targeting vector, to the region of the murine chromosome 13 containing the *Ryr2* (accession number NT_039578.8), as well as the corresponding mRNA (accession number NM_023868.2) using Nucleotide BLAST.¹⁴³ The translated protein was compared to the mouse RyR2 (accession number E9Q401).

4.4.3. *Experimental Animals*

All animal experiments were approved by the University of Michigan Institutional Animal Care and Use Committee. All experiments performed at institutional cores were single blind. Age- and gender-matched littermates and C57Bl/6J mice were used as WT controls.

4.4.4. *Echocardiography*

Transthoracic echocardiography (Echo) was performed by the Echocardiography Service of the Frankel Cardiovascular Center Animal Phenotyping Core at the University of Michigan as described in section 2.4.5.

4.4.5. *Electrocardiography*

Surface electrocardiograms were recorded as described previously.⁸⁷ Mice were anesthetized with isoflurane (2–5%) and maintained on a heated pad. Needle electrodes were placed under the skin to record in Lead-I and Lead-II configurations, using a PowerLab system (ADInstruments). After 5–10 minutes of stabilization and baseline recording, epinephrine (2 mg/mg) and caffeine (120 mg/kg) were applied through intraperitoneal injection. Animals were monitored for 30 minutes after injection in search

of arrhythmic events (typically ventricular bigeminy and ventricular tachycardia) defined as 3 or more ventricular ectopic beats, consecutive or alternated with normal beats. These events were further classified as non-sustained (lasting less than 5 seconds) or sustained (lasting 5 seconds or longer).

4.4.6. Histological Staining

Hearts were explanted, perfused with PBS, and fixed in 10% neutral buffered formalin. The tissue was processed by the Pathology Core of the Unit for Laboratory Animal Medicine at the University of Michigan. Briefly, hearts were cut transversely, embedded in paraffin and stained with hematoxylin/eosin and Masson's trichrome stains. A blinded veterinary pathologist performed the tissue assessment and fibrosis scoring.

4.4.7. Transient Expression of RyR2 in HEK293 Cells

HEK293 cells were grown in DMEM supplemented with 10% FBS, 100 U/mL penicillin and 100 µg/mL streptomycin on 100 mm tissue culture dishes. Cells were transfected with a plasmid containing the mouse *Ryr2* cDNA using the Xtreme-DNA reagent (Roche Laboratories), following the instructions of the manufacturer. Cell lysates were prepared from transfected cells as previously described.⁸⁹ 24 h after transfection, cells were washed twice with PBS, then scraped from the plate and solubilized in 200 µL of lysis buffer, containing 25 mM Tris/50 mM HEPES (pH 7.4), 137 mM NaCl, 1% CHAPS, 0.5% soybean phosphatidylcholine, 2.5 mM DTT, and protease inhibitors (2 µM leupeptin, 100 µM phenylmethylsulphonyl fluoride, 500 µM benzamidine, 100 nM aprotinin). The cells were incubated on ice for 1 h and lysates were obtained by centrifuging at 16,000 × g at 4 °C for 10 min to remove insoluble material. Protein concentrations were determined using the Bradford method (Bio-Rad).

4.4.8. Spontaneous Ca²⁺ Release in HEK293 Cells

Stable inducible HEK293 cells lines expressing WT or P1124L-RyR2 were cultured as described in section 4.4.7. Spontaneous Ca²⁺ release was measured using the FRET endoplasmic reticulum Ca²⁺ sensor D1ER (Addgene, 36325), as previously described.¹¹⁹ After 18-24 hours of subculture on 35 mm glass-bottom dishes, D1ER was transfected as described in section 4.4.7. 18–24 post-transfection, RyR2 expression was induced by adding culture medium supplemented with tetracycline 1 µg/mL. For imaging (performed 18–24 h after induction), cells were continually perfused with Krebs-Ringer-HEPES buffer containing (mM): 125 NaCl, 5 KCl, 1.2 KH₂PO₄, 1.2 MgCl₂, 6 glucose, 25 HEPES, pH 7.4. 2 mM CaCl₂, 1 mM tetracaine and 20 mM caffeine were added as indicated. Images were captured at room temperature on an Olympus FV-100 confocal microscope with a 40X objective at 405 nm excitation, and 535-565 (YFP) and 430-470 (CFP) emission. Images were collected every 1.644 seconds. FRET was calculated as the YFP/CFP ratio. The maximum store capacity, fractional release, and activation and termination thresholds were calculated using the following equations. The parameters for these equations were defined as described in Figure 4.7.

$$\begin{aligned} \text{Store Capacity} &= (F_{Max} - F_{Min}) & \text{Termination Threshold} &= \frac{F_{Term} - F_{Min}}{\text{Store Capacity}} \times 100\% \\ \text{Activation Threshold} &= \frac{F_{Act} - F_{Min}}{\text{Store Capacity}} \times 100\% & \text{Fractional Release} &= \frac{F_{Act} - F_{Term}}{\text{Store Capacity}} \times 100\% \end{aligned}$$

4.4.9. Tissue Homogenization

Whole heart homogenates were prepared as described in section 2.4.6.

4.4.10. Western Blotting

Western blots were carried out as described in section 2.4.7. In addition, we used primary antibodies for the following targets: CaMKII (1:1000; 4436, Cell Signaling), pT286-CaMKII (1:1000; 12716, Cell Signaling), p44/42 MAPK (Erk1/2) (1:1000; 9102, Cell Signaling), pT202/Y204-p44/42 MAPK (Erk1/2) (1:1000; 9101, Cell Signaling), Akt (1:1000; 9272, Cell Signaling), pS473-Akt (1:1000; 9271, Cell Signaling).

4.4.11. [³H]Ryanodine Binding Assays

[³H]Ryanodine binding assays were performed as described in section 3.4.5. Binding reactions contained 50–100 µg of cell lysates. Whatman GF/B filters were pre-soaked in 5% polyethyleneimine to maximize protein retention.

4.4.12. Single Channel Recordings

Cardiac SR-enriched microsomes for single channel recordings were prepared from mouse hearts using differential centrifugation, as previously described.⁸⁹ 10–15 pooled mouse hearts were homogenized as described in section 2.4.6. Homogenates were centrifuged a second time at 8000 x *g* for 20 minutes at 4°C. Supernatants were further centrifuged at 100,000 x *g* for 35 minutes at 4°C. The pellets containing SR-enriched microsomes were resuspended in homogenization buffer supplemented with 0.3 M sucrose.

RyR2 from cardiac microsomes were incorporated into planar lipid bilayer to record single channel activity as previously reported.⁸⁹ The *trans* (1000 µl) and the *cis* (1000 µl) chambers (corresponding to the luminal and cytoplasmic side of the channel, respectively) contained 300 and 50 mM CsCH₃SO₃ (cesium methanesulfonate), respectively, 20 mM MOPS (pH 7.2), and nominally free [Ca²⁺] (~5 µM). A phospholipid

bilayer of phosphatidylethanolamine : phosphatidylserine : phosphatidylcholine (1.0:0.8:0.2 ratio dissolved in n-decane to 20 mg/ml) was "painted" with a glass rod across an aperture of ~200 μm diameter in a Delrin cup. The *trans* chamber was the voltage control side connected to the head stage of a 200-A Axopatch amplifier, while the *cis* side was held at virtual ground. Channel activity was recorded after filtration with an 8-pole low pass Bessel filter set at 1.5 kHz, and digitized at a rate of 4 kHz using a Digidata 1200 AD/DA interface. Data acquisition and analysis was performed with Axon Instruments hardware and software (pClamp 10).

4.4.13. Confocal Ca^{2+} Imaging in Isolated Myocytes

Ventricular myocytes were isolated as described in section 2.4.9. Ca^{2+} transients triggered by field stimulation were recorded as described in section 2.4.10. To determine the susceptibility of developing spontaneous Ca^{2+} release, cells were paced at 3 Hz for 30 s at basal conditions and in the presence of 300 nM Iso. Following this train of stimulation, cells were monitored for 30 seconds for spontaneous Ca^{2+} waves.

4.4.14. Crystallization of SPRY2

Mouse RyR2 (residues 1080–1253) including the P1124L substitution were cloned, expressed and purified according to a similar strategy previously used for wild type RyR2 SPRY2 domain.³⁰ Protein crystals were grown using hanging drop method at 20°C. P1124L (5 mg/mL) was crystallized in 0.1 M potassium thiocyanate, 25-35% PEG2000MME with seeding of wild type crystals. Crystals were harvested and flash frozen in the original growth condition supplemented with 25-30% glycerol. Diffraction data were collected at the Advanced Photon Source (APS) beamline 23ID-D. Data were

processed with HKL2000. The wild type RyR2 SPRY2 structure (PDB ID 4P9I) was used as a search model for molecular replacement to solve the RyR2 SPRY2 P1124L mutant structure. The statistics for data collection and refinement is shown in Table 4.1. Coordinate and structure factor for P1124L is available in the PDB with accession code 5VSN.

4.4.15. Gene Expression Analysis

Total RNA extraction, cDNA synthesis and gene expression analysis were carried out as described in section 3.4.5. Expression levels of *Nppa* (Mm01255748_g1, ThermoFisher), *Nppb* (Mm01255770_g1, ThermoFisher), *Myh7* (Mm00600555_m1, ThermoFisher), and *Actb* (4352933E, ThermoFisher) were assessed using TaqMan gene expression probes (ThermoFisher).

4.4.16. Statistical Analysis

Data are presented as mean \pm SEM. Statistical significance was determined at $p \leq 0.05$ using t-test, one-way ANOVA with Holm-Sidak's post-hoc or two-way ANOVA with Holm-Sidak's post-hoc. Data without normal distribution are shown in box-plots with whiskers indicating a 1.5 inter-quartile range. These data were compared using one-way ANOVA on Ranks followed by Dunn's post-hoc. Analyses were carried out in SigmaPlot 12.5 (Systat Software).

4.5. Acknowledgments

This chapter was prepared to be submitted as a manuscript including data generated with the following collaborators: Filip Van Petegem and Michael Yuchi, University of British Columbia, Canada (X-ray crystallography); Carmen R. Valdivia and

Mario San Martin, University of Michigan (single channel recordings); Yan-Ting Zhao, University of Michigan (isolation of ventricular myocytes); Dawn Henderlong, University of Michigan (expansion of plasmids, maintenance and transfection of HEK cells); Jonathan J. Hernández, University of Wisconsin-Madison (gene expression analysis); Patricia Powers, University of Wisconsin-Madison (generation of the P1124L mouse); and J. Martijn Bos, Cherisse Marcou and Michael J. Ackerman, Mayo Clinic (clinical diagnosis and identification of P1124L).

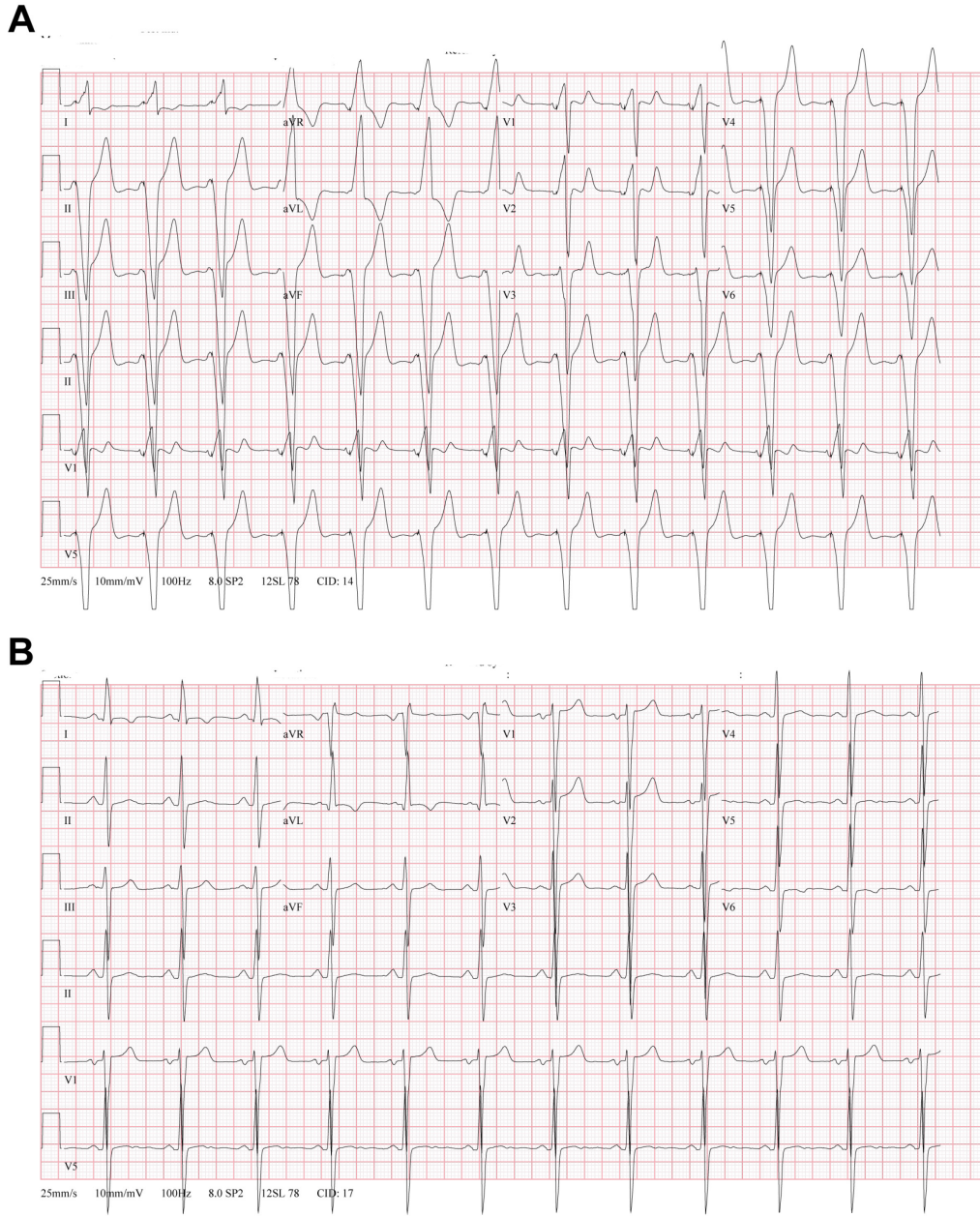


Figure 4.1. Electrocardiogram Recordings from the Patient Harboring the P1124L Mutation.

A. 12-lead ECG recorded upon admission at Mayo Clinic before undergoing surgery. Heart rate is normal, but rhythm is maintained by firing of the dual-chamber pacemaker previously implanted to alleviate symptoms of heart failure. Stimulation artifact is visible in all leads. **B.** ECG recording 1 day post- surgical myectomy to remove LVOT obstruction.

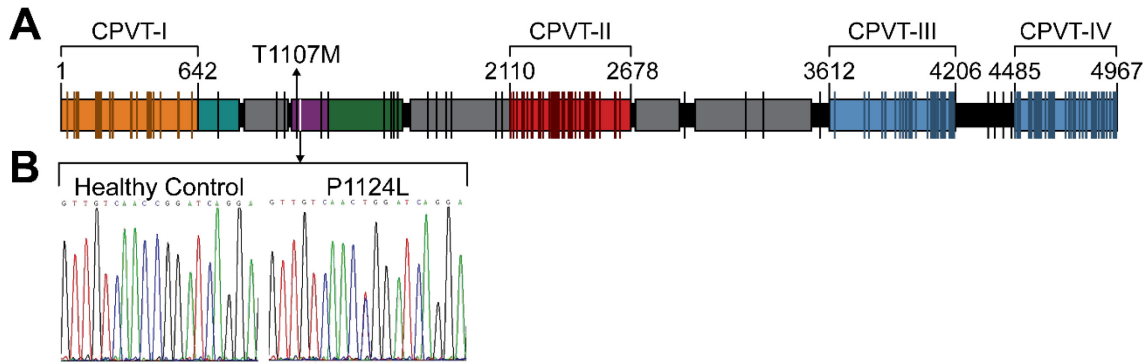


Figure 4.2. Location of P1124L in the Context of the RyR2 Mutation “Hotspots.”

A. Linear representation of an RyR2 subunit indicating the three mutation “hotspots.” **B.** Chromatograms for direct sequencing of RyR2 in a healthy patient and the patient harboring P1124L. Arrowhead indicates changed base.

Accession Number	Species	Protein	Sequence	Sequence	
				1107	1124
Q92736	Human	RyR2	1100	RWYFEFETVTAGDMRVGWSRPGCQ	PDQELGSDELA 1134
E9Q401	Mouse	RyR2	1100	RWYFEFEAVTAGDMRVGWSRPGCQ	PDLELGSDDELA 1134
B0LPN4	Rat	RyR2	1093	RWYFEFEAVTAGDMRVGWSRPGCQ	PDLELGSDDELA 1127
P30957	Rabbit	RyR2	1100	RWYFEFEAVTSGDMRVGWSRPGCQ	PDQELGSDELA 1134
*	Pig	RyR2	1100	RWYFEFETVTAGDMRVGWSRPGCQ	PDQELGSDELA 1134
P21817	Human	RyR1	1086	RWYFEFEAVTTGEMRVGWARPELR	PDVELGADELA 1120
E9PZQ0	Mouse	RyR1	1088	RWYFEFEAVTTGEMRVGWARPELR	PDVELGADDLA 1122
F1LMY4	Rat	RyR1	1088	RWYFEFEAVTTGR-ELGWARPELR	PDVELGADDLA 1121
P11716	Rabbit	RyR1	1087	RWYFEFEAVTTGEMRVGWARPELR	PDVELGADELA 1121
P16960	Pig	RyR1	1087	RWYFEFEAVTTGEMRVGWARPELR	PDVELGADELA 1121
Q15413	Human	RyR3	1086	KWYFEFEVVTGGDMRVGWARPGCR	PDVELGADDQA 1120
A2AGL3	Mouse	RyR3	1086	KWYFEFEVVTGGDMRVGWARPGCR	PDIELGADDQA 1120
Q9TS33	Rabbit	RyR3	1086	KWYFEFEVVTGGDMRVGWARPGCR	PDIELG 1115
Q24498	Drosophila	RyR	1093	KWYFEFEVLTSGPMRVGWARADCY	PGAMLGSED 1125

Figure 4.3. Amino Acid Sequence Alignment of RyR Isoforms from Various Species.

Sequence alignment of residues 1100–1134 of the human RyR2 with RyR isoforms from other species. Shaded residues are different from the human template. P1124 is conserved in all RyR isoforms from all the species compared. Accession numbers and protein sequences from UniProt.¹²⁸ *: Pig RyR2 sequence from Peng et al.³⁶

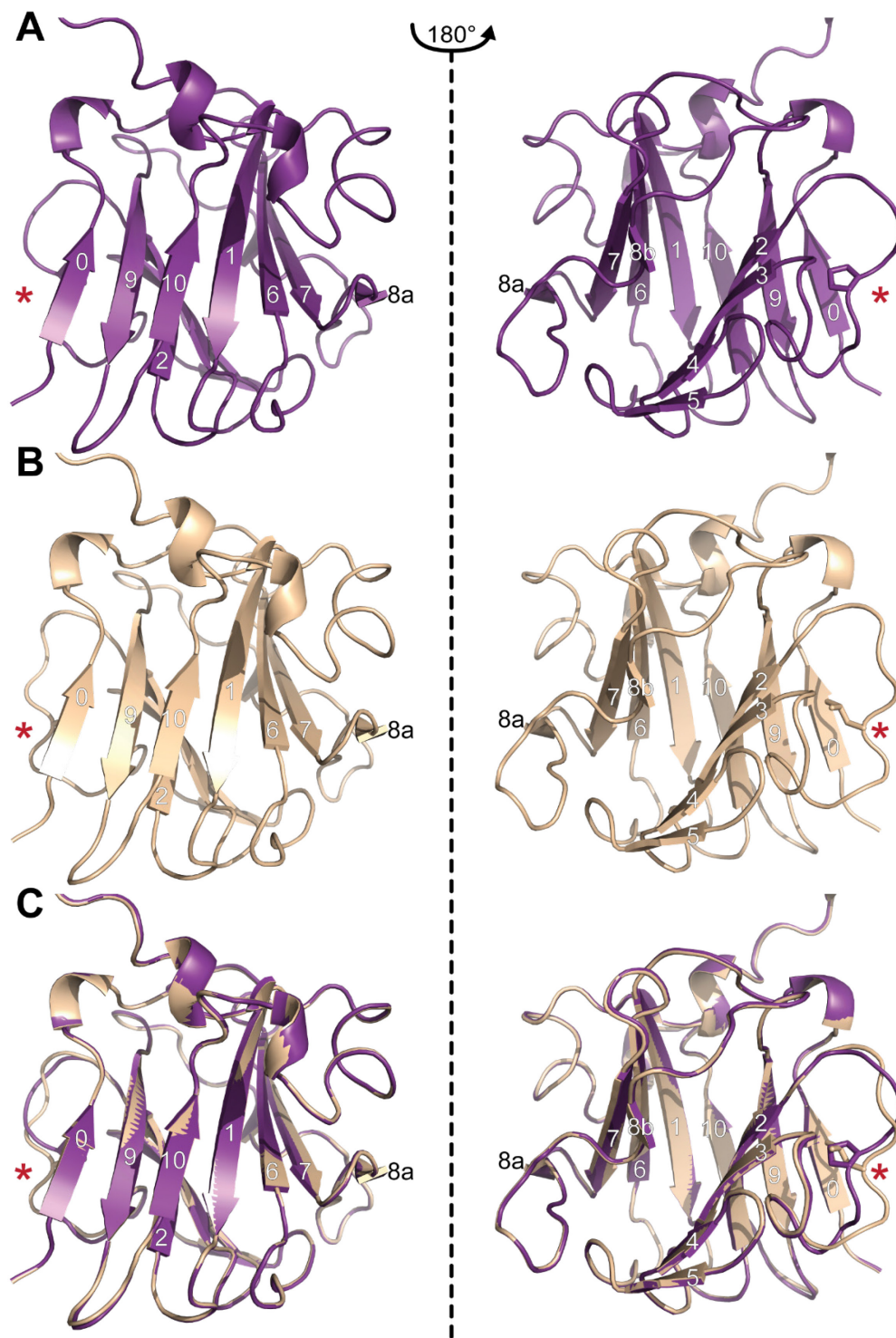


Figure 4.4. Structure of the SPRY2 Domain at 1.44 Å resolution.

A. Crystal structures of the WT SPRY2 domain. **B.** Crystal structure of the P1124L SPRY2. **C.** Overlap the structures from panels A and B. Numbers indicate β -sheets as defined by Lau et al.³⁰ Asterisk indicates the flexible linker containing residue 1124.

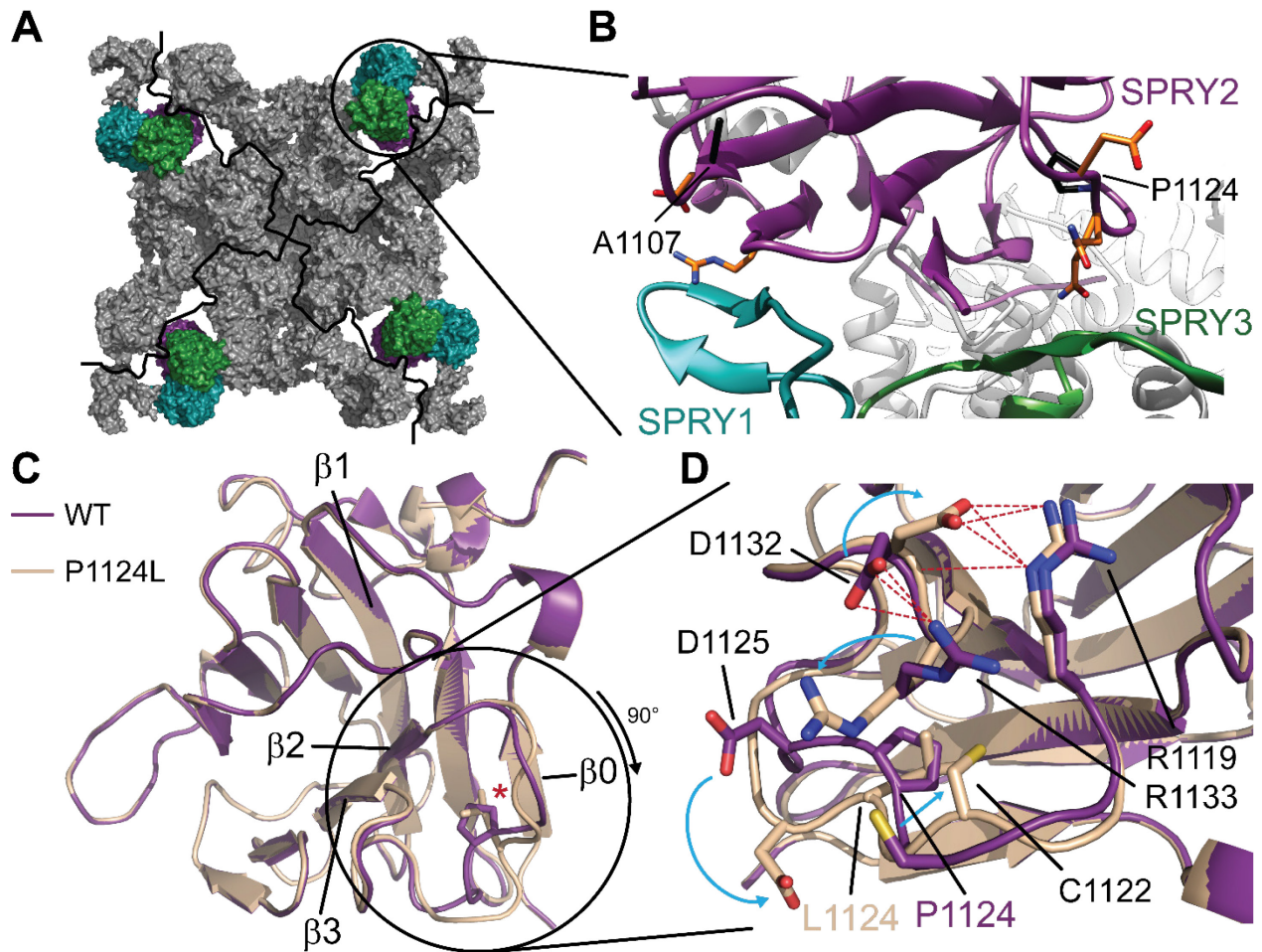


Figure 4.5. Location of P1124L Within the SPRY2 Domain of RyR2.

A. Electron density map of RyR2.³⁶ Subunits are delimited by black lines and the three SPRY domains area colored as indicated in B. **B.** Modeled interface between the three SPRY domains of RyR2. The position of the two HCM-associated mutations, A1107 and P1124, is indicated. **C-D.** Superimposed crystal structures of the WT and P1124L SPRY2 domains. Asterisk indicates positions of residue 1124 within the β 2- β 3 linker. Blue arrows indicate movement of four residues between WT and P1124L structures. Most notably: D1125 rotates and becomes exposed into the SPRY1-3 interface, D1132 rotates away from R1133 breaking a salt bridge, and moves closer to R1119 forming a new salt bridge. Red dashed lines indicate salt bridges.

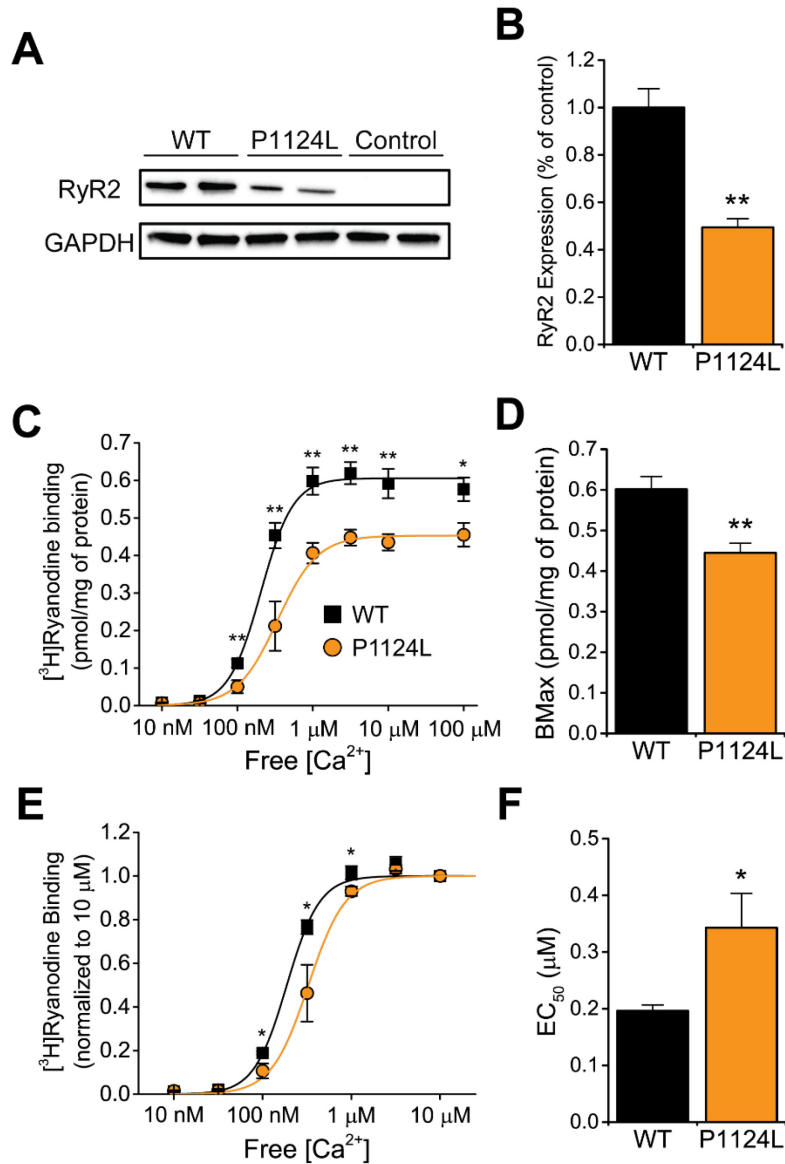


Figure 4.6. RyR2-P1124L Activity Measured with [³H]Ryanodine Binding Assays.

A. Representative Western blot of P1124L and WT RyR2 expression in transiently-transfected HEK 293 cells. **B.** P1124L expression is lower than WT expression (n = 6 transfections, **: p < 0.01). **C.** Ca²⁺-dependent [³H]ryanodine binding curve corrected for RyR2 expression. **D.** Maximum binding (BMax) calculated from the curves in C using Hill's equation. P1124L has lower Bmax than WT (0.44±0.02 vs. 0.60±0.03 pmol/mg of protein, p < 0.01). **E.** Ca²⁺-dependent [³H]ryanodine binding curve normalized to 10 μM [Ca²⁺]. **F.** P1124L required higher [Ca²⁺] for activation than WT (EC₅₀ = 362.9±74.5 vs. 190.6±9.8 nM, p = 0.04). Overall these data suggest P1124L is a loss-of-function mutation (n = 7 bindings. *: p < 0.05, ** p < 0.01 vs WT.).

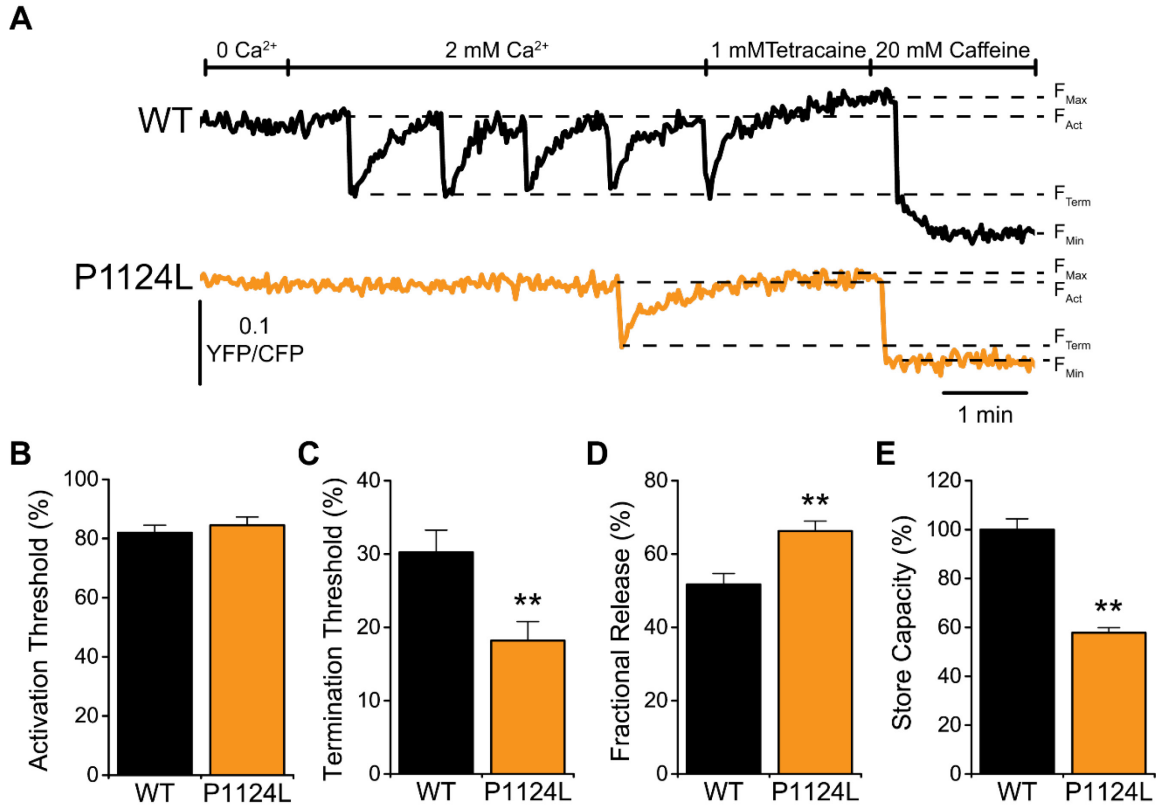


Figure 4.7. Abnormal Termination of Spontaneous Ca^{2+} Release in HEK293 Cells Expressing RyR2.

A. Representative traces of the intra-ER FRET signal using D1ER, from HEK cells with stable expression of RyR2. The $[\text{Ca}^{2+}]$ in the perfusion solution was increased to 2 mM to induce oscillations of intra-SR $[\text{Ca}^{2+}]$ due to spontaneous activation of RyR2 (spontaneous Ca^{2+} release, SCR). Tetracaine (1 mM) and caffeine (20 mM) were perfused to measure the store capacity and calculate other parameters. **B-C.** Activation and termination thresholds for SCR, as percentage of store capacity. **D.** Percentage of the store capacity release during SCR events. **E.** Store capacity, determined as $\text{FRET}_{\text{Tetracaine}} - \text{FRET}_{\text{Caffeine}}$. Data expressed as percentage of control ($n = \text{WT } 22, \text{ PL } 19$. $p < 0.01$ vs WT).

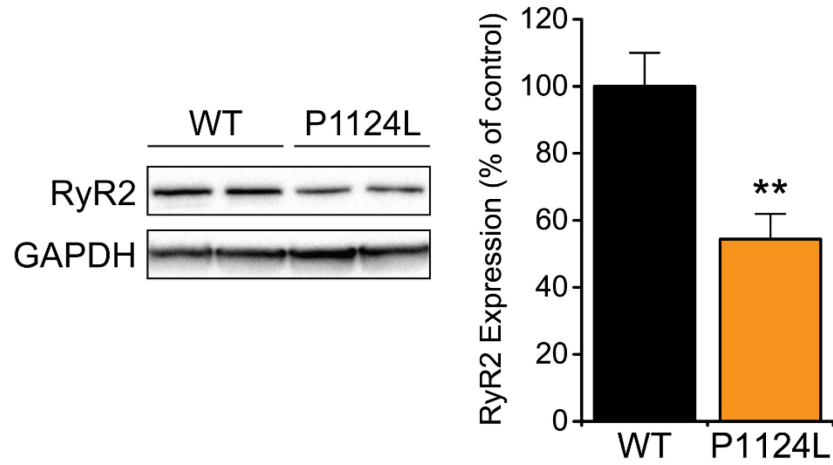


Figure 4.8. RyR2 Expression in Stable HEK Cells.

Representative Western blot and quantification of RyR2 level in HEK cell with stable expression induced by addition of tetracycline 1 $\mu\text{g}/\text{mL}$ to the culture medium (n = 6 WT, PL 5. $p < 0.01$ vs WT)

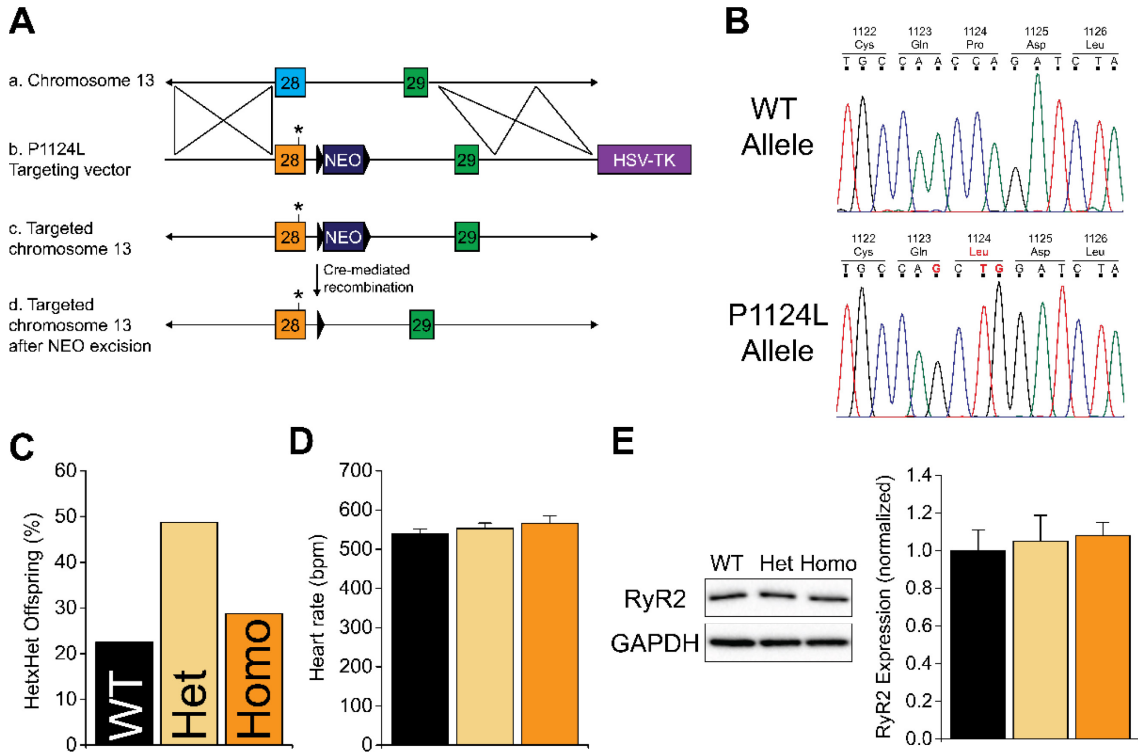


Figure 4.9. Generation of the P1124L Mouse Model.

A. Strategy for the generation of the mouse model by homologous recombination. Numbers indicate RyR2 exons. **B.** Direct sequencing of the WT and mutant allele of a heterozygous mouse. **C.** Offspring proportions of heterozygous mice mating (n = 160 pups, 25 litters). **D.** Heart rate measured during echocardiography (n = 8 per genotype). **E.** Quantification of RyR2 density in whole heart homogenates (n = 5 per genotype).

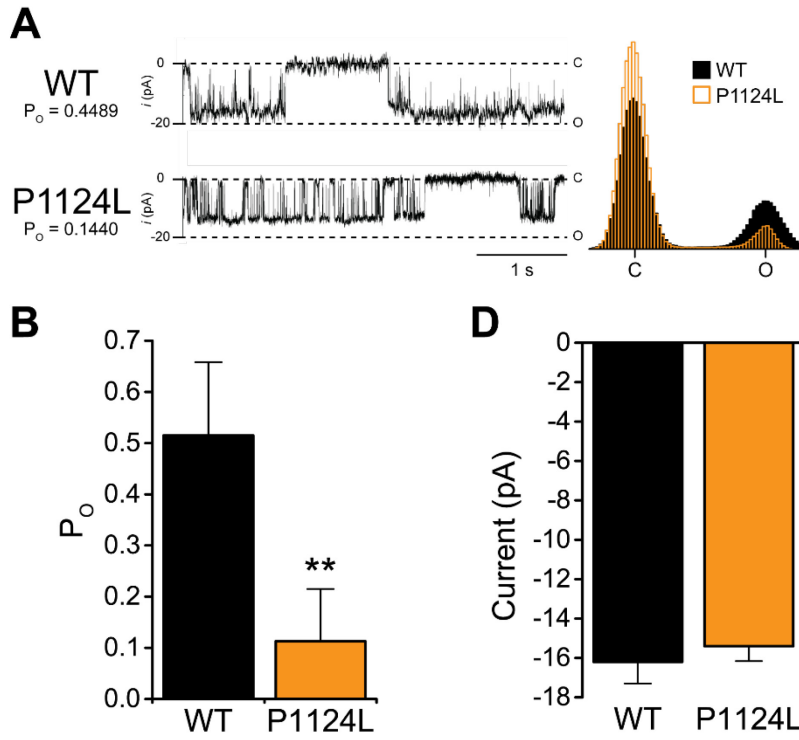


Figure 4.10. Single RyR2 Recordings from Cardiac Microsomes.

A. *Left.* Representative single RyR2 channel recordings from cardiac microsomes prepared WT and Homo P1124L hearts. *Right.* Overlapped histograms of normalized current calculated from two representative channels. **B.** Average open probability (P_o) recorded at nominally free $[Ca^{2+}]$ (~3-5 μM). **C.** Average single channel current calculated from single channel current recorded in with a 50/500 mM Cs^+ gradient. (n = 3 WT, 5 P1124L. **: $p < 0.05$ vs. WT).

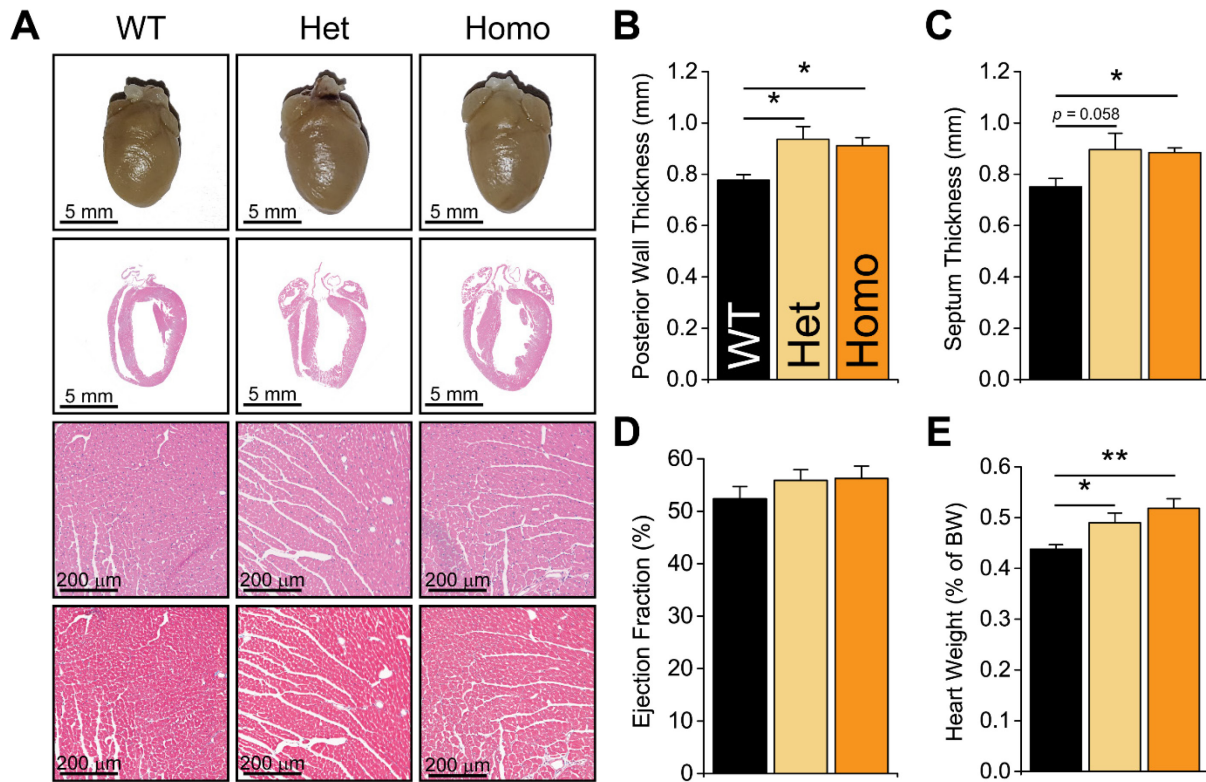


Figure 4.11. Cardiac Hypertrophy in 12-month-old P1124L Mice.

A. Representative pictures of whole hearts fixed in formalin (first row), H&E-stained coronal sections at low magnification of paraffin-embedded tissue (second row), high-magnification micrographs of H&E-stained tissue section (third row) and high-magnification micrographs of Masson's Trichrome-stained tissue sections (fourth row). **B-D.** M-Mode echocardiography measurements showing an increase in posterior wall (**B**) and septum thickness (**C**), and normal ejection fraction in homozygous mice (**D**) ($n = 8$ WT, 7 Het, 8 Homo. *: $p < 0.05$ vs WT). **E.** Heart weight normalized by body weight is also increased in homozygous mice ($n = 16$ WT, 13 Het, 14 Homo. *: $p < 0.05$, **: $p < 0.05$ vs WT).

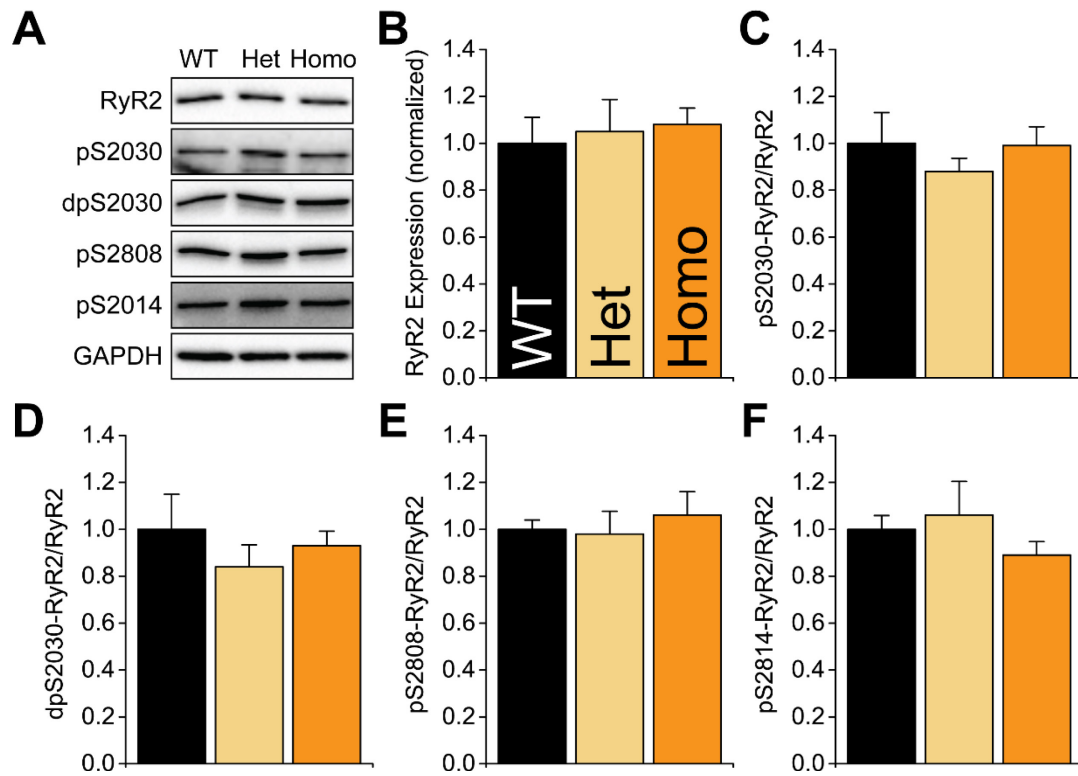


Figure 4.12. RyR2 Expression and Phosphorylation in 12-month-old Mice.

A. Representative blots. **B.** Quantification of RyR2 expression normalized to GAPDH. **C-F.** Phosphorylation levels of the three major RyR2 phospho-sites (dp: dephospho; p: phospho): S2031 (**C,D**), S2808 (**E**), and S2814 (**F**) (n = 4–5 per genotype).

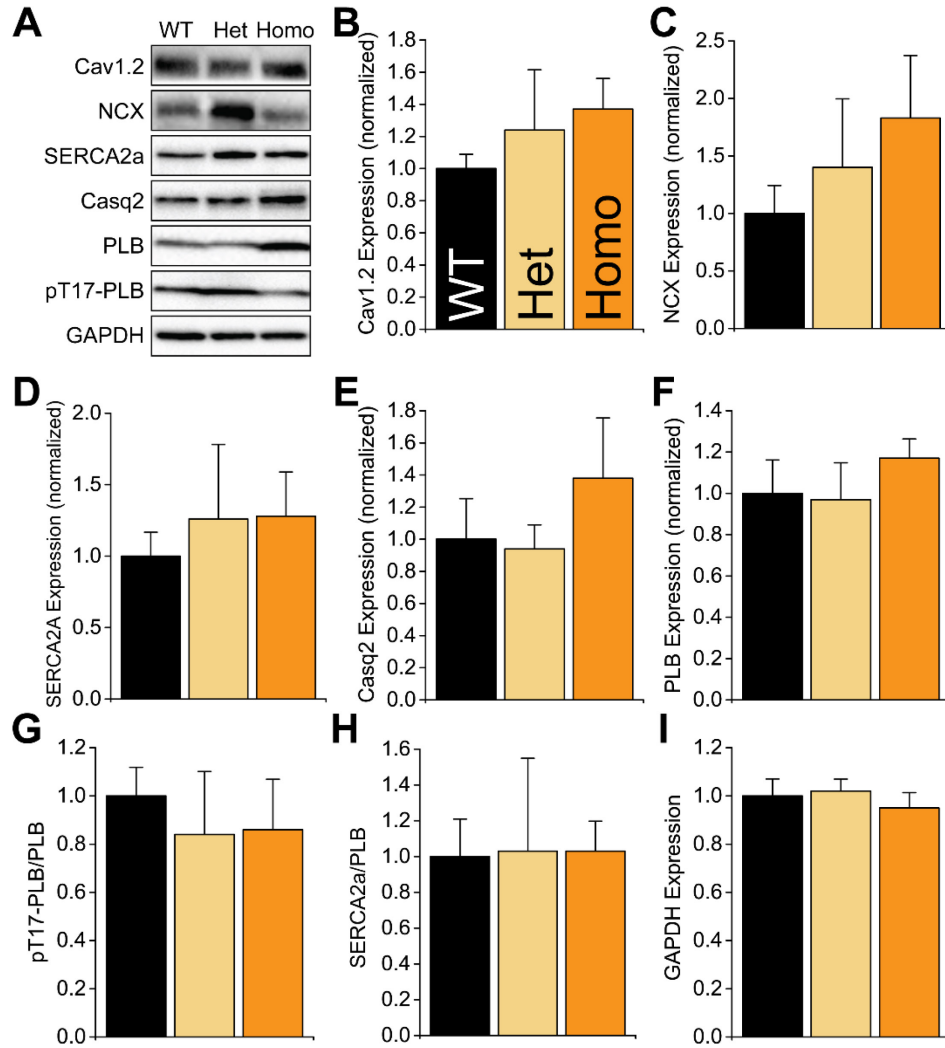


Figure 4.13. Expression of E-C Coupling Proteins in 12-month-old Mice.

A. Representative blots. **B-F.** Quantification of expression normalized to GAPDH of the e-c coupling proteins Cav1.2 (catalytic subunit of LTCC, **B**), NCX (**C**), SERCA2a (**D**), Casq2 (**E**) and PLB (**F**). **G.** Phosphorylation level of PLB at the CaMKII site, T17, normalized to total PLB expression. **H.** Ratio between the normalized expression of SERCA2A and PLB. **I.** Quantification of GAPDH expression (n = 4–5 per genotype). Samples and loading controls are the same as in Figure 4.12.

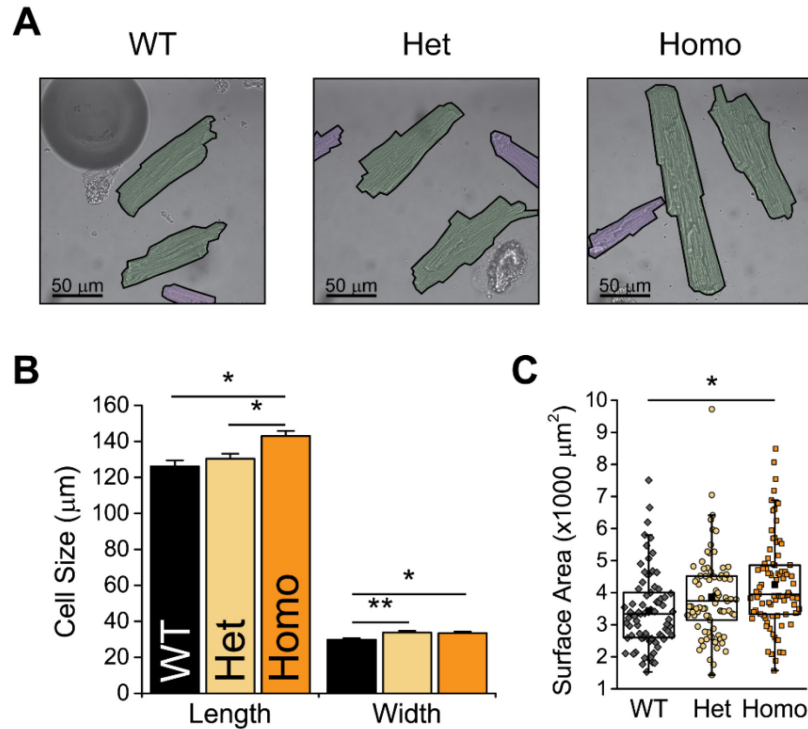


Figure 4.14. Ventricular Myocyte Size.

A. Representative transmitted light images of ventricular myocytes. Cells are delineated and colored green (measured cells) or purple (out of focus or out of frame). **B.** Average cell length and width measured from confocal images. **C.** Distribution of cell surface area per genotype ($n = \text{WT } 75, \text{ Het } 81, \text{ Homo } 84, N = 3$). * $p < 0.05$, ** $p < 0.01$ vs WT).

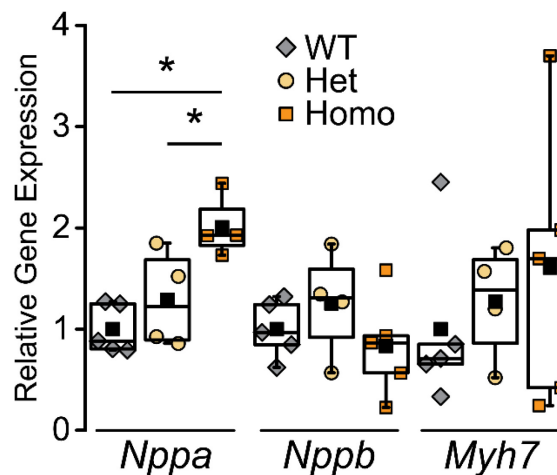


Figure 4.15. Expression of Hypertrophic Genes in 12-month-old Mice.

Box plots with data overlap expression level showing of three hypertrophic genes: atrial natriuretic peptide (*Nppa*), brain natriuretic peptide (*Nppb*), and β -myosin heavy chain (*Myh7*). Data normalized to actin expression (*Actb*) ($n = 4\text{--}5$ per genotype. * $p < 0.05$).

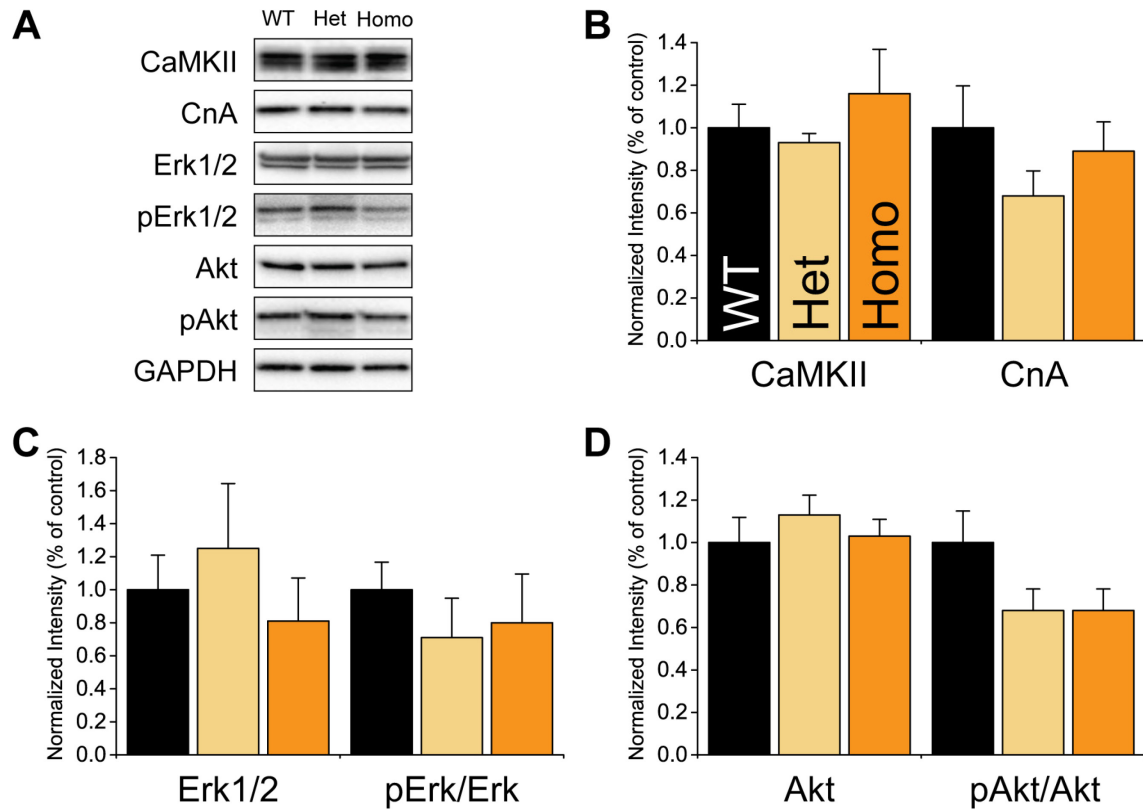


Figure 4.16. Hypertrophic Signaling Pathways.

A. Representative blots. **B-D.** Quantification of the expression and phosphorylation of proteins involved in three hypertrophic signaling pathways: CaMKII and CnA, the catalytic subunit of CaN (**B**); Erk1/2 and pT202/T204-Erk1/2 (**C**); and Akt and pS473Akt (**D**). (n = 4–5 per genotype).

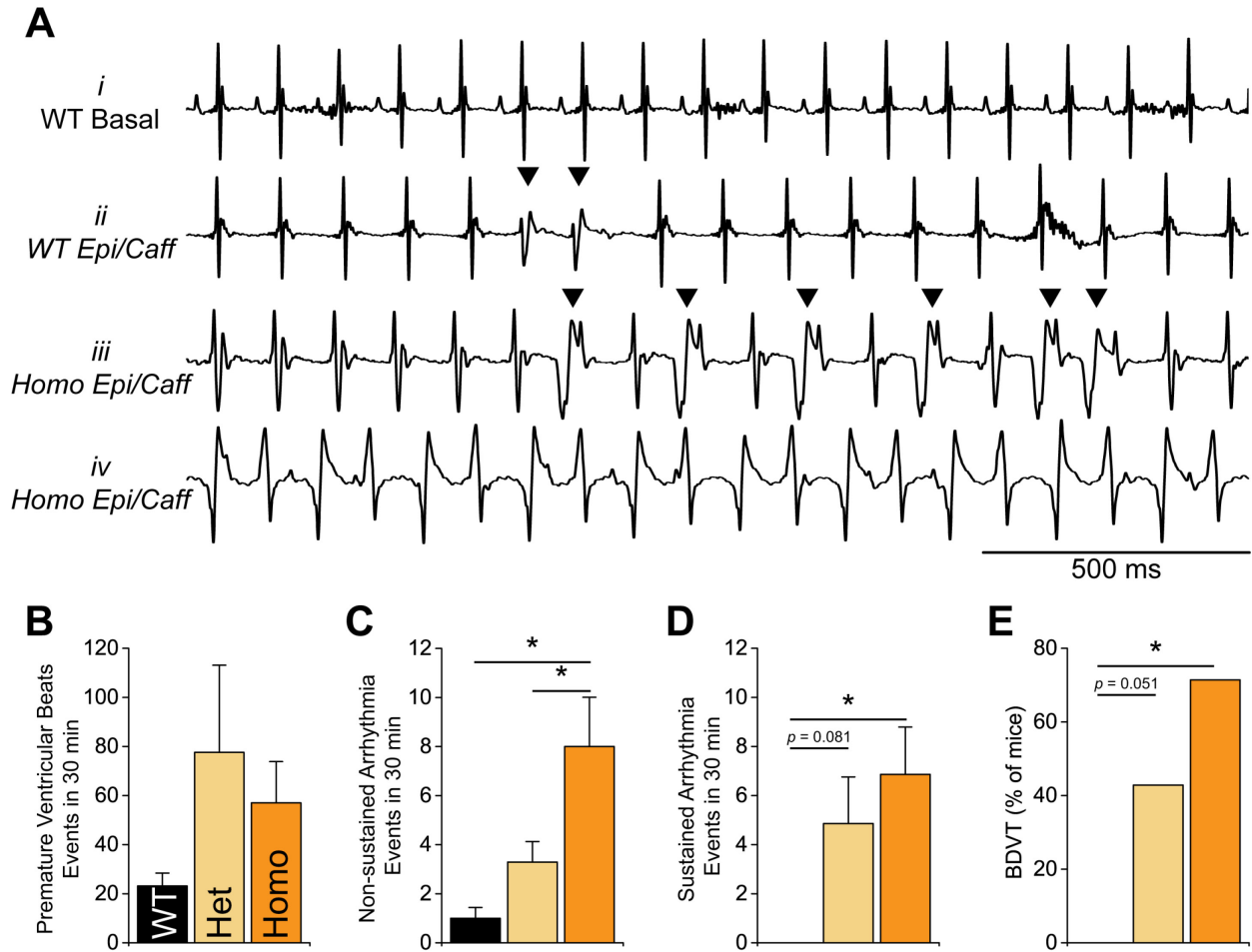


Figure 4.17. Susceptibility to Ventricular Arrhythmia in P1124L Mice Challenged with Epinephrine/Caffeine.

A. 2-second representative lead-II ECG traces from mice undergoing IP injection of 2 mg/kg of epinephrine and 120 mg/kg of caffeine (Epi/Caff). *i*- sinus rhythm in a WT mouse before treatment; *ii*- premature ventricular beats in a WT mouse; *iii*- non-sustained ventricular bigeminy in a Homo mouse; *iv*- bidirectional VT in a Homo mouse. **B.** Premature ventricular beats quantified after injection. **C-D.** Average number of episodes of non-sustained (lasting ≤ 5 s) and sustained arrhythmias (lasting > 5 s). **E.** Incidence if sustained bidirectional VT. **F-G.** Duration of non-sustained and sustained arrhythmia events. (n = 7 per genotype. * $p < 0.05$ vs WT).

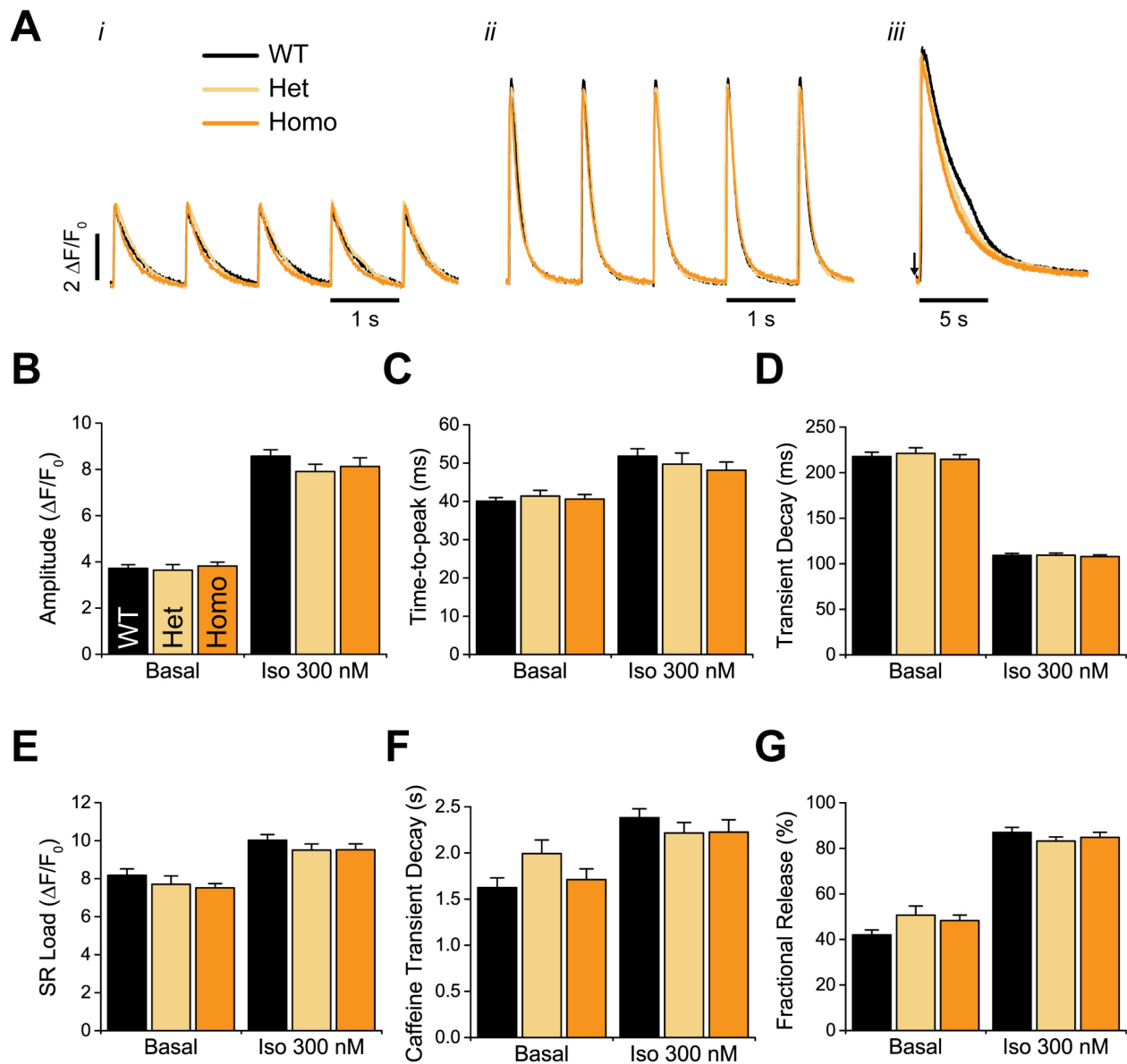


Figure 4.18. Ca²⁺ Transients and SR Load.

A. Representative traces of Ca²⁺ fluorescence produced by fluo-4, at control conditions (*i*), in the presence of 300 nM isoproterenol (*ii*) and upon rapid perfusion of 20 mM caffeine (*iii*, perfusion indicated by arrow). **B-D.** Quantification of Ca²⁺ transient amplitude (B), time-to-peak (C) and 50% transient decay time (D) during 1 Hz field stimulation (Basal WT: N = 5, n = 56; Het: N = 3, n = 15; Homo: N = 6, n = 47. Iso WT: N = 3, n = 22; Het: N = 3, n = 19; Homo: N = 3, n = 18). **E-G.** Quantification of SR load (E), 50% caffeine transient decay time (F) and fractional release of Ca²⁺ (G) (Basal WT: N = 5, n = 22; Het: N = 3, n = 15; Homo: N = 6, n = 25. Iso WT: N = 3, n = 21; Het: N = 3, n = 19; Homo: N = 3, n = 18). For all genotypes, $p < 0.01$ Basal vs Iso).

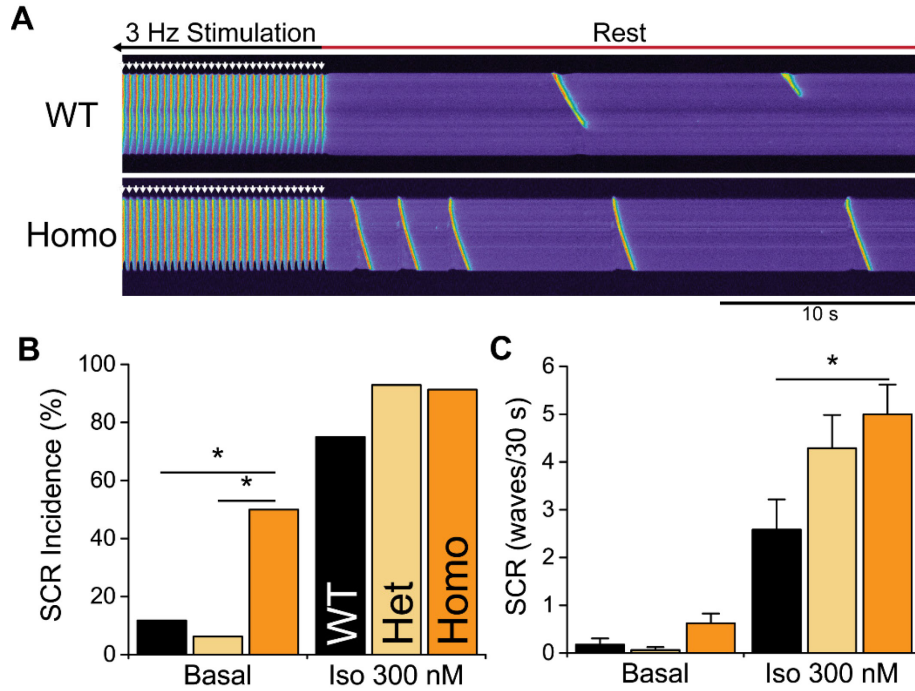


Figure 4.19. Susceptibility to Spontaneous Ca²⁺ Release in Ventricular Myocytes.

A. Representative traces of WT and Homo ventricular myocytes stimulated with 300 nM Isoproterenol (Iso), paced at 1 Hz for 30 s and monitored at rest for 30 s. **B.** Percentage of cells showing spontaneous Ca²⁺ release (SCR) during the monitoring period. SCR incidence is increased in Homo mice in basal conditions. **C.** Average number of SCR events (Ca²⁺ waves) during in 30 seconds. Homo myocytes show significantly more waves under Iso stimulation (Basal WT: n = 17; Het: n = 16; Homo: n = 16. Iso WT: n = 12; Het: n = 14; Homo: n = 23. N = 3 per genotype. * *p* < 0.05).

Table 4.1. X-ray crystallography data collected and refinement statistics.

Parameters	P1124L
Wavelength (Å)	1.00
Resolution range (Å)	23.55 - 1.439 (1.491 - 1.439)
Space group	P 2 21 21
Unit cell	36.29 66.23 66.98 90 90 90
Total reflections	29741
Unique reflections	29697 (2662)
Multiplicity	6.7 (5.2)
Completeness (%)	98.88 (89.81)
Mean I/sigma(I)	12.97 (1.96)
Wilson B-factor	21.94
R-merge (%)	0.109 (0.830)
R-meas	0.118 (0.918)
R-pim (%)	0.045 (0.384)
Reflections used in refinement	29665 (2643)
Reflections used for R-free	1480 (129)
R-work	0.1736 (0.2979)
R-free	0.1926 (0.2986)
Number of non-hydrogen atoms	1518
Macromolecules	1400
Ligands	7
Solvent	111
Protein residues	169
RMS(bonds)	0.005
RMS(angles)	0.76
Ramachandran favored (%)	97.01
Ramachandran allowed (%)	2.99
Ramachandran outliers (%)	0.00
Rotamer outliers (%)	0.00
Clash score	2.94
Average B-factor	31.74
Macromolecules	30.96
Ligands	49.03
Solvent	40.45

Statistics for the highest-resolution shell are shown in parentheses.

Table 4.2. Echocardiographic Parameters in 8-month-old P1124L Mice.

	WT	Het	Homo	ANOVA	t-test WT vs Homo
n	6	6	7	-	-
BW (g)	26.00±1.88	25.83±1.66	27.43±1.76	NS	NS
HR (bpm)	534±13	552±11	495±11	WT vs Homo $p = 0.056$ Het vs Homo $p = 0.008$	$p = 0.040$
IVSd (mm)	0.78±0.02	0.81±0.03	0.82±0.02	NS	NS
IVSs (mm)	1.07±0.03	1.20±0.08	1.29±0.03	WT vs Homo $p = 0.023$	$p < 0.001$
IVSth (%)	37.88±5.94	47.35±7.00	58.2±3.75	WT vs Homo $p = 0.056$	$p = 0.019$
PWd (mm)	0.78±0.02	0.8±0.04	0.86±0.03	NS	$p = 0.062$
PWs (mm)	1.06±0.03	1.05±0.07	1.22±0.05	WT vs Homo $p = 0.072$ Het vs Homo $p = 0.062$	$p = 0.016$
PWth (%)	35.56±5.01	31.83±5.04	42.08±2.81	NS	NS
LVDd (mm)	3.99±0.13	3.97±0.14	4.25±0.11	NS	NS
LVDs (mm)	2.96±0.15	2.98±0.19	3.03±0.13	NS	NS
FS (%)	26.09±1.63	25.04±2.63	28.73±2.06	NS	NS
LVVd (μL)	70.3±5.52	69.58±6.12	81.48±4.88	NS	NS
LVV s (μL)	34.54±4.52	35.45±5.6	36.57±3.81	NS	NS
EF (%)	51.53±2.84	50.06±4.1	55.33±3.13	NS	NS
SV (μL)	35.76±2.49	34.13±2.7	44.9±3.47	WT vs Homo $p = 0.087$ Het vs Homo $p = 0.061$	$p = 0.057$
CO (ml/min)	19.13±1.5	18.83±1.49	22.04±1.38	NS	NS
LVMass (% of BW)	0.44±0.02	0.45±0.02	0.51±0.03	NS	NS

BW: body weight; HR: heart rate; IVSd: interventricular septum thickness in diastole; IVSs: interventricular septum thickness in systole; IVSth: percent change in IVS between systole and diastole; PWd: posterior wall thickness in diastole; PWs: posterior wall thickness in systole; PWth: percent change in PW between systole and diastole; LVDd: left ventricle diameter in diastole; LVDs: left ventricle diameter in systole; FS: fractional shortening; LVVd: left ventricle volume in diastole; LVVs: left ventricle volume in systole; EF: ejection fraction; SV: stroke volume; CO: cardiac output; LVmass: left ventricle mass.

Table 4.3. Echocardiographic Parameters in 12-month-old P1124L Mice.

	WT	Het	Homo	ANOVA	t-test WT vs Homo
n	8	7	8	-	-
BW (g)	28.25±1.31	31.14±1.78	30.75±1.80	NS	NS
HR (bpm)	539±13	553±14	566±19	NS	NS
IVSd (mm)	0.75±0.03	0.9±0.06	0.88±0.02	WT vs Het <i>p</i> = 0.058 WT vs Homo <i>p</i> = 0.050	<i>p</i> = 0.005
IVSs (mm)	1.11±0.04	1.28±0.08	1.28±0.06	NS	<i>p</i> = 0.041
IVSth (%)	48.34±4.89	43.49±3.37	44.13±4.30	NS	NS
PWd (mm)	0.78±0.02	0.94±0.05	0.91±0.03	WT vs Het <i>p</i> = 0.013 WT vs Homo <i>p</i> = 0.021	<i>p</i> = 0.004
PWs (mm)	1.14±0.05	1.32±0.07	1.27±0.05	NS	<i>p</i> = 0.079
PWth (%)	46.22±5.54	41.79±4.13	39.8±4.04	NS	NS
LVDd (mm)	3.93±0.1	3.99±0.12	4.00±0.10	NS	NS
LVDs (mm)	2.89±0.12	2.84±0.11	2.84±0.11	NS	NS
FS (%)	26.56±1.42	28.8±1.3	29.12±1.53	NS	NS
LVVd (μL)	67.91±4.36	70.19±5.13	70.70±4.36	NS	NS
LVV _s (μL)	32.73±3.25	31.17±2.99	31.17±2.98	NS	NS
EF (%)	52.38±2.34	55.87±2.05	56.24±2.37	NS	NS
SV (μL)	35.18±1.87	39.02±2.74	39.53±2.38	NS	NS
CO (ml/min)	18.93±1.05	21.77±2	22.3±1.36	NS	NS
LVMass (% of BW)	0.38±0.02	0.47±0.05	0.45±0.01	NS	<i>p</i> = 0.003

BW: body weight; HR: heart rate; IVSd: interventricular septum thickness in diastole; IVSs: interventricular septum thickness in systole; IVSth: percent change in IVS between systole and diastole; PWd: posterior wall thickness in diastole; PWs: posterior wall thickness in systole; PWth: percent change in PW between systole and diastole; LVDd: left ventricle diameter in diastole; LVDs: left ventricle diameter in systole; FS: fractional shortening; LVVd: left ventricle volume in diastole; LVVs: left ventricle volume in systole; EF: ejection fraction; SV: stroke volume; CO: cardiac output; LVmass: left ventricle mass.

Table 4.4. Ca²⁺ Handling Parameters in Isolated P1124L Myocytes.Ca²⁺ transient amplitude and SR Ca²⁺ load measured in basal conditions and with 300 nM Iso stimulation.

	WT	Het	Homo
Cells (n)	21–56	15–36	18–47
Mice (N)	3–5	3	3–6
[Ca ²⁺] _i transient amplitude basal ($\Delta F/F_0$)	3.72±0.16	3.64±0.24	3.82±0.17
SR Ca ²⁺ Load basal ($\Delta F/F_0$)	8.17±0.34	7.70±0.44	7.52±0.22
Fractional release basal (%)	41.02±2.14	50.68±3.99	48.29±2.42
[Ca ²⁺] _i transient amplitude Iso ($\Delta F/F_0$)	8.57±0.28	7.91±0.32	8.13±0.38
SR Ca ²⁺ Load Iso ($\Delta F/F_0$)	10.02±0.30	9.50±0.33	9.52±0.31
Fractional release Iso (%)	86.95±2.25	83.21±1.79	84.82±2.23

** $p < 0.01$ vs. same genotype basal, paired t-test.

CHAPTER 5

Conclusions and Perspectives

5.1. Summary of Key Findings

In this dissertation, we examined different aspects of RyR2 regulation to obtain a better understanding of the role of this ion channel in the healthy and diseased heart. To follow this aim, we took advantage of three animal models with point mutations in RyR2. While each chapter of this dissertation focused on one specific question regarding RyR2's role in the regulation of cardiac function — channel phosphorylation in CHAPTER 2, haploinsufficiency in CHAPTER 3, and involvement in structural remodeling in CHAPTER 4 — this final chapter highlights key pieces of information that thread the dissertation together. The following sections provide a summary of the most important findings from each chapter, while the other sections provide technical, physiological, and clinical context to these data. This chapter contains references to the human RyR2 nomenclature, unless otherwise stated; however, sections 5.1.1, 5.1.2 and 5.1.3 refer to the nomenclature of the specific animal model used in the chapter summarized.

5.1.1. The Genetic Background of RyR2-S2808A Mice

In CHAPTER 2, we determined that the genetic background of S2808A mice does not affect their overall response to acute adrenergic stimulation, nor does it improve their outcome after myocardial infarction. This study was designed to determine the causes for

the inconsistent results obtained with S2808A generated by two different laboratories — Andrew Marks' at Columbia University and Héctor Valdivia's at the University of Michigan. Since the pioneering studies on this subject were published in 2000, the issue evolved into a contentious controversy. Until now, several investigators in the field have recognized the difference in the results of both groups,^{14,140} but no studies have been devoted to determining the causes for the discrepancy. There are several differences in the approach used to characterize the mice from each lab, but the most striking one is the mouse strain, which could have profound effects on the phenotypic presentation of a specific mutation^{138,189} or experimental manipulation.¹⁹⁰ Hence, the data presented in CHAPTER 2 are complementary to similar studies performed by our laboratory and several collaborators, but the novelty resides in the use of a congenic mouse strain in the C57Bl/6 background. This new line was derived for the specific purpose of performing all experiments in mice with the same genetic background used by the Marks laboratory — as opposed to the Sv129/B6 mixed strain originally developed by the Valdivia laboratory. Using an approach that involved some of the fundamental experiments that fueled the controversy, we demonstrated that the genetic background is an unlikely cause for the divergence between the results of both laboratories. In our hands, S2808A mice were indistinguishable from WT in most experiments. There was only a single exception: S2808A mice showed a significantly higher HR after MI than WT animals. Since this unexpected observation was not reported by any of the previous studies on S2808A mice, elucidating the underlying mechanisms will deserve further investigation. Nevertheless, this does not affect the overall conclusion stated in the title of CHAPTER 2: "Ablation of

RyR2-S2808 Phosphorylation Does Not Alter the Adrenergic Response or the Progression to Heart Failure in Mice.”

5.1.2. RyR2 Haploinsufficiency is not Deleterious in Rabbits

CHAPTER 3 looked at the compensatory mechanisms that preserve cardiac function and structure in a rabbit model of RyR2 haploinsufficiency. We showed that Het RyR2-KO rabbits have ~60% decrease in RyR2 expression but lack an obvious abnormal phenotype. The data presented in CHAPTER 3 suggest that this may be due to an upregulation of RyR2 function by decreasing the basal phosphorylation level of the S2031 phosphorylation site. Furthermore, our data indicated that increased association of RyR2 with PP2A may be responsible for maintaining the S2031 site at a lower phosphorylation level in Het animals. In basal conditions, this response was perhaps sufficient to compensate for the lower RyR2 expression. Under acute adrenergic stimulation, Het RyR2-KO rabbits responded similarly to WT animals; however, data from isolated hearts and Ca²⁺ imaging in cardiomyocytes suggested that this level of RyR2 expression could be insufficient to maintain a normal Ca²⁺ release flux during Iso stimulation. Hence, Het rabbits showed slower force generation and delayed Ca²⁺ transient time-to-peak during adrenergic stimulation. As stated in the title of CHAPTER 3, our conclusion is that “RyR2 Haploinsufficiency is Compensated by Fine-tuning Channel Activity Through Phosphorylation.” To determine whether decreased RyR2 expression affects the response of Het rabbits to chronic stress more experiments are necessary.

5.1.3. RyR2 Mutations Can Induce Structural Remodeling of the Heart

Finally, in CHAPTER 4 we performed a multi-level characterization of the novel P1124L mutation, identified in a patient with HCM. We determined that this mutation induces structural alterations in the SPRY2 domain of RyR2, likely affecting an interdomain interface with the neighboring SPRY3 domain. Functionally, P1124L channels show decreased cytosolic sensitivity to Ca^{2+} , but we also observed that when P1124L channels are activated by luminal Ca^{2+} they release a larger fraction of the store Ca^{2+} content compared to WT. In a mouse model, these alterations translated into a mild hypertrophy and increased susceptibility to arrhythmia. For the former phenotype, we attempted to identify the underlying signaling pathways; however, after probing three signaling cascades we have yet to determine the hypertrophic signaling acting in P1124L mice. As for the latter, we hypothesize that upon luminal activation, the larger mass of Ca^{2+} released by P1124L channels might coordinate isolated SCR events into arrhythmogenic Ca^{2+} waves and, hence, lead to ventricular arrhythmia. As stated in the title of CHAPTER 4, P1124L is “A Novel RyR2 Mutation Associated with Hypertrophic Cardiomyopathy [that] Induces Hypertrophy and Arrhythmia in Mice.” Therefore, these data suggest that it may be the disease-causing mutation in the patient with HCM where it was identified. A full elucidation of the pathogenic mechanisms induced by P1124L will require further investigation.

5.2. Genetically-Engineered Rabbit Models to Study Cardiac Physiology

For two of the chapters of this dissertation we took advantage of knock-in mouse models to study point mutations in RyR2. However, in terms of novelty, one of the most salient features of the research discussed in this dissertation is that the results outlined

in CHAPTER 3 were generated in one of only a handful of genetically-engineered rabbit models available today, and, to our knowledge, the first specifically targeting *RYR2*. This section gives brief technical context to the use of larger mammals, like the rabbit, for the study of cardiac physiology.

Mus musculus, the house mouse, is the animal species most widely used in biomedical research. Mice are small, reproduce quickly, reach adulthood in only a few months, have a relatively short lifespan, and exist as inbred strains of genetically identical animals. But these characteristics offer no clear advantage over smaller and simpler organisms, such as *Drosophila melanogaster* — the fruit fly — and the worm *Caenorhabditis elegans*. Instead, the reasons the mouse is the number one species used to model human disease are simple: mice and humans are genetically very similar, and mice are, to date, the only mammal in which *any* gene can be targeted through genetic engineering.¹⁹¹ While this genetic versatility makes the mouse the most powerful tool for biomedical research, this species is not the best to model human disease.

In the field of cardiac research, the characteristics that make the mouse an often-unsuitable model are particularly evident, as shown in Figure 5.1. Mice have a heart rate of ~500 bpm requiring short cardiac cycles and fast action potentials, while humans have significantly lower heart rate and a cardiac action potential (AP) with a completely different waveform. The phase-2 plateau observed in the human cardiac AP — formed by a transient balance between outward K^+ currents and I_{CaL} — is largely absent in mice.¹⁹² Because of the small role of I_{CaL} in shaping the mouse cardiac AP, e-c coupling must rely primarily on SR rather than extracellular Ca^{2+} . This explains why in the mouse heart the relative source/sink contribution to Ca^{2+} homeostasis of LTCC/NCX on the sarcolemma

and RyR2/SERCA2a on the SR is ~10% and ~90% respectively, while in the human heart they account for ~30% and ~70,% respectively (Figure 5.1).^{3,193} Furthermore, the repolarization phase of the mouse AP relies on transient outward currents (I_{to}), while in the human and rabbit this is mediated by delayed rectifier K⁺ currents (I_{Kr} and I_{Ks}).¹⁹⁴

Unfortunately, larger mammals such as the rabbit (Figure 5.1), the sheep, or the pig, that have cardiac physiology that better resembles that of the human,¹⁹⁵ are significantly more difficult to genetically engineer than the mouse. Transgenic expression of exogenous genes due to random insertion of DNA constructs is possible in these species,¹⁹⁶ but the lack of suitable embryonic stem cell lines has hindered the development of knock-in and knock-out strains.¹⁹⁷ Indeed, several transgenic rabbits overexpressing human genes are available^{198,199} — including the LQTS model mentioned in CHAPTER 3^{156,157} — but any study that requires manipulation of endogenous genes — such as the characterization of disease-causing mutations without protein overexpression — must be performed in mice (e.g. in CHAPTER 2 and CHAPTER 4).^{87,89,102} On the other hand, those studies requiring healthy animals or the use of experimental manipulations to induce heart disease are often performed in larger species (examples in refs. ^{8,147,200}). Rabbits are commonly preferred because their small size (2–4 kg adults), rapid sexual maturation (5–6 months), short gestational period (~30 days), and large litter size (4–12 kits/litter) make them convenient laboratory animals.²⁰¹

Lately, new gene editing techniques have been applied to create gene knock-outs in rabbits^{152,202,203} and pigs,^{204,205} overcoming a historic hurdle by microinjecting the targeting vectors into healthy pronuclear embryos that are then implanted into surrogate females. CRISPR/Cas9 technology, the most recent of these novel approaches, uses

carefully-designed RNA probes derived from the bacterial CRISPR system (clustered, regularly interspaced, short palindromic repeats) to recruit the nuclease Cas9 to the genomic region of interest. Cas9 then creates a double-stranded DNA cut, which the cell repairs by employing non-homologous end joining — introducing insertions or deletions that change the reading frame of the gene and, in some cases, knock out protein expression — or homology-directed repair — when the cell restores the DNA using a donor template provided to that effect.²⁰⁶ Adding specific mutations to this donor template is, theoretically, the means to create knock-in animals. While using this approach to create gene knock-out animals is relatively easy, introducing a DNA donor template to create knock-in animals is more challenging.

In 2014, Yang et al. published the first report of knock-out rabbits created using CRISPR/Cas9.¹⁵² The RyR2-KO rabbit model discussed in CHAPTER 3 is one of seven RyR2-KO founders reported in that publication, along with several KOs of three other genes — *CD36*, *APOE*, and *LDLR*.¹⁵² Since the DNA restoration performed by the cellular machinery is variable, each Cas9-damaged allele is repaired differently and founders are unique. Furthermore, two different types of repair can occur within the same cell on each gene allele, and if the targeting materials injected into the embryo are transmitted to the daughter cells, a second round of Cas9 targeting/DNA repair could result in mosaicism — i.e. animals containing more than two different alleles for each gene. Indeed, Yang et al. described 20 founders with at least two different mutations in the gene of interest, and three of those founders were mosaics with three different alleles for the gene.

While studying the RyR2-KO model in CHAPTER 3 we dealt with this issue: one of the founders selected had a 16 bp deletion in one allele — the knock-out allele — and

a 12 bp insertion in the second allele accounting for four additional residues in RyR2. This second mutation remained unnoticed for nearly two years because it behaved as a WT allele in the genotyping protocol. Hence, most of the animals we initially classified as WT littermates were not. When we changed the breeding pairs and observed inconsistent genotyping in the offspring, we performed an extensive genetic characterization and identified the 12 bp insertion. Then, using Punnett's diagrams we determined which animals carried this mutation without the need to perform additional genetic screening. Ultimately, the lesson is that, when using CRISPR/Cas9 to develop mutant animals and regardless of the species, a careful genetic characterization of the founders and the F1 offspring is paramount to avoid costly mistakes. Ultimately, the screening, selection, and breeding of the offspring carrying only the knock-out allele took over one year and required to purge all datasets from inadequate samples and repeat several experiments.

Finally, there is one piece of information we did not discuss in CHAPTER 3: the site of the mutation in the RyR2-KO allele. *RYR2* is formed by 105 exons and Cas9 was purposely targeted to exon 49 (Figure 3.1, Figure 3.2), a rather unusual choice to make a knock-out. Exon 49 encodes 56 residues from 2448 to 2504 in the middle of the protein. Our laboratory previously characterized the CPVT mutation V2475F in mice;⁸⁷ hence, the targeting site is in fact quite obvious: every single RyR2-KO founder generated by the Chen laboratory and described by Yang et al.¹⁵² was obtained while attempting to knock-in this mutation into *RYR2*. Fortunately, the fortuitous creation of the knock-outs allowed us to address important questions regarding cardiac function, Ca²⁺ homeostasis, and RyR2 regulation when lower RyR2 expression occurs. After several years of trial-and-error, our collaborators in the Chen laboratory recently succeeded in creating the first

RyR2-V2475F rabbit founders. The characterization of these animals and the comparison with the mouse results already published will be exciting new projects for the Valdivia Laboratory in coming years.

5.3. Mouse vs. Rabbit Cardiac Electrophysiology and Ca²⁺ Handling

The similarity in Ca²⁺ handling between the rabbit and human hearts makes RyR2 mutant rabbits particularly exciting to study in our field. One would expect that if the mouse heart relies mostly on the SR Ca²⁺ for contraction, RyR2 dysfunction might have a more deleterious effect in the mouse than in the rabbit, which requires a larger sarcolemmal Ca²⁺ contribution. With the RyR2-KO rabbit model we indirectly tested this hypothesis. Interestingly, both heterozygous RyR2-KO mice¹²¹ and rabbits have lower RyR2 expression but lack a basal abnormal phenotype. Hence, regardless of the specific contributions of the SR and the sarcolemma to Ca²⁺ homeostasis, both species maintain a normal cardiac function even with lower RyR2 expression. Nonetheless, this may not be the case for other types of mutations. We discussed in section 1.5.1 that the most accepted mechanism of CPVT involves extemporaneous release of Ca²⁺ that produces either DADs or EADs as this Ca²⁺ is extruded from the cell by the electrogenic NCX. Since the role of NCX is more prominent in the rabbit heart than in the mouse (Figure 5.1), it is reasonable to hypothesize that a rabbit model of CPVT may be more susceptible to arrhythmia. Indeed, inducing arrhythmia in a CPVT mouse model requires an extremely large, non-physiologic dose of epinephrine mixed with an even larger dose of caffeine (Figure 4.17). Hence, a systematic side-by-side comparison between rabbit and mouse models of CPVT will be an interesting experimental approach now that our laboratory has the mutation V2475F in both species. To address this issue, it is important to consider the

differences between the mouse, rabbit and human heart physiology. Since we discussed Ca^{2+} handling in the previous section, here we will make a brief comparison of specific parameters in the three species.

Evidently, mouse and rabbit cardiac physiology is significantly different from human; yet, the rabbit is typically an intermediate between the two. One of the most evident differences in cardiac physiology among the three species is the heart rate (HR): the resting human HR is 60–100 bpm and the parasympathetic/vagal tone, which restrains cardiac function, prevails over the sympathetic/adrenergic tone, which enhances cardiac function (section 1.3).²⁰⁷ Conscious mouse HR is significantly higher (450–750 bpm), and the rabbit HR, although lower than the mouse, is still significantly higher than that of the human (180–350 bpm).²⁰⁸ Remarkably, isolated mouse hearts, devoid of hemodynamic and neurohormonal regulation of cardiac function, have a HR significantly lower than anesthetized animals (396.5 ± 13.2 bpm vs. 522.9 ± 12.3 bpm, respectively; Figure 5.2 **A**), while in rabbits both anesthetized and isolated-heart HR are nearly-identical (186.6 ± 7.0 bpm vs. 206.3 ± 7.4 bpm; Figure 5.2 **A**). Similarly, small studies of human hearts explanted from organ donors have found either a slight decrease²⁰⁹ or no difference²¹⁰ in HR compared to the value before pre-explantation. This suggests that mice have a significantly higher adrenergic tone than rabbits and humans. Upon adrenergic stimulation, human HR can increase nearly 2-fold during exercise,²¹¹ whereas mice and rabbits respond to Iso stimulation with a ~10% and ~1.7-fold increase, respectively (Figure 5.2 **B**). Other functional parameters such as the EF and FS are more similar: the normal human EF is between 50–70%,²¹² and both mouse and rabbit EF falling on the lower end of that range (Figure 5.2 **C-D**). During exercise, humans show a

modest rise in EF (~15%),²¹¹ but Iso stimulation in anesthetized mice and rabbits produces a more robust increase: ~1.5 fold in EF and ~1.8 fold in FS (Figure 5.2 **C-D**). Therefore, the higher adrenergic tone in mice seems to be restricted to the sinus node. At the ventricle, the three species seem to have a similar sympathetic reserve. This is not the case for isolated hearts, because the mouse and rabbit HR have the same response to Iso (Figure 5.2 **E**), and rabbits show a larger increase in LVDP (Figure 5.2 **F**); unfortunately, LVDP measurements are difficult to obtain in isolated human hearts. Finally, it is important to note that the HR and EF measurements in exercising humans discussed above are likely to underestimate the maximum effect of adrenergic stimulation.

At the cellular level, the differences between species are empirically less obvious but equally striking. As shown in figure Figure 5.1 **B** and discussed in section 5.2, some of the ionic currents that form the mouse AP are different from those that shape the rabbit and human AP. Similarly, the source/sink contribution of specific e-c coupling components to Ca²⁺ homeostasis is similar between rabbit and human, and significantly different in the mouse (Figure 5.1 **C**, section 5.2). Figure 5.3 shows a comparison between Ca²⁺ transients and action potentials in mouse and rabbit ventricular myocytes. As previously shown by Maier & Bers,²¹³ rabbit myocytes show post-rest potentiation of Ca²⁺ release — i.e. Ca²⁺ transient amplitude increases progressively during pacing as the SR is loaded²¹⁴ — while in mouse myocytes Ca²⁺ transient amplitude decreases with pacing as the SR is progressively unloaded (Figure 5.3 **A,B**). The SR load in quiescent cells is a result of two factors: the balance between SERCA2a and NCX, and the resting SR Ca²⁺ leak.²¹³ Hence, the high SR load in resting mouse myocytes is likely the result of the

powerful contribution of SERCA2a to Ca^{2+} reuptake and low resting leak. Interestingly, healthy human myocardium shows post-rest decay (like the mouse), while failing myocardium shows post-rest potentiation (like the rabbit).²¹⁵ Considering the similarity in SERCA2a/NCX balance between rabbit and human, the different response of the Ca^{2+} transients to stimulation suggests that human myocytes have lower basal SR Ca^{2+} leak compared to rabbit myocytes. Finally, the kinetics of Ca^{2+} release is slower in rabbit than in mouse myocytes (Figure 5.3 **C**). While a mouse Ca^{2+} transient peaks within ~40 ms (Figure 4.18 **C**), rabbit transients peak within ~200 ms (Figure 3.10 **B**). This is likely a result of the AP waveform (Figure 5.3 **D**) and underlying ionic currents.¹⁹² At 1 Hz stimulation rate, a rabbit AP lasts ~300 ms and I_{CaL} is active during a large fraction of this time producing the phase 2 of the AP.¹⁹² A mouse AP, on the other hand, lasts ~150 ms; hence, the kinetics of activation and inactivation of I_{CaL} are compressed in a shorter period, as is RyR2 recruitment and activation. Furthermore, the overall contribution of I_{CaL} to AP waveform is more prominent in rabbit myocytes (as it is in human); therefore, Ca^{2+} transients are slower. To determine whether the responsiveness of RyR2 to I_{CaL} is also playing a role in the kinetics of Ca^{2+} , it would be interesting to make a systematic comparison of the kinetics of Ca^{2+} transients while controlling I_{CaL} with voltage clamp — i.e. e-c coupling gain. Interestingly, while isoproterenol stimulation clearly enhances Ca^{2+} flux in both species, it decreases the time-to-peak of rabbit Ca^{2+} transients (Figure 3.10 **B**) but has the opposite effect in the mouse (Figure 4.18 **C**). The reason for this observation difference is unclear, but it might be associated to the overall contribution of SR and sarcolemma to Ca^{2+} cycling as well.

In conclusion, the mouse is not human and the rabbit is not human. The selection of any species to model human cardiac pathophysiology will be inherently affected by the characteristics of such species at all levels — whole-organ, cellular and molecular. Hence, it is important to interpret the results carefully. Finally, while the use of genetically-engineered rabbits is hindered by the novelty of the technique, it is expected that, in the future, mutant rabbit models will be more frequently used in the field of cardiac physiology.

5.4. RyR2 Regulation by Phosphorylation

Two of the chapters in this dissertation looked at RyR2 phosphorylation as a regulatory mechanism of Ca²⁺ release during e-c coupling. In CHAPTER 2 we revisited the idea that S2808 phosphorylation is essential for the adrenergic response and critical for HF progression, while in CHAPTER 3 we identified a decrease in basal phosphorylation of S2031 as a possible compensatory mechanism for RyR2 haploinsufficiency. This section provides a brief experimental context for these findings.

Early work by Takasago et al. showed that at least four kinases — PKA, PKG, PKC, and CaMKII — phosphorylate RyR2 using ³²P incorporation studies.⁶⁸ Identifying the relevant phosphorylation targets of these kinases is, however, a difficult issue to tackle. We discussed before that the human RyR2 (hRyR2) contains 353 serine and 222 threonine residues (section 1.4.3). From these, ~40 residues are predicted phosphorylation sites based on computational analysis of consensus sequences.^{51,216} Therefore, a simple permutation analysis shows that there are ~1.1x10¹² possible different phosphorylation states for a *single* RyR2 subunit — ~1.5x10⁴⁸ for a fully-assembled channel. Thus, in physiological conditions there will be a heterogeneous population of channels in which the overall phosphorylation states may vary depending

on several factors, including the association of the channel with kinases and phosphatases, and the location of any given channel within the myocyte's SR network. In any case, it is unlikely that all these sites are *essential* for the regulation of the channel, especially because the access of any given kinase to some sites is likely limited by steric hindrance, and the phosphorylation of many of these sites will prevent or enhance the phosphorylation of others. Still, according to the experiments by Takasago et al., CaMKII phosphorylates at least four residues for every PKA, PKG or PKC site.⁶⁸ Considering only the two currently-known PKA sites (S2031, S2808) there should be at least six more for CaMKII — in addition to S2808 and S2814. Therefore, even as we argue to create a more comprehensive model contemplating the three phosphorylation sites known to date (S2031, S2808 and S2814; sections 2.3 and 3.3), such model may also be too simplistic. Indeed, Lau and Van Petegem³¹ showed that two additional putative phosphorylation sites — T2810 and S2811, phosphorylated by CaMKII and PKA *in vitro* — are part of the same “phosphorylation hotspot” loop of the P2 domain containing S2808 and S2814. To date, there are no published studies focusing on these novel sites. Most of the discussion regarding RyR2 phosphorylation has focused on S2808 and S2814 for historical reasons.

S2808 is a controversial phosphorylation site that we discussed at length in previous chapters. Since we have already discussed the studies that have fueled this controversy, it is not necessary to relitigate this issue here. Nevertheless, it is important to consider that a study reported slight differences in the velocity of Ca²⁺ wave propagation and luminal Ca²⁺ sensitivity between cardiac myocytes from WT and S2808A mice,¹³³ which do not affect the overall cardiac function of animals harboring the mutation. Therefore, considering the data presented in CHAPTER 2 and briefly summarized in

section 5.1.1, it is reasonable to conclude that this site is not *essential* for RyR2 regulation in physiologic or pathologic conditions. It is fascinating, however, that this is not the case for S2814: while this site is not required for the cardiac adrenergic response and the phospho-mimetic mutation S2814D does not produce an overt basal phenotype,²¹⁷ S2814A animals are resistant to non-ischemic HF,⁶⁰ ventricular arrhythmia,²¹⁷ atrial fibrillation,²¹⁸ and CaMKII-induced SR Ca²⁺ leak.^{15,217} Hence, despite the proximity between S2808 and S2814, both sites transduce different regulatory signals to the channel. One reason for this may be the specific location of the sites within the P2 domain: while both are contained within the same flexible linker,³¹ S2814 is closer to the C-terminus end of the loop and might have fewer structural constraints to convey conformational changes to rest the domain and the central tower scaffold. Since S2814 is a CaMKII phosphorylation site, CaMKII phosphorylation of RyR2 is branded as deleterious,^{58,219} and this idea also suggests that overall *increased* phosphorylation of RyR2 is detrimental to cardiac function.⁵¹ Hence, more phosphorylation would produce hyperactive channels, as seen in some forms of heart disease such as HF⁶⁰ and HCM⁹⁹ — following the same line of thought initially proposed by Marks et al. for S2808. Nevertheless, there is experimental support for the idea that dephosphorylation of RyR2 also increases channel activity: Lokuta et al. showed that dephosphorylation of rabbit cardiac SR vesicles with acid phosphatase increases [³H]ryanodine binding, and the open probability of channels embedded in artificial lipid bilayers;⁶⁵ Terentyev et al. demonstrated that perfusion of permeabilized rat myocytes with PP1 increases Ca²⁺ spark frequency and depletes the SR load,⁶⁶ Camors et al. proposed that the double mutation S2808A/S2814A in mice decreases RyR2 refractoriness and promotes SR Ca²⁺

leak and arrhythmia;¹⁶⁵ and in CHAPTER 3 we showed that a lower S2031 phosphorylation level in RyR2-KO rabbits may be responsible for increasing RyR2 activity to compensate for the lower expression (Figure 3.3 and Figure 3.6). Altogether, these data suggest that the relationship between RyR2 phosphorylation and channel activity is not a straight line but a parabola (Figure 5.4): from the lowest point of the curve, an increase or decrease in phosphorylation will activate RyR2. Different populations of channels, or models with specific genetic mutations that hamper or mimic phosphorylation will fall within an “optimal phosphorylation” range that will not produce deleterious phenotypes — such as the S2808A, S2814A, and RyR2-KO models. Extremes on both sides of the curve beyond the optimal range, however, will produce RyR2 dysfunction — as in the S2808A/S814 mouse on the left, and HF and HCM on the right.

So far, most of this discussion relies on the generalization of data from two of the three known phosphorylation sites and on reports that study global channel phosphorylation. Hence, it is difficult to assess where a normal human patient or experimental animal subject would fall on the phosphorylation-activity curve (Figure 5.4). To continue improving our understanding of this issue, similar in-depth studies of the S2031 site are required. Our laboratory has developed a mouse with genetic ablation of this site — S2030A as per the mouse nomenclature. To date, the only data available on this model suggests that the site regulates the sensitivity of RyR2 channels to Ca^{2+} during e-c coupling and CICR.²²⁰ These data are consistent with the idea that the low basal phosphorylation of this site provides a wide dynamic range during adrenergic stimulation — 16-fold, as opposed to 50% increase for S2808 and S2814. Further studies of the S2030A mice will provide more insights into the relevance of this site and must answer at

least two fundamental questions: is S2031 phosphorylation essential for the normal adrenergic response, and does genetic modification of this site lead to an overt basal phenotype? With this information, we can continue building a more comprehensive model of RyR2 regulation. Together with our data from CHAPTER 3 indicating that changes in S2031 phosphorylation potentially compensates for RyR2 deficiency, the limited data available from the S2030A mouse model suggest that this site is more relevant than previously anticipated.

5.5. Clinical Significance of RyR2 Variants and Polymorphisms

In 1999, Swan et al. used genetic linkage analysis of two unrelated families with clinical history of sudden cardiac death to map the underlying arrhythmogenic disorder to chromosome 1q42-43.²²¹ Shortly after, this region was narrowed to *RYR2*, when Priori et al. reported four specific mutations in a same number of probands with CPVT,⁷³ the syndrome studied by Swan et al.²²¹ One of these mutations, R4497C, was later introduced in mice (R4496C) and heterozygous animals recapitulated the most relevant clinical signs of CPVT: polymorphic ventricular tachycardia and ventricular fibrillation in response to catecholamines and exercise.²²² Hence, the research field devoted to elucidating the mechanisms of RyR2-mediated inherited cardiac disease was born. Today, there is enough evidence in the literature to assert beyond doubt that some RyR2 mutations produce CPVT. However, the spectrum of possible phenotypes induced by RyR2 dysfunction continues to grow. P1124L, the novel HCM mutation discussed in CHAPTER 4, is one example; but the Human Gene Mutation Database (HGMD)¹²⁷ — a resource compiling studies of potentially pathogenic mutations — also incorporates reports of RyR2 mutations possibly associated with LQTS, Brugada Syndrome,

arrhythmogenic right ventricular cardiomyopathy (ARVC), and even colorectal cancer and intellectual disability. Altogether, this information is stimulating to the field, but it deserves careful consideration. Landstrom et al. recently reported that 7.5% of individuals undergoing whole-exome sequencing (WES) carry *RYR2* variants, but only 1.2% of those were pathogenic based on clinical information.¹⁷⁶ Overall, RyR2 appears to be highly tolerant to variability: gnomAD — a public database containing WES and genome sequencing information from more than 120,000 individuals — reports 1422 residues susceptible to 1751 missense variants. These mutations are equally distributed throughout the protein, while those associated with CPVT cluster in three regions of the channel, as we discussed before (Figure 1.5, section 1.5.1). Remarkably, the 31 specific mutations summarized in Table 5.1 appear in gnomAD and HGMD. Then, what is the overall clinical significance of novel RyR2 mutations? If a patient carries any given RyR2 mutation and shows an abnormal phenotype, should this be labeled as *the* disease-causing mutation?

Ackerman recently addressed this issue arguing that, hierarchically, the phenotype must prevail over the genotype.⁸² Hence, if the clinical diagnosis is inconclusive, any rare mutation identified in a patient is likely a false-positive — i.e. a variant of unknown significance (VUS). But even with a robust phenotype, any RyR2 mutation could be merely coincidental. This is evident from Table 5.1: for many mutations compiled in HGMD, the original clinical report does not provide detailed information of the patients' phenotype (e.g. S1765C and R2359C), and considers a mutation as “pathogenic” even when the patient carries variants in other relevant genes (e.g. L73V found with mutations in *PKP2*, *MYBPC3* and *MYH7*) or provides a diagnosis without the appropriate clinical

tests (e.g. T1223A, the patient only had one episode of syncope). For other mutations, this issue is compounded by the high allelic frequency in the general population. Such is the case of T1107M (Table 5.1), reported in cases of CPVT⁸¹ and HCM,¹¹³ but occurring in approximately 4 of every 10,000 alleles in gnomAD (Table 5.1). Hence, T1107M is probably not disease-causing — as recognized by Landstrom et al.¹⁷⁶ — and in patients carrying this mutation, other epigenetic or environmental factors likely contribute to the phenotype. This residue is also subject to inter-species variation (Figure 4.3), and the functional and structural studies were performed with A1107M, the mouse analog.^{30,119}

Ultimately, the genetic variability in *RYR2* should not discourage the study of rare mutations from patients with phenotypes other than CPVT, since determining the pathogenic potential of any genetic variant, whether in *RYR2* or any other gene, needs confirmation at different levels. P1124L, for example, also appears in gnomAD (Table 5.1), but this residue is conserved in all species and RyR isoforms (Figure 4.3), and we provide experimental evidence in support of its pathogenicity, including the marked hypertrophic phenotype in the human patient (section 4.2.1), a molecular characterization showing structural and functional alterations in RyR2 (sections 4.2.3), and a mouse model showing cardiac hypertrophy (section 4.2.6) and arrhythmia (section 4.2.8). Nevertheless, the lack of segregation data within the patient's family and the mild phenotype in the animal model undermine the disease-causality of P1124L, even with our thorough characterization. Therefore, the data discussed in CHAPTER 4 might be insufficient to include *RYR2* in the clinical HCM panels — as suggested by a colleague at a conference — but it validates the hypothesis of a wider spectrum of RyR2-caused disease deserving further investigation. To date, P1124L is the only mutation strongly correlated with HCM;

hence, the field of RyR2-mediated HCM and structural remodeling is at the same developmental stage as the RyR2-mediated CPVT field was when Cerrone et al. reported the first CPVT mouse model nearly 12 years ago.²²²

Finally, there is another category of RyR2 mutations in gnomAD deserving discussion: 29 *RYR2* genetic variants produce premature termination of RyR2 synthesis, collectively accounting for ~1 of every 10,000 alleles. Overall, these truncations are compatible with that of the RyR2-KO rabbit model discussed in CHAPTER 3 (Figure 3.1). Like the rabbit model, these individuals are heterozygous; hence, it is conceivable that they have RyR2 haploinsufficiency as well. As we discussed earlier, our data suggest that lower RyR2 expression is readily compensated and does not trigger a deleterious phenotype. Therefore, even though these mutations produce significant disturbance of the *RYR2* gene, there is an insignificant effect on the e-c coupling apparatus. This may explain why no truncation mutations are currently associated with heart disease. If a report identified one of such mutations in a patient with a cardiac disease, like is the case of T1107M, our data would provide strong experimental evidence suggesting that this is likely a false-positive, i.e. not *the* disease-causing mutation.

5.6. RyR2-Associated Structural Cardiomyopathy

The attempt to study structural cardiomyopathy because of RyR2 dysfunction is not entirely new. Even before Fujino et al.¹¹³ presented at the 2006 American Heart Association Scientific Sessions the abstract reporting T1107M in a family with HCM, there were already reports of RyR2 mutations in patients with arrhythmogenic right ventricular cardiomyopathy (ARVC, section 1.5.3) — formerly ARVD2, for dysplasia. Rampazzo et al.¹²³ mapped some cases of ARVC to the region of chromosome 1 containing *RYR2* four

years before Swan et al. mapped CPVT to the exact same locus.²²¹ Later, Tiso et al. narrowed this region to *RYR2* when they reported four missense mutations in five families with ARVC.¹¹⁷ So far, the story of ARVC is very similar to that of CPVT (previous section), but the reason both have not received the same recognition is simple: instead of producing structural cardiomyopathy, three of the mutations described by Tiso et al. predisposed mice to stress-induced arrhythmia, *the* CPVT phenotype — L433P,²²³ N2386I,²²³ and R176Q.²²⁴ To our knowledge, the fourth mutation, T2504M, has not been expressed in mice but was found in the same allele as R176Q in the family described by Tiso et al.;¹¹⁷ hence, the R176Q mouse model is not representative of the clinical report. Ultimately, these mutations are likely pathogenic — they induce RyR2 channel dysfunction,²²⁵ produce a phenotype in mice and none of them appear in gnomAD — but their link with structural cardiomyopathy is weak. Therefore, a clear association between RyR2 mutations and ARVC remains unproven, even as the number of such mutations continues to grow.

As we discussed in previous sections, the relationship between other types of cardiomyopathy such as HCM and LVNC with RyR2 mutations also remains, at best, tantalizing. For exon 3 deletion the mouse model does not develop cardiomyopathy nor stress-induced arrhythmia, and for T1107M there are no animal models available. Still, both mutations appear in CPVT patients as well, which obscures any association. Nevertheless, there is a reasonable link between RyR2 dysfunction and cardiomyopathy: any mutation that produces a constitutive diastolic leak of SR Ca²⁺ might activate the two Ca²⁺-dependent hypertrophic signaling pathways — CaM-CaN-NFAT and CaM-CaMKII-HDAC. However, this may not be the case, since V2475F, a CPVT mutation, increases

channel activity at diastolic $[Ca^{2+}]$ (100 nM), even though heterozygous mice only show arrhythmia.⁸⁷ The characterization of P1124L in CHAPTER 4 addressed this issue, but we were not able to identify the link between the molecular phenotype of RyR2 channels and the hypertrophy in mice. Nevertheless, the fact that mice harboring the mutation develop hypertrophy is supportive of two hypotheses: (1) P1124L is *the* disease-causing mutation in the patient; and (2) that RyR2 dysfunction can indeed produce structural cardiomyopathy. In any case, we must also consider the possibility that any of these mutations could fail to trigger the expected phenotype just because of the cardiac physiology of the mouse, which we have addressed before.

Lastly, we must consider the possible signaling pathways underlying the development of hypertrophy due to RyR2 mutations. If CaM-CaN-NFAT and CaM-CaMKII-HDAC are not the culprits, the number of other possible hypertrophic cascades is overwhelming.¹⁷⁸ In CHAPTER 4 we selected two specific ones mediated by AKT and ERK based on the work by the Meissner laboratory with the RyR2-ADA mouse which expresses CaM-binding deficient RyR2.^{43,111} Until P1124L, this mouse model was the only one to develop cardiac hypertrophy as a result of an RyR2 mutation. However, the ADA mutation is not clinically relevant — i.e. not from a patient — and the phenotype is very severe: homozygous mice die 10–15 days after birth. At this stage, there are clear signs of activation of Ca^{2+} -dependent hypertrophic signaling: increased HDAC⁴³ and NFAT¹¹¹ activity, but none of these molecules is altered in embryos before the onset of hypertrophy. In P1124L we did not observe indications of increased Ca^{2+} , Erk1/2 or Akt-dependent signaling pathways; hence, these pathways are not likely involved in the phenotype of the mice. Thus, the link between RyR2 mutations and structural

cardiomyopathy remains elusive; but the association between RyR2 mutations and HCM seems promising.

5.7. Future Directions

5.7.1. S2808A Mouse Models and the Never-Ending Controversy

One of the reviewers of our article describing the results of CHAPTER 2¹⁰² commended us for addressing the issue of the genetic background in the S2808 phosphorylation controversy, but suggested to perform a side-by-side comparison with the S2808A mouse from the Marks Laboratory. Indeed, such study would likely solve this long-standing controversy. Since this has not been possible to date, we made our S2808A mouse models available to the entire scientific community. Recently, Dobrev and Wehrens¹⁴⁰ provided an extensive list of potential reasons for the divergent results that have fueled the S2808 debate. Environmental conditions (diet, microbiome, water quality) and circadian rhythms (light/dark cycles and time-of-day of the experiments) stand out among those possibly accounting for the opposite phenotypes of S2808A mice. It is unlikely, however, that all these factors selectively affect S2808A mice to assign diametrically different properties to this site depending on the laboratory. Hence, independent validation of all these experimental results is critical. This controversy will hardly be solved until a side-by-side comparison between the Mark and Valdivia S2808A mice is performed by an independent group.

5.7.2. The Three Phosphorylation Sites and Their Role in RyR2 Regulation

Complete ablation of S2808 and S2814 phosphorylation does not seem to affect cardiac function. Unlike the S2808A substitution, S2814A appears to be protective

against some forms of heart failure because it inhibits the CaMKII-mediated RyR2 leak. This is surprising because of the location and proximity of both residues. If we add to the equation the poor understanding of S2031, it is evident we need new comprehensive models of RyR2 regulation by phosphorylation. Hence, it is necessary to characterize several animal models, including S2030A, S2030A/S2808A (to determine whether PKA phosphorylation of RyR2 is necessary for the adrenergic response) and S2808A/S2814A (to determine whether CaMKII phosphorylation of RyR2 is necessary to regulate the channel). Our laboratory is currently working with these models and has plans to develop a mouse triple phospho-mutant mouse — S2030A/S2808A/S2814A — to assess cardiac function in the absence of all known phospho-sites. To meet the PKA:CaMKII phosphorylation stoichiometry proposed by Takasago et al.⁶⁸ more sites are likely to be discovered in the future. Hence, determining which of these new sites are important for RyR2 regulation is an exciting future research area. For every study considering RyR2 phosphorylation, at least two questions must be addressed systematically: is phosphorylation critical for the normal adrenergic response and is it involved in the pathogenesis of certain forms of heart disease?

5.7.3. RyR2 distribution and Ca²⁺ handling in RyR2-KO Rabbits

RyR2 haploinsufficiency is expected to reduce the number of channels in a CRU, decrease the number CRUs within a myocyte or, most likely, a combination thereof. However, it is possible that remodeling of the SR network in myocytes from RyR2-KO rabbits contributes to normalize Ca²⁺ release even with lower expression. In this case, corbular SR — terminal SR cisternae containing CRUs that do not forming junctions with the sarcolemma or TT, i.e. “orphan SR” — could reconfigure into junctional SR — SR

cisternae forming dyads with the TT or sarcolemma, and committed to activation by LTCC during an AP. Hence, it is fundamental to determine the extent to which haploinsufficiency alters the distribution of RyR2 in a cardiac myocyte. This would allow us to weigh the relevance of RyR2 organization and the decrease in pS2031 phosphorylation as possible mechanisms that normalize cardiac function in RyR2-KO rabbits. We have already started these studies by collecting cardiac myocytes for immunostaining of RyR2 and other relevant proteins such as LTCC; unfortunately, this technique might not offer enough sensitivity to address this question. Other approaches such as dual-tilt tomography²²⁶ might provide more conclusive data. This method uses three-dimensional reconstruction of electron micrographs of dyadic clefts to visualize the position, distribution, and orientation of individual RyR2 tetramers.^{226,227} With this information we could specifically compare dyad formation and RyR2 content between WT and Het RyR2-KO hearts.

We showed in Figure 3.10 that RyR2 deficiency does not seem to affect the amplitude of the global cytosolic Ca^{2+} transient, while it slightly prolongs the time-to-peak under Iso stimulation. Nevertheless, there are two essential aspects that remain to be addressed in this model. First, the distribution of RyR2 and composition of a CRU may affect the properties of the unitary Ca^{2+} release event: the Ca^{2+} spark. Hence, measuring the properties of Ca^{2+} sparks in intact and permeabilized myocytes could provide more insights into the extent to which haploinsufficiency affects Ca^{2+} handling. Second, the I_{CaL} density and responsiveness of RyR2 to activation by this current — e-c coupling gain — are critical measurements to be performed in the future. Although we did not observe differences in overall Cav1.2 expression, it is possible that post-translational modifications or compartmentalization of LTCC within the cell account for changes in I_{CaL} density in

RyR2-KO myocytes. If these experiments showed that I_{CaL} and/or e-c coupling gain are increased in RyR2-KO myocytes, these would most likely be dominant compensatory mechanisms for RyR2 deficiency in haploinsufficient hearts.

5.7.4. *Chronic Response of RyR2-KO Rabbits to Stress*

RyR2 haploinsufficiency is readily compensated in basal conditions, and the overall acute adrenergic response is maintained. To complete the results described in CHAPTER 3 and section 5.7.3, we must test how RyR2 haploinsufficient rabbits respond to chronic stress, such as myocardial infarction or aortic banding. Zou et al. suggested that RyR2 deficiency is beneficial in mice undergoing aortic constriction, as they develop less severe hypertrophy.¹²¹ In the near future, we will begin testing this in heterozygous RyR2-KO rabbits. These results will be reported in a separate publication.

5.7.5. *Hypertrophic Signaling Pathways Activated by P1124L*

The characterization of P1124L described in CHAPTER 4 was thorough, using several approaches from molecule to whole animal. Still, we have yet to identify the signaling pathways underlying the cardiac hypertrophy. Hence, the description of the clinical case and the level of characterization of P1124L and the in CHAPTER 4, may be suitable for a high impact factor journal such as *Circulation*. The elucidation of the signaling pathways, may be published in a follow-up report. It is possible that the phenotype of the P1124L mice is too mild to reach conclusive results as to specific hypertrophic pathways. In this case, it could be worth considering creating a P1124L rabbit model, as this mutation may produce a more pronounced phenotype in a species closer to human.

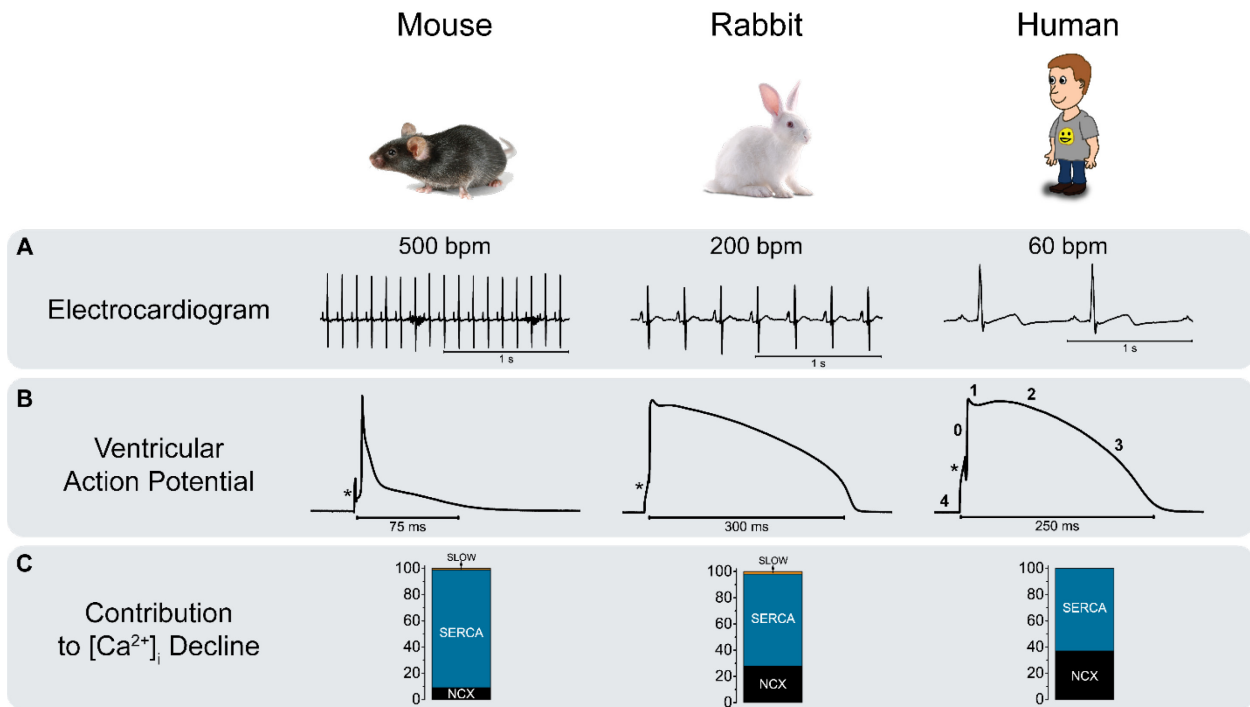


Figure 5.1. Overview of Cardiac Physiology in Mouse, Rabbit, and Human.

A. Representative 2-second traces of Lead-II Electrocardiograms recorded in a mouse and rabbit — anesthetized — and a conscious human subject. The approximate heart rate of the ECG trace is indicated above. **B.** Representative action potentials from ventricular myocytes of the same three species. Numbers indicate the phases of the human action potential. Asterisk indicates the stimulation artifact. Mouse AP courtesy of Yan-Ting Zhao, and human AP courtesy of Daniela Ponce from the University of Michigan Center for Arrhythmia Research. **C.** Contribution of SERCA2a and NCX to cytosolic Ca^{2+} removal. To maintain homeostasis, these percentages must match the contribution of RyR2 and LTCC, respectively, to the cytosolic Ca^{2+} transient. “Slow” indicates the mitochondrial Ca^{2+} uniporter and PMCA. Data from Bers.³

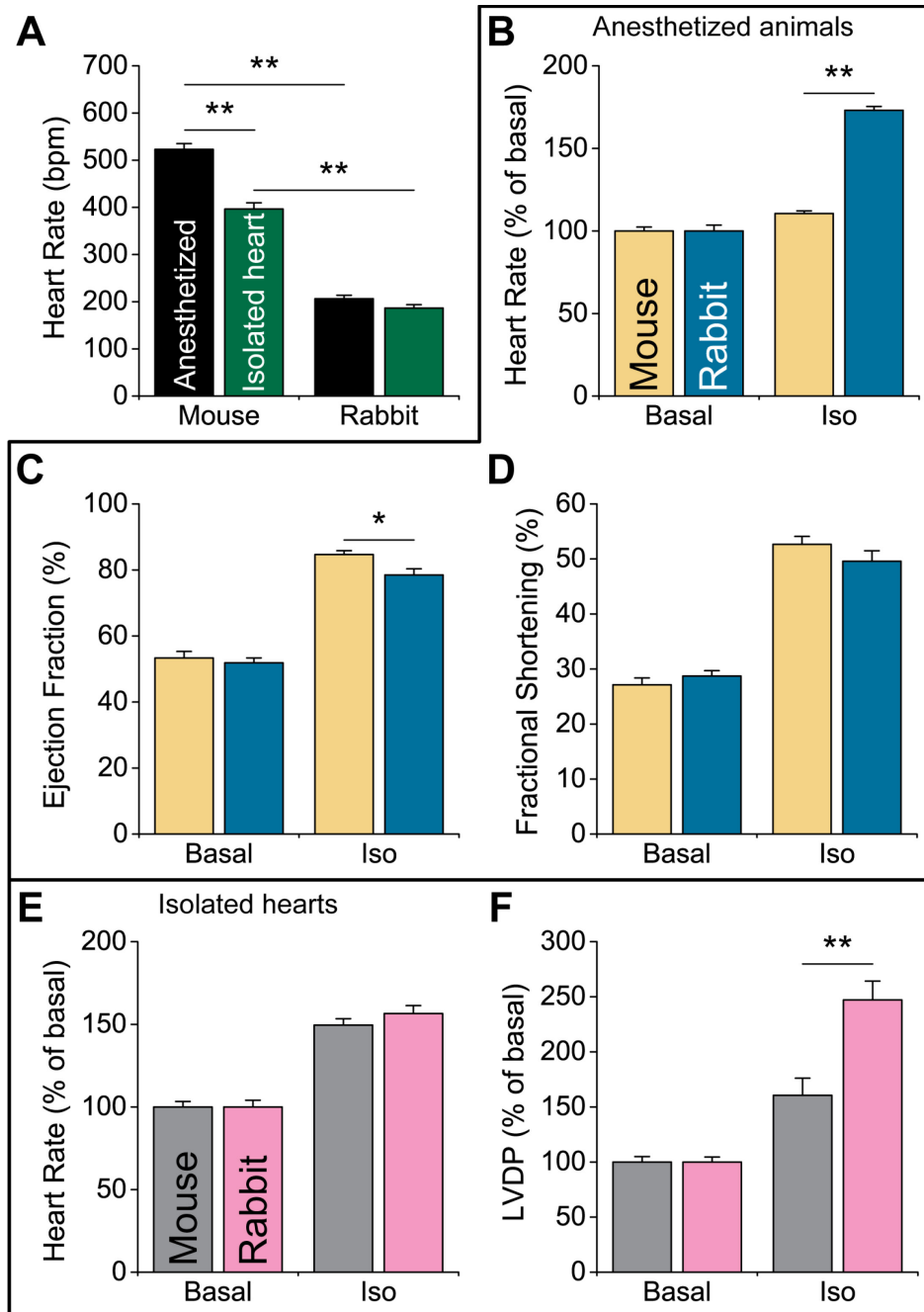


Figure 5.2. Comparison of Cardiac Function between Mouse and Rabbit.

A. Heart rate measurements during echocardiographic assessment of cardiac function in anesthetized mice and in isolated hearts mounted on a Langendorff apparatus. **B-D.** Cardiac function measured in anesthetized animals through echocardiography: HR (**B**, as percentage of basal), ejection fraction (**C**), and fractional shortening (**D**). Measurements performed in basal conditions and under isoproterenol stimulation (mouse: 2 mg/kg IP; rabbit 0.5 µg/kg/min IV). **E-F.** Cardiac function measured in Langendorff-perfused isolated hearts: HR (**E**, mouse: 60 s post-iso, rabbit: 300 s post-iso) and LVDP (**F**, mouse and rabbit: 10 s post-iso) in basal conditions and under Iso stimulation (mouse: 300 nM, rabbit: 100 nM). Data compiled from Figure 2.6 and Figure 3.8 after combining genotypes per species (n = 12 per group. *: $p < 0.05$, **: $p < 0.01$ as indicated).

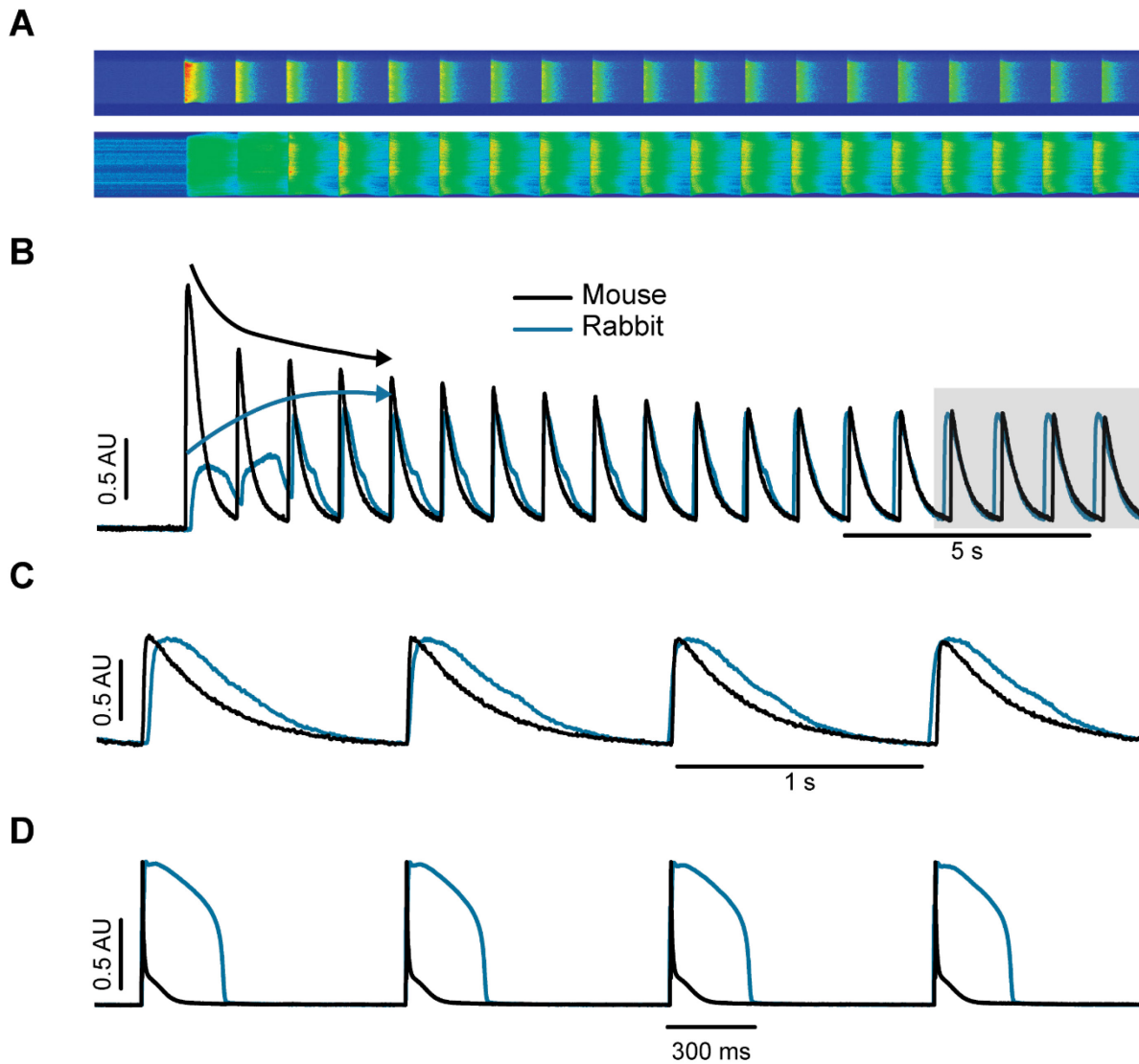


Figure 5.3. Comparison of Ca^{2+} Transients and Action Potentials in Ventricular Myocytes from Mouse and Rabbit.

A. Representative line-scans from mouse (*top panel*) and rabbit (*bottom panel*) myocytes loaded with the Ca^{2+} indicator fluo-4AM and paced at 1 Hz with field stimulation. **B.** Normalized intensity profile of the traces shown in A. $\Delta F/F_0$ values normalized to the peak Ca^{2+} transient. **C.** Ca^{2+} transients from the shaded box in panel B, temporally realigned and at a different time scale. **D.** Ventricular AP recordings from myocytes paced at 1 Hz. Voltage values were adjusted for the resting membrane potential and normalized to the peak of the action potential. Mouse AP courtesy of Yan-Ting Zhao from the University of Michigan Center for Arrhythmia Research

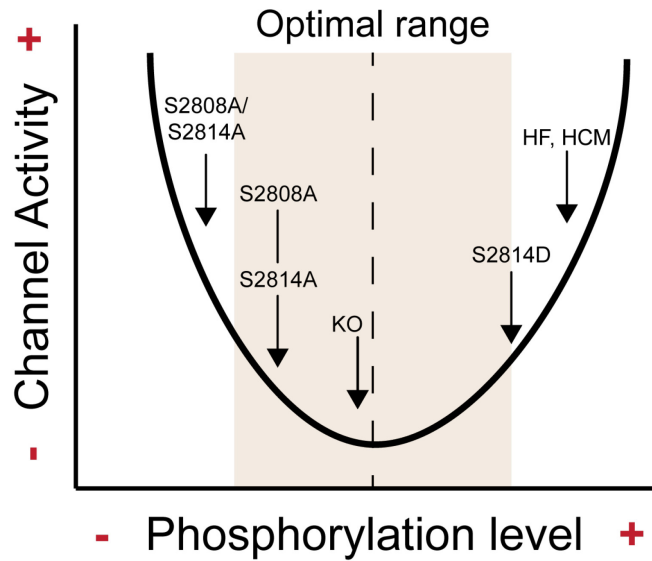


Figure 5.4. RyR2 Regulation by Phosphorylation.

Schematic representation of RyR2 regulation by phosphorylation. The dashed line indicates the phosphorylation level of the channel under normal, basal conditions. To the right, increased phosphorylation of the channel produces an increase in channel activity that can turn pathogenic as proposed in heart failure (HF) and hypertrophic cardiomyopathy (HCM). To the left of the dashed line, dephosphorylation of the channel also produces an increase in channel activity. The level of dephosphorylation determines whether the channel activity remains within an optimal range for the specific model — as in the S2808A mouse and in the RyR2-KO rabbit. Higher dephosphorylation of the channel can have pathological implications, as in the S2808A/S2814A mouse model, which shows increased susceptibility to cardiac arrhythmia.¹⁶⁵

Table 5.1. RyR2 Mutations Reported in both Clinical Cases and WES Studies.

Substitution	Variant Allele Frequency	Clinical Presentation	Pathogenic Potential ^A		Reference
			Frequency	Clinical	
L62F	4.06x10 ⁻⁶	CPVT	++	+	81
L73V	4.06x10 ⁻⁶	SCD ^B	++	-	228
V186M	2.44x10 ⁻⁵	CPVT	+	+	81
H240R	1.08x10 ⁻⁵	CPVT	+	+	81
S406L	2.17x10 ⁻⁵	CPVT	+	+	229
R414C	8.13x10 ⁻⁶	SCD	++	+	230
P466A ^C	8.68x10 ⁻⁵	ACA	+	+	231
L555V	4.07x10 ⁻⁶	diLQTS ^B	++	-	232
R739H	4.08x10 ⁻⁶	CPVT	++	+	81
R1013Q ^C	4.76x10 ⁻⁴	CPVT	-	+	81
T1107M	4.26x10 ⁻⁴	CPVT?, HCM	-	+	81,113
P1124L^C	2.03x10⁻⁵	HCM	+	+	Novel
A1136V	7.06x10 ⁻³	CPVT ^B	-	-	233
T1223A	4.07x10 ⁻⁶	Syncope	++	-	234
P1256T ^C	1.63x10 ⁻⁵	Syncope	+	-	234
N1551S	2.75x10 ⁻⁴	CPVT	+	+	235
S1765C ^C	1.73x10 ⁻⁴	?	+	-	236
V1810L	8.14x10 ⁻⁵	CPVT ^B	+	-	237
E1837K	2.04x10 ⁻⁵	CPVT	+	+	81
I2075T	8.15x10 ⁻⁶	iVF ^B	++	-	238
V2113M	3.97x10 ⁻⁴	CPVT	+	+	81
R2267H	2.85x10 ⁻⁵	SID	++	+	239
R2359Q	3.25x10 ⁻⁵	CPVT? ^B	+	-	240
Y2392C	4.07x10 ⁻⁶	CPVT, SCD	++	+	241
A2439T	1.62x10 ⁻⁵	?	+	-	236
A2498V ^C	4.82x10 ⁻⁵	CPVT?	+	-	242
K4392R	1.64x10 ⁻⁵	ACA, CPVT	+	+	243
G4471R	3.23x10 ⁻⁵	Family History of SCD	+	-	244
H4552R	1.63x10 ⁻⁵	SUD?	+	-	245
A4556T	3.98x10 ⁻⁵	?	+	-	231
R4790Q	4.06 x10 ⁻⁶	CPVT	++	+	81

ACA: aborted cardiac arrest; CPVT: catecholaminergic polymorphic ventricular tachycardia; diLQTS: drug-induced long QT syndrome; iVF: idiopathic ventricular fibrillation; SCD: sudden cardiac death; SID: sudden infant death; SUD: sudden unexplained death.

?: Report does not give specific details of the patient.

^A: Pathogenic potential based on variant frequency (< 1x10⁻⁵: ++, < 4x10⁻⁴: +) and reported clinical diagnosis.

^B: Mutation identified with other variants in RyR2 or other genes.

^C: More variants reported for this residue. Only the one indicated appears in HGMD.

Table compiled from the indicated references and the following databases: variants and allele frequency from the Genome Association Database (gnomAD);⁸³ disease-associated mutations from the Human Gene Mutation Database (HGMD).¹²⁷

BIBLIOGRAPHY

1. Moore B. In Memory of Sidney Ringer [1835-1910]: Some account of the Fundamental Discoveries of the Great Pioneer of the Bio-Chemistry of Crystallo-colloids in Living Cells. *Biochem J.* 1911;5:i b3-xix.
2. Bers DM. Cardiac excitation-contraction coupling. *Nature.* 2002;415:198-205.
3. Bers DM. *Excitation-contraction coupling and cardiac contractile force.* Dordrecht, The Netherlands: Kluwer Academic Publishers; 2001.
4. Fabiato A and Fabiato F. Calcium release from the sarcoplasmic reticulum. *Circ Res.* 1977;40:119-129.
5. Gyorke S and Fill M. Ryanodine receptor adaptation: control mechanism of Ca(2+)-induced Ca²⁺ release in heart. *Science.* 1993;260:807-809.
6. Gyorke S and Terentyev D. Modulation of ryanodine receptor by luminal calcium and accessory proteins in health and cardiac disease. *Cardiovasc Res.* 2008;77:245-255.
7. Valdivia HH, Kaplan JH, Ellis-Davies GC and Lederer WJ. Rapid adaptation of cardiac ryanodine receptors: modulation by Mg²⁺ and phosphorylation. *Science.* 1995;267:1997-2000.
8. Zima AV, Picht E, Bers DM and Blatter LA. Termination of cardiac Ca²⁺ sparks: role of intra-SR [Ca²⁺], release flux, and intra-SR Ca²⁺ diffusion. *Circ Res.* 2008;103:e105-115.
9. Sato D, Shannon TR and Bers DM. Sarcoplasmic Reticulum Structure and Functional Properties that Promote Long-Lasting Calcium Sparks. *Biophys J.* 2016;110:382-390.
10. Cheng H and Lederer WJ. Calcium sparks. *Physiol Rev.* 2008;88:1491-1545.
11. Bers DM. Cardiac sarcoplasmic reticulum calcium leak: basis and roles in cardiac dysfunction. *Annu Rev Physiol.* 2014;76:107-127.
12. Lakatta EG and DiFrancesco D. What keeps us ticking: a funny current, a calcium clock, or both? *J Mol Cell Cardiol.* 2009;47:157-170.
13. Benkusky NA, Weber CS, Scherman JA, Farrell EF, Hacker TA, John MC, Powers PA and Valdivia HH. Intact beta-adrenergic response and unmodified progression toward heart failure in mice with genetic ablation of a major protein kinase A phosphorylation site in the cardiac ryanodine receptor. *Circ Res.* 2007;101:819-829.

14. Houser SR. Role of RyR2 Phosphorylation in Heart Failure and Arrhythmias: Protein Kinase A-Mediated Hyperphosphorylation of the Ryanodine Receptor at Serine 2808 Does Not Alter Cardiac Contractility or Cause Heart Failure and Arrhythmias. *Circ Res*. 2014;114:1320-1327.
15. Pereira L, Cheng H, Lao DH, Na L, van Oort RJ, Brown JH, Wehrens XH, Chen J and Bers DM. Epac2 mediates cardiac beta1-adrenergic-dependent sarcoplasmic reticulum Ca²⁺ leak and arrhythmia. *Circulation*. 2013;127:913-922.
16. Grimm M and Brown JH. Beta-adrenergic receptor signaling in the heart: role of CaMKII. *J Mol Cell Cardiol*. 2010;48:322-330.
17. Anderson ME, Brown JH and Bers DM. CaMKII in myocardial hypertrophy and heart failure. *J Mol Cell Cardiol*. 2011;51:468-473.
18. Valdivia HH. Ryanodine receptor phosphorylation and heart failure: phasing out S2808 and "criminalizing" S2814. *Circ Res*. 2012;110:1398-1402.
19. Bers DM. Ryanodine receptor S2808 phosphorylation in heart failure: smoking gun or red herring. *Circ Res*. 2012;110:796-799.
20. Bovo E, Huke S, Blatter LA and Zima AV. The effect of PKA-mediated phosphorylation of ryanodine receptor on SR Ca²⁺ leak in ventricular myocytes. *J Mol Cell Cardiol*. 2017;104:9-16.
21. Rogers EF, Koniuszy FR and et al. Plant insecticides; ryanodine, a new alkaloid from *Ryania speciosa* Vahl. *J Am Chem Soc*. 1948;70:3086-3088.
22. Fill M and Copello JA. Ryanodine receptor calcium release channels. *Physiol Rev*. 2002;82:893-922.
23. Lai FA, Erickson HP, Rousseau E, Liu QY and Meissner G. Purification and reconstitution of the calcium release channel from skeletal muscle. *Nature*. 1988;331:315-319.
24. Inui M, Saito A and Fleischer S. Purification of the ryanodine receptor and identity with feet structures of junctional terminal cisternae of sarcoplasmic reticulum from fast skeletal muscle. *J Biol Chem*. 1987;262:1740-1747.
25. Capes EM, Loaiza R and Valdivia HH. Ryanodine receptors. *Skelet Muscle*. 2011;1:18.

26. McPherson PS and Campbell KP. Characterization of the major brain form of the ryanodine receptor/Ca²⁺ release channel. *J Biol Chem*. 1993;268:19785-19790.
27. el-Hayek R, Lokuta AJ, Arevalo C and Valdivia HH. Peptide probe of ryanodine receptor function. Imperatoxin A, a peptide from the venom of the scorpion *Pandinus imperator*, selectively activates skeletal-type ryanodine receptor isoforms. *J Biol Chem*. 1995;270:28696-28704.
28. Rebbeck RT, Nitu FR, Rohde D, Most P, Bers DM, Thomas DD and Cornea RL. S100A1 Protein Does Not Compete with Calmodulin for Ryanodine Receptor Binding but Structurally Alters the Ryanodine Receptor-Calmodulin Complex. *J Biol Chem*. 2016;291:15896-15907.
29. Ludtke SJ, Serysheva, II, Hamilton SL and Chiu W. The pore structure of the closed RyR1 channel. *Structure*. 2005;13:1203-1211.
30. Lau K and Van Petegem F. Crystal structures of wild type and disease mutant forms of the ryanodine receptor SPRY2 domain. *Nat Commun*. 2014;5:5397.
31. Yuchi Z, Lau K and Van Petegem F. Disease mutations in the ryanodine receptor central region: crystal structures of a phosphorylation hot spot domain. *Structure*. 2012;20:1201-1211.
32. Tung CC, Lobo PA, Kimlicka L and Van Petegem F. The amino-terminal disease hotspot of ryanodine receptors forms a cytoplasmic vestibule. *Nature*. 2010;468:585-588.
33. Yan Z, Bai XC, Yan C, Wu J, Li Z, Xie T, Peng W, Yin CC, Li X, Scheres SH, Shi Y and Yan N. Structure of the rabbit ryanodine receptor RyR1 at near-atomic resolution. *Nature*. 2015;517:50-55.
34. Zalk R, Clarke OB, des Georges A, Grassucci RA, Reiken S, Mancina F, Hendrickson WA, Frank J and Marks AR. Structure of a mammalian ryanodine receptor. *Nature*. 2015;517:44-49.
35. Efremov RG, Leitner A, Aebersold R and Raunser S. Architecture and conformational switch mechanism of the ryanodine receptor. *Nature*. 2015;517:39-43.
36. Peng W, Shen H, Wu J, Guo W, Pan X, Wang R, Chen SR and Yan N. Structural basis for the gating mechanism of the type 2 ryanodine receptor RyR2. *Science*. 2016;354:ahh5324.

37. des Georges A, Clarke OB, Zalk R, Yuan Q, Condon KJ, Grassucci RA, Hendrickson WA, Marks AR and Frank J. Structural Basis for Gating and Activation of RyR1. *Cell*. 2016;167:145-157 e117.
38. Valdivia HH. Structural and molecular basis of sarcoplasmic reticulum ion channel function. In: D. P. Zipes and J. Jalife, eds. *Cardiac Electrophysiology: from bench to bedside* Philadelphia: Saunders; 2014: 55-69.
39. Van Petegem F. Ryanodine receptors: allosteric ion channel giants. *J Mol Biol*. 2015;427:31-53.
40. Kushnir A and Marks AR. The ryanodine receptor in cardiac physiology and disease. *Adv Pharmacol*. 2010;59:1-30.
41. Babu YS, Sack JS, Greenhough TJ, Bugg CE, Means AR and Cook WJ. Three-dimensional structure of calmodulin. *Nature*. 1985;315:37-40.
42. Xu L and Meissner G. Mechanism of calmodulin inhibition of cardiac sarcoplasmic reticulum Ca²⁺ release channel (ryanodine receptor). *Biophys J*. 2004;86:797-804.
43. Yamaguchi N, Takahashi N, Xu L, Smithies O and Meissner G. Early cardiac hypertrophy in mice with impaired calmodulin regulation of cardiac muscle Ca release channel. *J Clin Invest*. 2007;117:1344-1353.
44. Jeyakumar LH, Ballester L, Cheng DS, McIntyre JO, Chang P, Olivey HE, Rollins-Smith L, Barnett JV, Murray K, Xin HB and Fleischer S. FKBP binding characteristics of cardiac microsomes from diverse vertebrates. *Biochem Biophys Res Commun*. 2001;281:979-986.
45. Farrell EF, Antaramian A, Benkusky N, Zhu X, Rueda A, Gomez AM and Valdivia HH. Regulation of cardiac excitation-contraction coupling by sorcin, a novel modulator of ryanodine receptors. *Biol Res*. 2004;37:609-612.
46. Farrell EF, Antaramian A, Rueda A, Gomez AM and Valdivia HH. Sorcin inhibits calcium release and modulates excitation-contraction coupling in the heart. *J Biol Chem*. 2003;278:34660-34666.
47. Lokuta AJ, Meyers MB, Sander PR, Fishman GI and Valdivia HH. Modulation of cardiac ryanodine receptors by sorcin. *J Biol Chem*. 1997;272:25333-25338.
48. Matsumoto T, Hisamatsu Y, Ohkusa T, Inoue N, Sato T, Suzuki S, Ikeda Y and Matsuzaki M. Sorcin interacts with sarcoplasmic reticulum Ca(2+)-ATPase and

modulates excitation-contraction coupling in the heart. *Basic Res Cardiol.* 2005;100:250-262.

49. Zamparelli C, Macquaide N, Colotti G, Verzili D, Seidler T, Smith GL and Chiancone E. Activation of the cardiac Na(+)-Ca(2+) exchanger by sorcin via the interaction of the respective Ca(2+)-binding domains. *J Mol Cell Cardiol.* 2010;49:132-141.

50. Seidler T, Miller SL, Loughrey CM, Kania A, Burow A, Kettlewell S, Teucher N, Wagner S, Kogler H, Meyers MB, Hasenfuss G and Smith GL. Effects of adenovirus-mediated sorcin overexpression on excitation-contraction coupling in isolated rabbit cardiomyocytes. *Circ Res.* 2003;93:132-139.

51. George CH. Sarcoplasmic reticulum Ca²⁺ leak in heart failure: mere observation or functional relevance? *Cardiovasc Res.* 2008;77:302-314.

52. Witcher DR, Kovacs RJ, Schulman H, Cefali DC and Jones LR. Unique phosphorylation site on the cardiac ryanodine receptor regulates calcium channel activity. *J Biol Chem.* 1991;266:11144-11152.

53. Wehrens XH, Lehnart SE, Reiken S, Vest JA, Wronska A and Marks AR. Ryanodine receptor/calcium release channel PKA phosphorylation: a critical mediator of heart failure progression. *Proc Natl Acad Sci U S A.* 2006;103:511-518.

54. Marx SO, Reiken S, Hisamatsu Y, Jayaraman T, Burkhoff D, Rosemlit N and Marks AR. PKA phosphorylation dissociates FKBP12.6 from the calcium release channel (ryanodine receptor): defective regulation in failing hearts. *Cell.* 2000;101:365-376.

55. Shan J, Kushnir A, Betzenhauser MJ, Reiken S, Li J, Lehnart SE, Lindegger N, Mongillo M, Mohler PJ and Marks AR. Phosphorylation of the ryanodine receptor mediates the cardiac fight or flight response in mice. *J Clin Invest.* 2010;120:4388-4398.

56. Shan J, Betzenhauser MJ, Kushnir A, Reiken S, Meli AC, Wronska A, Dura M, Chen BX and Marks AR. Role of chronic ryanodine receptor phosphorylation in heart failure and beta-adrenergic receptor blockade in mice. *J Clin Invest.* 2010;120:4375-4387.

57. Huke S and Bers DM. Ryanodine receptor phosphorylation at Serine 2030, 2808 and 2814 in rat cardiomyocytes. *Biochem Biophys Res Commun.* 2008;376:80-85.

58. Camors E and Valdivia HH. CaMKII regulation of cardiac ryanodine receptors and inositol triphosphate receptors. *Front Pharmacol.* 2014;5:101.

59. Wehrens XH, Lehnart SE, Reiken SR and Marks AR. Ca²⁺/calmodulin-dependent protein kinase II phosphorylation regulates the cardiac ryanodine receptor. *Circ Res.* 2004;94:e61-70.
60. Respress JL, van Oort RJ, Li N, Rolim N, Dixit SS, deAlmeida A, Voigt N, Lawrence WS, Skapura DG, Skardal K, Wisloff U, Wieland T, Ai X, Pogwizd SM, Dobrev D and Wehrens XH. Role of RyR2 phosphorylation at S2814 during heart failure progression. *Circ Res.* 2012;110:1474-1483.
61. Xiao B, Jiang MT, Zhao M, Yang D, Sutherland C, Lai FA, Walsh MP, Wartier DC, Cheng H and Chen SR. Characterization of a novel PKA phosphorylation site, serine-2030, reveals no PKA hyperphosphorylation of the cardiac ryanodine receptor in canine heart failure. *Circ Res.* 2005;96:847-855.
62. Xiao B, Zhong G, Obayashi M, Yang D, Chen K, Walsh MP, Shimoni Y, Cheng H, Ter Keurs H and Chen SR. Ser-2030, but not Ser-2808, is the major phosphorylation site in cardiac ryanodine receptors responding to protein kinase A activation upon beta-adrenergic stimulation in normal and failing hearts. *Biochem J.* 2006;396:7-16.
63. Ginsburg KS and Bers DM. Modulation of excitation-contraction coupling by isoproterenol in cardiomyocytes with controlled SR Ca²⁺ load and Ca²⁺ current trigger. *J Physiol.* 2004;556:463-480.
64. Cheng H, Fill M, Valdivia H and Lederer WJ. Models of Ca²⁺ release channel adaptation. *Science.* 1995;267:2009-2010.
65. Lokuta AJ, Rogers TB, Lederer WJ and Valdivia HH. Modulation of cardiac ryanodine receptors of swine and rabbit by a phosphorylation-dephosphorylation mechanism. *J Physiol.* 1995;487 (Pt 3):609-622.
66. Terentyev D, Viatchenko-Karpinski S, Gyorke I, Terentyeva R and Gyorke S. Protein phosphatases decrease sarcoplasmic reticulum calcium content by stimulating calcium release in cardiac myocytes. *J Physiol.* 2003;552:109-118.
67. Li Y, Kranias EG, Mignery GA and Bers DM. Protein kinase A phosphorylation of the ryanodine receptor does not affect calcium sparks in mouse ventricular myocytes. *Circ Res.* 2002;90:309-316.
68. Takasago T, Imagawa T, Furukawa K, Ogurusu T and Shigekawa M. Regulation of the cardiac ryanodine receptor by protein kinase-dependent phosphorylation. *J Biochem.* 1991;109:163-170.

69. Priori SG and Chen SR. Inherited dysfunction of sarcoplasmic reticulum Ca²⁺ handling and arrhythmogenesis. *Circ Res*. 2011;108:871-883.
70. Leenhardt A, Denjoy I and Guicheney P. Catecholaminergic polymorphic ventricular tachycardia. *Circ Arrhythm Electrophysiol*. 2012;5:1044-1052.
71. Leenhardt A, Lucet V, Denjoy I, Grau F, Ngoc DD and Coumel P. Catecholaminergic polymorphic ventricular tachycardia in children. A 7-year follow-up of 21 patients. *Circulation*. 1995;91:1512-1519.
72. Priori SG, Napolitano C, Memmi M, Colombi B, Drago F, Gasparini M, DeSimone L, Coltorti F, Bloise R, Keegan R, Cruz Filho FE, Vignati G, Benatar A and DeLogu A. Clinical and molecular characterization of patients with catecholaminergic polymorphic ventricular tachycardia. *Circulation*. 2002;106:69-74.
73. Priori SG, Napolitano C, Tiso N, Memmi M, Vignati G, Bloise R, Sorrentino V and Danielli GA. Mutations in the cardiac ryanodine receptor gene (hRyR2) underlie catecholaminergic polymorphic ventricular tachycardia. *Circulation*. 2001;103:196-200.
74. Lahat H, Pras E, Olender T, Avidan N, Ben-Asher E, Man O, Levy-Nissenbaum E, Khoury A, Lorber A, Goldman B, Lancet D and Eldar M. A missense mutation in a highly conserved region of CASQ2 is associated with autosomal recessive catecholamine-induced polymorphic ventricular tachycardia in Bedouin families from Israel. *Am J Hum Genet*. 2001;69:1378-1384.
75. Roux-Buisson N, Cacheux M, Fourest-Lieuvin A, Fauconnier J, Brocard J, Denjoy I, Durand P, Guicheney P, Kyndt F, Leenhardt A, Le Marec H, Lucet V, Mabo P, Probst V, Monnier N, Ray PF, Santoni E, Tremeaux P, Lacampagne A, Faure J, Lunardi J and Marty I. Absence of triadin, a protein of the calcium release complex, is responsible for cardiac arrhythmia with sudden death in human. *Hum Mol Genet*. 2012;21:2759-2767.
76. Rooryck C, Kyndt F, Bozon D, Roux-Buisson N, Sacher F, Probst V and Thambo JB. New Family With Catecholaminergic Polymorphic Ventricular Tachycardia Linked to the Triadin Gene. *J Cardiovasc Electrophysiol*. 2015;26:1146-1150.
77. Nyegaard M, Overgaard MT, Sondergaard MT, Vranas M, Behr ER, Hildebrandt LL, Lund J, Hedley PL, Camm AJ, Wettrell G, Fosdal I, Christiansen M and Borglum AD. Mutations in calmodulin cause ventricular tachycardia and sudden cardiac death. *Am J Hum Genet*. 2012;91:703-712.
78. Cerrone M, Noujaim SF, Tolkacheva EG, Talkachou A, O'Connell R, Berenfeld O, Anumonwo J, Pandit SV, Vikstrom K, Napolitano C, Priori SG and Jalife J. Arrhythmogenic mechanisms in a mouse model of catecholaminergic polymorphic ventricular tachycardia. *Circ Res*. 2007;101:1039-1048.

79. Herron TJ, Milstein ML, Anumonwo J, Priori SG and Jalife J. Purkinje cell calcium dysregulation is the cellular mechanism that underlies catecholaminergic polymorphic ventricular tachycardia. *Heart Rhythm*. 2010;7:1122-1128.
80. Willis BC, Pandit SV, Ponce-Balbuena D, Zarzoso M, Guerrero-Serna G, Limbu B, Deo M, Camors E, Ramirez RJ, Mironov S, Herron TJ, Valdivia HH and Jalife J. Constitutive Intracellular Na⁺ Excess in Purkinje Cells Promotes Arrhythmogenesis at Lower Levels of Stress Than Ventricular Myocytes From Mice With Catecholaminergic Polymorphic Ventricular Tachycardia. *Circulation*. 2016;133:2348-2359.
81. Medeiros-Domingo A, Bhuiyan ZA, Tester DJ, Hofman N, Bikker H, van Tintelen JP, Mannens MM, Wilde AA and Ackerman MJ. The RYR2-encoded ryanodine receptor/calcium release channel in patients diagnosed previously with either catecholaminergic polymorphic ventricular tachycardia or genotype negative, exercise-induced long QT syndrome: a comprehensive open reading frame mutational analysis. *J Am Coll Cardiol*. 2009;54:2065-2074.
82. Ackerman MJ. Genetic purgatory and the cardiac channelopathies: Exposing the variants of uncertain/unknown significance issue. *Heart Rhythm*. 2015;12:2325-2331.
83. Database TGA, gnomAD Browser. <http://gnomad.broadinstitute.org/>, 2017 (accessed 03.29.2017).
84. Yamamoto T, Yano M, Xu X, Uchinoumi H, Tateishi H, Mochizuki M, Oda T, Kobayashi S, Ikemoto N and Matsuzaki M. Identification of target domains of the cardiac ryanodine receptor to correct channel disorder in failing hearts. *Circulation*. 2008;117:762-772.
85. Wehrens XHT, Lehnart SE, Huang F, Vest JA, Reiken SR, Mohler PJ, Sun J, Guatimosim S, Song L-S, Rosemblyt N, D'Armiento JM, Napolitano C, Memmi M, Priori SG, Lederer WJ and Marks AR. FKBP12.6 Deficiency and Defective Calcium Release Channel (Ryanodine Receptor) Function Linked to Exercise-Induced Sudden Cardiac Death. *Cell*. 2003;113:829-840.
86. Lehnart SE, Mongillo M, Bellinger A, Lindegger N, Chen BX, Hsueh W, Reiken S, Wronska A, Drew LJ, Ward CW, Lederer WJ, Kass RS, Morley G and Marks AR. Leaky Ca²⁺ release channel/ryanodine receptor 2 causes seizures and sudden cardiac death in mice. *J Clin Invest*. 2008;118:2230-2245.
87. Loaiza R, Benkusky NA, Powers PP, Hacker T, Noujaim S, Ackerman MJ, Jalife J and Valdivia HH. Heterogeneity of ryanodine receptor dysfunction in a mouse model of catecholaminergic polymorphic ventricular tachycardia. *Circ Res*. 2013;112:298-308.

88. Jiang D, Chen W, Wang R, Zhang L and Chen SR. Loss of luminal Ca²⁺ activation in the cardiac ryanodine receptor is associated with ventricular fibrillation and sudden death. *Proc Natl Acad Sci U S A*. 2007;104:18309-18314.
89. Zhao YT, Valdivia CR, Gurrola GB, Powers PP, Willis BC, Moss RL, Jalife J and Valdivia HH. Arrhythmogenesis in a catecholaminergic polymorphic ventricular tachycardia mutation that depresses ryanodine receptor function. *Proc Natl Acad Sci U S A*. 2015;112:E1669-1677.
90. Yancy CW, Jessup M, Bozkurt B, Butler J, Casey DE, Jr., Drazner MH, Fonarow GC, Geraci SA, Horwich T, Januzzi JL, Johnson MR, Kasper EK, Levy WC, Masoudi FA, McBride PE, McMurray JJ, Mitchell JE, Peterson PN, Riegel B, Sam F, Stevenson LW, Tang WH, Tsai EJ and Wilkoff BL. 2013 ACCF/AHA guideline for the management of heart failure: executive summary: a report of the American College of Cardiology Foundation/American Heart Association Task Force on practice guidelines. *Circulation*. 2013;128:1810-1852.
91. Hasenfuss G and Pieske B. Calcium cycling in congestive heart failure. *J Mol Cell Cardiol*. 2002;34:951-969.
92. Houser SR, Piacentino V, 3rd and Weisser J. Abnormalities of calcium cycling in the hypertrophied and failing heart. *J Mol Cell Cardiol*. 2000;32:1595-1607.
93. Gwathmey JK, Copelas L, MacKinnon R, Schoen FJ, Feldman MD, Grossman W and Morgan JP. Abnormal intracellular calcium handling in myocardium from patients with end-stage heart failure. *Circ Res*. 1987;61:70-76.
94. Gomez AM, Valdivia HH, Cheng H, Lederer MR, Santana LF, Cannell MB, McCune SA, Altschuld RA and Lederer WJ. Defective excitation-contraction coupling in experimental cardiac hypertrophy and heart failure. *Science*. 1997;276:800-806.
95. Piacentino V, 3rd, Weber CR, Chen X, Weisser-Thomas J, Margulies KB, Bers DM and Houser SR. Cellular basis of abnormal calcium transients of failing human ventricular myocytes. *Circ Res*. 2003;92:651-658.
96. Zima AV, Bovo E, Mazurek SR, Rochira JA, Li W and Terentyev D. Ca handling during excitation-contraction coupling in heart failure. *Pflugers Arch*. 2014;466:1129-1137.
97. Pogwizd SM, Schlotthauer K, Li L, Yuan W and Bers DM. Arrhythmogenesis and contractile dysfunction in heart failure: Roles of sodium-calcium exchange, inward rectifier potassium current, and residual beta-adrenergic responsiveness. *Circ Res*. 2001;88:1159-1167.

98. Shannon TR, Pogwizd SM and Bers DM. Elevated sarcoplasmic reticulum Ca²⁺ leak in intact ventricular myocytes from rabbits in heart failure. *Circ Res*. 2003;93:592-594.
99. Coppini R, Ferrantini C, Yao L, Fan P, Del Lungo M, Stillitano F, Sartiani L, Tosi B, Suffredini S, Tesi C, Yacoub M, Olivotto I, Belardinelli L, Poggesi C, Cerbai E and Mugelli A. Late sodium current inhibition reverses electromechanical dysfunction in human hypertrophic cardiomyopathy. *Circulation*. 2013;127:575-584.
100. Helms AS, Alvarado FJ, Yob J, Tang VT, Pagani F, Russell MW, Valdivia HH and Day SM. Genotype-Dependent and -Independent Calcium Signaling Dysregulation in Human Hypertrophic Cardiomyopathy. *Circulation*. 2016;134:1738-1748.
101. Zhang H, Makarewich CA, Kubo H, Wang W, Duran JM, Li Y, Berretta RM, Koch WJ, Chen X, Gao E, Valdivia HH and Houser SR. Hyperphosphorylation of the cardiac ryanodine receptor at serine 2808 is not involved in cardiac dysfunction after myocardial infarction. *Circ Res*. 2012;110:831-840.
102. Alvarado FJ, Chen X and Valdivia HH. Ablation of the cardiac ryanodine receptor phospho-site Ser2808 does not alter the adrenergic response or the progression to heart failure in mice. Elimination of the genetic background as critical variable. *J Mol Cell Cardiol*. 2017;103:40-47.
103. Eschenhagen T. Is ryanodine receptor phosphorylation key to the fight or flight response and heart failure? *J Clin Invest*. 2010;120:4197-4203.
104. Guo T, Cornea RL, Huke S, Camors E, Yang Y, Picht E, Fruen BR and Bers DM. Kinetics of FKBP12.6 binding to ryanodine receptors in permeabilized cardiac myocytes and effects on Ca sparks. *Circ Res*. 2010;106:1743-1752.
105. Maron BJ, Towbin JA, Thiene G, Antzelevitch C, Corrado D, Arnett D, Moss AJ, Seidman CE, Young JB, American Heart A, Council on Clinical Cardiology HF, Transplantation C, Quality of C, Outcomes R, Functional G, Translational Biology Interdisciplinary Working G, Council on E and Prevention. Contemporary definitions and classification of the cardiomyopathies: an American Heart Association Scientific Statement from the Council on Clinical Cardiology, Heart Failure and Transplantation Committee; Quality of Care and Outcomes Research and Functional Genomics and Translational Biology Interdisciplinary Working Groups; and Council on Epidemiology and Prevention. *Circulation*. 2006;113:1807-1816.
106. Maron BJ. The 2006 American Heart Association classification of cardiomyopathies is the gold standard. *Circ Heart Fail*. 2008;1:72-75.
107. Ommen SR. Hypertrophic cardiomyopathy. *Curr Probl Cardiol*. 2011;36:409-453.

108. Mozaffarian D, Benjamin EJ, Go AS, Arnett DK, Blaha MJ, Cushman M, de Ferranti S, Despres JP, Fullerton HJ, Howard VJ, Huffman MD, Judd SE, Kissela BM, Lackland DT, Lichtman JH, Lisabeth LD, Liu S, Mackey RH, Matchar DB, McGuire DK, Mohler ER, 3rd, Moy CS, Muntner P, Mussolino ME, Nasir K, Neumar RW, Nichol G, Palaniappan L, Pandey DK, Reeves MJ, Rodriguez CJ, Sorlie PD, Stein J, Towfighi A, Turan TN, Virani SS, Willey JZ, Woo D, Yeh RW, Turner MB, American Heart Association Statistics C and Stroke Statistics S. Heart disease and stroke statistics--2015 update: a report from the American Heart Association. *Circulation*. 2015;131:e29-322.
109. Maron BJ, Maron MS and Semsarian C. Genetics of hypertrophic cardiomyopathy after 20 years: clinical perspectives. *J Am Coll Cardiol*. 2012;60:705-715.
110. Landstrom AP and Ackerman MJ. Beyond the cardiac myofilament: hypertrophic cardiomyopathy- associated mutations in genes that encode calcium-handling proteins. *Curr Mol Med*. 2012;12:507-518.
111. Yamaguchi N, Chakraborty A, Pasek DA, Molkentin JD and Meissner G. Dysfunctional ryanodine receptor and cardiac hypertrophy: role of signaling molecules. *Am J Physiol Heart Circ Physiol*. 2011;300:H2187-2195.
112. Yamaguchi N, Chakraborty A, Huang TQ, Xu L, Gomez AC, Pasek DA and Meissner G. Cardiac hypertrophy associated with impaired regulation of cardiac ryanodine receptor by calmodulin and S100A1. *Am J Physiol Heart Circ Physiol*. 2013;305:H86-94.
113. Fujino N, Ino H, Hayashi K, Uchiyama K, Nagata M, Kenno T, Katoh H, Sakamoto Y, Tsubokawa T, Ohsato K, Mizuno S and Yamagishi M. A Novel Missense Mutation in Cardiac Ryanodine Receptor Gene as a Possible Cause of Hypertrophic Cardiomyopathy: Evidence From Familial Analysis [Abstract]. *Circulation*. 2006;114:II_165.
114. Bhuiyan ZA, van den Berg MP, van Tintelen JP, Bink-Boelkens MT, Wiesfeld AC, Alders M, Postma AV, van Langen I, Mannens MM and Wilde AA. Expanding spectrum of human RYR2-related disease: new electrocardiographic, structural, and genetic features. *Circulation*. 2007;116:1569-1576.
115. Campbell MJ, Czosek RJ, Hinton RB and Miller EM. Exon 3 deletion of ryanodine receptor causes left ventricular noncompaction, worsening catecholaminergic polymorphic ventricular tachycardia, and sudden cardiac arrest. *Am J Med Genet A*. 2015;167:2197-2200.
116. Ohno S, Omura M, Kawamura M, Kimura H, Itoh H, Makiyama T, Ushinohama H, Makita N and Horie M. Exon 3 deletion of RYR2 encoding cardiac ryanodine receptor is associated with left ventricular non-compaction. *Europace*. 2014;16:1646-1654.

117. Tiso N, Stephan DA, Nava A, Bagattin A, Devaney JM, Stanchi F, Larderet G, Brahmbhatt B, Brown K, Bauce B, Muriago M, Basso C, Thiene G, Danieli GA and Rampazzo A. Identification of mutations in the cardiac ryanodine receptor gene in families affected with arrhythmogenic right ventricular cardiomyopathy type 2 (ARVD2). *Hum Mol Genet.* 2001;10:189-194.
118. d'Amati G, Bagattin A, Bauce B, Rampazzo A, Autore C, Basso C, King K, Romeo MD, Gallo P, Thiene G, Danieli GA and Nava A. Juvenile sudden death in a family with polymorphic ventricular arrhythmias caused by a novel RyR2 gene mutation: evidence of specific morphological substrates. *Hum Pathol.* 2005;36:761-767.
119. Tang Y, Tian X, Wang R, Fill M and Chen SR. Abnormal termination of Ca²⁺ release is a common defect of RyR2 mutations associated with cardiomyopathies. *Circ Res.* 2012;110:968-977.
120. Liu Y, Wang R, Sun B, Mi T, Zhang J, Mu Y, Chen J, Bround MJ, Johnson JD, Gillis AM and Chen SR. Generation and characterization of a mouse model harboring the exon-3 deletion in the cardiac ryanodine receptor. *PLoS One.* 2014;9:e95615.
121. Zou Y, Liang Y, Gong H, Zhou N, Ma H, Guan A, Sun A, Wang P, Niu Y, Jiang H, Takano H, Toko H, Yao A, Takeshima H, Akazawa H, Shiojima I, Wang Y, Komuro I and Ge J. Ryanodine receptor type 2 is required for the development of pressure overload-induced cardiac hypertrophy. *Hypertension.* 2011;58:1099-1110.
122. Fressart V, Duthoit G, Donal E, Probst V, Deharo JC, Chevalier P, Klug D, Dubourg O, Delacretaz E, Cosnay P, Scanu P, Extramiana F, Keller D, Hidden-Lucet F, Simon F, Bessirard V, Roux-Buisson N, Hebert JL, Azarine A, Casset-Senon D, Rouzet F, Lecarpentier Y, Fontaine G, Coirault C, Frank R, Hainque B and Charron P. Desmosomal gene analysis in arrhythmogenic right ventricular dysplasia/cardiomyopathy: spectrum of mutations and clinical impact in practice. *Europace.* 2010;12:861-868.
123. Rampazzo A, Nava A, Erne P, Eberhard M, Vian E, Slomp P, Tiso N, Thiene G and Danieli GA. A new locus for arrhythmogenic right ventricular cardiomyopathy (ARVD2) maps to chromosome 1q42-q43. *Hum Mol Genet.* 1995;4:2151-2154.
124. Roux-Buisson N, Gandjbakhch E, Donal E, Probst V, Deharo JC, Chevalier P, Klug D, Mansencal N, Delacretaz E, Cosnay P, Scanu P, Extramiana F, Keller D, Hidden-Lucet F, Trapani J, Fouret P, Frank R, Fressart V, Faure J, Lunardi J and Charron P. Prevalence and significance of rare RYR2 variants in arrhythmogenic right ventricular cardiomyopathy/dysplasia: results of a systematic screening. *Heart Rhythm.* 2014;11:1999-2009.
125. Valdivia CR, Landstrom AP, Capes EM, Zhang J, Alvarado FJ, Powers PP, Ackerman MJ and Valdivia HH. Common Polymorphism RYR2-Q2958R Increases

Spontaneous Calcium Release Under Stress and May be Associated With Increased Risk of Sudden Cardiac Death [Abstract]. *Circulation*. 2013;128:A17670.

126. Bers DM. Calcium cycling and signaling in cardiac myocytes. *Annu Rev Physiol*. 2008;70:23-49.

127. IMGC, The Human Gene Mutation Database (HGMD). <http://www.hgmd.cf.ac.uk/ac/index.php>, 2015 (accessed 10.16.2015).

128. Consortium U, UniProt: the universal protein knowledgebase. <http://www.uniprot.org/>, 2017 (accessed 03.29.2017).

129. Pogwizd SM and Bers DM. Calcium cycling in heart failure: the arrhythmia connection. *J Cardiovasc Electrophysiol*. 2002;13:88-91.

130. Hasenfuss G. Alterations of calcium-regulatory proteins in heart failure. *Cardiovasc Res*. 1998;37:279-289.

131. MacDonnell SM, Garcia-Rivas G, Scherman JA, Kubo H, Chen X, Valdivia H and Houser SR. Adrenergic regulation of cardiac contractility does not involve phosphorylation of the cardiac ryanodine receptor at serine 2808. *Circ Res*. 2008;102:e65-72.

132. Liu B, Ho HT, Velez-Cortes F, Lou Q, Valdivia CR, Knollmann BC, Valdivia HH and Gyorke S. Genetic ablation of ryanodine receptor 2 phosphorylation at Ser-2808 aggravates Ca(2+)-dependent cardiomyopathy by exacerbating diastolic Ca²⁺ release. *J Physiol*. 2014;592:1957-1973.

133. Ullrich ND, Valdivia HH and Niggli E. PKA phosphorylation of cardiac ryanodine receptor modulates SR luminal Ca²⁺ sensitivity. *J Mol Cell Cardiol*. 2012;53:33-42.

134. Lehnart SE, Terrenoire C, Reiken S, Wehrens XH, Song LS, Tillman EJ, Mancarella S, Coromilas J, Lederer WJ, Kass RS and Marks AR. Stabilization of cardiac ryanodine receptor prevents intracellular calcium leak and arrhythmias. *Proc Natl Acad Sci U S A*. 2006;103:7906-7910.

135. Bellinger AM, Reiken S, Carlson C, Mongillo M, Liu X, Rothman L, Matecki S, Lacampagne A and Marks AR. Hypernitrosylated ryanodine receptor calcium release channels are leaky in dystrophic muscle. *Nat Med*. 2009;15:325-330.

136. Montagutelli X. Effect of the genetic background on the phenotype of mouse mutations. *J Am Soc Nephrol*. 2000;11 Suppl 16:S101-105.

137. Doetschman T. Influence of genetic background on genetically engineered mouse phenotypes. *Methods Mol Biol.* 2009;530:423-433.
138. Rubinstein M, Westenbroek RE, Yu FH, Jones CJ, Scheuer T and Catterall WA. Genetic background modulates impaired excitability of inhibitory neurons in a mouse model of Dravet syndrome. *Neurobiol Dis.* 2015;73:106-117.
139. Tu PH, Raju P, Robinson KA, Gurney ME, Trojanowski JQ and Lee VM. Transgenic mice carrying a human mutant superoxide dismutase transgene develop neuronal cytoskeletal pathology resembling human amyotrophic lateral sclerosis lesions. *Proc Natl Acad Sci U S A.* 1996;93:3155-3160.
140. Dobrev D and Wehrens XH. Role of RyR2 Phosphorylation in Heart Failure and Arrhythmias: Controversies Around Ryanodine Receptor Phosphorylation in Cardiac Disease. *Circ Res.* 2014;114:1311-1319.
141. Neco P, Torrente AG, Mesirca P, Zorio E, Liu N, Priori SG, Napolitano C, Richard S, Benitah JP, Mangoni ME and Gomez AM. Paradoxical effect of increased diastolic Ca(2+) release and decreased sinoatrial node activity in a mouse model of catecholaminergic polymorphic ventricular tachycardia. *Circulation.* 2012;126:392-401.
142. Wong GT. Speed congenics: applications for transgenic and knock-out mouse strains. *Neuropeptides.* 2002;36:230-236.
143. Information NCfB, Basic Local Alignment Search Tool (BLAST). <http://blast.ncbi.nlm.nih.gov/Blast.cgi>, 2016 (accessed 09.09.2016).
144. Gao E, Lei YH, Shang X, Huang ZM, Zuo L, Boucher M, Fan Q, Chuprun JK, Ma XL and Koch WJ. A novel and efficient model of coronary artery ligation and myocardial infarction in the mouse. *Circ Res.* 2010;107:1445-1453.
145. Harris SP, Bartley CR, Hacker TA, McDonald KS, Douglas PS, Greaser ML, Powers PA and Moss RL. Hypertrophic cardiomyopathy in cardiac myosin binding protein-C knockout mice. *Circ Res.* 2002;90:594-601.
146. Hoit BD, Khoury SF, Kranias EG, Ball N and Walsh RA. In vivo echocardiographic detection of enhanced left ventricular function in gene-targeted mice with phospholamban deficiency. *Circ Res.* 1995;77:632-637.
147. Pogwizd SM, Qi M, Yuan W, Samarel AM and Bers DM. Upregulation of Na(+)/Ca(2+) exchanger expression and function in an arrhythmogenic rabbit model of heart failure. *Circ Res.* 1999;85:1009-1019.

148. Ai X, Curran JW, Shannon TR, Bers DM and Pogwizd SM. Ca²⁺/calmodulin-dependent protein kinase modulates cardiac ryanodine receptor phosphorylation and sarcoplasmic reticulum Ca²⁺ leak in heart failure. *Circ Res*. 2005;97:1314-1322.
149. Sallinen P, Manttari S, Leskinen H, Ilves M, Ruskoaho H and Saarela S. Time course of changes in the expression of DHPR, RyR(2), and SERCA2 after myocardial infarction in the rat left ventricle. *Mol Cell Biochem*. 2007;303:97-103.
150. Bround MJ, Asghari P, Wambolt RB, Bohunek L, Smits C, Philit M, Kieffer TJ, Lakatta EG, Boheler KR, Moore ED, Allard MF and Johnson JD. Cardiac ryanodine receptors control heart rate and rhythmicity in adult mice. *Cardiovasc Res*. 2012;96:372-380.
151. Bround MJ, Wambolt R, Cen H, Asghari P, Albu RF, Han J, McAfee D, Pourrier M, Scott NE, Bohunek L, Kulpa JE, Chen SR, Fedida D, Brownsey RW, Borchers CH, Foster LJ, Mayor T, Moore ED, Allard MF and Johnson JD. Cardiac Ryanodine Receptor (Ryr2)-mediated Calcium Signals Specifically Promote Glucose Oxidation via Pyruvate Dehydrogenase. *J Biol Chem*. 2016;291:23490-23505.
152. Yang D, Xu J, Zhu T, Fan J, Lai L, Zhang J and Chen YE. Effective gene targeting in rabbits using RNA-guided Cas9 nucleases. *J Mol Cell Biol*. 2014;6:97-99.
153. Takeshima H, Komazaki S, Hirose K, Nishi M, Noda T and Iino M. Embryonic lethality and abnormal cardiac myocytes in mice lacking ryanodine receptor type 2. *EMBO J*. 1998;17:3309-3316.
154. Tong J, Oyamada H, Demaurex N, Grinstein S, McCarthy TV and MacLennan DH. Caffeine and halothane sensitivity of intracellular Ca²⁺ release is altered by 15 calcium release channel (ryanodine receptor) mutations associated with malignant hyperthermia and/or central core disease. *J Biol Chem*. 1997;272:26332-26339.
155. Meng X, Xiao B, Cai S, Huang X, Li F, Bolstad J, Trujillo R, Airey J, Chen SR, Wagenknecht T and Liu Z. Three-dimensional localization of serine 2808, a phosphorylation site in cardiac ryanodine receptor. *J Biol Chem*. 2007;282:25929-25939.
156. Brunner M, Peng X, Liu GX, Ren XQ, Ziv O, Choi BR, Mathur R, Hajjiri M, Odening KE, Steinberg E, Folco EJ, Pringa E, Centracchio J, Macharzina RR, Donahay T, Schofield L, Rana N, Kirk M, Mitchell GF, Poppas A, Zehender M and Koren G. Mechanisms of cardiac arrhythmias and sudden death in transgenic rabbits with long QT syndrome. *J Clin Invest*. 2008;118:2246-2259.
157. Terentyev D, Rees CM, Li W, Cooper LL, Jindal HK, Peng X, Lu Y, Terentyeva R, Odening KE, Daley J, Bist K, Choi BR, Karma A and Koren G. Hyperphosphorylation of

RyRs Underlies Triggered Activity in Transgenic Rabbit Model of LQT2 Syndrome. *Circ Res.* 2014;115:919-928.

158. Sicari R, Nihoyannopoulos P, Evangelista A, Kasprzak J, Lancellotti P, Poldermans D, Voigt JU, Zamorano JL and European Association of E. Stress echocardiography expert consensus statement: European Association of Echocardiography (EAE) (a registered branch of the ESC). *Eur J Echocardiogr.* 2008;9:415-437.

159. White JF and Carlson GP. Epinephrine-induced cardiac arrhythmias in rabbits exposed to trichloroethylene: potentiation by caffeine. *Fundam Appl Toxicol.* 1982;2:125-129.

160. Beach CA, Mays DC, Sterman BM and Gerber N. Metabolism, distribution, seminal excretion and pharmacokinetics of caffeine in the rabbit. *J Pharmacol Exp Ther.* 1985;233:18-23.

161. Ikemoto T, Komazaki S, Takeshima H, Nishi M, Noda T, Iino M and Endo M. Functional and morphological features of skeletal muscle from mutant mice lacking both type 1 and type 3 ryanodine receptors. *J Physiol.* 1997;501 (Pt 2):305-312.

162. Takeshima H, Iino M, Takekura H, Nishi M, Kuno J, Minowa O, Takano H and Noda T. Excitation-contraction uncoupling and muscular degeneration in mice lacking functional skeletal muscle ryanodine-receptor gene. *Nature.* 1994;369:556-559.

163. Bround MJ, Wambolt R, Luciani DS, Kulpa JE, Rodrigues B, Brownsey RW, Allard MF and Johnson JD. Cardiomyocyte ATP production, metabolic flexibility, and survival require calcium flux through cardiac ryanodine receptors in vivo. *J Biol Chem.* 2013.

164. Federico M, Portiansky EL, Sommese L, Alvarado FJ, Blanco PG, Zanuzzi CN, Dedman J, Kaetzel M, Wehrens XH, Mattiazzi A and Palomeque J. Calcium-calmodulin-dependent protein kinase mediates the intracellular signalling pathways of cardiac apoptosis in mice with impaired glucose tolerance. *J Physiol.* 2017.

165. Camors E, Loaiza R, Alvarado F, Zhao Y, Powers P and Valdivia HH. Preventing RyR2-S2808 and RyR2-S2814 Phosphorylation does not Alter the β -Adrenergic Response of Mouse Hearts [Abstract]. *Biophys J.* 2014;102:108a.

166. Shannon TR, Ginsburg KS and Bers DM. Potentiation of fractional sarcoplasmic reticulum calcium release by total and free intra-sarcoplasmic reticulum calcium concentration. *Biophys J.* 2000;78:334-343.

167. Eisner DA, Choi HS, Diaz ME, O'Neill SC and Trafford AW. Integrative analysis of calcium cycling in cardiac muscle. *Circ Res*. 2000;87:1087-1094.
168. Trafford AW, Diaz ME, Sibbring GC and Eisner DA. Modulation of CICR has no maintained effect on systolic Ca²⁺: simultaneous measurements of sarcoplasmic reticulum and sarcolemmal Ca²⁺ fluxes in rat ventricular myocytes. *J Physiol*. 2000;522 Pt 2:259-270.
169. Eisner DA, Diaz ME, O'Neill SC and Trafford AW. Physiological and pathological modulation of ryanodine receptor function in cardiac muscle. *Cell Calcium*. 2004;35:583-589.
170. Fu Y, Shaw SA, Naami R, Vuong CL, Basheer WA, Guo X and Hong T. Isoproterenol Promotes Rapid Ryanodine Receptor Movement to Bridging Integrator 1 (BIN1)-Organized Dyads. *Circulation*. 2016;133:388-397.
171. Pandit SV, Kaur K, Zlochiver S, Noujaim SF, Furspan P, Mironov S, Shibayama J, Anumonwo J and Jalife J. Left-to-right ventricular differences in I(KATP) underlie epicardial repolarization gradient during global ischemia. *Heart Rhythm*. 2011;8:1732-1739.
172. Ho CY. Hypertrophic cardiomyopathy: preclinical and early phenotype. *J Cardiovasc Transl Res*. 2009;2:462-470.
173. Braunwald E. Hypertrophic cardiomyopathy: the early years. *J Cardiovasc Transl Res*. 2009;2:341-348.
174. Maron BJ. Sudden death in hypertrophic cardiomyopathy. *J Cardiovasc Transl Res*. 2009;2:368-380.
175. Bos JM, Ommen SR and Ackerman MJ. Genetics of hypertrophic cardiomyopathy: one, two, or more diseases? *Curr Opin Cardiol*. 2007;22:193-199.
176. Landstrom AP, Dailey-Schwartz AL, Rosenfeld JA, Yang Y, McLean MJ, Miyake CY, Valdes SO, Fan Y, Allen HD, Penny DJ and Kim JJ. Interpreting Incidentally Identified Variants in Genes Associated With Catecholaminergic Polymorphic Ventricular Tachycardia in a Large Cohort of Clinical Whole-Exome Genetic Test Referrals. *Circ Arrhythm Electrophysiol*. 2017;10.
177. Van Petegem F. Ryanodine receptors: structure and function. *J Biol Chem*. 2012;287:31624-31632.

178. Frey N and Olson EN. Cardiac hypertrophy: the good, the bad, and the ugly. *Annu Rev Physiol.* 2003;65:45-79.
179. Teare D. Asymmetrical hypertrophy of the heart in young adults. *Br Heart J.* 1958;20:1-8.
180. Geisterfer-Lowrance AA, Kass S, Tanigawa G, Vosberg HP, McKenna W, Seidman CE and Seidman JG. A molecular basis for familial hypertrophic cardiomyopathy: a beta cardiac myosin heavy chain gene missense mutation. *Cell.* 1990;62:999-1006.
181. Jabbari J, Jabbari R, Nielsen MW, Holst AG, Nielsen JB, Haunso S, Tfelt-Hansen J, Svendsen JH and Olesen MS. New exome data question the pathogenicity of genetic variants previously associated with catecholaminergic polymorphic ventricular tachycardia. *Circ Cardiovasc Genet.* 2013;6:481-489.
182. McConnell BK, Jones KA, Fatkin D, Arroyo LH, Lee RT, Aristizabal O, Turnbull DH, Georgakopoulos D, Kass D, Bond M, Niimura H, Schoen FJ, Conner D, Fischman DA, Seidman CE and Seidman JG. Dilated cardiomyopathy in homozygous myosin-binding protein-C mutant mice. *J Clin Invest.* 1999;104:1235-1244.
183. Chen PP, Patel JR, Powers PA, Fitzsimons DP and Moss RL. Dissociation of Structural and Functional Phenotypes in Cardiac Myosin Binding Protein-C Conditional Knock-Out Mice. *Circulation.* 2012.
184. Maron BJ and Ho CY. Hypertrophic cardiomyopathy without hypertrophy: an emerging pre-clinical subgroup composed of genetically affected family members. *JACC Cardiovasc Imaging.* 2009;2:65-68.
185. Jiang D, Xiao B, Yang D, Wang R, Choi P, Zhang L, Cheng H and Chen SR. RyR2 mutations linked to ventricular tachycardia and sudden death reduce the threshold for store-overload-induced Ca²⁺ release (SOICR). *Proc Natl Acad Sci U S A.* 2004;101:13062-13067.
186. Liu P, Jenkins NA and Copeland NG. A highly efficient recombineering-based method for generating conditional knockout mutations. *Genome Res.* 2003;13:476-484.
187. Copeland NG, Jenkins NA and Court DL. Recombineering: a powerful new tool for mouse functional genomics. *Nat Rev Genet.* 2001;2:769-779.
188. Cadinanos J and Bradley A. Generation of an inducible and optimized piggyBac transposon system. *Nucleic Acids Res.* 2007;35:e87.

189. Yang T, Huang YG, Ye W, Hansen P, Schnermann JB and Briggs JP. Influence of genetic background and gender on hypertension and renal failure in COX-2-deficient mice. *Am J Physiol Renal Physiol*. 2005;288:F1125-1132.
190. Waters SB, Diak DM, Zuckermann M, Goldspink PH, Leoni L and Roman BB. Genetic background influences adaptation to cardiac hypertrophy and Ca(2+) handling gene expression. *Front Physiol*. 2013;4:11.
191. Austin CP, Battey JF, Bradley A, Bucan M, Capecchi M, Collins FS, Dove WF, Duyk G, Dymecki S, Eppig JT, Grieder FB, Heintz N, Hicks G, Insel TR, Joyner A, Koller BH, Lloyd KC, Magnuson T, Moore MW, Nagy A, Pollock JD, Roses AD, Sands AT, Seed B, Skarnes WC, Snoddy J, Soriano P, Stewart DJ, Stewart F, Stillman B, Varmus H, Varticovski L, Verma IM, Vogt TF, von Melchner H, Witkowski J, Woychik RP, Wurst W, Yancopoulos GD, Young SG and Zambrowicz B. The knockout mouse project. *Nat Genet*. 2004;36:921-924.
192. Nerbonne JM. Studying cardiac arrhythmias in the mouse--a reasonable model for probing mechanisms? *Trends Cardiovasc Med*. 2004;14:83-93.
193. Bassani JW, Bassani RA and Bers DM. Relaxation in rabbit and rat cardiac cells: species-dependent differences in cellular mechanisms. *J Physiol*. 1994;476:279-293.
194. Pogwizd SM and Bers DM. Rabbit models of heart disease. *Drug Discovery Today: Disease Models*. 2008;5:185-193.
195. Milani-Nejad N and Janssen PM. Small and large animal models in cardiac contraction research: advantages and disadvantages. *Pharmacol Ther*. 2014;141:235-249.
196. Hammer RE, Pursel VG, Rexroad CE, Jr., Wall RJ, Bolt DJ, Ebert KM, Palmiter RD and Brinster RL. Production of transgenic rabbits, sheep and pigs by microinjection. *Nature*. 1985;315:680-683.
197. Fan J and Watanabe T. Transgenic rabbits as therapeutic protein bioreactors and human disease models. *Pharmacol Ther*. 2003;99:261-282.
198. Christensen ND and Peng X. Rabbit Genetics and Transgenic Models. In: M. A. Suckow, K. A. Stevens and R. P. Wilson, eds. *The laboratory rabbit, guinea pig, hamster, and other rodents*. 1st ed. London ; Waltham, MA: Academic Press/Elsevier; 2012: 165-193.

199. Bosze Z, Major P, Baczko I, Odening KE, Bodrogi L, Hiripi L and Varro A. The potential impact of new generation transgenic methods on creating rabbit models of cardiac diseases. *Prog Biophys Mol Biol*. 2016;121:123-130.
200. Martins RP, Kaur K, Hwang E, Ramirez RJ, Willis BC, Filgueiras-Rama D, Ennis SR, Takemoto Y, Ponce-Balbuena D, Zarzoso M, O'Connell RP, Musa H, Guerrero-Serna G, Avula UM, Swartz MF, Bhushal S, Deo M, Pandit SV, Berenfeld O and Jalife J. Dominant frequency increase rate predicts transition from paroxysmal to long-term persistent atrial fibrillation. *Circulation*. 2014;129:1472-1482.
201. Quinn RH. Rabbit Colony Management and Related Health Concerns. In: M. A. Suckow, K. A. Stevens and R. P. Wilson, eds. *The laboratory rabbit, guinea pig, hamster, and other rodents*. 1st ed. London ; Waltham, MA: Academic Press/Elsevier; 2012: 217-241.
202. Yang D, Song J, Zhang J, Xu J, Zhu T, Wang Z, Lai L and Chen YE. Identification and characterization of rabbit ROSA26 for gene knock-in and stable reporter gene expression. *Sci Rep*. 2016;6:25161.
203. Yang D, Zhang J, Xu J, Zhu T, Fan Y, Fan J and Chen YE. Production of apolipoprotein C-III knockout rabbits using zinc finger nucleases. *J Vis Exp*. 2013:e50957.
204. Yang D, Yang H, Li W, Zhao B, Ouyang Z, Liu Z, Zhao Y, Fan N, Song J, Tian J, Li F, Zhang J, Chang L, Pei D, Chen YE and Lai L. Generation of PPARgamma mono-allelic knockout pigs via zinc-finger nucleases and nuclear transfer cloning. *Cell Res*. 2011;21:979-982.
205. Park KE, Powell A, Sandmaier SE, Kim CM, Mileham A, Donovan DM and Telugu BP. Targeted gene knock-in by CRISPR/Cas ribonucleoproteins in porcine zygotes. *Sci Rep*. 2017;7:42458.
206. Sander JD and Joung JK. CRISPR-Cas systems for editing, regulating and targeting genomes. *Nat Biotechnol*. 2014;32:347-355.
207. Electrophysiology TFoTESoCaTNASoPa. Heart rate variability. Standards of measurement, physiological interpretation, and clinical use. Task Force of the European Society of Cardiology and the North American Society of Pacing and Electrophysiology. *Eur Heart J*. 1996;17:354-381.
208. Fielder SE, Merck Veterinary Manual: Resting Heart Rate. <http://www.merckvetmanual.com/appendixes/reference-guides/resting-heart-rates>, 2017 (accessed 07.17.2017).

209. Goff RP, Howard BT, Quallich SG, Iles TL and Iazzo PA. The novel in vitro reanimation of isolated human and large mammalian heart-lung blocs. *BMC Physiol.* 2016;16:4.
210. Hill AJ, Laske TG, Coles JA, Jr., Sigg DC, Skadsberg ND, Vincent SA, Soule CL, Gallagher WJ and Iazzo PA. In vitro studies of human hearts. *Ann Thorac Surg.* 2005;79:168-177.
211. Miller DD, Ruddy TD, Zusman RM, Okada RD, Strauss HW, Kanarek DJ, Christensen D, Federman EB and Boucher CA. Left ventricular ejection fraction response during exercise in asymptomatic systemic hypertension. *Am J Cardiol.* 1987;59:409-413.
212. Lang RM, Badano LP, Mor-Avi V, Afilalo J, Armstrong A, Ernande L, Flachskampf FA, Foster E, Goldstein SA, Kuznetsova T, Lancellotti P, Muraru D, Picard MH, Rietzschel ER, Rudski L, Spencer KT, Tsang W and Voigt JU. Recommendations for cardiac chamber quantification by echocardiography in adults: an update from the American Society of Echocardiography and the European Association of Cardiovascular Imaging. *J Am Soc Echocardiogr.* 2015;28:1-39 e14.
213. Maier LS, Bers DM and Pieske B. Differences in Ca(2+)-handling and sarcoplasmic reticulum Ca(2+)-content in isolated rat and rabbit myocardium. *J Mol Cell Cardiol.* 2000;32:2249-2258.
214. Bassani RA, Altamirano J, Puglisi JL and Bers DM. Action potential duration determines sarcoplasmic reticulum Ca²⁺ reloading in mammalian ventricular myocytes. *J Physiol.* 2004;559:593-609.
215. Pieske B, Sutterlin M, Schmidt-Schweda S, Minami K, Meyer M, Olschewski M, Holubarsch C, Just H and Hasenfuss G. Diminished post-rest potentiation of contractile force in human dilated cardiomyopathy. Functional evidence for alterations in intracellular Ca²⁺ handling. *J Clin Invest.* 1996;98:764-776.
216. Terentyev D and Hamilton S. Regulation of sarcoplasmic reticulum Ca²⁺ release by serine-threonine phosphatases in the heart. *J Mol Cell Cardiol.* 2016;101:156-164.
217. van Oort RJ, McCauley MD, Dixit SS, Pereira L, Yang Y, Respress JL, Wang Q, De Almeida AC, Skapura DG, Anderson ME, Bers DM and Wehrens XH. Ryanodine receptor phosphorylation by calcium/calmodulin-dependent protein kinase II promotes life-threatening ventricular arrhythmias in mice with heart failure. *Circulation.* 2010;122:2669-2679.
218. Chelu MG, Sarma S, Sood S, Wang S, van Oort RJ, Skapura DG, Li N, Santonastasi M, Muller FU, Schmitz W, Schotten U, Anderson ME, Valderrabano M,

Dobrev D and Wehrens XH. Calmodulin kinase II-mediated sarcoplasmic reticulum Ca²⁺ leak promotes atrial fibrillation in mice. *J Clin Invest.* 2009;119:1940-1951.

219. Grimm M, Ling H, Willeford A, Pereira L, Gray CB, Erickson JR, Sarma S, Respress JL, Wehrens XH, Bers DM and Brown JH. CaMKII δ mediates beta-adrenergic effects on RyR2 phosphorylation and SR Ca(2+) leak and the pathophysiological response to chronic beta-adrenergic stimulation. *J Mol Cell Cardiol.* 2015;85:282-291.

220. Potenza DM, Janicek R, Fernandez-Tenorio M, Valdivia HH and Niggli E. Ablation of the RyR2-Ser2030 Phosphorylation Site Limits Changes in RyR2 Sensitivity during β -Adrenergic Stimulation. *Biophys J.* 2017;112:541a-542a.

221. Swan H, Piippo K, Viitasalo M, Heikkila P, Paavonen T, Kainulainen K, Kere J, Keto P, Kontula K and Toivonen L. Arrhythmic disorder mapped to chromosome 1q42-q43 causes malignant polymorphic ventricular tachycardia in structurally normal hearts. *J Am Coll Cardiol.* 1999;34:2035-2042.

222. Cerrone M, Colombi B, Santoro M, di Barletta MR, Scelsi M, Villani L, Napolitano C and Priori SG. Bidirectional ventricular tachycardia and fibrillation elicited in a knock-in mouse model carrier of a mutation in the cardiac ryanodine receptor. *Circ Res.* 2005;96:e77-82.

223. Shan J, Xie W, Betzenhauser M, Reiken S, Chen BX, Wronska A and Marks AR. Calcium leak through ryanodine receptors leads to atrial fibrillation in 3 mouse models of catecholaminergic polymorphic ventricular tachycardia. *Circ Res.* 2012;111:708-717.

224. Kannankeril PJ, Mitchell BM, Goonasekera SA, Chelu MG, Zhang W, Sood S, Kearney DL, Danila CI, De Biasi M, Wehrens XH, Pautler RG, Roden DM, Taffet GE, Dirksen RT, Anderson ME and Hamilton SL. Mice with the R176Q cardiac ryanodine receptor mutation exhibit catecholamine-induced ventricular tachycardia and cardiomyopathy. *Proc Natl Acad Sci U S A.* 2006;103:12179-12184.

225. Jiang D, Wang R, Xiao B, Kong H, Hunt DJ, Choi P, Zhang L and Chen SR. Enhanced store overload-induced Ca²⁺ release and channel sensitivity to luminal Ca²⁺ activation are common defects of RyR2 mutations linked to ventricular tachycardia and sudden death. *Circ Res.* 2005;97:1173-1181.

226. Asghari P, Scriven DR, Sanatani S, Gandhi SK, Campbell AI and Moore ED. Nonuniform and variable arrangements of ryanodine receptors within mammalian ventricular couplons. *Circ Res.* 2014;115:252-262.

227. Asghari P, Scriven DRL, Zhao Y, Ramos-Mondragon R, Valdivia H, Wehrens X and Moore EDW. RyR2 Tetramer Distributions in Ventricular Myocytes from Phosphomutant Mice [Abstract]. *Biophys J*. 2017;112:161a.
228. Campuzano O, Sanchez-Molero O, Allegue C, Coll M, Mademont-Soler I, Selga E, Ferrer-Costa C, Mates J, Iglesias A, Sarquella-Brugada G, Cesar S, Brugada J, Castella J, Medallo J and Brugada R. Post-mortem genetic analysis in juvenile cases of sudden cardiac death. *Forensic Sci Int*. 2014;245:30-37.
229. Jung CB, Moretti A, Mederos y Schnitzler M, Iop L, Storch U, Bellin M, Dorn T, Ruppenthal S, Pfeiffer S, Goedel A, Dirschinger RJ, Seyfarth M, Lam JT, Sinnecker D, Gudermann T, Lipp P and Laugwitz KL. Dantrolene rescues arrhythmogenic RYR2 defect in a patient-specific stem cell model of catecholaminergic polymorphic ventricular tachycardia. *EMBO Mol Med*. 2012;4:180-191.
230. Creighton W, Virmani R, Kutys R and Burke A. Identification of novel missense mutations of cardiac ryanodine receptor gene in exercise-induced sudden death at autopsy. *J Mol Diagn*. 2006;8:62-67.
231. Tester DJ, Kopplin LJ, Will ML and Ackerman MJ. Spectrum and prevalence of cardiac ryanodine receptor (RyR2) mutations in a cohort of unrelated patients referred explicitly for long QT syndrome genetic testing. *Heart Rhythm*. 2005;2:1099-1105.
232. Ramirez AH, Shaffer CM, Delaney JT, Sexton DP, Levy SE, Rieder MJ, Nickerson DA, George AL, Jr. and Roden DM. Novel rare variants in congenital cardiac arrhythmia genes are frequent in drug-induced torsades de pointes. *Pharmacogenomics J*. 2013;13:325-329.
233. Krahn AD, Healey JS, Chauhan V, Birnie DH, Simpson CS, Champagne J, Gardner M, Sanatani S, Exner DV, Klein GJ, Yee R, Skanes AC, Gula LJ and Gollob MH. Systematic assessment of patients with unexplained cardiac arrest: Cardiac Arrest Survivors With Preserved Ejection Fraction Registry (CASPER). *Circulation*. 2009;120:278-285.
234. Ohno S, Hasegawa K and Horie M. Gender Differences in the Inheritance Mode of RYR2 Mutations in Catecholaminergic Polymorphic Ventricular Tachycardia Patients. *PLoS One*. 2015;10:e0131517.
235. Kawamura M, Ohno S, Naiki N, Nagaoka I, Dochi K, Wang Q, Hasegawa K, Kimura H, Miyamoto A, Mizusawa Y, Itoh H, Makiyama T, Sumitomo N, Ushinohama H, Oyama K, Murakoshi N, Aonuma K, Horigome H, Honda T, Yoshinaga M, Ito M and Horie M. Genetic background of catecholaminergic polymorphic ventricular tachycardia in Japan. *Circ J*. 2013;77:1705-1713.

236. Brion M, Blanco-Verea A, Sobrino B, Santori M, Gil R, Ramos-Luis E, Martinez M, Amigo J and Carracedo A. Next generation sequencing challenges in the analysis of cardiac sudden death due to arrhythmogenic disorders. *Electrophoresis*. 2014;35:3111-3116.
237. Kim NY, Kang JK, Park SH, Bae MH, Lee JH, Yang DH, Park HS, Chae SC, Jun JE and Cho Y. Catecholaminergic polymorphic ventricular tachycardia in a patient with recurrent exertional syncope. *Korean Circ J*. 2012;42:129-132.
238. Paech C, Gebauer RA, Karstedt J, Marschall C, Bollmann A and Husser D. Ryanodine receptor mutations presenting as idiopathic ventricular fibrillation: a report on two novel familial compound mutations, c.6224T>C and c.13781A>G, with the clinical presentation of idiopathic ventricular fibrillation. *Pediatr Cardiol*. 2014;35:1437-1441.
239. Tester DJ, Dura M, Carturan E, Reiken S, Wronska A, Marks AR and Ackerman MJ. A mechanism for sudden infant death syndrome (SIDS): stress-induced leak via ryanodine receptors. *Heart Rhythm*. 2007;4:733-739.
240. Aizawa Y, Mitsuma W, Ikrar T, Komura S, Hanawa H, Miyajima S, Miyoshi F, Kobayashi Y, Chinushi M, Kimura A, Hiraoka M and Aizawa Y. Human cardiac ryanodine receptor mutations in ion channel disorders in Japan. *Int J Cardiol*. 2007;116:263-265.
241. Bauce B, Rampazzo A, Basso C, Bagattin A, Daliento L, Tiso N, Turrini P, Thiene G, Danieli GA and Nava A. Screening for ryanodine receptor type 2 mutations in families with effort-induced polymorphic ventricular arrhythmias and sudden death: early diagnosis of asymptomatic carriers. *J Am Coll Cardiol*. 2002;40:341-349.
242. Hayashi M, Denjoy I, Extramiana F, Maltret A, Buisson NR, Lupoglazoff JM, Klug D, Hayashi M, Takatsuki S, Villain E, Kamblock J, Messali A, Guicheney P, Lunardi J and Leenhardt A. Incidence and risk factors of arrhythmic events in catecholaminergic polymorphic ventricular tachycardia. *Circulation*. 2009;119:2426-2434.
243. Arakawa J, Hamabe A, Aiba T, Nagai T, Yoshida M, Touya T, Ishigami N, Hisadome H, Katsushika S, Tabata H, Miyamoto Y and Shimizu W. A novel cardiac ryanodine receptor gene (RyR2) mutation in an athlete with aborted sudden cardiac death: a case of adult-onset catecholaminergic polymorphic ventricular tachycardia. *Heart Vessels*. 2015;30:835-840.
244. Wang D, Shah KR, Um SY, Eng LS, Zhou B, Lin Y, Mitchell AA, Nicaj L, Prinz M, McDonald TV, Sampson BA and Tang Y. Cardiac channelopathy testing in 274 ethnically diverse sudden unexplained deaths. *Forensic Sci Int*. 2014;237:90-99.

245. Narula N, Tester DJ, Paulmichl A, Maleszewski JJ and Ackerman MJ. Post-mortem Whole exome sequencing with gene-specific analysis for autopsy-negative sudden unexplained death in the young: a case series. *Pediatr Cardiol.* 2015;36:768-778.